Active Mode-Locking of Semiconductor Lasers and Study of Optical Amplification in Diode Lasers.

Thesis submitted for the degree of Doctor of Philosophy of the University of London

by

Jeremy Tsz-Kong CHANG B.Sc., A.R.C.S., M.Sc., D.I.C.

Optics Section, The Blackett Laboratory,
Imperial College of Science and Technology,
London SW7 2BZ, U.K.

February 1988

Abstract

Experimental work on generation and detection of short optical pulses from semiconductor lasers are described. Active mode-locking was used and by applying this technique onto an external cavity Brewster angled stripe semiconductor laser, pulses of durations of 10 picoseconds were produced at a repetition rate of 0.3 GHz. Pulse profile was measured using a synchronscan streak camera with extended infra red sensitivity (From ultra-violet to 1.55μm). Channel plate intensifier which has a gain of 10^5 was also used to enhance the streaked images.

Characterisation of external cavity lasers using various feedback elements are presented. External reflectors such as optical fibre gratings, plane metal coated mirrors, and ruling gratings were used. The spectral outputs were found to be depended strongly on the feedback mechanism. For the selective feedback, single mode emission was obtained. The subcavity effect of a laser diode also plays an important role. In order to reduce this effect, the facets were polished (or cleaved) such that they were at Brewster angles to the metalisation stripe, i.e. transforming a laser into an amplifier. The transformed diodes could not lase on their own. However, under high pumping condition, small modulations were observed around the fluorescence peak.

The possible lasing-wavelengths of a composite resonator has been carried out based on the multiple beam interference equations. A single, consistent lasing-wavelengths equation has been derived for composite resonator of four mirrors. This equation can also be used to describe the transmission bandwidth of a passive composite cavity by taking all the gain media as 1. The computed results showed that the excitations of modes in a composite cavity depend strongly on the reflectivities of the mirrors. It was also found that the lasing band of composite cavity may not be a continuum, as it is generally assumed.

Optical amplification using Brewster angled laser diodes was investigated.

Since a semiconductor laser inherently possesses high optical amplification by stimulated emission, it is thus an attractive optical amplifier which is one of the key components of a future lightwave communication system. An external cavity laser was used as a signal source which can produce either c.w. output or picoseconds pulses when mode-locked. Spectra and pulse-profiles of the amplified signals were studied. Single-pass-gain of 32dB was obtained for an input peak-power of -26 dBm.

Acknowledgements

I am indebted to:

Dr. John I. Vukusic (my supervisor) for his "**smoky**" supervision on the above reported work and his "**black coffee**"-like encouragements through out the last three years.

Professor Wilson Sibbett* (my ex-supervisor) for giving me this wonderful opportunity.

Dr. Pete J. William† (my industrial supervisor) for his tolerance and useful advice, also for the supply of InGaAsP laser chips. Without them, this work would have not been possible.

Mr. Doug C.J. Reid† and Mr. Christ J. Rowe† for their help and guidence in fabricating the 1.3μm optical fibre grating.

Drs. Roy J. Taylor, Paul M.W. French, Jian-Ying Zhou, Dave W. Crust*, Nigel Langford*, Hercules Avramopoulos, Anderson S.L. Gomes and Artur S. Gouveia Neto for allowing the use of their equipment, and their technical advice, and stimulating discussions.

Professor Walter Welford for his help and deep insight into the problems involved in Chapter Three on the lasing wavelengths of composite cavities.

Mr. Rolf Bachen for editing and correcting the thesis, and for giving me some useful lessons on English grammar.

Mr. Wing C. Pang and Mr. Ernest S.M. Tsui, who have enlightened my obsession of life and borne my exasperations of living ever since we were freshmen, also to their families for their warm hospitalities many times.

Thanks are also due to all the staff in the Optics Section and especially to Mr. T.Bates and Mr. R.S. Morrison for constructing the laser mounts, and to Mr. J. Bean for building the casings for the streak camera and the intensifier.

Last but not least, I wish to express my thanks to the Plessey Research

(Caswell) Centre, Towcester, England for providing the CASE award and to the Science and Engineering Research Council (SERC) for giving me the financial support.

* : Physics Department, St.Andrews University, Fife, Scotland.

† : Plessey Research Centre, Caswell, Towcester, England.

To all those who have made me what I am to date, and those who will make me even better tomorrow.

Contents

CHAPTER ONE

General introductions

To a certain extent, it is justified to say that men have been using optical communication systems ever since the pre-historic times. The most renowned evidence was found in America where the red-indians have used the smoke-signals to send messages. The intermittent puffs of smoke they generated from a mountain top can be regarded as digital signals. Light is the information-carrier which travels through the air (the transmission medium). The human eyes are the photodetectors. For transmitting messages over a long distance, puffs of smoke can be relayed from one mountaintop to another. The use of such a system was also recorded by the early Chinese in the time well before the erection of Great Wall. News of invasions around the borders could swiftly reach the capital via a network of smoke-towers in all the strategic points across China. Presumably, similar techniques of optical communications were also used by other earliest civilisations.

Today, the optical communication system relies mainly on:

(1) the near-infra-red optical sources that can be modulated by the information bearing signals.

(2) a low-loss transmission medium that is capable of guiding optical energy along it.

(3) the sensitive photodetectors that can recover the optical modulations and transform them into electrical signals.

The first commercial optical communication system was installed in 1977. The data transmission rate was around 10Mbit/s over several kilometres. This would not have been possible if the three major technologies were not matured at the time. The first was the invention of semiconductor (or current-injection) laser in 1962 and later in 1977, the demonstration of continuous operation for over one million hours. The second technology involved the attainment of 20dB/km doped silica fibre in 1970. Nowadays, Ge-doped silica-based fibres have losses as low as 0.12dB/km at

wavelengths around 1.55μm and have zero-dispersion at wavelengths around 1.3μm. The third technology is the development of low-noise photodetectors in the 1970s, which brought the ultrahigh-sensitivity photo-receivers into realisation.

Over the last two decades, exciting advances have been made in optical communications which greatly increased the transmission capacity and stretched the communication-links further apart. Recently, the optical transmission systems have just broken the Gbit/s barrier and communication-links over 50km long have been installed. It has been speculated that by implementing with the wavelength multiplexing, systems operating at many Gbit/s over much longer distances may well be available before 1990. Surely, the quest for better systems will not stop there. The progress in lightwave communications will still be made. In addition, the interdisciplinary efforts as well as the strong interaction with the needs of the ever-expanding information technology will fuel further revolutions in optical communications. It does not take a great deal of imagination to realise the impact of such technological advances on the world.

The whole architecture of optical communications is essentially based on the modulation of light. For the pulse-coded-modulation, faster modulation speed and shorter pulse-widths will result in greater transmission capacity. For the semiconductor laser, its light output can be easily modulated by varying the amount of injected currents. Other modulation techniques which have already demonstrated on its precursors- the gas, dye, and solid-state lasers, can also be applied. One of which is the mode-locking technique. Using such a technique, sub-picoseconds pules have been generated on the "big" lasers. In this thesis, the study of actively mode-locking external semiconductor laser cavities is described together with the characterisation of various external cavity lasers. Preliminary work on the Brewster angled stripe laser amplifier is also described. Since semiconductor lasers possess the high amplification properties by stimulated emissions, they thus have the potential as linear repeaters in the future lightwave communication systems.

Being one of the key components in optical communication systems, semiconductor lasers have been subjected to extensive research in both the fabrication and performance. Since its birth in 1962, various types of semiconductor lasers have been evolved to suit different applications. In chapter two, basic concepts of laser diodes in terms of electron-band structures are presented. Various well-known semiconductor lasers are briefly outlined.

In certain applications such as mode-locking experiments and coherent systems, the use of semiconductor lasers are not appropriate unless they have external (or extended) cavities. Chapter three deals theoretically with the lasing-bands (i.e. all the possible lasing-wavelengths) of such external cavity lasers. In chapter four, fabrications of Brewster angled stripe lasers are described. Experimental results which characterised the performance of the zero-degree, A.R. coated, and Brewster angled stripe lasers are presented. In addition, the spectral properties of these lasers operating within different external cavities are also discussed.

Chapter five is a review of the three major but different analysis on active mode-locking of semiconductor lasers. Since the initial boundary conditions strongly determine the final outcome of a mathematical derivation, detailed examinations on the validities of these conditions are given. Physical interpretations of the derived equations are presented together with the effect on the pulse-widths due to several important experimental parameters. The experimental results on the actively mode-locked systems are discussed in chapter six. In addition, the diagnostic systems used in measuring the pulse-widths are described. Chapter seven is devoted entirely to the Brewster angled stripe laser amplifier because of its potential as linear repeater in a optical communication system. Its operational characteristics in terms of single-pass-gain, spectral output, and distortions in pulse-widths are described together with the experimental set-up. Finally, the general conclusions and the prospects of the present reported work will be discussed in chapter eight.

CHAPTER TWO

Semiconductor lasers

2.1 Introduction

Semiconductor lasers are probably the most widely used optical devices in optical information technology. These can be utilised as optical signal sources in lightwave communication systems. They are also used as laser amplifiers in a wide range of optoelectronic devices to improve the devices' sensitivities. Laser diodes are also employed in the optical reading devices such as the video disc recorders, compact disc player, and in optical writing appliances such as the laser printers. Semiconductor lasers are also used as the pump sources for solid state lasers instead of the flash lamps to increase the pumping efficiency. With this improved pumping efficiency, the compact hand-held Nd:Yad lasers can now be manufactured. In the high output power regime, semiconductor laser arrays can now generate c.w. output powers exceeding 1 watt. However, intensive research and development is still being carried out on laser diodes to tailor their operating characteristics for various applications in science and engineering.

This chapter is intended to serve as an introduction to semiconductor lasers and their various structures. The discussion starts on the basic principles of lasing

in semiconductor lasers. Rigorous mathematical derivations on the occupation states densities are avoided since these formulations can be found in many standard text books of solid state physics and semiconductor lasers and thus it is unnecessary to re-derive them here but the important formulations of the threshold current, gain, etc, will be quoted whenever they are needed.

After establishing the necessary conditions for lasing to occur, the band structures of p-n (homojunction) lasers will be described and this follows by the principles of operation of heterostructure lasers which form the basis of to date's semiconductor lasers. From this point, the discussion branches into sub-topics. Each of which outlines various laser diodes which are tailored to suit particular applications.

2.2 General concept of semiconductor lasers

The basic components of a laser are (1) the gain (or active) medium through which light is amplified via the stimulated emission and (2) the cavity (or resonator) inside which the light can set up a standing wave to take full advantage of the gain medium. Lasing occurs when the optical gain of the active medium overcomes the net optical losses which are due to the absorptions by the medium and diffraction losses by the resonator. Thus, there exits a certain threshold level below which the lasing cannot occur. Within the gain medium, there are three primary types of electron-photon recombination processes which can occur. These are the photon absorption, spontaneous (fluorescence) and stimulated emissions. Below the lasing threshold, the active medium only emits spontaneous radiation. This fluorescence is also regarded as the origin of noise because of its random nature.

Prior to lasing, the amount of stimulated emission is much smaller than the fluorescence. As the pumping increases, the corresponding stimulated emission also becomes larger. It will become the dominant process above the lasing threshold. This is when the population inversion can be established among the upper and lower states. The stimulated photons will have the same propagation phases as the incoming (the

stimulus) photons.

In some lasers, all of these recombinations occur among the discrete states of the gain medium. For a semiconductor material, the electron-hole recombinations take place between bands of states, namely the valence and conduction bands. These bands of states are caused by a strong overlapping of electron distributions which bond the atoms together to form a crystalline structure. Electrons in the valence band are bounded to the vicinity of their parent atoms. While in the conduction band, they are mobile and free to move around the crystal when subjected to external forces such as applied electric or magnetic fields. For an intrinsic semiconductor, the "free" electrons in the conduction band are normally excited from the valence band by thermal agitation. These "free" electrons are responsible for the material's electric conductivity. For an extrinsic semiconductor which is doped with small amount of impurity atoms. If each impurity atom carries more electrons than it is needed for the crystalline bonding, more "free" electrons are thus made available. This type of doped semiconductor material is referred to as the n-type material. On the other hand, if a doped atom has insufficient amount of electrons for crystalline bonding; then there is not enough electrons within the crystal for bonding the atoms together. This creates the empty electron states (or holes) in the valency band. Such a material is referred to as the p-type material.

The distribution of electrons in either bands is governed by Fermi-Dirac statistics. At absolute zero (0^oK), the electrons fill all the lowest states and the upper bound is denoted by E_f, the Fermi level. Figure 2.1 shows the band structures which are expressed in electron energy (E) and crystal momentum (k) for intrinsic, extrinsic p-type and extrinsic n-type semiconductors at 0^oK. For the intrinsic materials, the Fermi levels are situated in the middle of the band gap (E_g). When impurity atoms are doped, the Fermi levels will shift to either the conduction or valence bands depending on whether the atoms have more or insufficient "bonding" electrons respectively. For the n-type materials, because of the excess electrons, the Fermi levels are positioned inside the conduction band. Conversely, the presence of holes in the

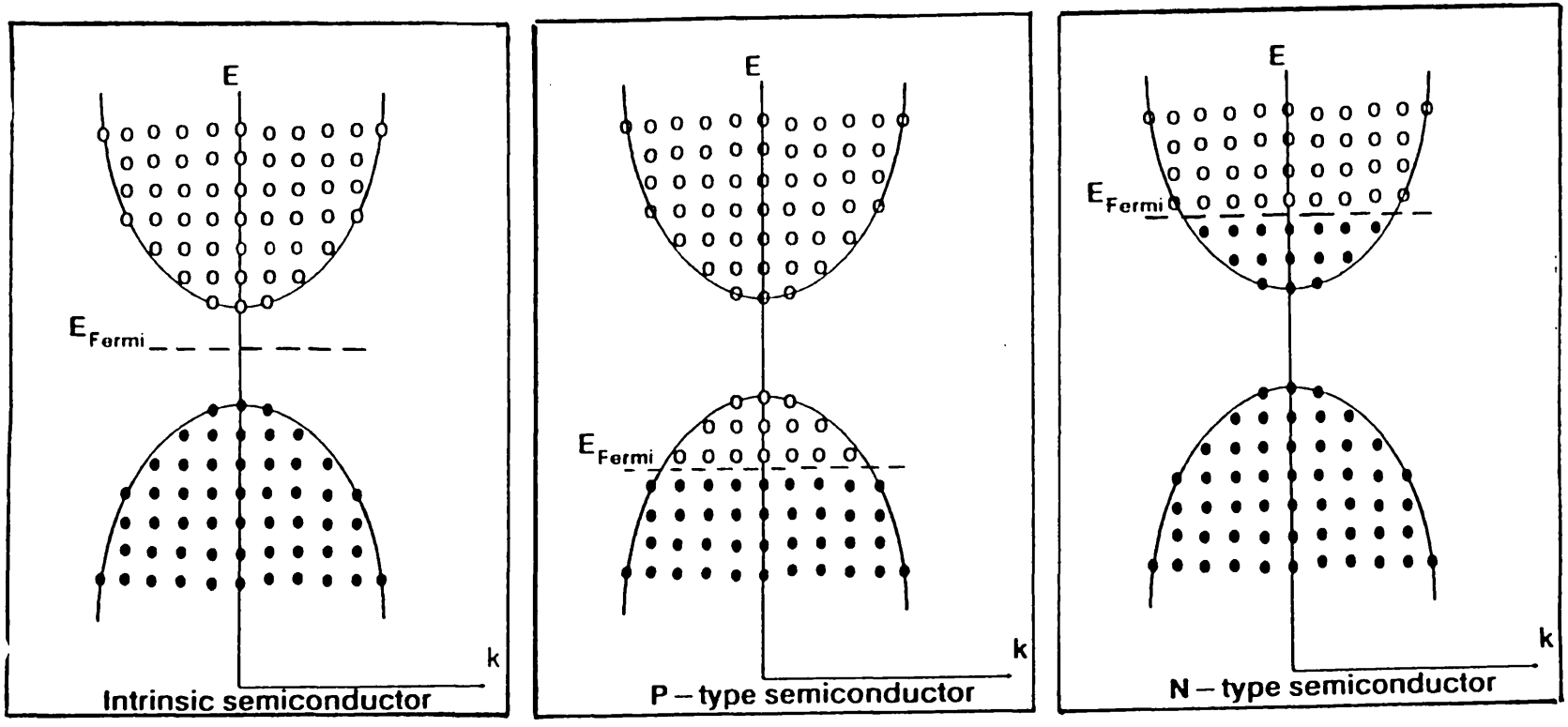

Figures (2.1a), (2.1b), and (2.1c) : The band structures of intrinsic, n-type, and p-type semiconductor materials respectively.

Figure (2.2) : The band structure of a "double degenerated" semiconductor material.

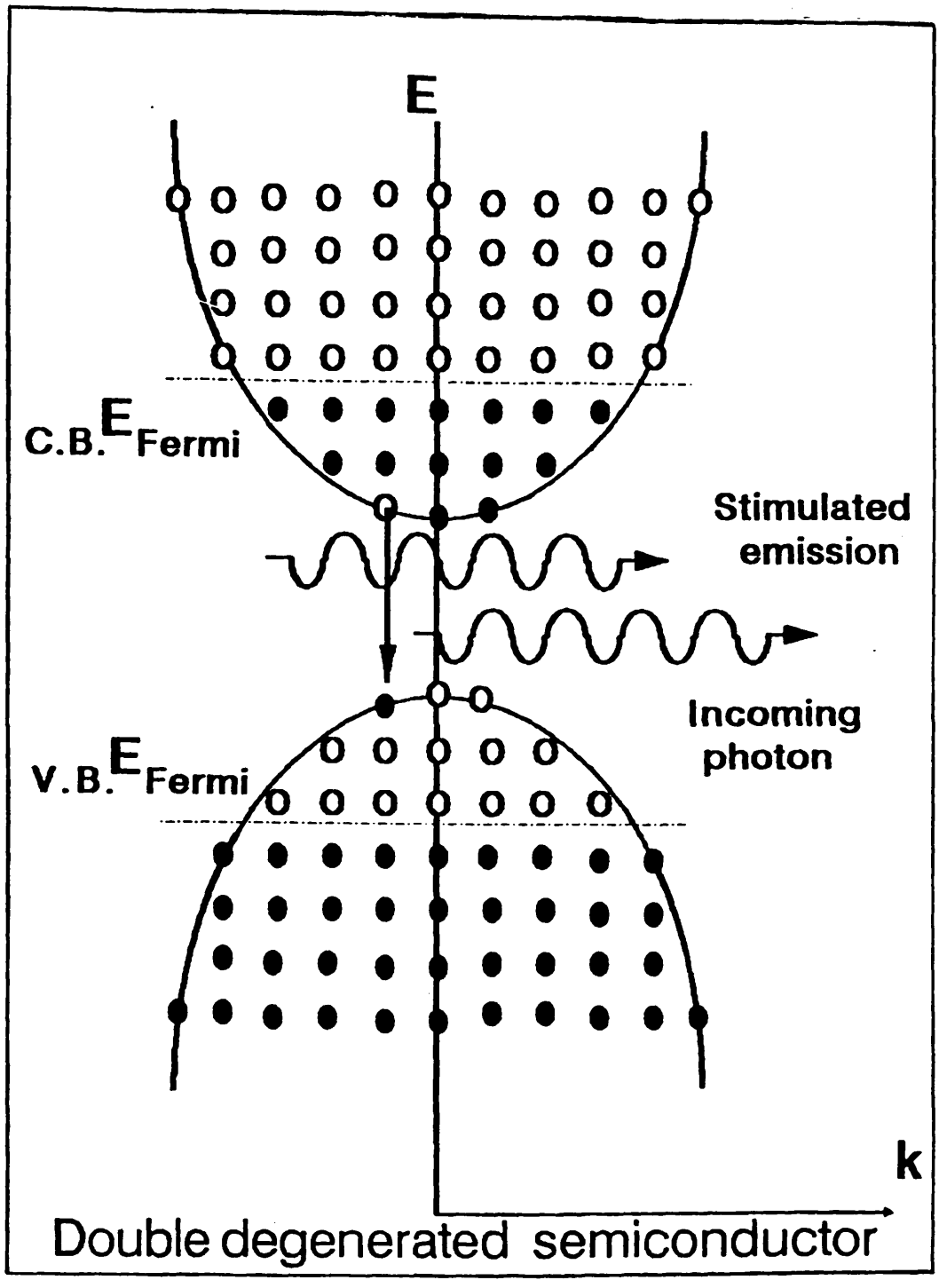

p-type materials confine the Fermi-levels within the valence bands. These two different types of extrinsic semiconductors are sometimes referred to as the "degenerate" materials.

When in thermal equilibrium, the electrons distribute themselves among the lowest states. The corresponding probability of an electron relaxing to a lower state is small. For lasing to occur, inverted population has to be established first, i.e. more electrons in the upper states than in the lower states. Such a condition of inverted population is the same as a "double degenerated" semiconductor material (fig 2.2) which is characterised by two Fermi levels, E_fv and E_fc, inside the valence and conduction bands respectively, i.e. a hybrid between n- and p-type materials. Stimulated emission is only possible if the energy ($h\nu$) of an incoming photon satisfies the Bernard and Duraffourg condition [79]:

$$E_{gap} < h\nu < E_{fc} - E_{fv} \qquad (2-1)$$

The formation of such a "double degenerated" condition can be brought about by electron beam excitation or by optical pumping. But forward biasing a p-n junction can also create this inverted populations in the conduction band.

2.3 P-n junction (Homojunction) lasers

When p- and n-type semiconductor materials are fused together, the electrons in the conduction band of the n-type material will flow toward the p-type material trying to fill up any vacancies in the valence band. This flow of electrons will stop once the Fermi levels of either materials are matched with each other. Thus an equilibrium condition is reached and the resultant junction's characteristics can be calculated using the Poission's electric field equation with the appropriate boundary conditions [79]. When the junction is forward biased, the equilibrium in electron distribution is disrupted (fig 2.3) causing the Fermi level to split into two parts: one being inside the conduction band of the n-type material and the other within the valence band of the p-type material. Thus, the band structure becomes "double degenerated" as

Figures (2.3a), (2.3b), and (2.4) : The band structures of a p-n junction and, when it is forward-biased and of a forward-biased heterojunction laser respectively.

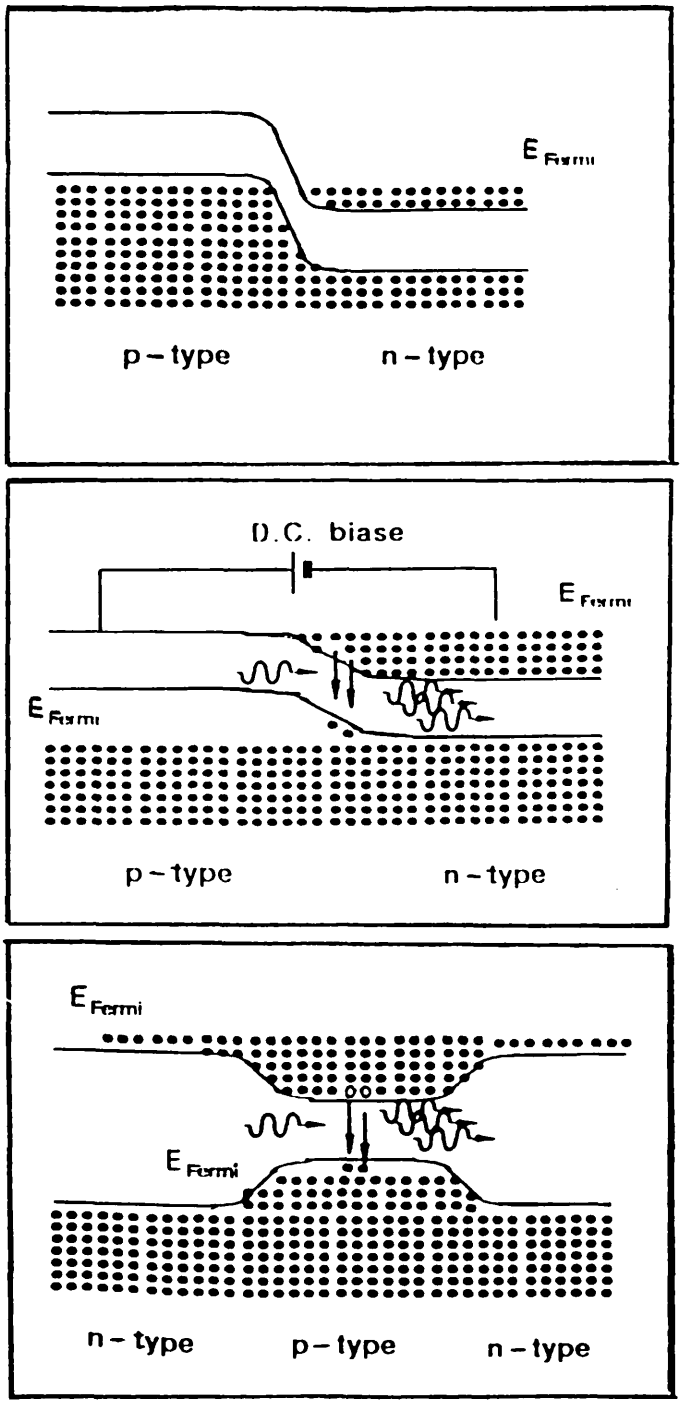

described earlier and stimulated recombinations are now possible within the junction. But as mentioned in the previous section, lasing also requires an optical resonator, which in the case of a semiconductor laser is formed by the cleaved facets in the crystal axis. Each facet has same normal incident reflectivity of 30% for a typical semiconductor material of refractive index equals to 3.5.

The earliest semiconductor lasers were made from GaAs materials and consisted of p-n junctions. These lasers were operated under pulsed condition at $77^{o}K$. Such critical operation conditions are due to the high losses by large electron carrier diffusion through the junction, and due to the poor optical confinement within the active layer. This led to the development of heterostructure lasers which have better carrier and optical confinement characteristics. Using this improved structure of reduced overall losses, continuous wave operation of semiconductor lasers at room temperature were brought into realisation in 1965.

2.4 Heterojunction lasers

A heterojunction (fig 2.4) is defined as the junction joining the two semiconductor materials of unequal band gaps. It was found that [105] by incorporating two heterojunction between GaAs and $Al_xGa_{1-x}As$, good carrier and optical confinement barriers can be set up within the active layer of GaAs. The carrier confinement is due to the "electron reservoir" formed by matching the unequal bandgaps of the claddings and the active layer. This reservoir confines the injected carriers which are used for recombinations with the "holes" in the valence band. Optical confinement is due to the higher refractive index of the active layer which acts as an optical waveguide and thus the propagation of light is confined within the active layer.

Since the invention of double heterostructure lasers, a tremendous amount of work has been carried out on a variety of band structures and material parameters so that the laser diodes can be tailored for particular applications. The desired characteristics of these applications can be grouped into:

(1) a narrow spectral output,

(2) with emission wavelengths at 1.3 and 1.55μm,

(3) a high frequency response,

(4) a high power output,

(5) a lower lasing threshold.

The discussion will now proceed onto the basic principles and operational characteristics of a variety of semiconductor lasers which were developed to meet these requirements.

2.5 Various types of semiconductor lasers

2.5a Narrow spectral output lasers

For the past several years, the design of novel semiconductor lasers, the work on highly sensitive detection systems, and the fabrication of low attenuation polarization-preserving optical fibres are all geared toward the commercialization of coherent optical transmission system which has the transmission capacity from 805 Mbits/s to 1.6 Gbits/s [17]. Submarine telecom. cables, terrestrial long-lines, and the subscriber loop are the potential area of use. To make such transmission system commercially viable, one of the important key requirements must be met. This is the narrow spectral linewidth emission from semiconductor lasers and the emission must be highly frequency stable because of the use of high frequency phase modulators.

The linewidth of a solitary semiconductor laser is about 100MHz which is very broad compared to the desired linewidth of a few KHz. The broadening in linewidth is assumed [72] to result from phase fluctuations of the laser field induced by two independent processes. One of which is the phase change caused directly by each spontaneous emission event $\delta\nu_\phi$ and the other is the change of the cavity resonance frequency due to a refractive index changes caused by the carrier density fluctuation $\delta\nu_N$. It has been shown that by feeding some of light back into the active region, these linewidth broadening factors $(\delta\nu_\phi, \delta\nu_N)$ can be suppressed. These factors are

proportional to the L^{-1} and L^{-2} respectively where L is the external cavity length (or the distance of an external reflector from the laser diode). Also, the linewidth reduction depends strongly on both the magnitude and the phase of the external optical feedback.

Using this technique, a spectral linewidth of 10KHz was achieved for 1.5μm InGaAsP lasers [94] using a diffraction grating of 1200 lines/mm as an external reflector. Other types of reflectors such as GRIN-ROD [47] and optical fibres [51] were used to reduce the spectral linewidth from semiconductor lasers. Various stabilisation schemes were developed [25,39,63] for maintaining the phase of external optical feedback. Although external cavity semiconductor lasers can generate very narrow linewidths, they are rather cumbersome, and various complicated optoelectronic devices are needed to control the phase and cavity stabilisations. Because of this, part of the development of coherent semiconductor lasers has been proceeded into an area where the linewidth reduction mechanism is introduced inside the laser structures. This gave birth to the cleaved-coupled-cavity (C^3), distributed-feedback (DFB) and distributed-Bragg-reflector (DBR) lasers.

A C^3 laser is basically two semiconductor lasers in tandem. The lasers are separated by about a few tens of micrometers. The two lasers are optically coupled but electrically, they are isolated from each other. The frequency selectivity results from the resonance condition that the light must form a standing wave pattern between each two reflecting surfaces. The spectral spacing of the dual cavity modes is significantly wider than either of the individual lasers' mode spacings and it is approximately given by [82]:

$$\Lambda \approx \frac{\lambda_o^2}{2|\Delta(n_{eff}L)|} \qquad (2-2)$$

where $\Delta(n_{eff}L)$ is the difference in cavity lengths of the two lasers.The frequency tunability is controlled by varying the bias currents to each lasers. This will change the refractive indices of the lasers and thus, altering the optical lengths of the laser cavities.

For a distributed-Bragg-reflector laser, the optical feedback is provided by two external Bragg reflectors instead of the cleaved facets. These reflectors are positioned outside the active region and their frequency selectivities depend on the Bragg wavelength and the depth of the corrugation [76,85]. In some respects, these DBR semiconductor lasers can be regarded as miniature versions of external cavity (grating) lasers.

The operational principle of a distributed feedback [71] (DFB) laser is similar to a DBR laser, in which an index corrugation pattern is introduced into the guiding layer. Within such a index pattern, part of the light is reflected back upon crossing each index step of the corrugation. Therefore, the feedback process is extended over the whole gain region or in other words, the feedback is distributed over the entire diode length. Resonance occurs when all distributed feedbacks are in phase. i.e. the lasing wavelength has to satisfy the Bragg condition.

2.5b 1.3 and 1.55μm lasers

Numerous lightwave communication systems have been installed throughout the world. Most of the systems ,installed to date, employing short-wavelengths (0.82-0.88μm) GaAlAs/GaAs lasers as light sources. However, longer-wavelength sources have been developed and are now being used in many new installations to take advantage of the lower losses and lower dispersion at λ=1.3 and 1.55μm respectively, in the present silica fibres.

At present, the semiconductor materials which have been widely used to emit at these wavelengths are In_{1-x}-Ga_x-As_y-P_{1-y} materials, where x and y are the material concentrations. The bandgap energy of this quarternary compound [62] can be approximated by:

$$E_g(y) = (1.35 - 0.72y + 0.12y^2)eV \qquad (2-3)$$

The widely used quarternary composition for emission at 1.3μm is $In_{0.74}$-$Ga_{0.26}$-$As_{0.6}$-$P_{0.4}$; whereas for 1.55μm devices, it is $In_{0.6}$-$Ga_{0.4}$-$As_{0.9}$-$P_{0.1}$. The x composition

parameter is to control the lattice matching of the active layer with the cladding materials.

Spectral dependence [21] of the optical gain for 1.3μm InGaAsP materials varies with the injected electron densities (n) and the peak gain increases with n. The threshold current density can be approximated by:

$$J_{th} = 2400\frac{d}{\eta} + 17.54\frac{d}{\eta\Gamma}\left[\alpha + \frac{1}{2L}Ln(R_1R_2)\right]\frac{d}{\eta\Gamma} \qquad (2-4)$$

where η is the internal quantum efficiency, d is the thickness of active layer, R's are the facet reflectivities, Γ is the optical confinement factor within the active guide, L is the diode length, and α is the net losses.

Unlike the GaAlAs lasers, the threshold currents of InGaAsP lasers are very sensitive to temperature. This imposes severe limitations for high-temperature operation.

2.5c High frequency response lasers

High frequency modulation is presently demanded in some specialised systems such as the laser-optical-fibre systems for synchronisation of air borne radar arrays [40] and will form the basis of future high-bit rate lightwave communication systems. For the D.H. III-V semiconductors, their practical direct-modulation bandwidths are within the lower gigahertz (1 to 2GHz) range regardless of their specific laser structures. But above this range, only the ones which are appropriately designed can be used.

The problems usually encountered in high-speed modulation are:

(1) the transient response (or relaxation oscillations) which causes a series of sharp optical spikes in response to a rapid increase of pumping. These oscillations will continue for some time before the light output settles to a steady state values. Thus, these highly irregular spikes can interfere with the bit pattern.

(2) the parasitic capacitance and inductance which are caused by the internal electrical parameters of the semiconductor lasers and by the external elements such as

the bonding wires and cables. The overall impedance due to these parasitic elements imposes an upper frequency limit.

The effect of parasitic elements on the modulation response can be [56] modelled by an equivalent circuit of the intrinsic laser diode which includes the conductivity of the substrate, the submount capacitance, and the band wire inductance. It appears that parasitic elements are not detrimental to high speed modulation for frequencies up to ≈4GHz. But beyond which, suitable electrode designs, and the use of semi-insulating substrates instead of the conventional conductive substrate are required to reduce these parasitics.

The transient response can be predicted from the spatially uniform rate equations [54]:

$$\frac{dn_e}{dt} = \frac{J}{ed} - \frac{n_e}{\tau_{sp}} - \frac{cg_oS}{\Gamma n_g} \qquad (2-5a)$$

$$\frac{dS}{dt} = \frac{\gamma D_o n_e}{\tau_{sp}} + \frac{c}{n_g}(g_o - \alpha)S \qquad (2-5b)$$

where g_o=$\Gamma n_g A(D_o n_e - n_o)/c$, Γ is the optical confinement factor, n_g is the group refractive index, $\tau_s p$ is the spontaneous electron lifetime, e is the electronic charge, J is the current density, c is the speed of light, d is the thickness of the active layer, A is the stimulated emission factor, n_o is the nominal electron density which determines the transparency of the active layer, D_o is the peak of the line shape function. The electron and photon densities are denoted as n_e and S respectively.

The intensities of the optical spikes are usually calculated using numerical methods since the rate equations cannot be analytically solved. However, the relaxation frequency can be approximated [53] using the small signal analysis:

$$\omega_r = \sqrt{\frac{1 + \Gamma A n_o \tau_{ph}}{\tau_{sp}\tau_{ph}}\left(\frac{J}{J_{th}} - 1\right)} \qquad (2-6)$$

where J_{th} is the threshold current density and τ_{ph} is the photon lifetime within the resonator.

In order to attain the highest modulation frequency, ω_r should be made as large as possible and this can be achieved by:

(1) operating the laser at higher currents but this will not be compatible with reliability, also the corresponding increase in optical power may cause catastrophic facet damage.

(2) designing new laser structures which have better internal parameters such as smaller τ_{ph} and τ_{sp}, or large A and n_o, but in doing so, it will simultaneously increase the lasing threshold. Thus, fundamentally speaking (in terms of increasing ω_r), the possible modulation frequencies can be pushed well into the X-band region, i.e.≈10GHz, or even higher but at the expense of increasing the threshold current and shortening the laser lifetime.

In order to reduce the necessary high lasing threshold and to alleviates the problem of catastrophic damage, smaller active volume and semi-insulating substrate should be employed. In addition, an extra window near the end facet is required. With these modifications, direct modulation and active mode-locking at frequencies up to 18GHz were demonstrated [3,24,46,83,84].

5.2d High output power lasers

Most c.w. semiconductor lasers to date can readily generate output power up to ten milliwatts. But beyond which, the optical damage on the facets can occur, also both the thermal effect around the active stripe, and the non-uniformity of the gain distribution along the active stripe will affect the performance in the high power region. Early types of high-power devices have concentrated on using wider stripes to increase the emission area and thus push up the facet damage threshold. The wide stripe also defines a larger active volume which is capable of providing a higher optical gain. With the wide stripe (≈30μm), peak optical power above 1 watts at pulsed pumping has been reported. However, the general problems encountered in the wide stripe lasers were:

(1) that the c.w. operation can no longer be maintained due to the corresponding increase in thermal effect and the only remedy would be to operate the lasers at lower temperature or to design better heatsinks.

(2) because of the large active volume, higher order lateral modes can be excited and oscillated in different wavelengths.

In order to discriminate the excitation of higher lateral modes, large optical cavity (LOC) has been used [10] which is to introduce between the active and cladding layers one or two extra layers with refractive index intermediate between those of the active and claddings. These additional layers are also called the "guiding" layers which allow a larger transverse spot size. Recently, the unstable resonator cavity [93] has been proposed for obtaining high power instead of the conventional parallel cleaved facets. With the improved lateral mode control, the quantum efficiencies can also be increased.

To date, the forerunner in the high power regime is the laser-array which is basically a multi-channel waveguide device and capable of generating output powers above 1 watt in c.w. operation before sustaining any facet damages. However, since each active stripe of the laser-array being so close to each other that the optical interference can occur between each propagating mode. This leads to the formations of several lateral modes (supermodes). These supermodes generally oscillate at different frequencies and their far-field patterns differ significantly from each other. Intensive work[16,42] has been carried out on improving the control on these supermodes. It was found that by phase-locking the laser-array, discrimination in supermodes could be possible and single supermode oscillation of a four-element, separate contact GaAlAs laser array has been reported[41].

2.5e Low threshold lasers

In most laser applications, it is an advantage to have a low threshold current density for reducing the energy dissipation, and for minimising the deleterious effects. In addition, the small threshold density gives a lower total operating current. The lasing threshold, as mentioned previously, is a point at which the optical gain balances with the net losses. Therefore, in order to achieve low lasing threshold, the net losses

must be reduced and the higher optical gain should be maintained, i.e. to increase the laser efficiency. The gain depends primarily on the electronic properties of the semiconductor, and also on the confinement factor, Γ. Whereas the losses are caused by:

(1) the spreading of carrier density before it reaches the active region.

(2) the cavity losses which are determined by the facet reflectivities and the length.

(3) the presence of the electron traps which are introduced into the active region and in the adjacent cladding layers during the growth of the wafer.

To improve the quality of the laser material, various fabrication techniques such as the two-phase solution growth[100], Low-pressure metalorganic chemical vapour deposition (LP-MOCVD)[99] have been developed which minimise the amount of defects within each layers. Additional current-blocking elements such as the reversed biased n-p-n buried infil structure[68] have been used to reduce the amount of leakage current and hence localise the injected carrier density within the active stripe. Optical confinement can also be improved by using the crescent-shaped active cross-section instead of the conventional rectangular cross-section.

To date, various types of low-threshold InGaAsP diode lasers have been developed. These are the: (1) buried heterostructure (B.H.)[101],

(2) planar buried heterostructure (P.B.H.)[103],

(3) double channel planar buried heterostructure[104] (D.C.B.H.),

(4) V-groove substrate buried heterostructure (V.S.B.H.)[102],

(5) buried crescent (B.C.)[67],

(6) Buried infill structure[68],

(7) V-channel substrate inner-stripe (V.S.I.S.)[98] lasers.

Among them the buried crescent and buried heterostructure laser diodes are the most promising due to their additional superior characteristics, such as the stable fundamental transverse mode oscillation and the c.w. operation at an elevated tem-

perature. The typical lasing threshold currents of these lasers are around 15 to 20 mA.

2.6 Conclusion

In this chapter, the basic principles of the lasing properties of semiconductor lasers have been described in the context of valence- and conduction-band structures and based on which, both the homojunction (p-n) and heterostructure lasers were discussed. For the heterostructure, because of its good optical and carrier confinements, it has formed the basis of all semiconductor lasers to date.

A variety of well known semiconductor lasers were briefly described. They were grouped into five categories of different applications, namely the:

(1) lasers with narrow linewidth output which are of potential light sources in the coherent communication systems.

(2) lasers emitting at the spectral window of to date's optical silica fibres.

(3) lasers capable of operating within the X-band or even higher modulation frequencies.

(4) high output power devices in area where high power is the primary requirement such as in the study of semiconductor soliton lasers.

(5) the lasers which have low lasing threshold currents.

Emphasis was placed on the basic operating principles, on the problems involved, and on how to improve the required performance that has led to the development of to date's semiconductor lasers. However, due to the new requirements and some foreseeable important applications, the search for better and novel devices are still continuing and although, in some area where the obstacles may seem to be insuperable; the continuing new discoveries in other areas of science and engineering may well, one day, overcome these seemingly impossibilities.

CHAPTER THREE

Interferometric study on composite cavity (axial)modes

3.1 Introduction

Referring to figure (3.1), for a two-mirror (Fabry-Perot) cavity, the possible lasing wavelengths (or the axial modes) extend to infinity in either direction and the mode separation is given as $c/2nL$ or $\lambda^2/2nL$, where nL is the optical cavity length. It is generally assumed that when an extra mirror is added to the cavity, there will still be a continuous band of possible lasing wavelengths but with the mode separation determined by the composite cavity length, i.e. $c/2(n_1L_1 + n_2L_2)$. In addition, this continuous lasing band will be subjected to another modulation caused by the subcavity effect. However, it was found using the following analysis that this is not always true and the formation of modes in a composite cavity depends strongly on the mirror reflectivities. In addition, a lasing-mode may not necessary form nodes at the mirrors.

The analysis is based on the interferometric equation which describes the net light output due to the multiple beam interference between reflected waves. The derivation starts on a simple two-mirror (Fabry-Perot) cavity and it is then progressed onto the composite cavities consisting of three and four mirrors. Throughout the

Figures (3.1a) and (3.1b) : The lasing bands of Fabry-Perot and composite cavity lasers respectively.

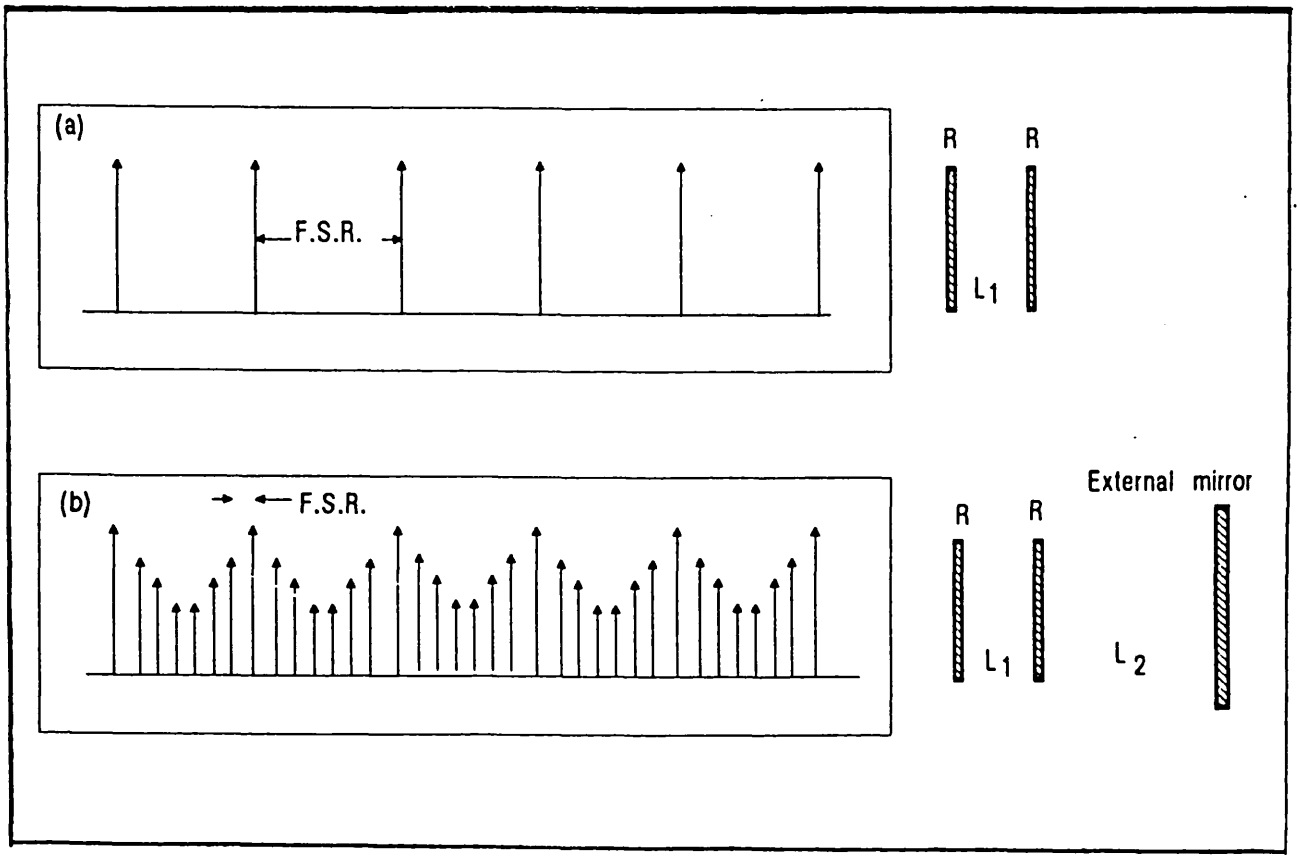

entire mathematical derivation, the mirror reflectivities r's are expressed as $\overleftarrow{r}$ or $\overrightarrow{r}$, where the arrows indicate the direction of the reflected waves at the mirrors. All the previous theoretical studies [115,116] on interferometric lasing modes of the composite cavity have neglected this dual parity in mirror reflectivity. As it will be shown in this chapter such a parity can greatly affect the lasing-wavelengths equation.

3.2 Fabry-Perot (two mirror) cavities

3.2a Multiple beams interference

Considering the system depicted in figure (3.2). The absolute amplitude reflectivities of the mirrors are denoted by r_1 and r_2 and their corresponding power reflectivities are R_1 and R_2 respectively. The sum of all the reflections to the right and to the left are given by:

$$\overleftarrow{r}_{sum} = \overleftarrow{r}_1 + \frac{t_1^2 \overleftarrow{r}_2 e^{-2\Gamma L}}{(1 - \overrightarrow{r}_1 \overleftarrow{r}_2 e^{-2\Gamma L})} \qquad (3-1)$$

$$\overrightarrow{r}_{sum} = \overrightarrow{r}_2 + \frac{t_2^2 \overrightarrow{r}_1 e^{-2\Gamma L}}{(1 - \overrightarrow{r}_1 \overleftarrow{r}_2 e^{-2\Gamma L})} \qquad (3-2)$$

and the transmission is found to be independent of direction and it is given by:

$$\overleftarrow{t}_{sum} = \overrightarrow{t}_{sum} = \frac{t_1 t_2 e^{-\Gamma L}}{(1 - \overrightarrow{r}_1 \overleftarrow{r}_2 e^{-2\Gamma L})} \qquad (3-3)$$

The relationship between $\overleftarrow{r}_i$'s and $\overrightarrow{r}_i$'s is defined as:

$$-\overrightarrow{r}_i = \overleftarrow{r}_i \qquad (3-4)$$

The negative sign is because of a phase shift of π when light reflects from a less dense medium. Due to this "odd" parity in mirror reflectivity, the equation representing the sum of reflectivity (R_{sum}) can take on other forms beside that in equations 3-1 and 3-2. In order to generalise these set of possible equations into just a single consistent equation, two boundary conditions are taken in this analysis. The first boundary condition is defined as: for every term that contains a pair, or multiple of pairs of reflectivities r_i's, each pair must be "directionless". i.e. each r_i within a pair must

Figure (3.2) : Multiple beams interference of a Fabry-Perot cavity laser.

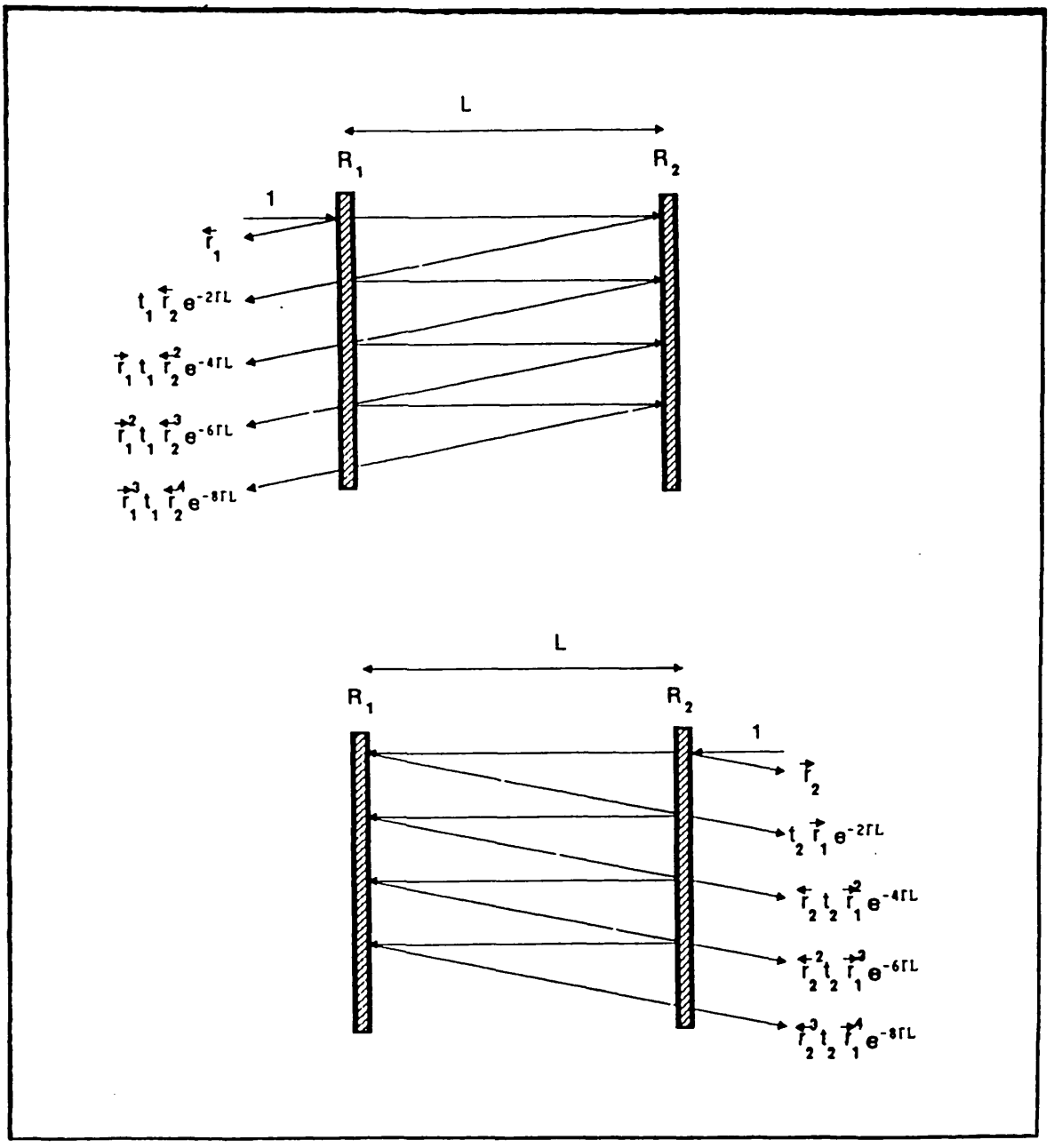

have an opposite direction to its partner. For example, if A $=\overleftarrow{r}_1\overleftarrow{r}_2$, then according to the boundary condition of "directionless", A has to be expressed as $-\overleftarrow{r}_1\overrightarrow{r}_2$ or $-\overrightarrow{r}_1\overleftarrow{r}_2$.

The second boundary condition is that the reflectivities of the two outermost mirrors must be taken as if they were seen by an observer. i.e. referring to figure (3.1), the reflectivities of the outermost mirrors must be taken as $\overleftarrow{r}_1$ and $\overrightarrow{r}_2$.

Applying these conditions to equations 3-1 and 3-2, the net reflectivities are given as:

$$\overleftarrow{r}_{sum} = \frac{\overleftarrow{r}_1 - \overrightarrow{r}_2 e^{-2\Gamma L}}{(1 - \overleftarrow{r}_1\overrightarrow{r}_2 e^{-2\Gamma L})} \qquad (3-5)$$

$$\overrightarrow{r}_{sum} = \frac{\overrightarrow{r}_2 - \overleftarrow{r}_1 e^{-2\Gamma L}}{(1 - \overleftarrow{r}_1\overrightarrow{r}_2 e^{-2\Gamma L})} \qquad (3-6)$$

The power reflectivity is defined as the square modulus of the amplitude reflectivities. i.e. $R_{sum} = |r_{sum}|^2$ and similarly power transmissivity is defined as $T_{sum} = |t_{sum}|^2$. If the enclosed medium is gain-free, i.e. the system is a passive cavity, then the propagation constant Γ is given as $2\pi n/\lambda$. Thus, the power reflectivity then becomes directionally independent:

$$\overrightarrow{R}_{sum} = \overleftarrow{R}_{sum} = \frac{R_1 + R_2 - 2\sqrt{R_1 R_2}\cos 4\pi nL/\lambda}{1 + R_1 R_2 - 2\sqrt{R_1 R_2}\cos 4\pi nL/\lambda} \qquad (3-7)$$

Suppose that the enclosed medium has a single pass gain denoted by g, then the propagation constant is represented by $2\pi n/\lambda$ - g/2 and the reflectivities will become directionally dependent which are given as:

$$\overleftarrow{R}_{sum} = \frac{R_1 + g^2 R_2 - 2g\sqrt{R_1 R_2}\cos 4\pi nL/\lambda}{(1 + g^2 R_1 R_2 - 2g\sqrt{R_1 R_2}\cos 4\pi nL/\lambda)} \qquad (3-8)$$

$$\overrightarrow{R}_{sum} = \frac{R_2 + g^2 R_1 - 2g\sqrt{R_1 R_2}\cos 4\pi nL/\lambda}{(1 + g^2 R_1 R_2 - 2g\sqrt{R_1 R_2}\cos 4\pi nL/\lambda)} \qquad (3-9)$$

but the power transmission is found to be always directionally independent despite of whether the cavity is active or passive:

$$\overleftarrow{T}_{sum} = \overrightarrow{T}_{sum} = \frac{gT_1 T_2}{1 + g^2 R_1 R_2 - 2g\sqrt{R_1 R_2}\cos 4\pi nL/\lambda} \qquad (3-10)$$

For a passive cavity, the sum of power transmissions and reflections always equals to 1, i.e. (R+T=1). But in the case of active cavity, this conservation becomes invalid because of the extra amount of light being generated inside the gain medium.

3.2b Lasing-wavelengths equation

For a Fabry-Perot semiconductor laser, the lasing wavelength depends primarily on the bandgap of the active medium, the injected carrier density, and on the spectral window of the laser cavity which is the main objective of this chapter. Theoretically, the lasing condition defined as the transmitted light through an active cavity grows to an infinite amount. i.e. the denominator of equation 3-10 becomes zero. Thus, the lasing condition is defined as:

$$0 = (1 + g^2 R_1 R_2 - 2g\sqrt{R_1 R_2}\cos 4\pi nL/\lambda) \qquad (3-11)$$

or

$$0 = (1 - \vec{g}\overleftarrow{r}_1\vec{r}_2 e^{4\pi nL/\lambda}) \qquad (3-12)$$

The possible lasing wavelengths from a semiconductor laser or any two-mirror laser resonator can be found by solving either one of these "lasing-wavelength" equations.

3.2c Description of the numerical analysis

Equation 3-12 contains both real and imaginary parts. The real part has two terms of which, the first term is unity. The second term is the difference in intensities of any two consecutive reflected beams. For lasing to occur, a beam must not be attenuated after a transit through the active cavity, i.e. the second term is equal to unity, and this leads to the real part becoming zero. Therefore, the real part represents only the changes in intensities of the multiple reflected beams. The imaginary part, on the other hand, represents the phase changes in the light beam after a single transit through the cavity and at lasing, this phase change should be zero. In the case of a two-mirror cavity, this means the standing-waves are being formed within the cavity. However, as will be shown later on, in the cases of composite cavities, this zero-phase

condition may not necessary correspond to the standing-wave patterns between the mirrors.

In order to find the solutions to equation 3-12, the real and imaginary parts have to be solved simultaneously. This implies that at a lasing-wavelength the transmission through the gain medium must be infinitely large and the phase change per transit is zero. Other wavelengths which only satisfy just one of these parts cannot be the lasing wavelengths.

Because of the periodicity nature of equation 3-12, there will be more than one solution. These multiple solutions represent a set of possible axial modes of the active cavity. The amplitude of each mode can be expressed in terms of the amount of gain required to overcome the cavity losses, i.e. the "cavity-modal" gain or the degree of "cavity-transparency" at each lasing mode.

The gain, g, can be derived by solving the real and imaginary parts of equation 3-12 and it is expressed as:

$$g = \frac{1}{|r_1 r_2| \cos(4\pi n L/\lambda)} \qquad (3-13a)$$

The corresponding phase equation is expressed as:

$$Phase = -g\sqrt{R_1 R_2} \sin(4\pi n L/\lambda) \qquad (3-13b)$$

The R.H.S. of the equation 3-13a represents the "cavity" losses at the possible lasing-wavelengths and the L.H.S. is the amount of gain required in the active medium in order to overcome the "cavity" losses. Figure (3.6a) shows the computed results of equations 3-13a and 3-13b. The possible lasing-wavelengths can be found by comparing the two curves so that at the lasing-wavelengths, the "phase" curve must be zero and the "gain" curve must be positive. It was found, as expected, that a mode only exists when an integral number of its half wavelengths equals the cavity length ($n\lambda/2 = L$), this also means that the cosine terms, $\cos(4\pi n L/\lambda)$, will always be 1 for every mode and thus, the "cavity" modal gain is constant over all axial modes. Because the "material" gain dependence has been neglected in the analysis,

the axial modes are thus represented as Dirac delta-functions and their amplitudes are expressed in terms of the "cavity" modal losses.

3.3 Composite (three- and four-mirror) cavities

3.3a Cavity reduction scheme

The mathematical derivation of a three mirror cavity would be much simpler if any two of the mirrors are reduced to a single effective reflector of reflectivity r_{eff} and thus transforming the three-mirror cavity into a two-mirror (Fabry-Perot) cavity. Referring to figure (3.3), such transformation does not alter the physical nature of the system. Since every beam which is incident onto the mirror r_2 will subsequently undergo multiple reflections within mirrors r_2 and r_3; and the net reflection back to r_1 is given by r_{eff}. Thus, the number of multiple reflections will remain unchanged regardless of whether it is a composite cavity of mirrors r_1, r_2, r_3, or a F.P. cavity of mirrors r_1, r_{eff}.

Using the results which were derived previously for the Fabry-Perot cavity, the field transmission of a reduced three-mirror system is given by:

$$\overleftarrow{t}_{123} = \overrightarrow{t}_{123} = \frac{t_1 t_{eff} e^{-\gamma l}}{(1 - \overrightarrow{r}_1 \overleftarrow{r}_{eff} e^{-2\gamma l})} \qquad (3-14)$$

Substitute t_{eff} with t_2 and t_3; r_{eff} with r_2 and r_3, and apply the boundary conditions to equation 3.13, the field transmission then becomes:

$$t_{123} = \frac{t_1 t_2 t_3 e^{-(\Gamma L + \gamma l)}}{1 - \overleftarrow{r}_2 \overrightarrow{r}_3 e^{-2\Gamma L} - \overleftarrow{r}_1 \overrightarrow{r}_2 e^{-2\gamma l} - \overleftarrow{r}_1 \overrightarrow{r}_3 e^{-2(\Gamma L + \gamma l)}} \qquad (3-15)$$

It is noted that the equation is symmetrical with the mirror image of the system, i.e. if mirrors r_1 and r_3 were to be replaced by each other, the above equation will still be unchanged. If one of the mirrors is reduced to zero reflectivity, equation 3-14 will reduce itself back to a Fabry-Perot equation. Buus and Adams[115] also derived a similar equation, but the equation has an asymmetry in the mirror reflectivities. This is because they have not imposed any conditions for the generalisation and without these conditions, a branch of equations is possible and the consistency is lost.

Figure (3.3) : Cavity reduction scheme.

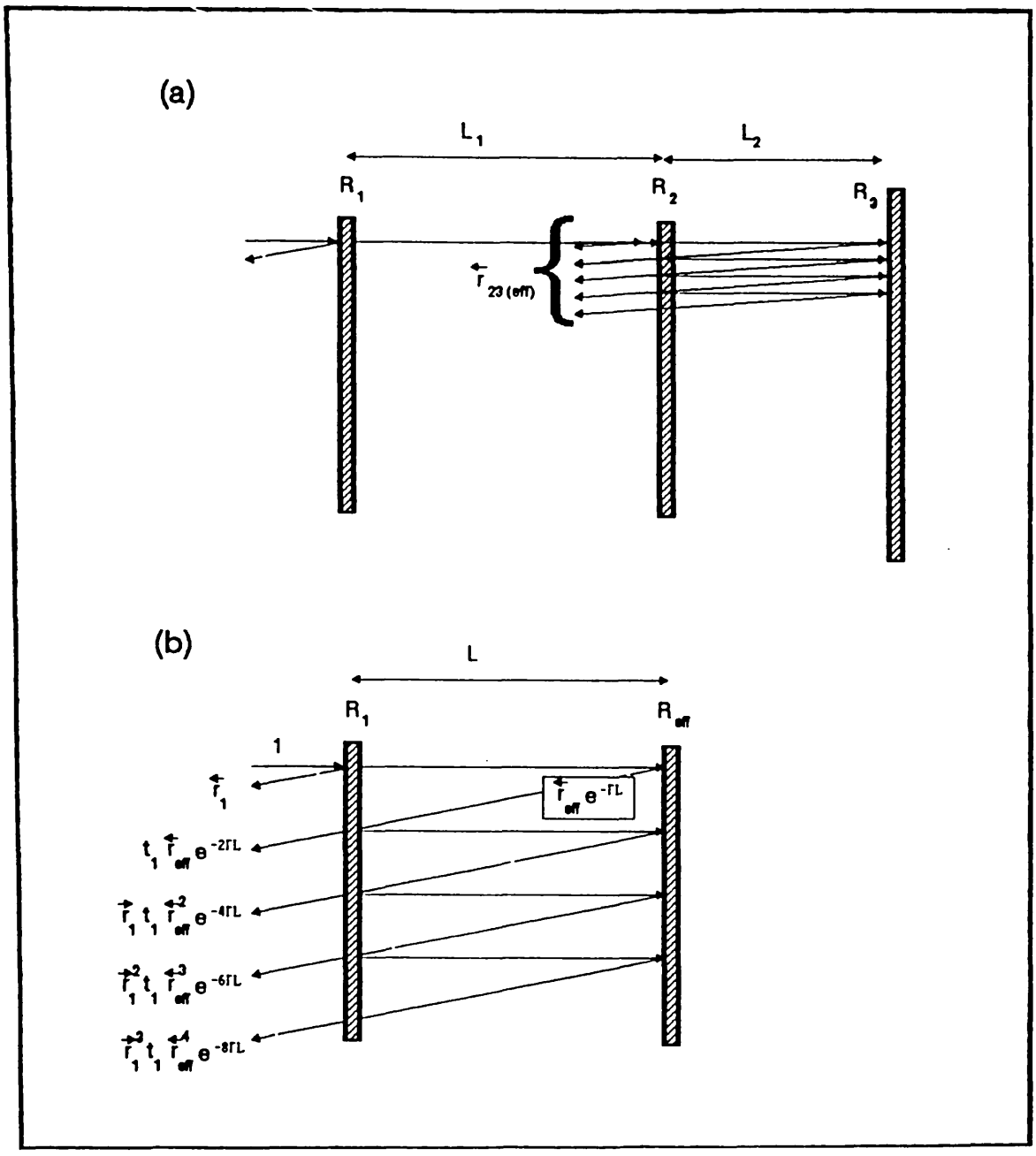

For an active cavity, the transmission is given by:

$$t_{123} = \frac{t_1 t_2 t_3 \sqrt{g_1 g_2}\, e^{\frac{-2\pi(n_1 L + n_2 l)}{\lambda}}}{1 - \overleftarrow{r}_2 g_1 \overrightarrow{r}_3 e^{\frac{-4\pi n_1 L}{\lambda}} - \overleftarrow{r}_1 g_2 \overrightarrow{r}_2 e^{\frac{-4\pi n_2 l}{\lambda}} - \overleftarrow{r}_1 g_1 g_2 \overrightarrow{r}_3 e^{\frac{-4\pi(n_1 L + n_2 l)}{\lambda}}} \qquad (3-16)$$

and the power transmission is :

$$T_{123} = \frac{T_1 T_2 T_3 g_1 g_2 \cos\frac{2\pi(n_1 L + n_2 l)}{\lambda}}{D_{123}} \qquad (3-17)$$

where

$$\begin{aligned} D_{123} = 1 &+ R_2 R_3 g_2^2 + R_1 R_2 g_1^2 + R_1 R_3 (g_1 g_2)^2 \\ &- 2\sqrt{R_2 R_3} g_2 \cos\frac{4\pi n_1 L}{\lambda} \\ &- 2\sqrt{R_1 R_2} g_1 \cos\frac{4\pi n_2 l}{\lambda} \\ &- 2\sqrt{R_1 R_3} g_1 g_2 \cos\frac{4\pi(n_1 L + n_2 l)}{\lambda} \\ &+ 2\sqrt{R_1 R_3} R_2 g_1 g_2 \cos\frac{4\pi(n_1 L - n_2 l)}{\lambda} \\ &+ 2\sqrt{R_1 R_2} R_3 g_1 g_2^2 \cos\frac{4\pi n_2 l}{\lambda} \\ &+ 2\sqrt{R_2 R_3} R_1 g_1^2 g_2 \cos\frac{4\pi n_1 L}{\lambda} \end{aligned}$$

The above equation can also be applied to a passive cavity by taking g_1 and g_2 equal to 1.

The polarity (i.e. positive or negative) of the cosine terms in the denominator has an significant effect on the formation of the standing waves. Considering "negative" cosine term, say, $-2\sqrt{R_2 R_3} g_2 \cos(4\pi n_1 L/\lambda)$, the maximum transmission will occur whenever $\cos(4\pi n_1 L/\lambda)$ equals 1 and this leads to a free spectral range (F.S.R) of $\Delta\nu = c/2L$ or $\Delta\lambda = \lambda^2/2L$ and this corresponds to the formation of "pure" standing waves, i.e. $m\lambda/2 = L$. Thus, the "negative" terms in the above denominator can be visualised as the intensity modulations which correspond to these "$\lambda/2$" standing waves enclosed within the cavities of $n_1 L$, $n_2 l$, and $(n_1 L + n_2 l)$. i.e. nodes are being formed at either end of these cavities.

A "positive" cosine term on the other hand will cause a maximum transmission when the cosine is negative and its corresponding F.S.R. is $\Delta\nu = c/4L$ or $\Delta\lambda = \lambda^2/4L$

Figure (3.4) : Various ways of reducing a composite cavity into Fabry-Perot cavity.

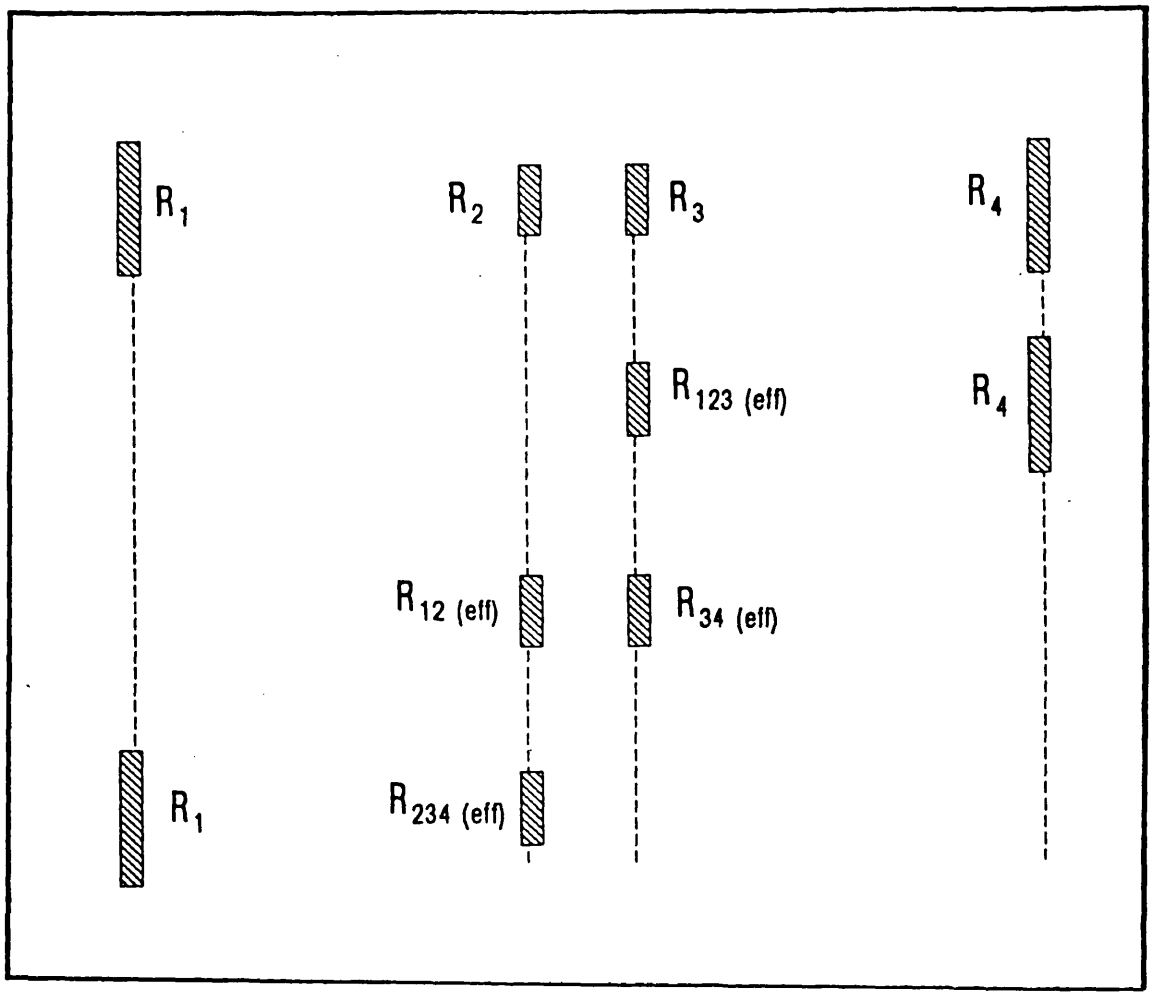

and that the waves which are enclosed within the cavity must satisfy $m\lambda/4 = L$, i.e. the "positive" cosine terms correspond to a mixture of standing waves and "non-resonant" waves. The former type of waves have nodes at either end of a cavity. But the latter type has a node at one end of the cavity and an anti-node at the other. Thus, the "positive" cosine terms of the above equation represent the intensity modulations caused by these mixture of "resonant" and "non-resonant" waves within the cavities of $(n_1L - n_2l)$, n_2l, and n_1L respectively. Thus, the excitations of the possible lasing wavelengths of a composite cavity are not as straight forward as it seems.

For the four-mirror cavity, the cavity reduction scheme can also be used. Figure (3.4) shows the various ways of reducing such system to a two-mirror (Fabry-Perot) cavity of mirrors ${}_1r_{eff}$ and ${}_2r_{eff}$. Using equation 3-3, the field transmission is given as:

$$t_{1234} = \frac{t_{12_{eff}} t_{34_{eff}} e^{-\Gamma L}}{(1 - \overleftarrow{r}_{12_{eff}} \overrightarrow{r}_{34_{eff}} e^{-2\Gamma L})} \qquad (3-18)$$

Replacing all the effective transmissivities and reflectivities with the fundamental parameters r'$_i$s and t'$_i$s using equation 3-3. The transmission becomes :

$$t_{1234} = \frac{t_1 t_2 t_3 t_4 e^{-\gamma l + \Gamma L + \beta k}}{\sqrt{D_{1234}}} \qquad (3-19)$$

where

$$\begin{aligned} D_{1234} = 1 &- \overleftarrow{r}_1 \overrightarrow{r}_2 e^{-2\gamma l} - \overleftarrow{r}_3 \overrightarrow{r}_4 e^{-2\beta k} - \overleftarrow{r}_2 \overrightarrow{r}_3 e^{-2\Gamma L} \\ &- \overleftarrow{r}_1 \overrightarrow{r}_3 e^{-2(\gamma l + \Gamma L)} - \overleftarrow{r}_2 \overrightarrow{r}_4 e^{-2(\Gamma L + \beta k)} \\ &+ \overleftarrow{r}_1 \overrightarrow{r}_2 \overleftarrow{r}_3 \overrightarrow{r}_4 e^{-2(\gamma l + \beta k)} \end{aligned}$$

It was found that if the reduction is carried out in any other way, same transmission equation will be obtained. The above equation is different from that derived by Van de Stadt and Muller[116] who used the thin film matrix calculations based on the travelling wave analysis. Their physical model only considered individual plane mirrors separated by media of the same refractive index on either side and this resulted the identical signs to every reflection coefficients. This made all the cosine terms in the

denominator of their transmission equations having positive signs even for a Fabry-Perot cavity which is usually given with minus signs. This also explains why they did not find the resonance at kπ; but at (2k+1)$\pi/2$. Because their equations only apply to composite cavity with the same refractive indices, they cannot be used to calculate the lasing wavelength of a semiconductor external cavity laser. The present analysis offers a generalised interferometric description to both passive and active composite cavities.

From equation 3-19, it can be found that the power transmission is given by:

$$T_{1234} = \frac{T_1 T_2 T_3 T_4 g_1 g_2 g_3}{D_{1234}} \qquad (3-20)$$

where

$$\begin{aligned} D_{1234} = 1 &+ g_1^2 R_1 R_2 + g_3^2 R_2 R_3 + g_1^2 g_2^2 R_1 R_3 + g_1^2 g_3^2 R_2 R_4 \\ &+ g_1^2 g_2^2 g_3^2 R_1 R_4 + g_1^2 g_4^2 R_1 R_2 R_3 R_4 \\ &- 2C_1 \cos(2\Gamma L) \\ &- 2C_2 \cos(2\gamma l) \\ &- 2C_3 \cos(2\beta k) \\ &- 2C_4 \cos 2(\gamma l + \Gamma L) \\ &- 2C_5 \cos 2(\Gamma L + \beta k) \\ &- 2C_6 \cos 2(\gamma l + \beta k) \\ &- 2C_7 \cos 2(\gamma l - \Gamma L) \\ &- 2C_8 \cos 2(\gamma l - \beta k) \\ &- 2C_9 \cos 2(\beta k - \Gamma L) \\ &- 2C_{10} \cos 2(\gamma l - \Gamma L - \beta k) \\ &- 2C_{11} \cos 2(\Gamma L - \beta k - \gamma l) \\ &- 2C_{12} \cos 2(\beta k - \gamma l - \Gamma L) \\ &- 2C_{13} \cos 2(\gamma l + \Gamma L + \beta k) \end{aligned}$$

where

$$C_1 = +g_2\sqrt{R_2R_3} - g_1g_3^2\sqrt{R_2R_3R_4^2} - g_1^2g_2\sqrt{R_1^2R_2R_3} + g_1^2g_2g_3^2\sqrt{R_1^2R_2R_3R_4^2}$$

$$C_2 = +g_1\sqrt{R_1R_2} + g_1g_3^2\sqrt{R_1R_2R_3^2R_4^2} - g_1g_2^2\sqrt{R_1R_2R_3^2} - g_1g_2^2g_3^2\sqrt{R_1R_2R_4^2}$$

$$C_3 = +g_3\sqrt{R_3R_4} + g_1^2g_3\sqrt{R_1^2R_2^2R_3R_4} - g_2^2g_3\sqrt{R_2^2R_3R_4} - g_1^2g_2^2g_3\sqrt{R_1^1R_3R_4}$$

$$C_4 = +g_1g_2\sqrt{R_1R_3} - g_1g_2g_3^2\sqrt{R_1R_3R_4^2}$$

$$C_5 = -g_2g_3\sqrt{R_2R_4} - g_1^2g_2g_3\sqrt{R_1^1R_2R_4}$$

$$C_6 = -g_1g_3\sqrt{R_1R_2R_3R_4} - g_1g_2^2g_3\sqrt{R_1R_2R_3R_4}$$

$$C_7 = -g_1g_3\sqrt{R_1R_2R_3R_4} - g_1g_2^2g_3\sqrt{R_1R_2R_3R_4}$$

$$C_8 = -g_1g_2\sqrt{R_1R_2^2R_3} + g_1g_2g_3^2\sqrt{R_1^2R_2R_3R_4^2}$$

$$C_9 = -g_2g_3\sqrt{R_2R_3^2R_4} + g_1^2g_2g_3\sqrt{R_1^2R_2R_3^2R_4}$$

$$C_{10} = -g_1g_2g_3\sqrt{R_1R_2^2R_4}$$

$$C_{11} = +g_1g_2g_3\sqrt{R_1R_2^2R_3^2R_4}$$

$$C_{12} = -g_1g_2g_3\sqrt{R_1R_3^2R_4}$$

$$C_{13} = +g_1g_2g_3\sqrt{R_1R_4}$$

As before the lasing wavelength can be calculated by solving denominator $\sqrt{D_{1234}}$ and for a passive cavity, all the gain coefficients g_i's can be taken as equal to 1.

The four-mirror cavity equation contains 13 cosine terms caused by the various possible combinations of the subcavities L, l, and k. Among all the coefficients, six of them: C_1, C_2, C_3, C_4, C_8, and C_9; have a mixture of positive and negative values. This means that the pure resonant waves and the hybrid resonant/non-resonant waves are competing with each other in these seven cavity configurations. There are five coefficients, C_5, C_6, C_7, C_{11}, and C_{12}; are purely negative and thus they correspond only to the hybrid waves. The other two coefficients, C_{11}, and C_{13}; are purely positive and thus correspond to the pure resonant waves. Therefore, for a four-mirror

Figure (3.5) : A family of solutions to the four-mirror cavity.

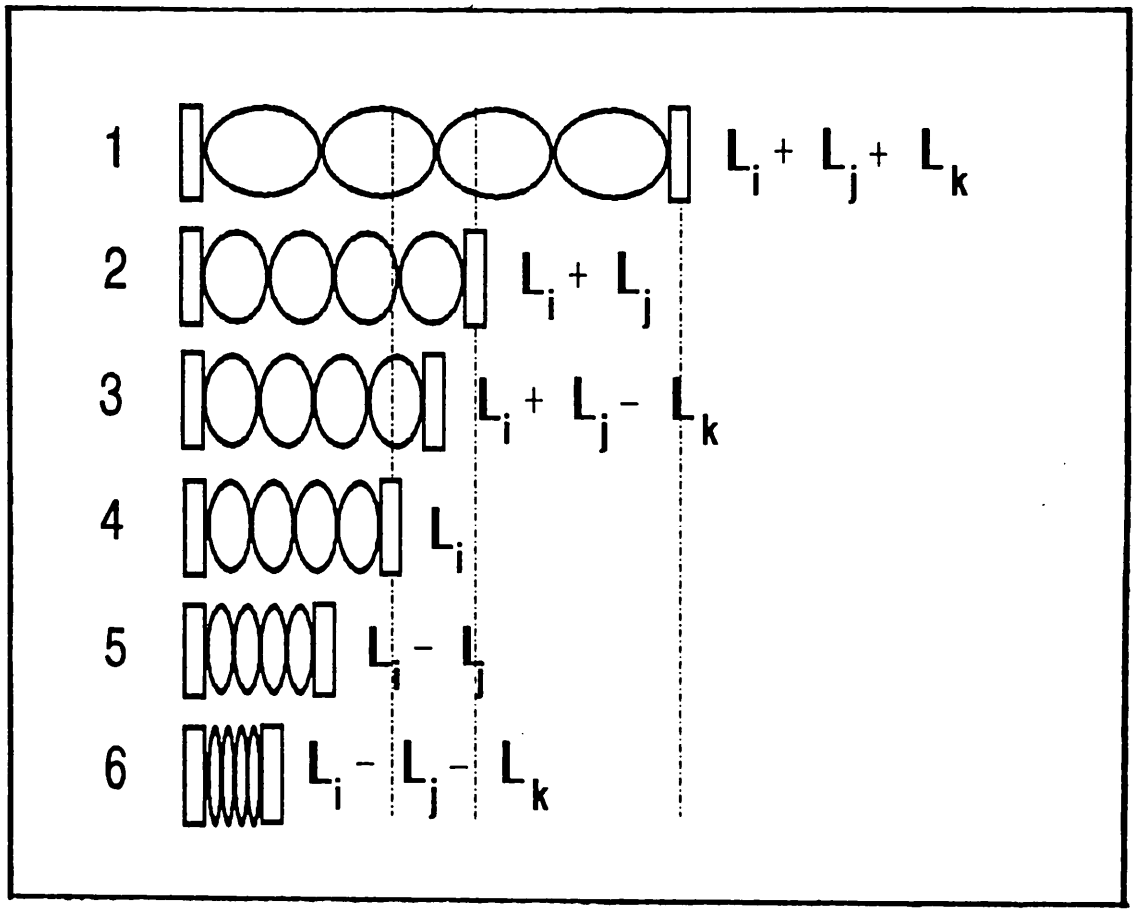

resonator, there could exist a variety of both "resonant" and "non-resonant" waves depending on the combinations of the subcavities.

Figure (3.5) shows a family of resonant waves formed inside various cavity configurations and there are six types of resonant waves in the four-mirror cavity and three types in the three-mirror cavity and as expected, only one type of resonant waves in the two-mirror cavity. For the four-mirror cavity, the third and sixth sets are identical to each other. This is because $\cos(-L_i + L_j + L_k) = \cos(L_i - L_j - L_k)$ and thus basically, there should only be five types of resonant waves. In the case of subtracting the subcavities, the resonant waves are bounded by the mirrors M_i and M_* where M_i is any one of the mirrors and M_* is a virtual mirror of reflectivity determined by the rest of the mirrors. The subcavity subtraction arises from the cross-multiplications in converting the amplitude transmission into intensity transmission.

3.3b Lasing-wavelength equations

For the three-mirror cavity, the lasing condition is defined as when t_{123} becomes infinite and the lasing wavelength can be found by solving denominator of equation 3-14 which equals zero. The real and imaginary parts of the denominator are separated and both are set to zero:

$$0 = 1 - \overleftarrow{r}_2 g_1 \overrightarrow{r}_3 \cos\Phi_1 - \overleftarrow{r}_1 g_2 \overrightarrow{r}_2 \cos\Phi_2 - \overleftarrow{r}_1 g_1 g_2 \overrightarrow{r}_3 \cos(\Phi_1 + \Phi_2) \qquad (3-21a)$$

$$0 = \overleftarrow{r}_2 g_1 \overrightarrow{r}_3 \sin\Phi_1 + \overleftarrow{r}_1 g_2 \overrightarrow{r}_2 \sin\Phi_2 + \overleftarrow{r}_1 g_1 g_2 \overrightarrow{r}_3 \sin(\Phi_1 + \Phi_2) \qquad (3-21b)$$

Using these two equations and let g_2=0, i.e. passive cavity, the threshold gain of the three-mirror cavity can be expressed as:

$$g = \frac{1 - r_1 r_2 \cos(2\Phi_1)}{r_2 r_3 \cos(2\Phi_2) + r_1 r_2 \cos(\Phi_1 + \Phi_2)} \qquad (3-22)$$

For the four-mirror cavity, the same procedure can be applied and by assuming g_1=g_3=1, the phase and gain equations can be expressed as:

$$g = \frac{1 - r_1 r_2 \cos 2\Phi_1 - r_3 r_4 \cos 2\Phi_2 + r_1 r_2 r_3 r_4 \cos 2(\Phi_1 + \Phi_3)}{(r_2 r_3 \cos 2\Phi_2 + r_1 r_3 \cos 2(\Phi_1 + \Phi_2) + r_2 r_4 \cos 2(\Phi_2 + \Phi_3) +}$$

$$r_1 r_4 \cos 2(\Phi_1 + \Phi_2 + \Phi_3)) \qquad (3-23a)$$

and

$$\begin{aligned} 0 = & -r_1 r_2 \sin 2\Phi_1 - r_3 r_4 \sin 2\Phi_3 - g r_2 r_3 \sin 2\Phi_2 \\ & - g r_1 r_3 \sin 2(\Phi_1 + \Phi_2) - g r_2 r_4 \sin 2(\Phi_2 + \Phi_3) \\ & - g r_1 r_4 \sin 2(\Phi_1 + \Phi_2 + \Phi_3) + r_1 r_2 r_3 r_4 \sin 2(\Phi_1 + \Phi_3) \qquad (3-23b) \end{aligned}$$

It can be shown that the above equations can convert to a fundamental two-mirror cavity by taking the reflectivities of the unwanted mirrors to zero.

3.3c Computed lasing-modes

Three different cases were investigated, of which two were the three-mirror cavities and one was a four-mirror cavity. The smallest cavity length of 250μm-typical length of a laser diode, was chosen. Initially, a 50cm long cavity was chosen but in order to maintain the computational accuracy, a shorter length of 5cm was used instead.

1. Three-mirror cavity (R_1 is variable, $R_2 = R_3$ =0.3, L_{12}=5cm, L_{23}=250μm):

Figure (3.6) shows a set of graphs representing the gain, phase, and the lasing modes, for various R_1's, i.e. varying the amount of external feedback. For R_1=0, the phase curve only crosses the x-axis once so that there is only one mode being excited within a F.S.R. of the laser diode. For R_1 greater than zero, ringings appear in both the phase and gain curves. The periodicity of these ringings corresponds to the F.S.R. of the composite cavity. Despite of these ringings, the phase curve still has one intersection point with the x-axis if R_1 is below 0.0001. For R_1 which is greater than this limit, four side-modes are excited around the diode mode and the transition occurs very rapidly that neither one, two, nor three side-modes were observed, i.e. the transition always jumped to four side modes. A plateau was also seen at this mode number (fig (3.7)). Further increase in R_1 will excite more of these side-modes

Figure (3.6a) :Computed solutions of a three-mirror cavity laser ($R_1 = 0$, $R_2 = R_3 = 30\%$).

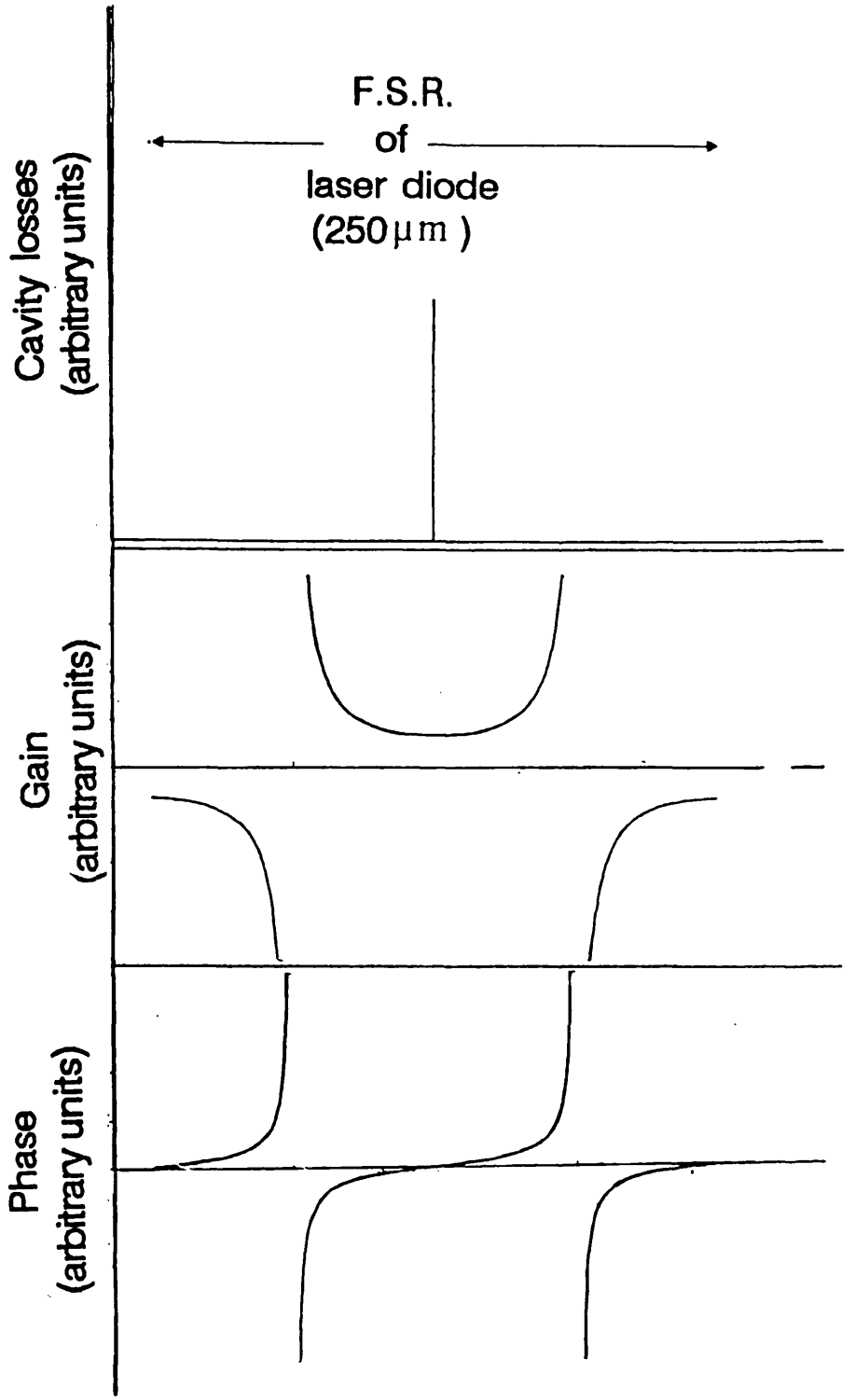

Figure (3.6b) : Computed solutions of a three-mirror cavity laser ($R_1 = 0.1\%$, $R_2 = R_3 = 30\%$)

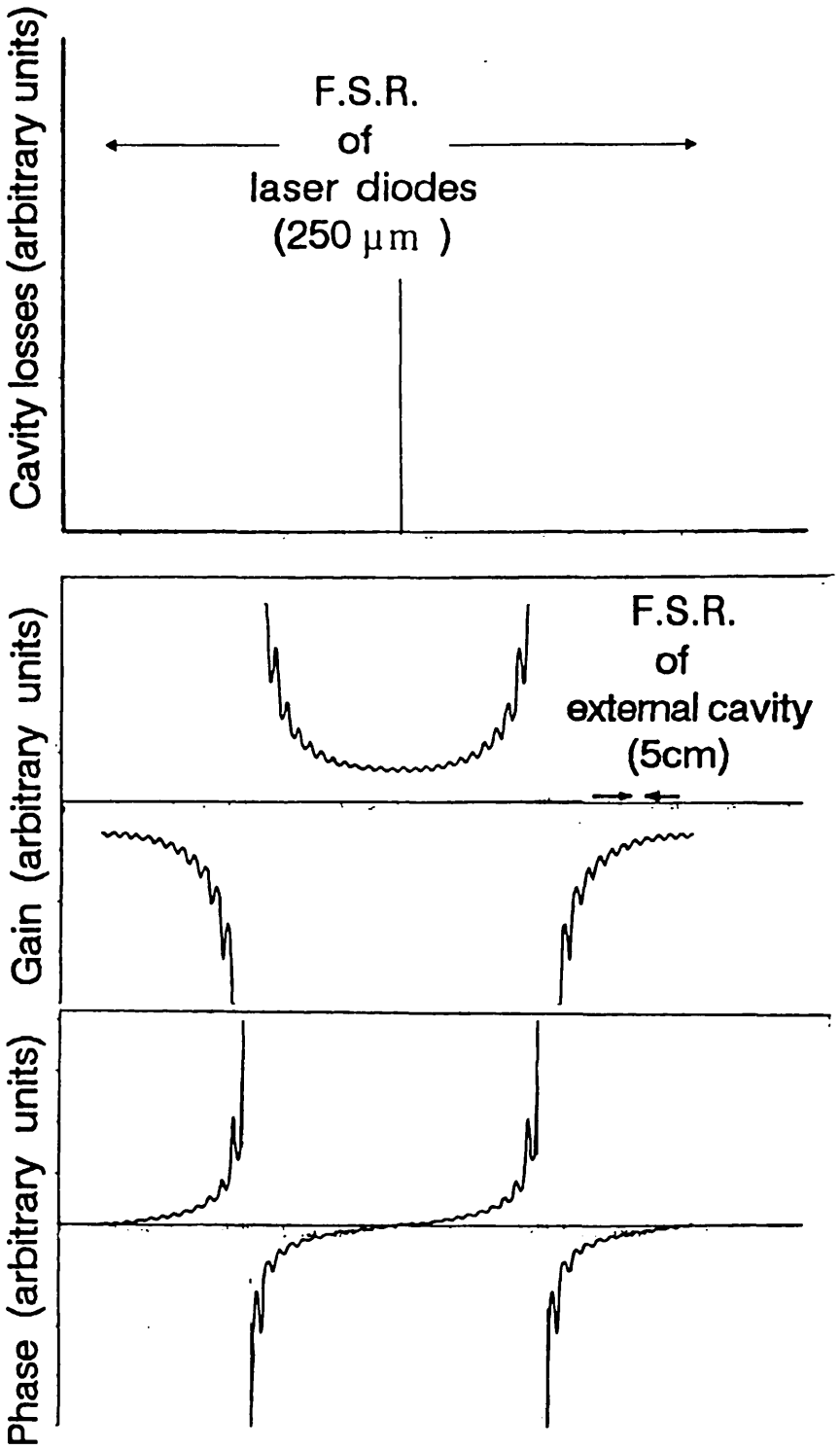

Figure (3.6c) : Computed solutions of a three-mirror cavity laser ($R_1 = 1\%$, $R_2 = R_3 = 30\%$)

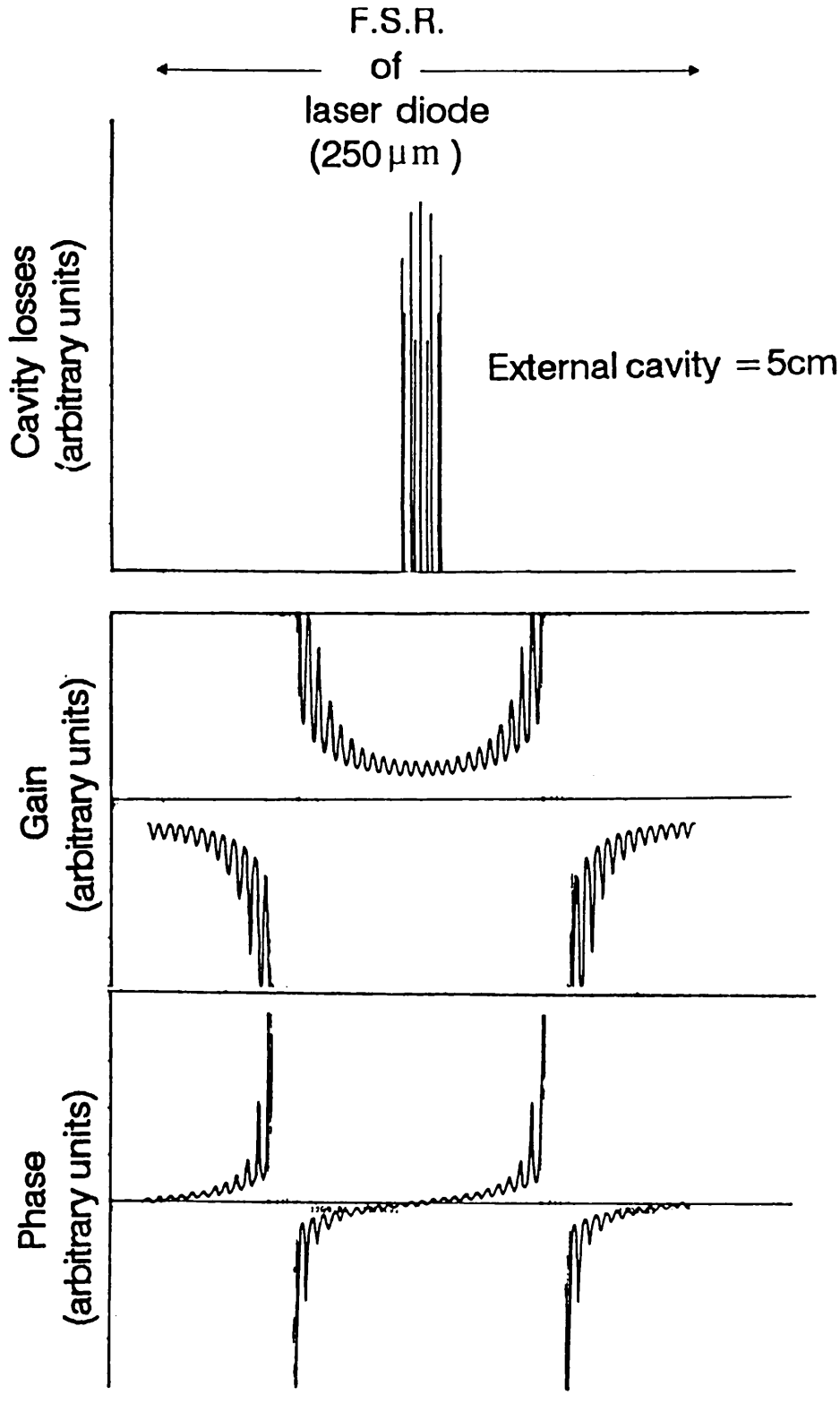

Figure (3.6d) : Computed solutions of a three-mirror cavity laser ($R_1 = 10\%$, $R_2 = R_3 = 30\%$)

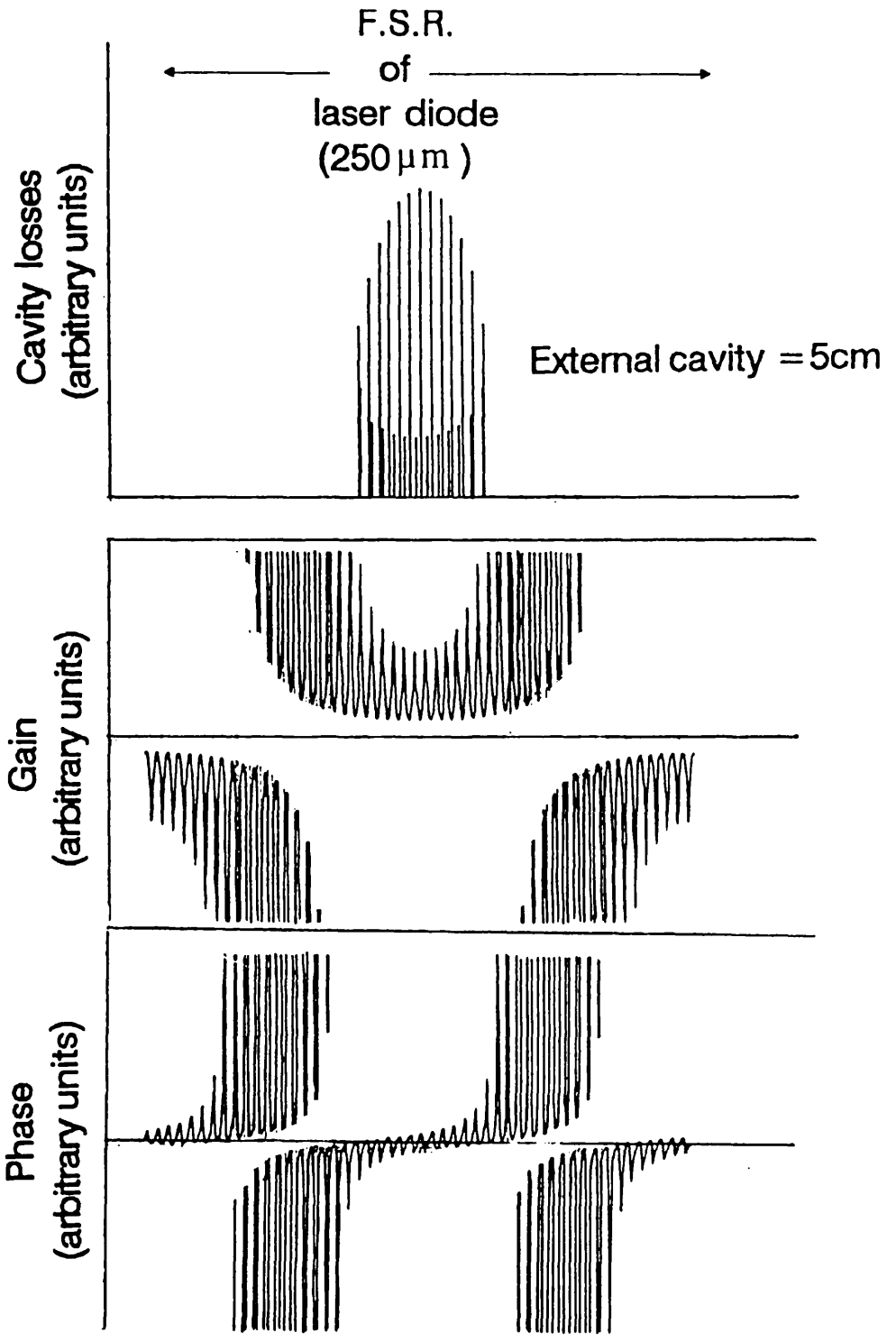

Figure (3.7) : The variations of possible lasing-wavelengths and reflectivities of external reflectors.

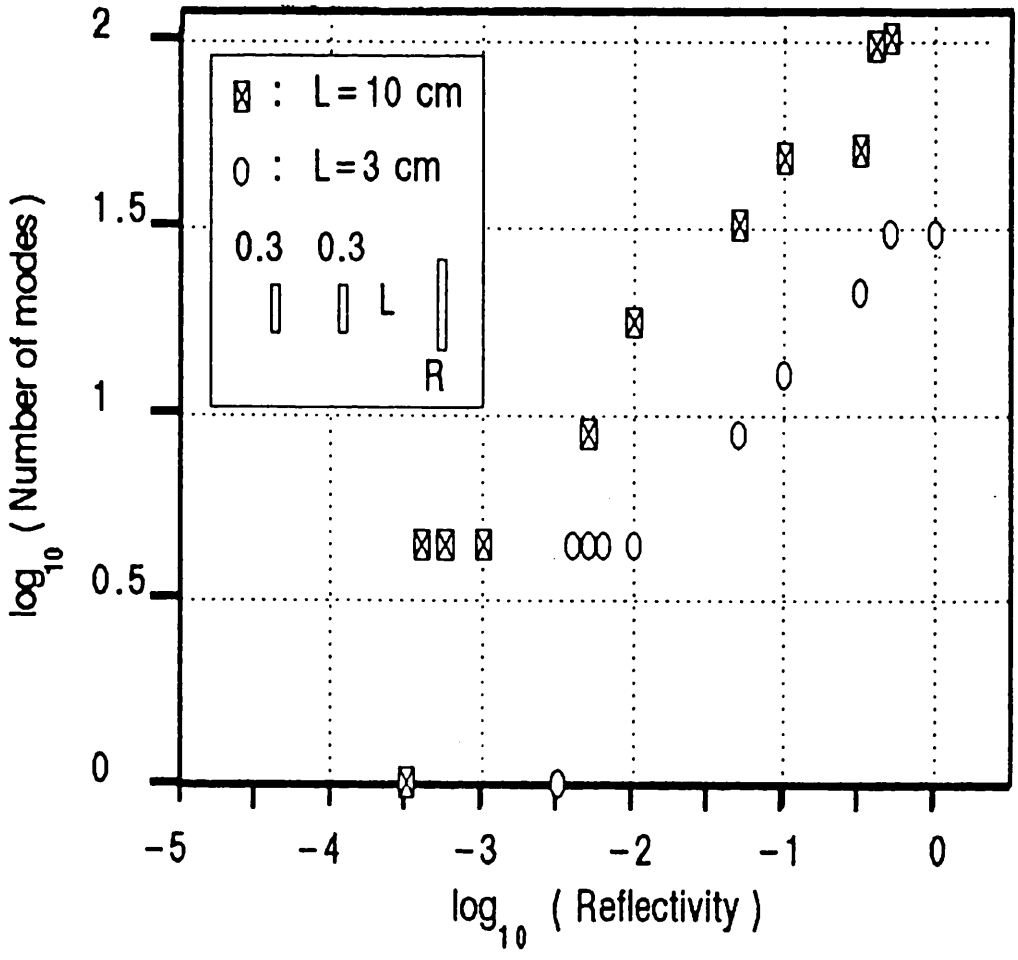

Figure (3.8a) : Computed solutions of a three-mirror cavitv laser ($R_1 = R_2 = R_3 =$ 30%).

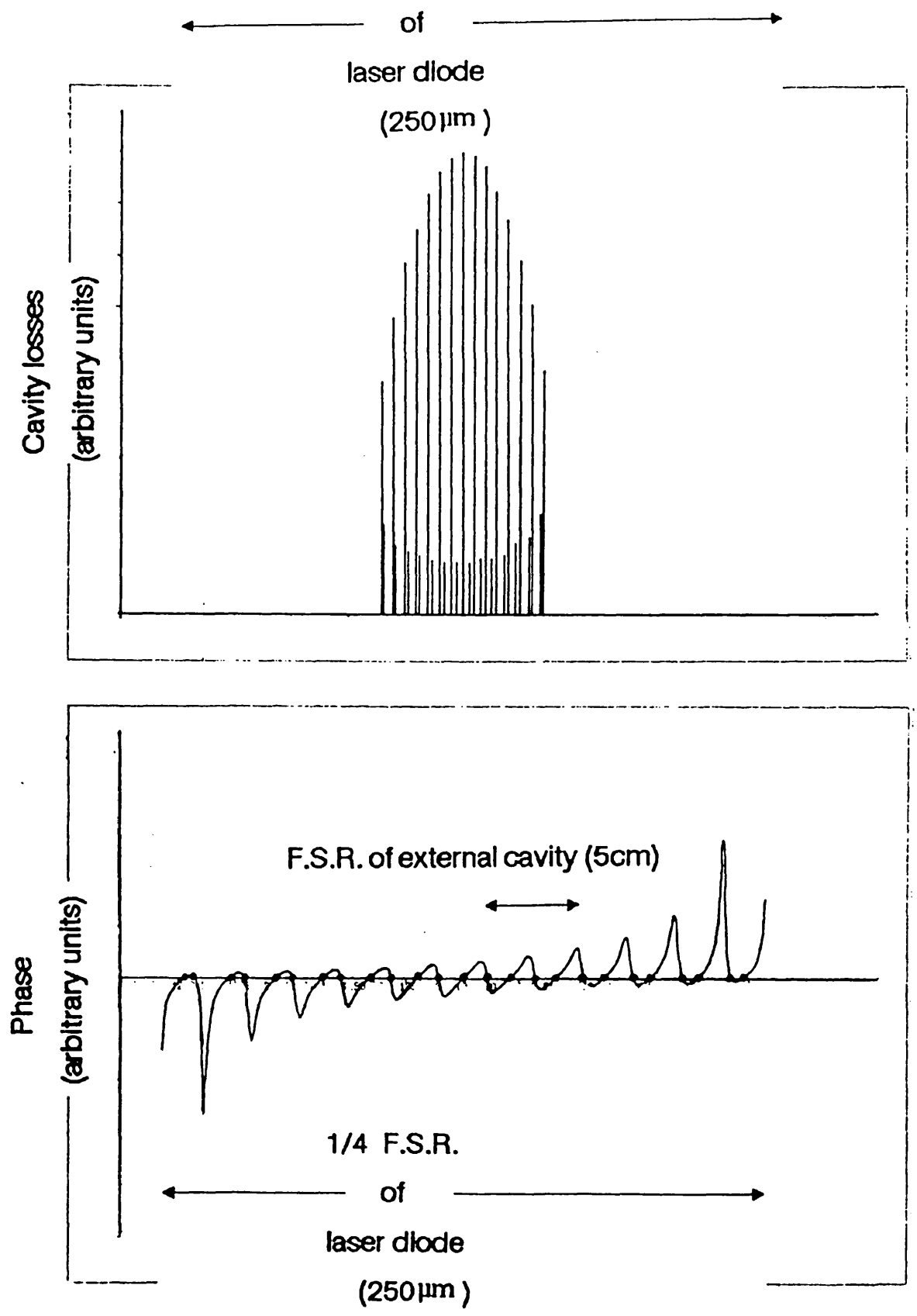

Figure (3.8b) : Computed solutions of a three-mirror cavity laser ($R_1 = 15\%$, $R_2 = R_3 = 30\%$).

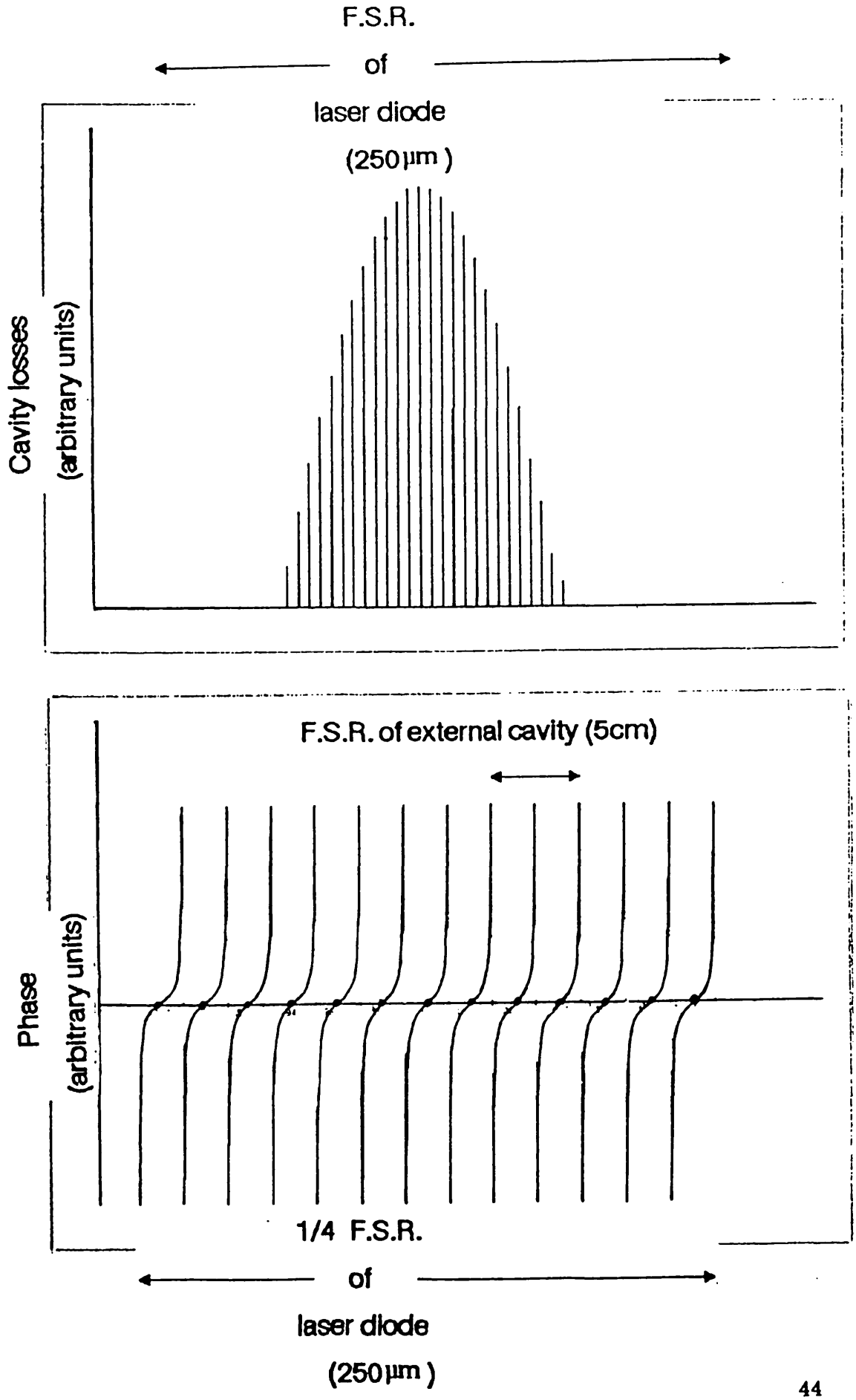

and the number of side-modes saturates at a value equal to the ratio of the cavity lengths :L_{123} and L_{23}.

The computed mode spectra of various R_1's indicated that at low R_1, there exist two sets of side modes which will now be referred to as the odd and even modes. According to the magnified phase curve in figure (3.8), the odd modes were due to the up-slopes of the ringings which crossed the x-axis at equal spacings; whereas the even modes corresponded to the down-slopes which had unequal spaced intersection points. For large R_1, the individual ringings turned into a F.P. phase curves and the down-slopes were no longer existed, and thus the even modes disappeared. The spacing of these odd modes correspond to the length of the composite cavity and thus they are the pure resonant modes of the composite cavity.

The physical explanation of the excitation of side modes, is that at low R_1, the presence of an external mirror actually perturbs the "stability" of the pure resonant diode modes and this weak perturbation causes the excitation of side-modes around the diode mode. The induced side-modes are not the resonant modes of the composite cavity because R_1 is still too low to support them. Henceforth, these side modes can be regarded as the "transition" modes and according to equation 3-20, the "transition" modes are described by the hybrid resonant/non-resonant waves, i.e. arises from the $\frac{1}{4}\lambda$ condition. It therefore seems that the hybrid waves can only be brought into existence during the transition from a steady state composite cavity to the next. This is why these "transition" modes can never exist in a two-mirror cavity because the Fabry-Perot cavity is the "fundamental" resonator which only has one state and that is the steady state.

2. Three-mirror cavity (R_1=0.15, R_2 is variable, R_3=0.3, L_{12}=5cm, L_{23}=250μm):

This cavity configuration corresponds to an external cavity laser in which only one facet of reflectivity, R_2, is coupled to an external reflector. The reflectivity of the external reflector, R_1, is chosen to be 15% which corresponded to a 100% mirror with a coupling efficiency of 15%. Figure (3.9) shows possible lasing-modes within

Figure (3.9a) : Computed solutions of a three-mirror cavity laser ($R_1 = 15\%$, R_2 is a variable, $R_3 = 30\%$).

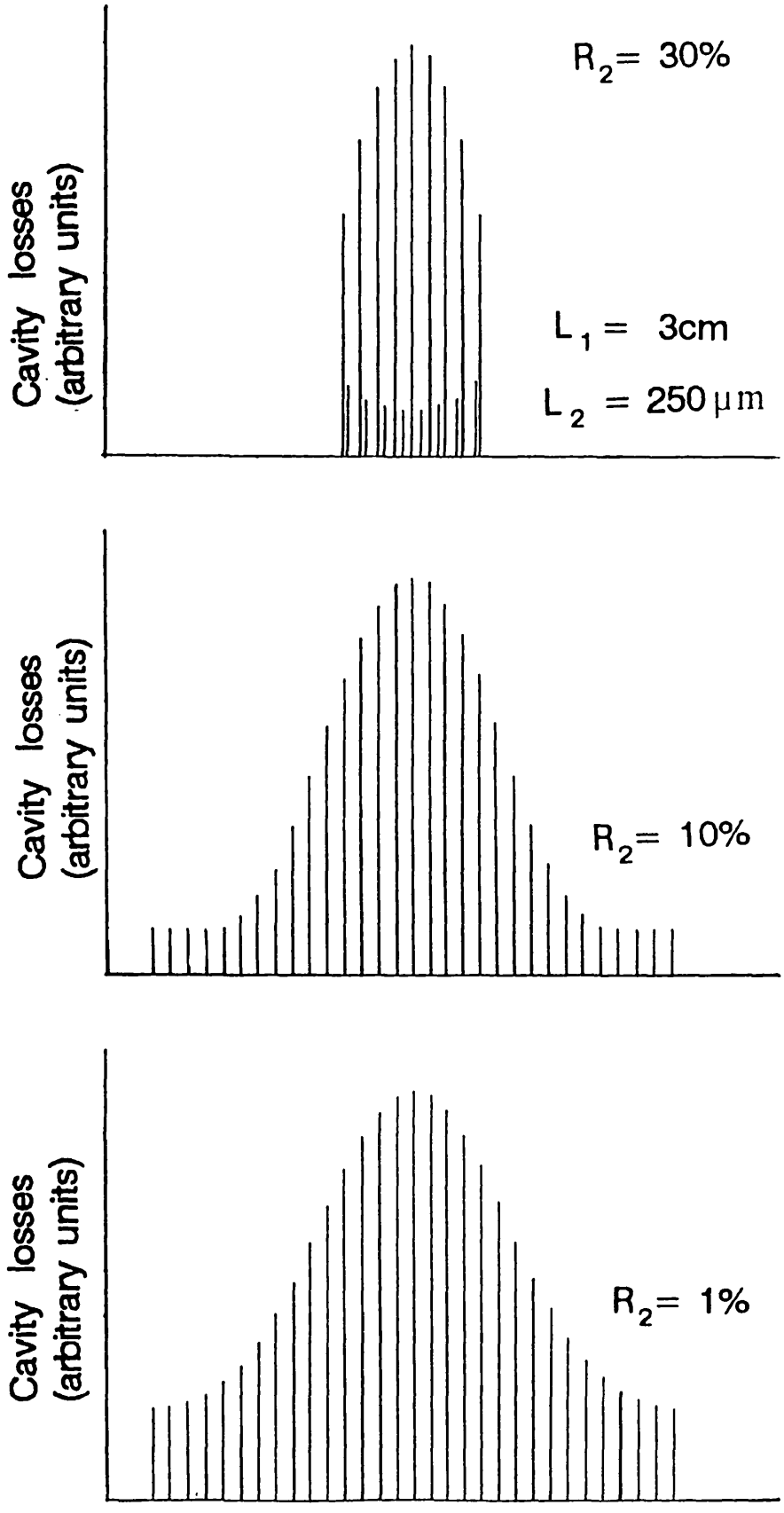

Figure (3.9b) : Computed solutions of a three-mirror cavity laser ($R_1 = 15\%$, R_2 is a variable, $R_3 = 30\%$).

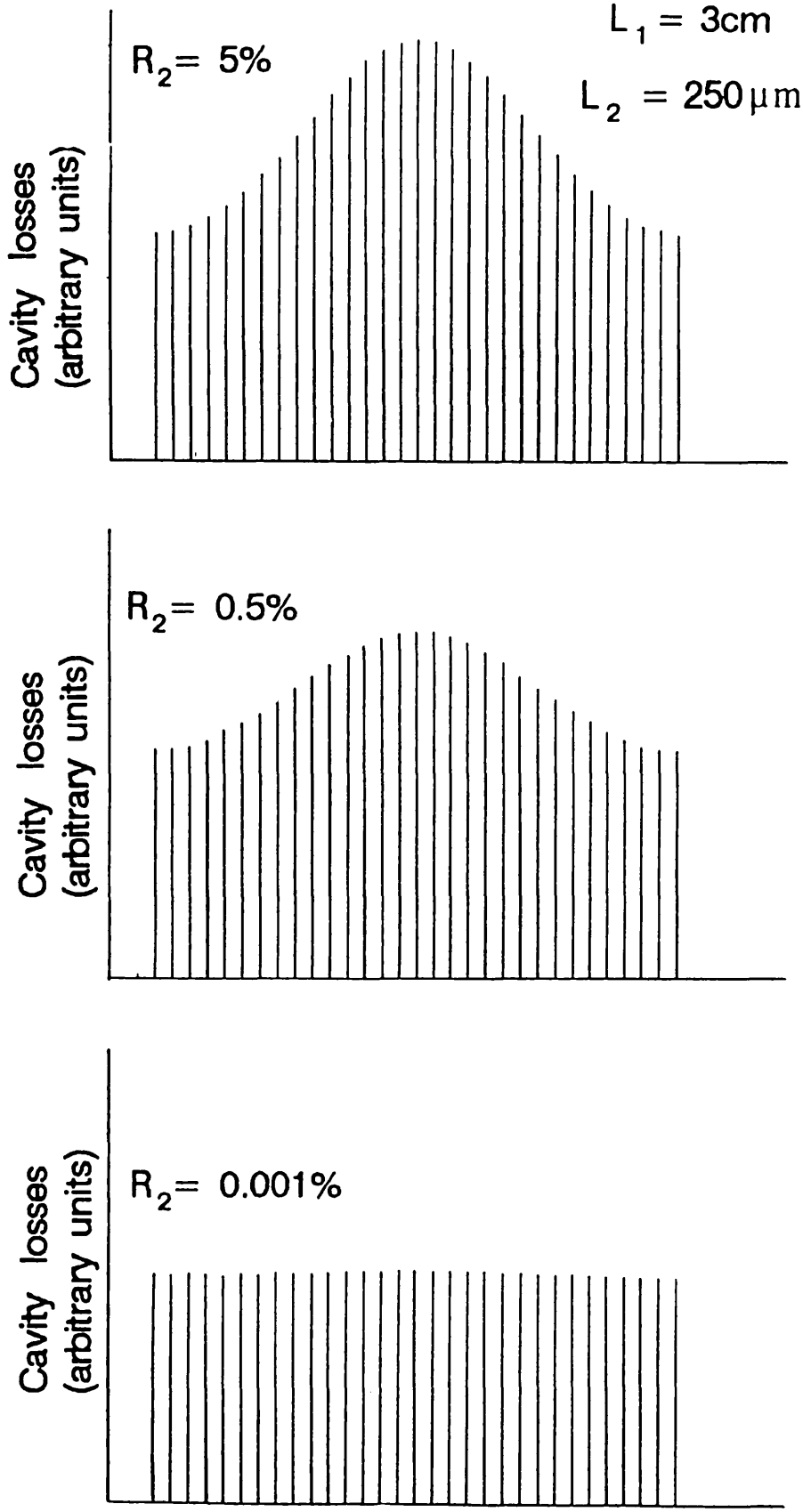

Figure (3.10a) : Computed solutions of four-mirror cavity laser ($R_1 = 15\%$, $R_2 = R_3$ are variables, $R_4 = 7.5\%$).

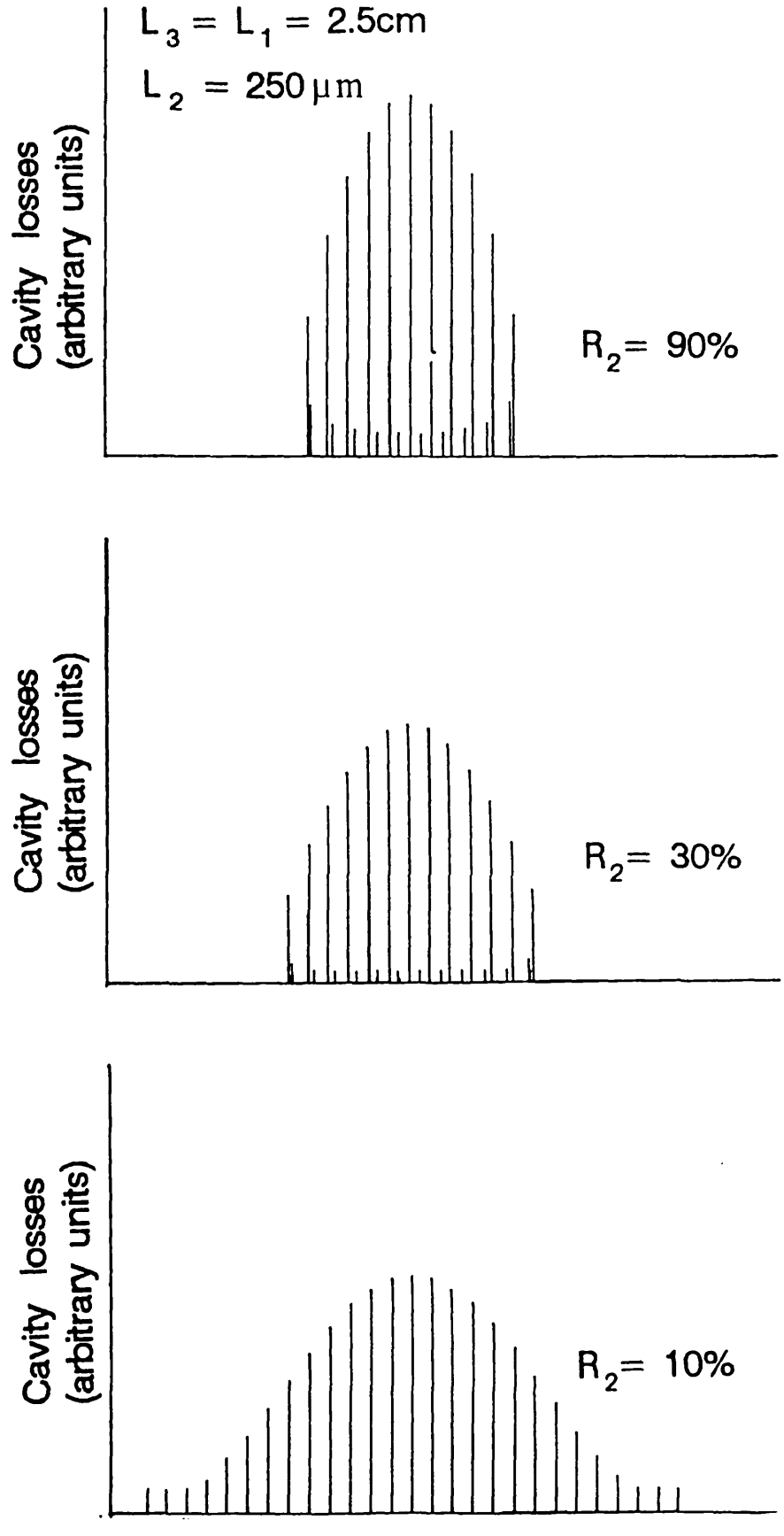

Figure (3.10b) : Computed solutions of a four mirror cavity laser ($R_1 = 15\%$, $R_2 = R_3$ are variables, $R_4 = 7.5\%$).

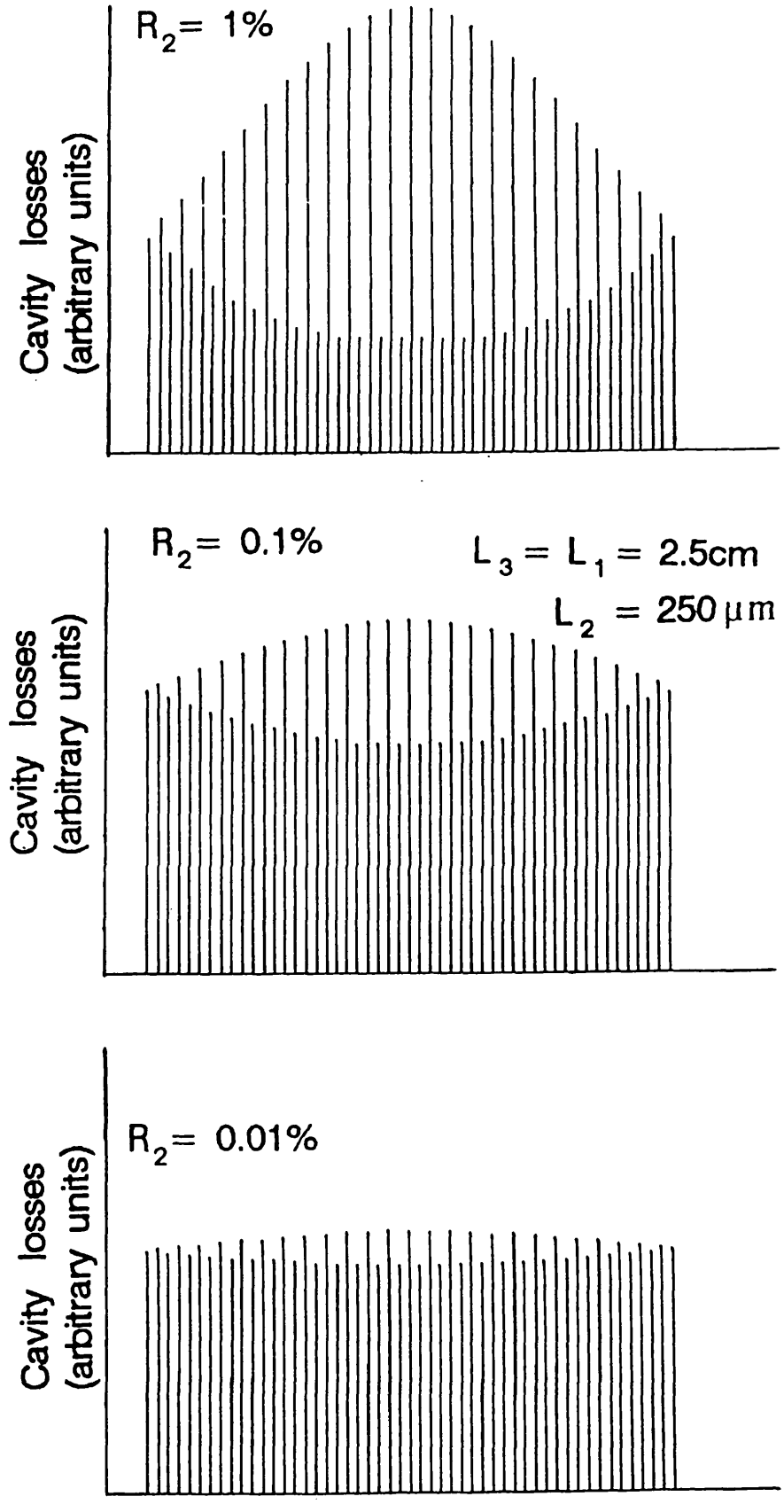

a single F.S.R. of the diode for various values of R_2. For R_2 is greater than 20%, both even and odd modes are excited and the lasing band within a F.S.R. is isolated from other bands in the neighbouring F.S.R.'s. For smaller R_2, the lasing-bands will connect to each other forming a continuous band of lasing wavelengths. However, there still exists a strong wavelength selectivity (or the sub-cavity modulation) even for R_2=0.5%. But below 0.001%, the lasing band becomes more or less constant for all modes, i.e. the sub-cavity effect diminishes significantly.

3. Four-mirror cavity (R_1=0.15, R_2=R_3=R which are variables, R_4=0.075, L_{12}=5cm, L_{23}=250μm, L_{34}=5cm):

This cavity configuration corresponds to an external cavity laser in which the facets' reflectivities, R's, can be varied. When the R's are greater than 20%, isolated lasing-bands are formed in each F.S.R. As before, both even and odd modes are excited around the centre diode mode (fig. (3.10)). At R=10%, the bands begin to join with each other forming a continuous lasing-band. At R=0.1%, two sets of modes are excited and together, they form an eye pattern in the lasing-band. As the facets' reflectivities are reduced, the eye pattern becomes smaller. Even at R=0.01%, the eye pattern is still apparent.

3.3e Computational errors

The F.S.R. of an resonator depends strongly on the wavelength but is independent of the the frequencies. Thus an intrinsic error will occur in calculating the lasing wavelengths if the computation were to be carried out in the wavelength domain. All the examples which were shown above were computed in the frequency domain so that this intrinsic error can be avoided and after which, the frequencies were then converted into wavelengths. A subcavity was set to be an integral number of the diode's optical lengths (i.e. $L_{i_{ext}} = M_i n L_{diode}$, where M_i is an integer) so that the "mode-splitting" could occur evenly around the "diode" lasing-wavelength.

The other source of error was in the computational step, i.e. $\Delta\nu$, which should

ideally be infinitesimally small. However, in practice this is impossible. For the above calculations, the value of $\Delta\nu$ was chosen such that the ratio of $\Delta\mu/F.S.R._{composite}$ was less than 0.01.

5.4 Conclusion

An interferometric study of the possible wavelengths of the composite cavity has been presented. A cavity reduction scheme has also been described and was used to reduce a composite cavity into a two-mirror cavity. The boundary conditions used in deriving the lasing-wavelengths equation are:

(1) a mirror reflectivity can take on two forms: $\overleftarrow{r}, \overrightarrow{r}$.

(2) a pair of r's must be directionless, i.e. $\overleftarrow{r}_1\overrightarrow{r}_2$.

(3) the reflectivities of the two outmost mirrors must be taken as if they were seen by an outside observer.

Using these boundary conditions, a single, consistent lasing-wavelengths equation has been derived for the composite cavity. The equation can also be used to describe a passive cavity by taking all the gain media, g's, equal to 1. In addition, the equation can reduce itself back to a Fabry-Perot equation if all the unwanted mirrors' reflectivities are set to zero, except any two mirrors.

From the lasing-wavelengths equation, it can be understood that the possible lasing wavelengths are determined by two set of solutions. These are:

(1) pure "resonant" waves,

(2) hybrid "resonant/non-resonant" waves.

The pure "resonant" waves correspond to the standing waves having nodes at the outmost mirrors. The phase condition for these waves is the well known "$\frac{\lambda}{2}$" criteria, i.e. $\frac{m\lambda}{2}$=cavity length. The hybrid waves can be visualised as a superposition of both the standing waves and non-standing waves. Thus, the lasing-modes arising from these waves may not have nodes at the outmost mirrors and in some cases, antinodes may form instead.

Using the lasing-wavelengths equation, the possible modes were calculated for

three- and four-mirror cavities of various mirror configurations. It was found that there exists a steady-state condition which is determined by the mirrors' reflectivities. Below this condition, the hybrid and pure waves compete with each other and this gives rise to the formation of even and odd modes. Their mode separations do not correspond to the length of the composite cavity. In addition, the possible lasing bandwidth is not a continuum.

At the steady state condition, the lasing band resumes back to a continuum and only the pure "resonant" waves are excited. This is because mode-spacings are now corresponding to the length of the composite cavity. Thus it seems that the excitation of the hybrid waves only occur during the transition of stable composite cavity to a higher order composite cavity, i.e. say, from a Fabry-Perot cavity to a three-mirror cavity. The reason why these modes cannot be seen in a Fabry-Perot resonator is because the two-mirror resonator (or cavity) is the fundamental "composite" cavity and it only has one state which is the steady state. Therefore, the formation of lasing modes in a composite cavity is not as simple as it is generally assumed.

CHAPTER FOUR

Characterisation of solitary and external cavity semiconductor lasers

4.1 Introduction

The architecture of a semiconductor laser is based on two foundations, of which, one is the inherent high optical gain in a semiconductor material. The other is its high refractive index (≈ 3.5) which provides facets' reflectivities of about 30%. This is why the laser diodes can be made so small and efficient. However, in some applications such as the "mode-locked" pulse generators and the single-pass optical amplifiers; the presence of facet reflectivities limits the devices' performance. Thus, the removal or reduction of the facet reflectivities is of the utmost importance to such a device.

Introducing anti-reflection coatings onto the facets can reduce the reflectivities; but cannot be completely eliminated due to the difficulties in obtaining a perfect index-matching. More detailed historical background on the antireflection coatings will be given in chapter VII. Alternatively, Brewster angled facets with respect to the

active stripe can also suppress the diode's cavity effect due to the facets' reflectivities. The first reported angled stripe semiconductor can be dated back to 1967[107]. Later on, other workers [13,15,36] have also applied the same technique to various laser diodes and claimed to have completely eliminated the facet reflections.

In this chapter, ways of fabricating Brewster angled stripe laser chips are described for two types of structures. These are the gain- and index-guided lasers. Procedures for mounting, and electrically connecting the chips onto heat-sinks are given. Thermal effects on both the lasing wavelengths and threshold currents of mounted chips are also discussed.

At the present, actively mode-locking still requires semiconductor lasers to have extended (or external) cavities. Different types of external cavities and their alignments are presented. A brief description is given on the fabrication of an optical fibre grating[106] which was specially made for this project. After which, the lasing characteristics of zero-degree, A.R. coated, and Brewster angled stripe lasers are discussed. The main emphasis is on both the spectral and intensity outputs. Finally the important results are summarised in the conclusion.

4.2 Fabrication of Brewster angled stripe semiconductor lasers

4.2a. Cleaving

For stripe geometry D.H. (i.e. gain guided structure) semiconductor lasers, the Brewster angled facets can be easily introduced during the fabrication process in the clean room. After the growth of the wafers; the metallization stripes are deposited at Brewster angles to the natural cleavage planes [110]. After which, the individual chips can then be obtained by either cleaving the crystal planes [111], which are perpendicular to the cleaved facets or cutting parallel to the stripe directions. Figure (4.1) shows photographs of both zero degree and Brewster angled stripe laser diodes which were fabricated using the angled-stripe technique, and the two cutting methods.

Figure (4.1) : Zero-degree and Brewster angled stripe lasers.

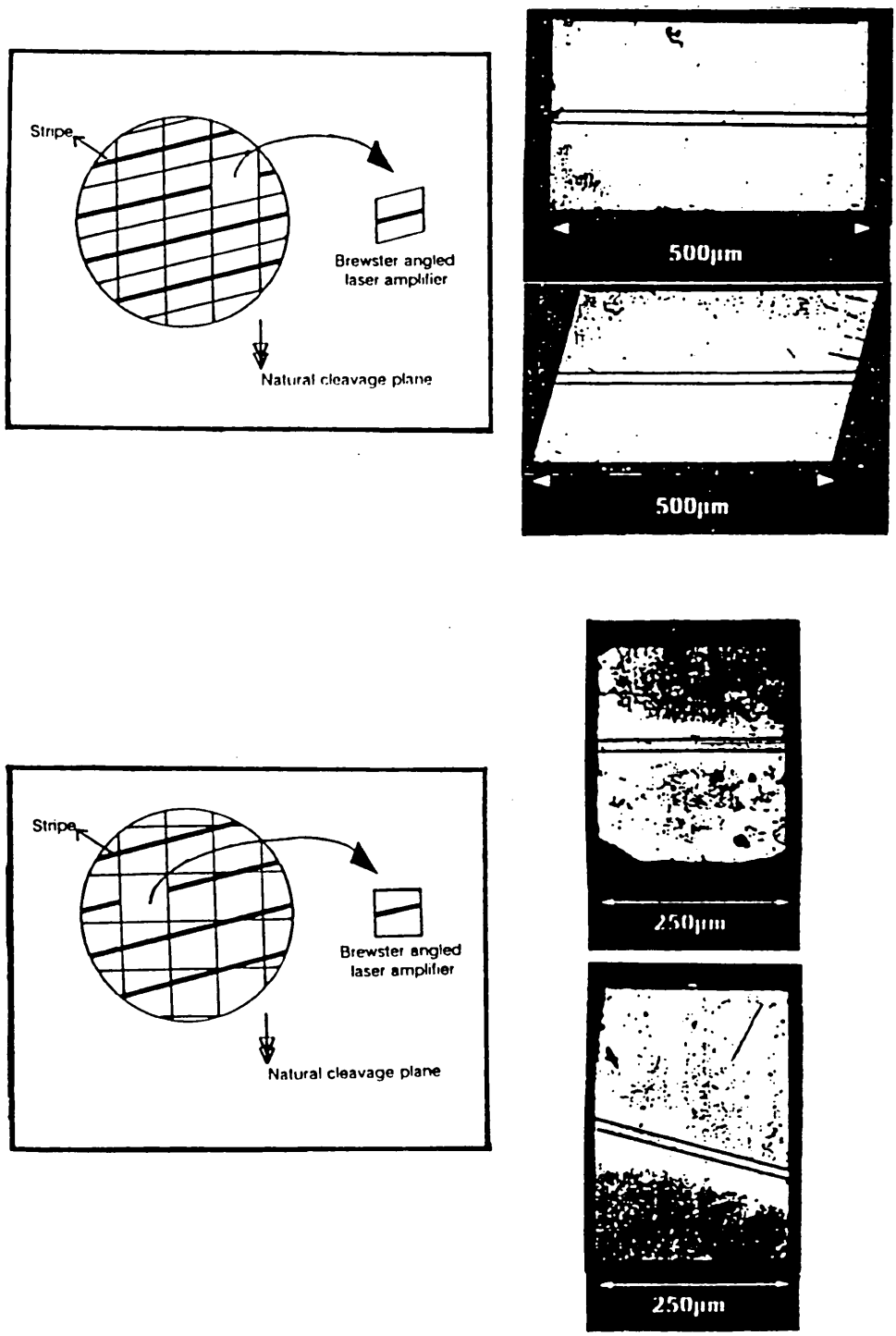

To achieve a high yield of laser diodes from the wafer, the latter cutting method is preferred.

For index guided structure semiconductor lasers such as the buried active crescent[67] or the multiple infill buried[68] laser diodes, the growth technique requires the active stripe to be laid perpendicular to the natural cleavage planes and thus, it is not possible to introduce Brewster angled facets by the described "cleaving" process. An alternative way is to polish the cleaved facets to Brewster angles (with respect to the stripe). An optical polishing technique has been developed for such purpose and will be described in the next subsection.

4.2b Optical polishing

There are basically two processes involved in polishing the "lose" laser chip. The first involves mounting of a laser chip on to a "glass-jig" which is much larger than the chip. Then, the grinding action is used to polish this "*loaded* glass-jig". The purpose of using a large "glass-jig" is that it can be easily manipulated than a single chip during the polishing process. The "glass jig" consists of two pieces of glass blocks (alternatively, one microscopic glass slide and one glass block can also be used). One of the blocks is marked with a line angled at 75^o to its edge and placed on to a hot plate and is heated to a temperature of 75^oC. A piece of thermoplastic polymer (crystal bond, grade 509, manufactured by Aremco Product Inc.) is then put on the glass block. At this temperature, the polymer softens enough to allow a chip to be immersed into it. Viewed through an optical microscope (40X), the chip is carefully positioned so that its stripe is parallel to the marked line. When this is achieved, the second block is then placed onto the hot plate and is allowed to reach a temperature of 70^oC. A wax which also melts at this temperature is used to cement the glass blocks together. During the cementing, extra care is needed in positioning the glass blocks. This is because any rapid movement of the top glass block will introduce a strong sheering force which can rotate or translate the immersed chip from its correct position. If this occurs, the cementing has to be terminated and the realignment

Figure (4.2a) : Photographs of the facet at various polishing stages.

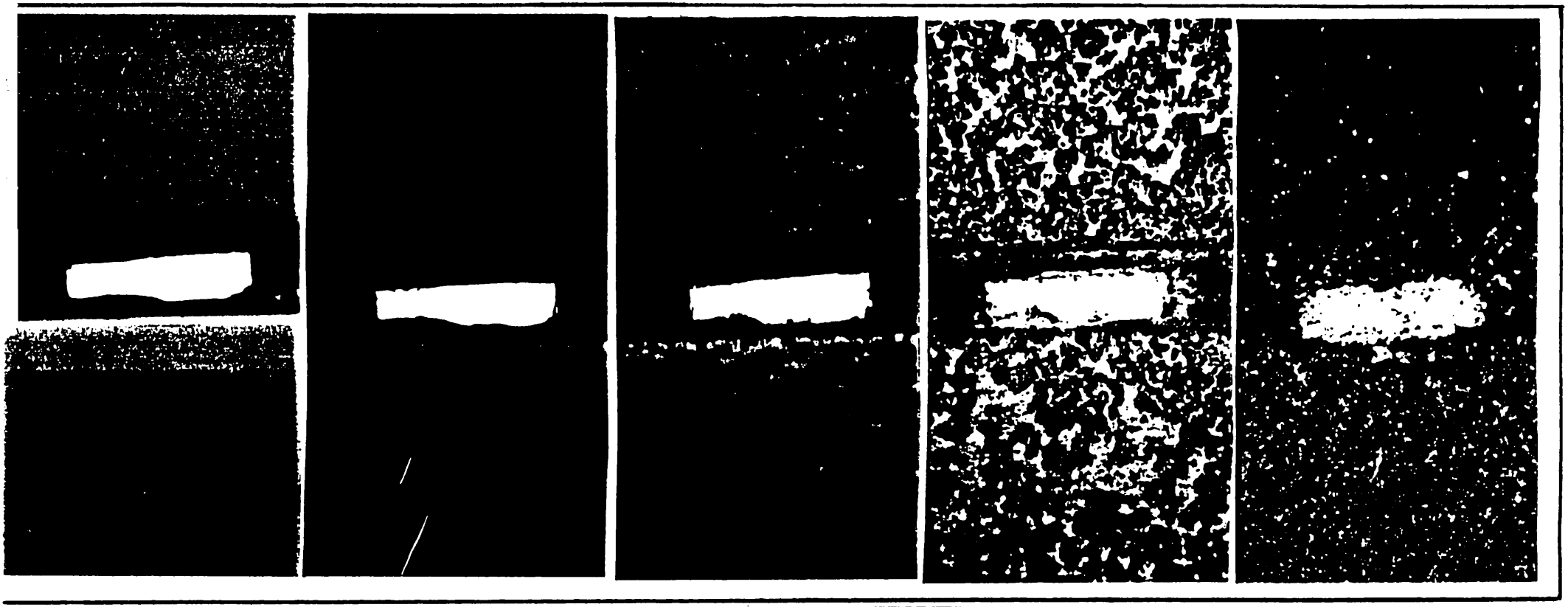

The final stage

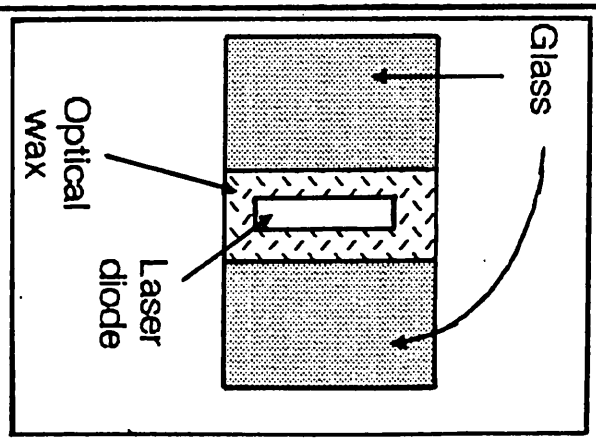

Figure (4.2b) : A laser diode prior and after the polishing.

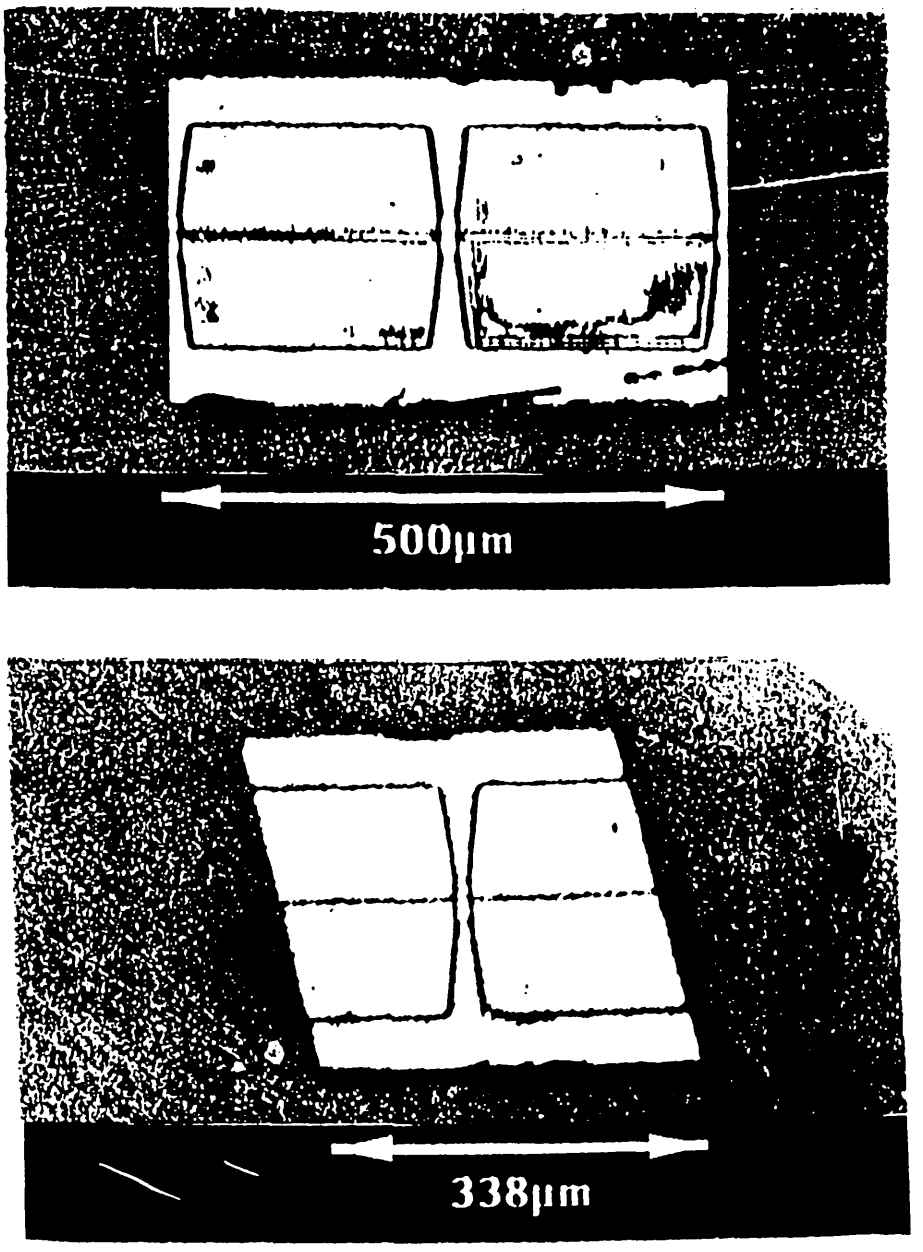

of laser chip must be repeated. Once the chip remains in its correct position after fusing the glass blocks, the "*loaded* glass-jig" is then removed from the hot plate and is allowed to cool down to room temperature.

For the polishing process, five types of powder are used. These are the (a) silicon carbide powder, (b) to (d) the Aluminium oxide powder type 225,150 and 95 respectively; and finally (e) the lapping powder (Tacepol 3, finest grade, supplied by Arafract, Sheffield). The first four powders are used on a cast iron polishing plate; while the lapping powder is used with a self adhesive cloth (Angus Ltd., Maidston, Kent) on a flat glass substrate. The silicon carbide powder which is of the largest granule size is merely used to grind the glass surface near to the laser chip. This follows by the polishing with powders (b), (c) and (d) to further smoothen the glass surface i.e. to remove the "pits" which are left over by the previous powder. Finally, through the lapping process, a polished facet of optical quality is obtained.

During the polishing process, the facet is frequently examined under the microscope to check the surface quality especially at the last two stages. If cracks or chippings appear in the proximity of the active region which is normally very close to the p-side of the chip, then polishing has to continue until they disappear before switching to the next powder. A sequence of photographs showing the facet quality at every polishing stage is shown in figure (4.2). The lapping process will stop whenever the "pits" are smoothened out and no cracks or chippings can be seen on the facet. When the polishing has been completed, the "*loaded* glass-jig" is then heated to 75°C and the laser chip is removed from the glass blocks, and is cleaned in acetone. To obtain Brewster angled facets at either ends, the described mounting and polishing processes have to be repeated twice for each facet.

4.3 Diode mounting technique & electrical connection

Initially, the surface of the oxygen free copper heatsink is polished with two abrasive papers: grade 600 and 400, followed by a diamond paste of granule size of

5μm using either paraffin or acetone as lubricant. It is then cleaned thoroughly by acetone and is heat-bathed in a cleaning solvent (P.C.81, Multicore solvent cleaner) for about thirty minutes. After which, it is again cleaned with acetone.

The preparation of a laser chip starts with the visual inspection through a high resolution microscope checking for any chippings or damage to the facets. It is very important during the handling of the laser chip that direct contact with the facets must be avoided but other surfaces can be in contact with the tools. The chip is then rinsed with alcohol (I.P.A.) or acetone.

Indium spheres (diameter of about 125μm) were used to bond the chip onto the heatsink. To bond the chip with the indium sphere, the copper stud is first heated on a hot plate to the melting temperature of indium (about 190°C). The temperature is monitored by an electrical thermocouple. Once the copper stud reaches the desired temperature it is then wetted with soldering flux. After which, the indium sphere is placed onto the heatsink and more flux is applied onto the sphere to assist it to melt and spread evenly on the surface. Then the laser diode is carefully placed with its p-side down onto the molten solder. Further adjustment is made to correctly position the chip with respect to the heatsink. Once, this is achieved the copper stud is removed from the hot plate and allowed to cool to room temperature. Visual inspection is carried out again at this stage to check the facet quality. Any excess flux or dirt is brushed off using a thin stripe of filter paper wetted with I.P.A. or acetone.

For the electrical connections (fig. 4.3a), a relay terminal, which can be made from a single-side printed circuit broad, is used to connect the coaxial cable to the laser chip. The terminal is glued near the bonded chip and a wire from the coaxial cable is connected onto the relay using ordinary solder. Following this, silver epoxy is applied onto both the chip and relay post. A piece of gold wire (diameter 25μm) is laid over them. The package is then heated in order to cure the epoxy before applying the voltage.

The D.C. current is generated from a power supply unit (Racal-Dana, 9331).

Figures (4.3a) and (4.3b) : The schematic diagram of the laser mount and the output voltages vs currents respectively.

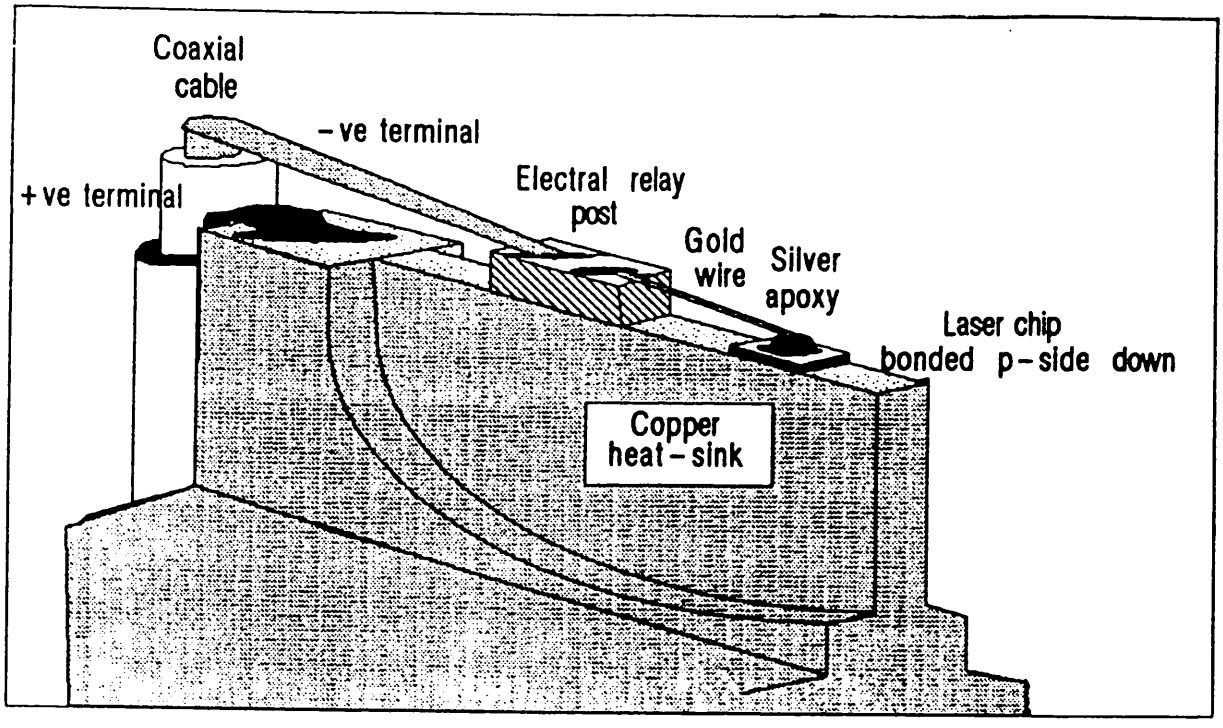

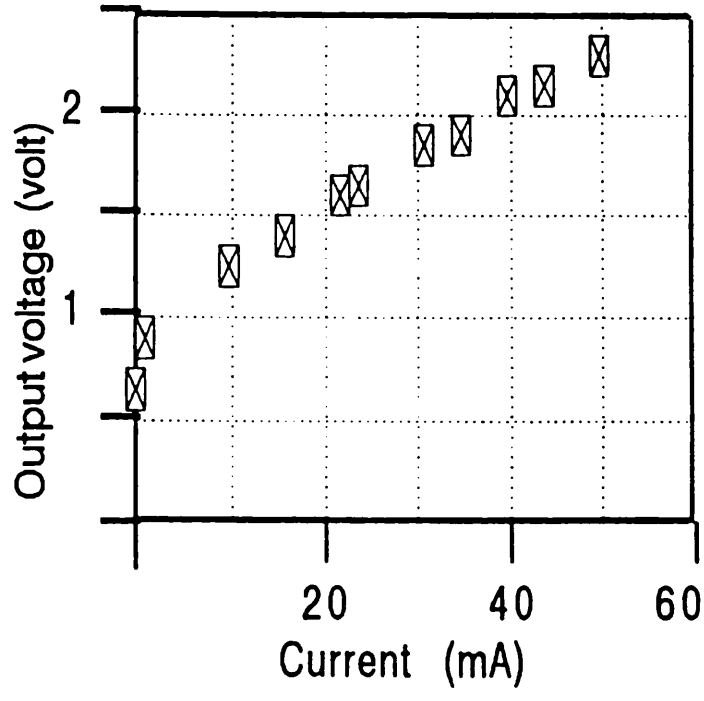

The output voltage and current are monitored on a L.E.D. display panel. In order to measure the current applied onto the laser diode, a 10Ω resistor was connected in series with the laser diode. Applying this voltage to the chart recorder allowed the applied currents to be monitored. The output voltage and current from the unit is plotted in figure (4.3b) for a typical laser diode. Generally, the net resistance decreases with voltage and the turn-on voltage is about 0.8 volts for the 1.3 μm diodes. The resistance gradients are typically around 25 to 40 Ω/mA at the lasing thresholds.

4.4 Temperature dependence of the lasing thresholds and wavelengths

The temperature dependence of the threshold current density in a laser diode is usually determined by a semi-empirical formula:

$$I_{th}(T) = I_o exp\frac{T}{T_o} \qquad (4-1)$$

where I_o is the lasing threshold at zero degree kelvin, T_o is the characteristic temperature which describes the degree of sensitivity to the changing ambient temperature. Ideally, T_o is preferred to be as large as possible, so that the performance of the laser diode should remain unchanged over a large temperature range.

Since the advent of the quaternary laser InGaAsP, there has been a strong interest in the thermal dependence of the lasing thresholds. This is because these types of lasers have stronger dependence on temperature than the ternary GaAsAl devices[5]. Intensive investigations [5,12,67,80] were conducted on these laser diodes and various explanations were suggested. These suggestions were:

(1) non-radiative Auger recombinations within the active region,

(2) electron leakage over the hetero-barrier into the confining InP layers,

(3) internal optical losses by intervalence band absorption, and

(4) non-radiative recombination due to the defects within the active layer or at the interfaces.

These effects are also responsible for the temperature dependence of lasing wavelengths. It was found[20] that the gain bandwidth sharpened with lower temperature

but that the lasing energy was linearly proportional to the temperature. Later on, similar results were obtained from 1.3μm InGaAsP lasers by Tsang et al[80] who used a frequency selective feedback technique.

Experimental set-up and results

The laser package(laser diode, copper stud and electrical wiring) was inserted in a heatsink which was fixed onto one end of a two inches thick aluminium plate. The other end was placed in a heating element or cooling tank. A thermal insulator was inserted in the middle, to block out any possible thermal radiations from the heater. The temperature of the heatsink was monitored jointly by a mercury thermometer and a thermocouple device. The light from one facet was collected by a standard x20 microscope objective and focused onto a large area germanium diode.

First, the heatsink was heated up and after a steady temperature was attained, the heater temperature was then reduced slowly such that the temperature dropped at a rate of about 0.5°C/min. When the heatsink had reached the room temperature, liquid nitrogen was poured into the cooling tank and the cooling rate was maintained at around 0.8°C/min.

A 1.3 μm InGaAsP diode which lased at 25mA in room temperature was tested. The light/current characteristics at different heat sink temperatures are shown in figure (4.4) revealing that the lasing threshold increased rapidly with temperature and that lasing was still possible even at as high temperatures as 55°C. The variation of threshold (Ln I_{th}) with temperature (T) is shown in figure (4.5). The characteristic temperature T_o was found to be smaller at higher temperatures, i.e. strong temperature dependence. T_o's of 166.6, 46, and 18.3 were measured at -10°C, 25°C and 55°C respectively. These results were compared with those obtained by other workers[5,12] who have also observed a nonlinear relationship between LnI_{th} and T. In particular, the experimental results agree well with the theoretical prediction by Asada et al[5]. In their case, T_o was calculated to be 145°K. Thus, according to their analysis, the

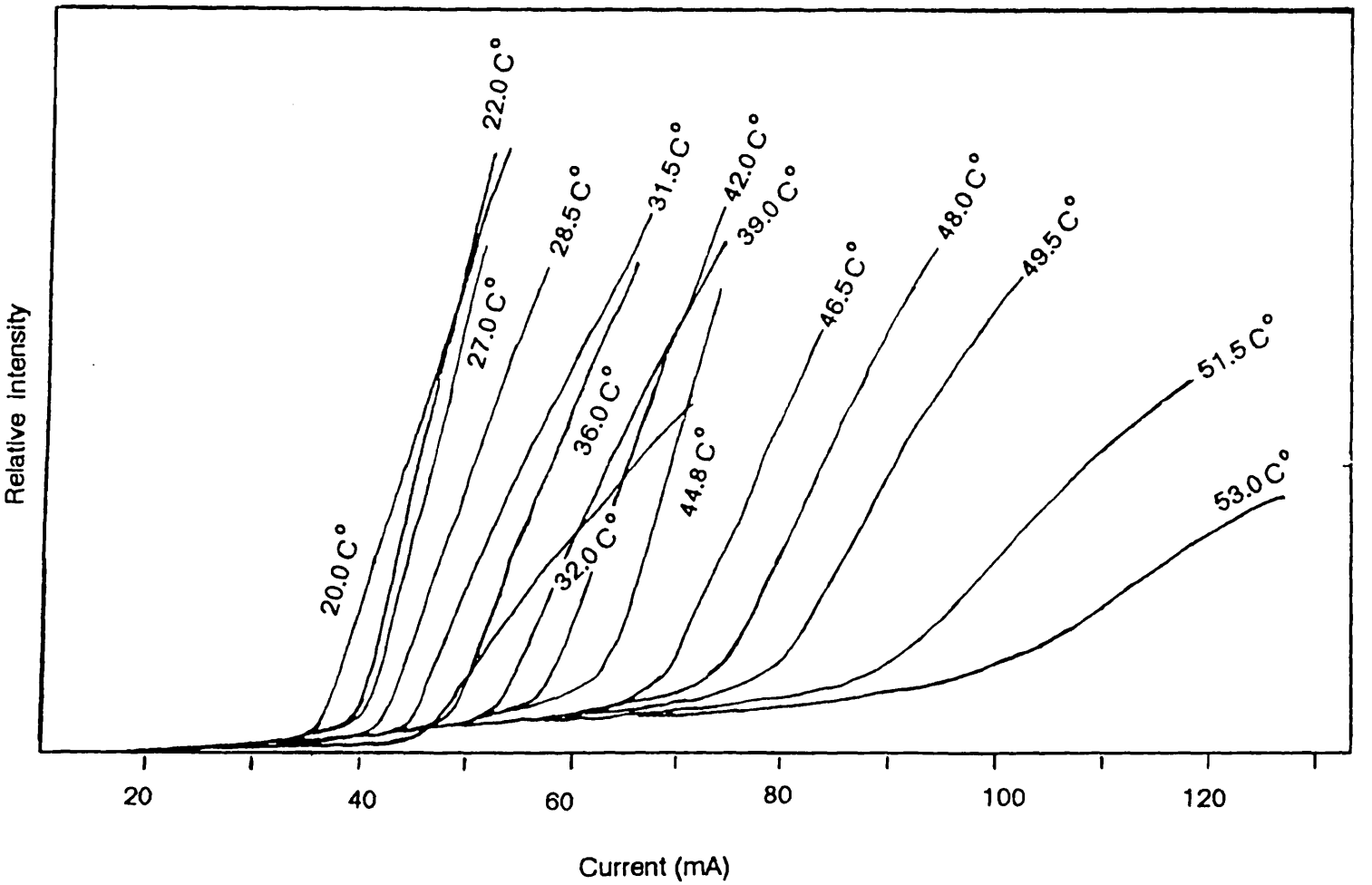

Figure (4.4) : Light/currents characteristics at various temperatures.

Figure (4.5) : Natural logarithm of threshold currents vs temperatures.

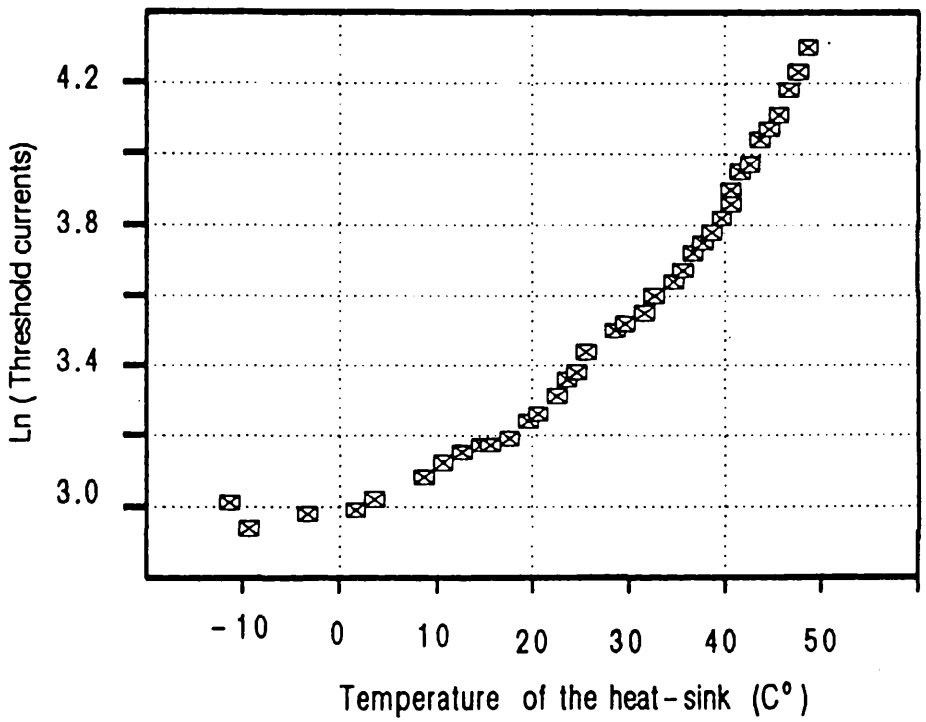

Figure (4.6) : Lasing spectra at various temperatures.

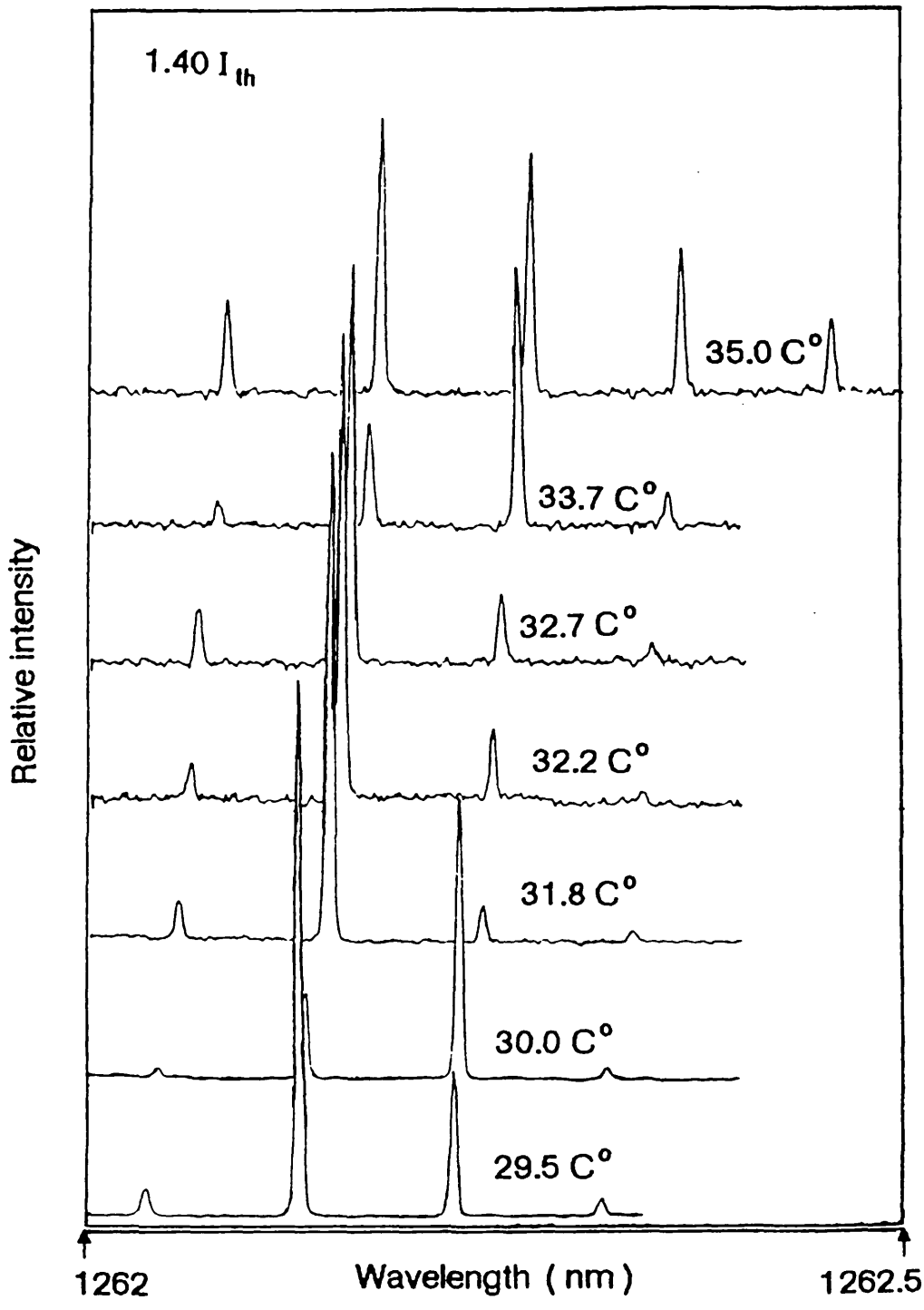

Figures (4.7a), (4.7b), (4.8a), and (4.8b) : Plane mirrors and grating cavity lasers.

(4.8a)

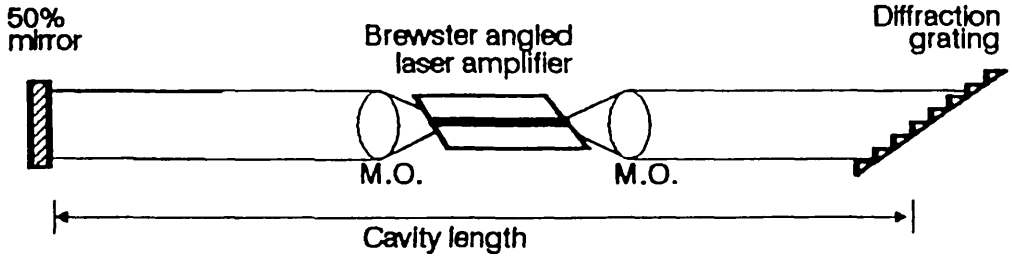

(4.8b)

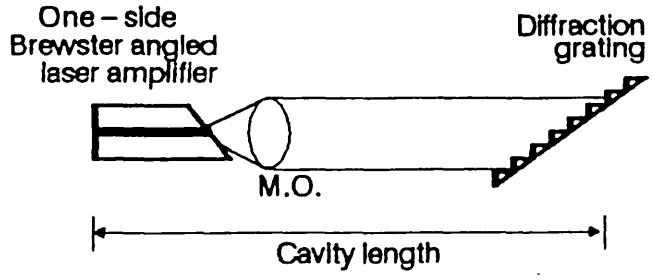

(4.7a)

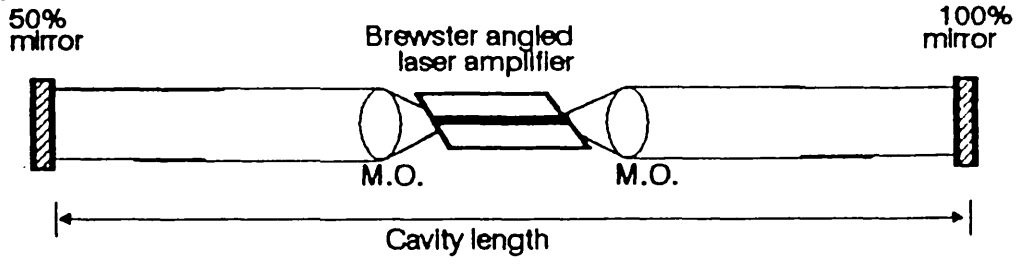

(4.7b)

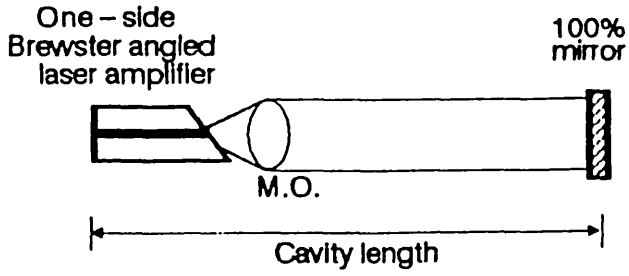

tested diodes' main losses were due to absorption in transitions between the split-off and heavy hole valence bands.

Spectra at different temperatures (fig. 4.6) showed that under fixed pumping, the mode intensity decreases with higher temperatures. This was mainly due to the temperature dependence of the lasing thresholds. Other key features were:

(1) the Fabry Perot modes drifted toward longer wavelengths at an average rate of 1.2Å/°C. The drifting was caused by thermal expansions which increased the optical length of the laser diode. No changes on the mode spacing were observed. However, the calculation showed that for a shift of 5Å, the mode separation will also be reduced by 0.003Å. But since the resolution of the spectrograph is about 0.2Å, which is wider than any changes in the mode-spacing. This is why the changes in mode spacing were not observed.

(2) the gain peak also moved toward longer wavelengths. This conforms with the suggestion[12] that an increase in the temperature will decrease the band-gap energy, E_g.

(3) Broadening of the gain bandwidth with higher temperatures was also observed. Referring to figure (4.6), there were only two strong modes at 29.5°C, but at 35°C, five modes have been excited. When the current was increased to 43mA, the gain bandwidth sharpened and only one mode was observed. A similar result was also observed by Dutta and Nelson [21], who have found that the spectral gain distribution sharpened with decreasing temperature. They also suggested that it is because the Fermi factors have a sharper tail at higher temperatures.

4.5 External cavity configurations and wavelength-tunabilities

4.5a Plane-mirror cavities

This type of external cavity consists of either one or two plane mirrors (fig. (4.7)). When two plane mirrors are used, one of them usually has high reflectivity (≈100%) while the other is a partially transmitting mirror. Microscope objectives are used to collimate (or focus) the light from the laser diode on to the mirrors, and to couple the returned light back to the active region. Graded index rod (GRIN)

lens can also be used to couple together both the laser and external reflectors. The refractive index of a GRIN lens varies continuously toward the centre axis. This index variation bends the light ray in the same fashion as a conventional (fixed refractive index) spherical lens. The amount of bending depends on the distance which the ray has travelled. If after traversing a distance l, the ray is bent such that it reaches the centre axis; then l is regarded as the "1/4 pitch", i.e. quarter of a wavelength. Similarly, if the ray passes the centre twice within the GRIN lens, then the lens is said to be "1/2 pitch". Thus, if a point source is placed at one end of a 1/4 pitch lens, the output through the other end will be collimated. In this project, 1/4 pitch (commercially available) GRIN lenses were used, but since the experimental set-up required a small working distance between the lenses and the laser diode, these GRIN lenses were polished to accommodate such requirement.

For the x20 microscope objective, a net coupling efficiency of 10 to 15% was estimated (see Chapter VII) for a wavelength of 1.3μm. The feedback condition did not improve with the 40x microscope objectives even though their numerical apertures were larger than the 20x objectives. It therefore seemed that instead of depending on the numerical apertures, the coupling was limited by a certain acceptance-angle characterised by the waveguiding mechanism of the active stripe. For the GRIN lenses, the measured threshold currents were the same as those measured using 20x objectives. Hence, both the GRIN lens and microscope objectives have the same coupling coefficients at 1.3μm.

The alignment was carried out using both the fluorescence cards and an infra-red viewer to trace and steer the beam back to the microscope objectives. Initially, large current was applied onto the laser diode to increase the amount of fluorescence which would make the beam easier to trace. A pelicle was inserted inside the cavity which reflected $\approx$8% of the intracavity flux onto a large area germanium detector (GA5, connected as a photovoltaic detector). The converted electrical signals were then monitored on a chart recorder.

If a good feedback condition was established, the intracavity flux would increase substantially compared to the fluorescence flux. After which, the applied current

should then be reduced gradually during the optimisation of the cavity. This is to avoid any optical damage which may incur to the facets because of the rapid build-up of intracavity flux. For a two-mirror cavity, this alignment procedure was repeated again for the second mirror. After the external cavity has been set up, the light current characteristics were then plotted on the chart recorder and the absolute value of the output power could be calibrated with an optical power meter (Photodyne).

It was found that the stability was critical and that cavity losses was high in a "collimated beam" alignment in which the beam was collimated throughout the external cavity. Conversely, for the "focused beam" alignment, the cavity feedback condition was less sensitive to the movements or orientations of the mirrors. Compared with other external cavities, which will be described later on, the plane-mirror cavities were the easiest to set up. This is because the returning light from a plane reflector is more intense so that the beam is more "visible". However, due to the lack of disperse or frequency selective elements, these external cavities do not have the facilities of wavelength tunability. The plane mirror cavity was often used for a quick assessment of the performance of laser diodes to see whether or not they can lase with external feedback. Also, they were used in some cases where the frequency selective elements could not be used or a strong coupling was needed.

4.5b Blazed grating cavities

The purpose of using a grating as an external reflector (fig. (4.8)) is that the optical feedback can be tuned spectrally, as well as restricting the oscillation bandwidth. The procedure for aligning the external grating cavity is the same as that of the plane-mirror cavity, except that the alignment became more difficult because of the weak dispersed-feedback. To overcome this problem, large currents but below the facet damage threshold, were applied to the laser diodes to increase the "beam visibility".

A blazed grating of 600 line pairs per mm was used, its wavelength selectivity (i.e. the spectral window) can be approximated by:

$$\Delta\lambda = \frac{\lambda}{N} \qquad (4-2)$$

where $\Delta\lambda$ and λ are the width of the spectral window and the emission wavelength respectively. N is the number of grating line pairs covered by the beam cross section. For the "collimated beam" alignment in which the beam diameter was normally 2.5mm, the corresponding spectral width is 7.8$\mathring{A}$ at a wavelength of 1.3μm. For the "focused beam", the $\Delta\lambda$ is about 43$\mathring{A}$. Since the light reflected from the grating is dispersed in space and therefore the spectral width will also depend on the apertures of coupling lenses. However, such dependence was found to be very small and in the case of "focused beam" alignment, no spectral selectivity was observed but the lasing wavelengths could still be tuned. Also, similar to the plane-mirror cavity, the stability and losses of the grating cavities were less critical in the "focused beam" alignment.

4.5e Optical fibre grating

The optical fibre gratings were fabricated from a commercially available step-index monomode silica fibre of core diameter 17.5μm which was cemented in a curved groove in a glass substrate (fig. (4.9)) and polished to about two micrometers inside the fibre core. This was followed by spinning a layer of resist (thinned Shipley AZ1350) of 90nm thick on to the polished surface. A two-beam interference pattern at 457.9 nm from an argon laser was then exposed on to the photoresist. A grating pattern was produced on the photoresist after the chemical development. A rectangular aperture mask was then placed in contact with the grating. This would define the length of corrugations within the core during the ion etching process using trifluoromethane. After residual photoresist was removed by ashing in an oxygen plasma, a 80nm thick film of aluminium oxide (n=1.68) was sputter-deposited over the surface containing the corrugations.

The corrugation period, Λ, was set at 449nm which corresponded to the wavelength of 1.3μm in air. This can be calculated using the Bragg equation of $\lambda = 2n_e\Lambda$, where n_e is the refractive index of the core. The wavelength tunability was controlled by placing different index-matching oils over the aluminium oxide layer. Since according to the Bragg condition, the resonance wavelength varies with effective refractive index of the fibre mode.

Figure (4.9) : Fabrication of an optical fibre grating.

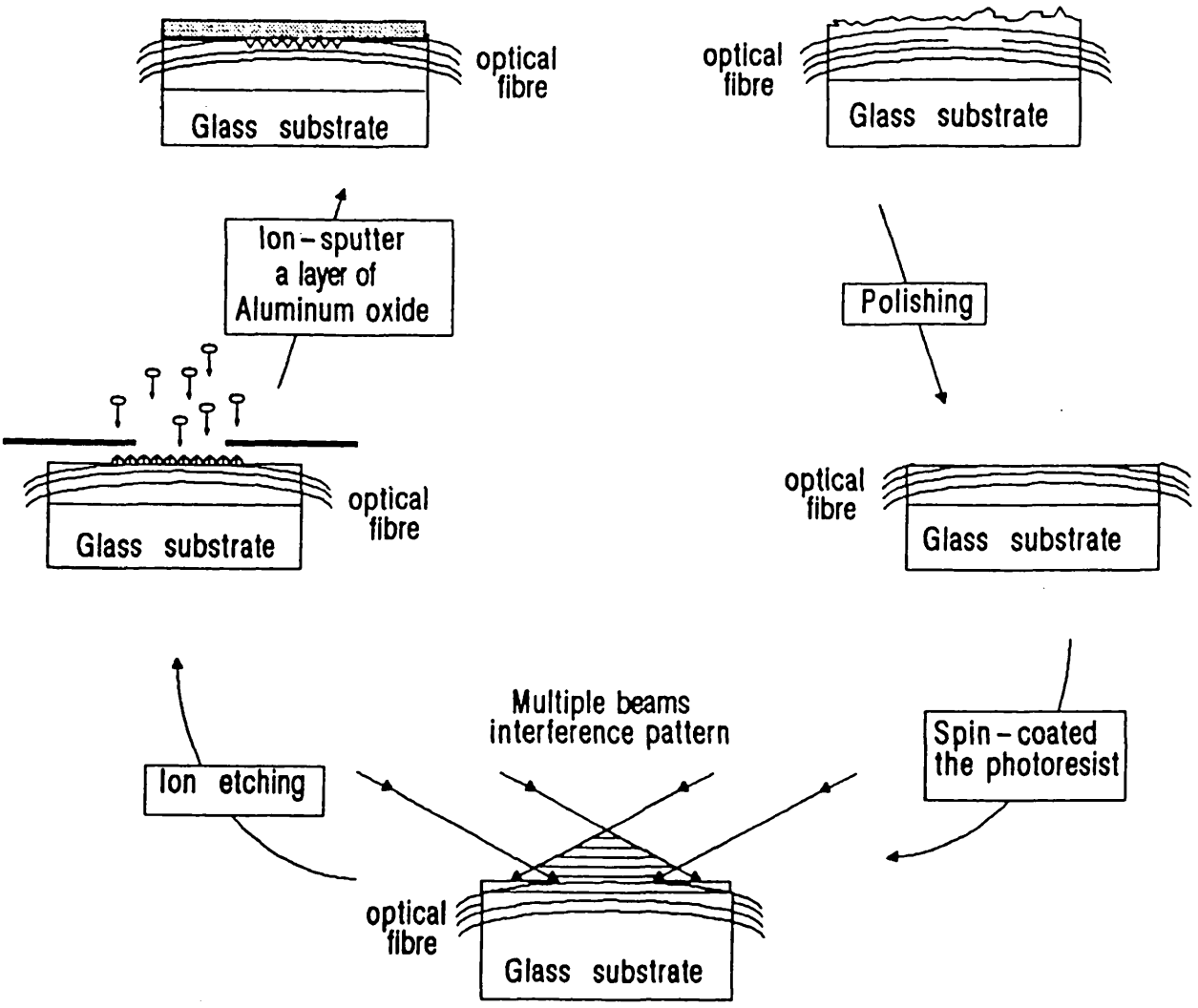

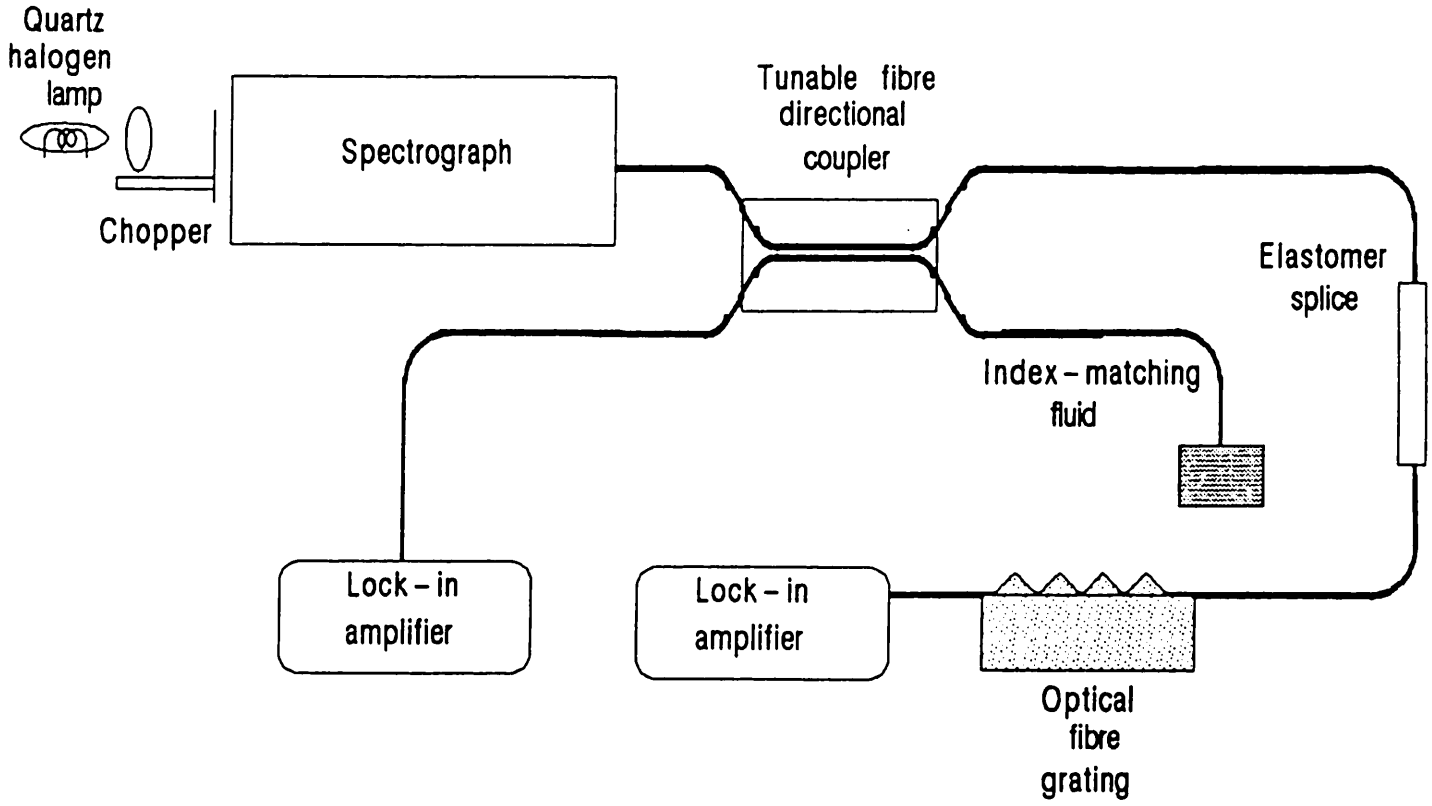

Figure (4.10) : Experiment set-up for characterising the optical fibre grating.

Figure (4.11) : Transmissivities and reflectivities of the optical fibre grating for different index-oils.

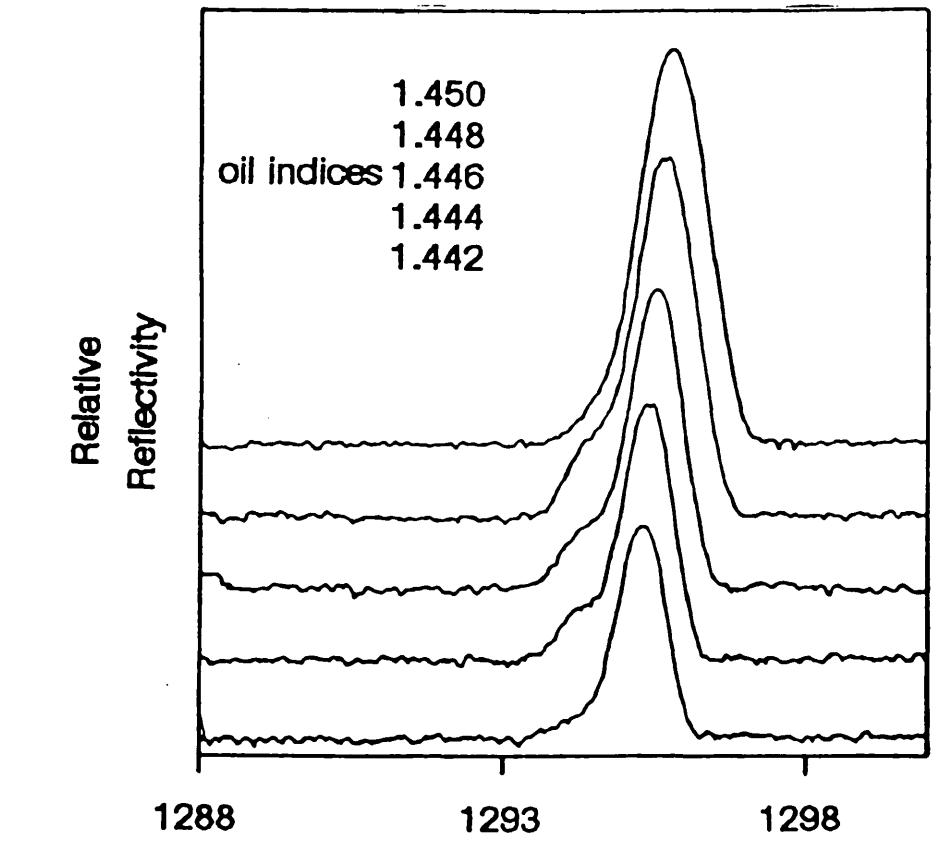

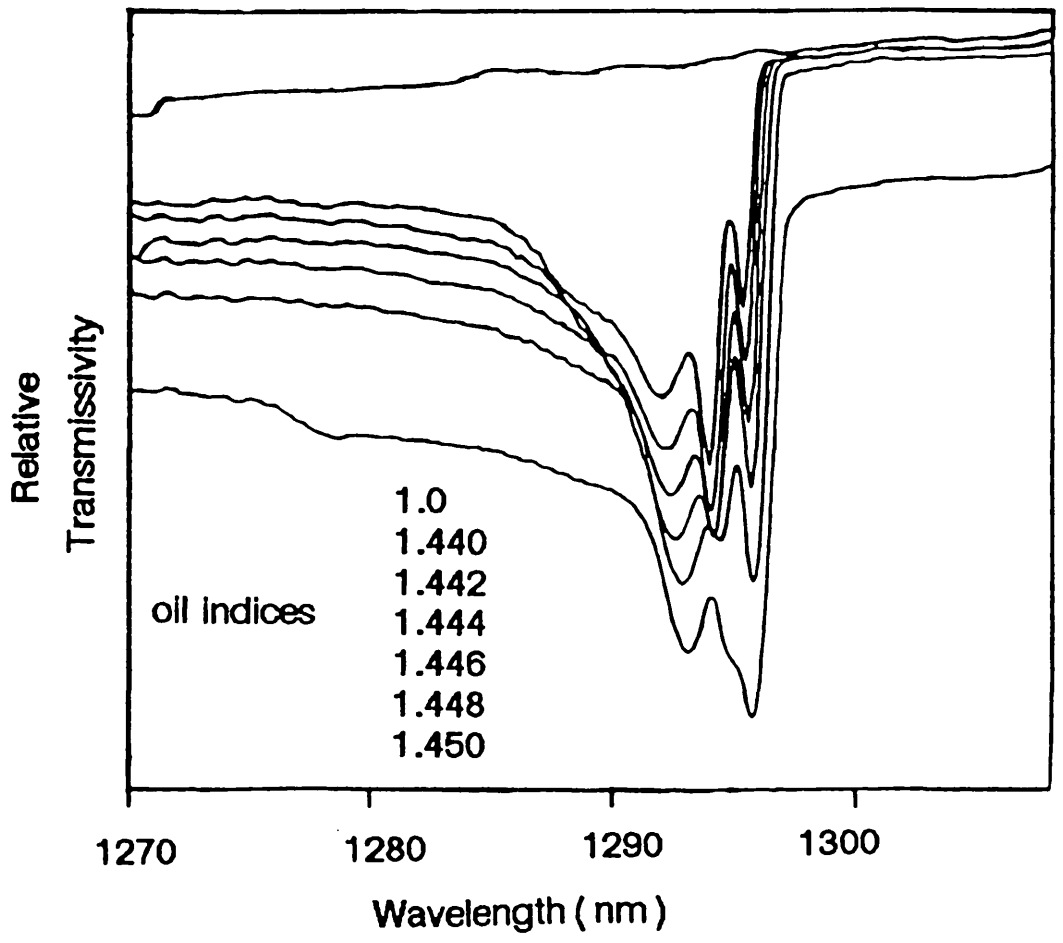

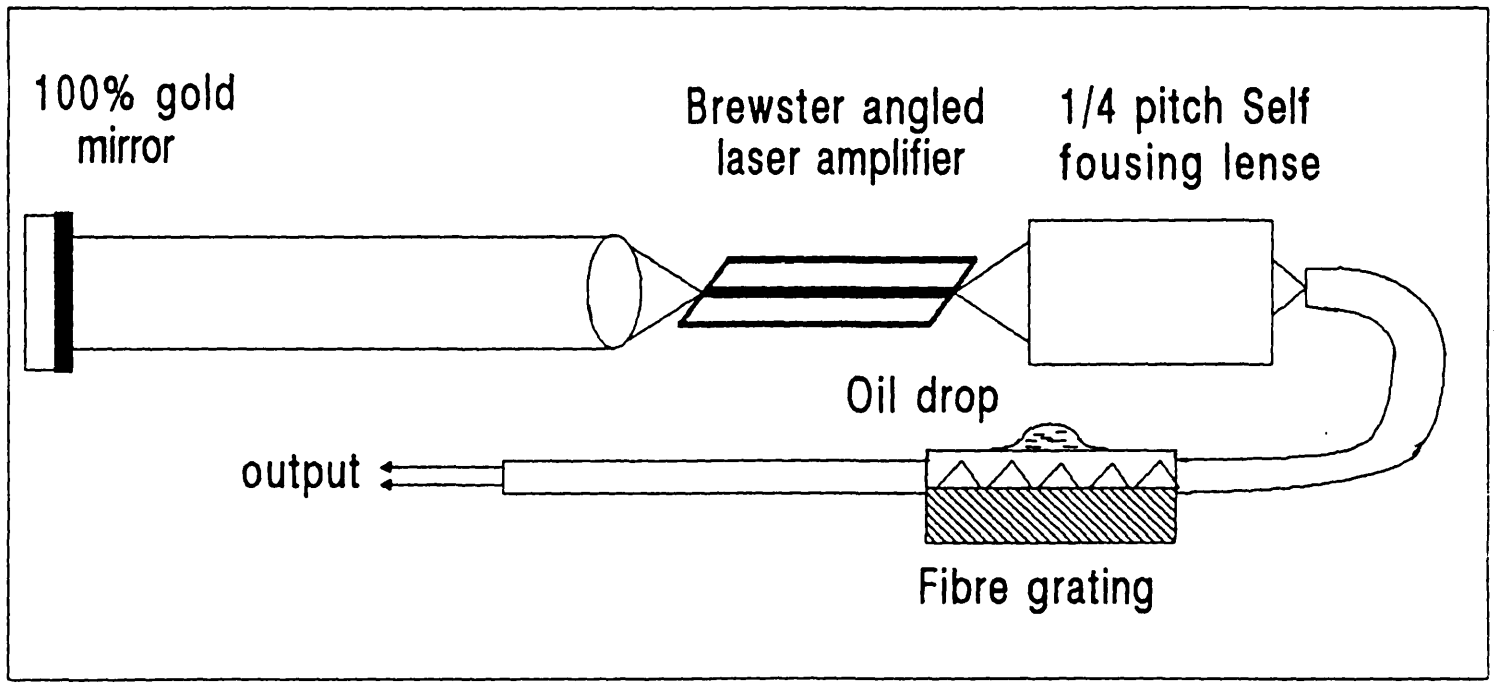

Figure (4.12) : Optical fibre grating cavity laser.

Figure (4.13) : Light output vs currents of the mounted laser diodes.

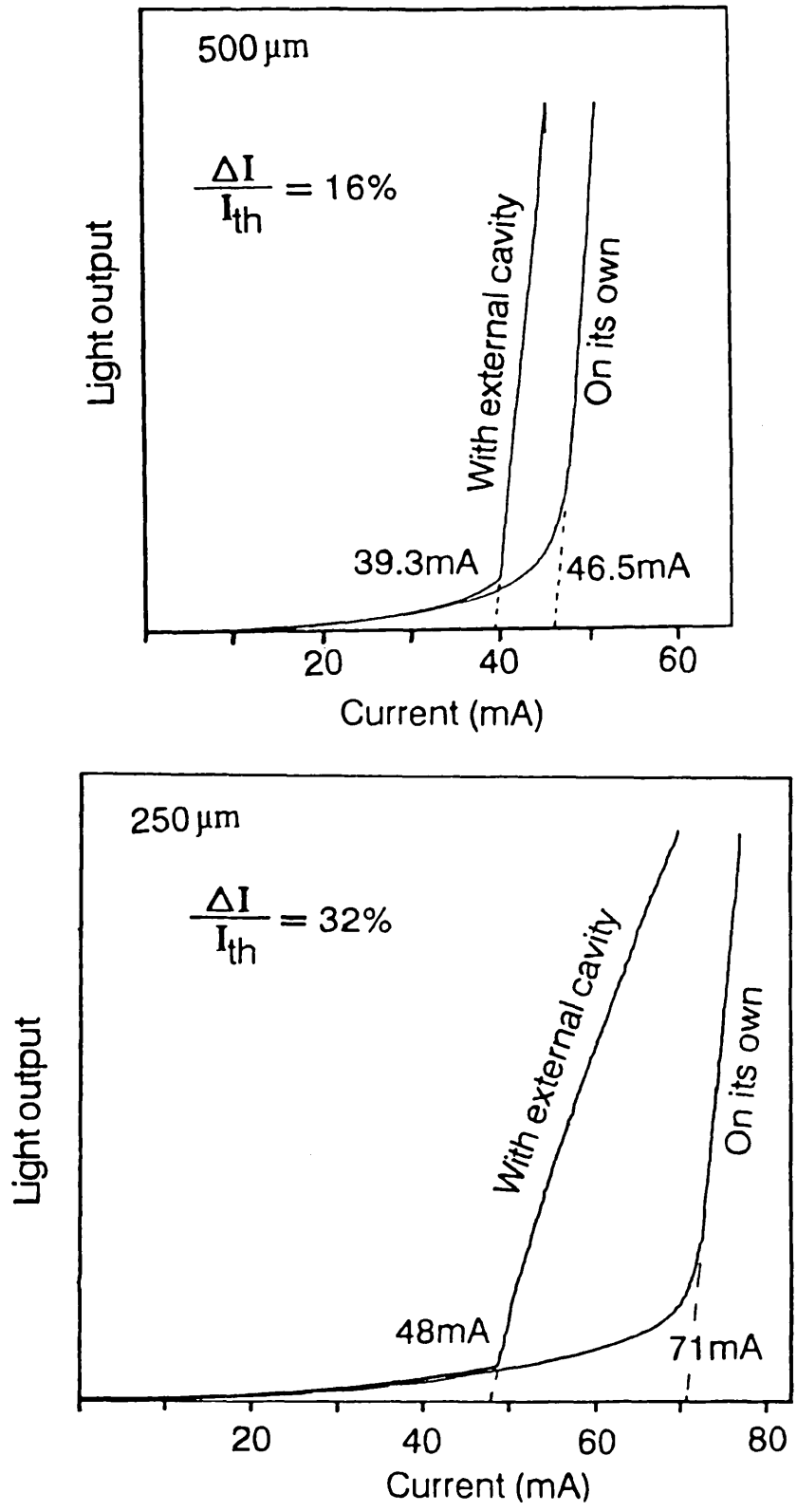

After the fabrication, characterisation on the grating was carried out using a set-up depicted in figure (4.10), in which the light from a quartz halogen lamp was chopped and passed through a spectrograph. The dispersed light from the exit slit was then fed into the fibre which was coupled to one of the ports of a fibre directional coupler using an elastomer splice. Using a directional coupler, both the transmission through the fibre grating and the reflected light were measured simultaneously. A lock-in amplifier was used to enhance the detection sensitivity. The transmissions and reflections for various index-matching oils are shown in figure (4.11). The bandwidth is about 12Å and the reflection coefficient is about 70% for the 1.448 index oil. The reflection peak also shifts toward the longer wavelengths for large indices.

To form an optical fibre grating external cavity (fig. (4.12)), a GRIN lens was used to couple together both the fibre grating and laser. The microscope objectives cannot be used because they do not have equally spaced conjugate focuses. For the GRIN rod lens, the best coupling condition was attained when the laser facet and the fibre end were at the same distance from the rod lens.

4.6 InGaAsP (1.3μm) semiconductor lasers

4.6a Zero degree lasers

The zero degree semiconductor lasers[68] were 250μm long and with 5μm stripes. After the chips were cleaved from the wafers, their light output characteristics were measured by spring-probing the chips with electrical pulses at 5% duty cycle. All the lasers which were used, did not have kinks in their light output curves.

After mounting onto the copper stud, most chips had an average increase of 10mA in threshold currents (fig. (4.13)). An increase of 30mA has also been observed, but in several cases, the mounted chips did not lase at all. The amount of the increased threshold depended inversely on the degree of contaminations, the fractures in the facets, and the poor heat resistance of a badly laid bonding (indium) layer. Therefore, the laser's performance is determined strongly by the mounting process. This is why a strong emphasis was made on the handling and mounting of the laser chip, especially

in getting a good thermal contact between the chip and the heat sink.

The light output characteristics were different from chip to chip even though some chips were from the same wafer. The reason for this was that the quality of the wafer (i.e. the material parameters) was not uniform throughout the whole of its region. Unfortunately, at present, this is still very difficult to achieve because of many processes involved in fabricating a wafer. Another reason may be due to the damages occurred in the mounting process.

The light output curve normally consisted of two parts, the first part represents the amount of spontaneous emissions below the threshold current I_{th}. The second part represents the current dependence of stimulated emissions beyond the threshold. For mode-locking experiments, the requirements are that:

(1) the spontaneous emission and threshold current are low, and

(2) the light output (stimulated emission curve) versus current was steep and linear beyond I_{th}.

The zero degree lasers often lased in multiple axial-modes. This originated from the fact that semiconductor lasers are quasi-homogeneously broadened. Also unlike the D.F.B. or C^3 lasers, these buried infill lasers do not have any built-in wavelength selective elements. However, some lasers did exhibit single mode emissions but as the currents were increased, they then switched back to multi-mode emissions. The measured axial mode spacing was about $10\mathring{A}$ which corresponded to a refractive index of 3.6 for a cavity length of 250μm.

For some lasers, the intensities varied randomly from one mode to another. Such intensity distributions were probably due to optical absorption at electron-traps inside the active region or due to the axial mode competition. Both of these effects are random in nature. In the case of a "snappy" laser, i.e. laser which exhibited very steep stimulated emission slope, current instability in D.C. bias may also cause sporadic intensity distribution of the axial modes.

When the zero degree lasers were coupled to external cavities, reductions in the threshold currents were observed. This is due to the extra optical feedback from the

Figure (4.14a) : Spectra of external cavity zero-degree laser.

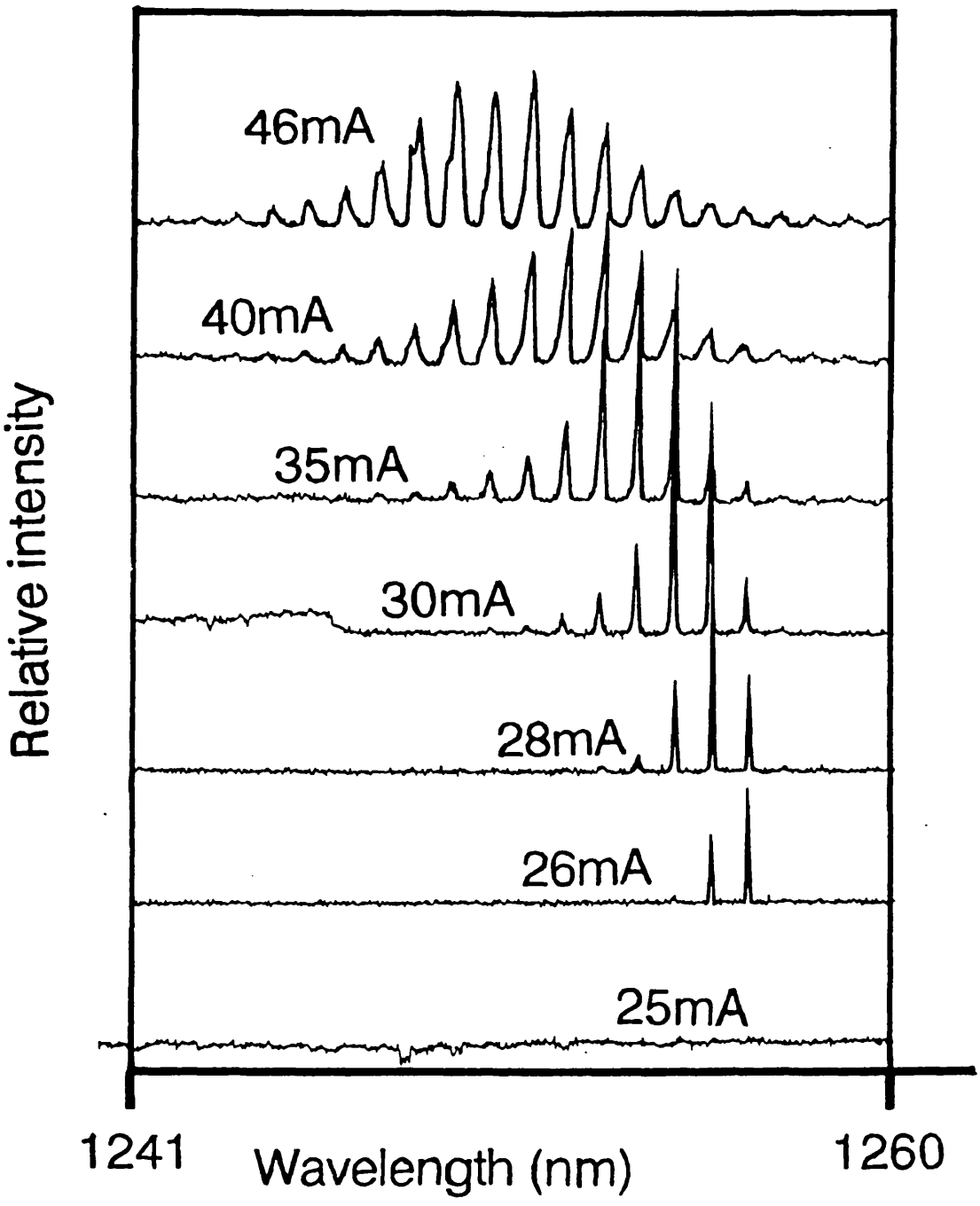

Figure (4.14b) : Spectra of external cavity zero-degree laser.

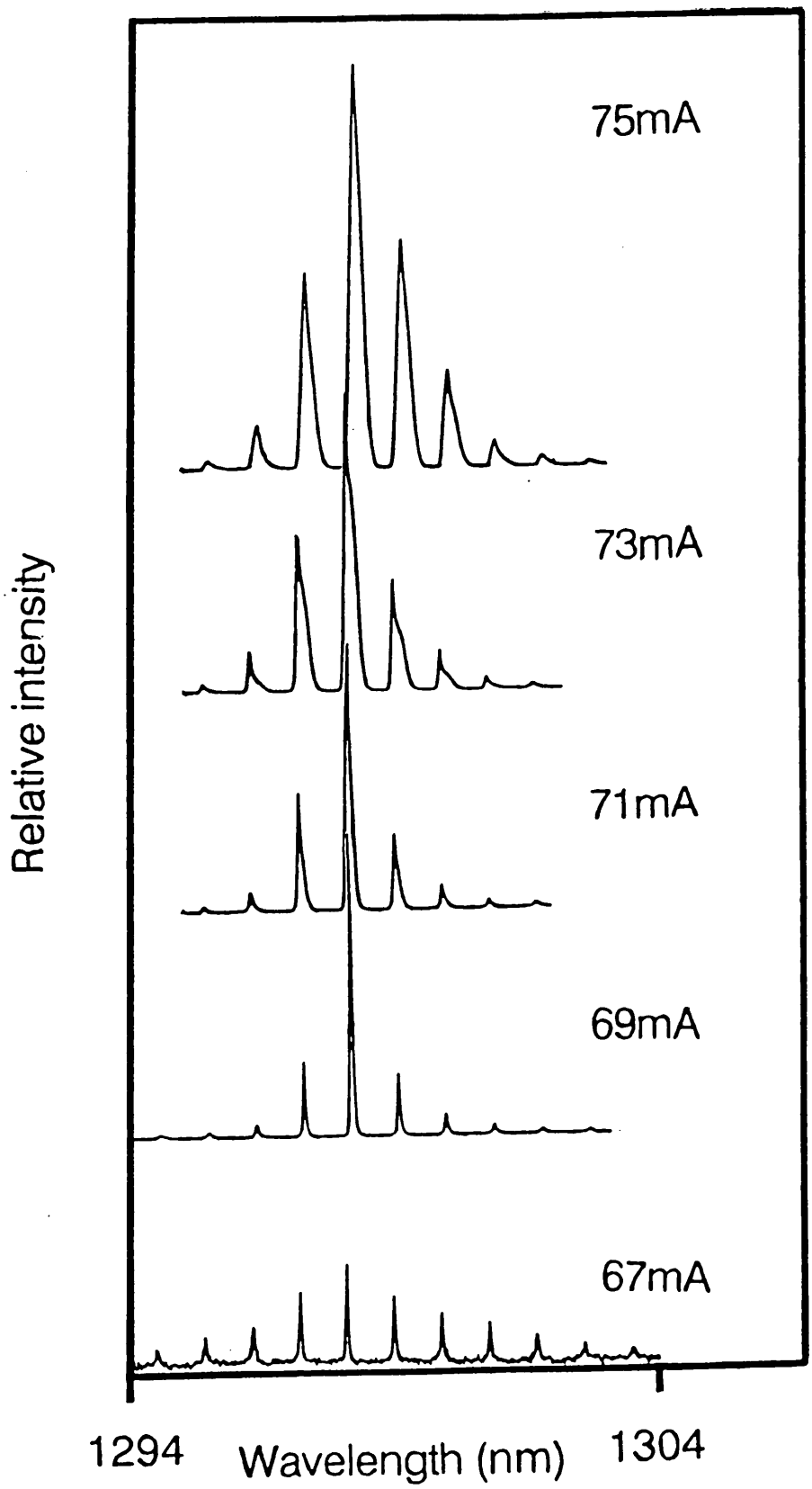

Figure (4.15a) : High resolution trace of the broadened mode-clusters.

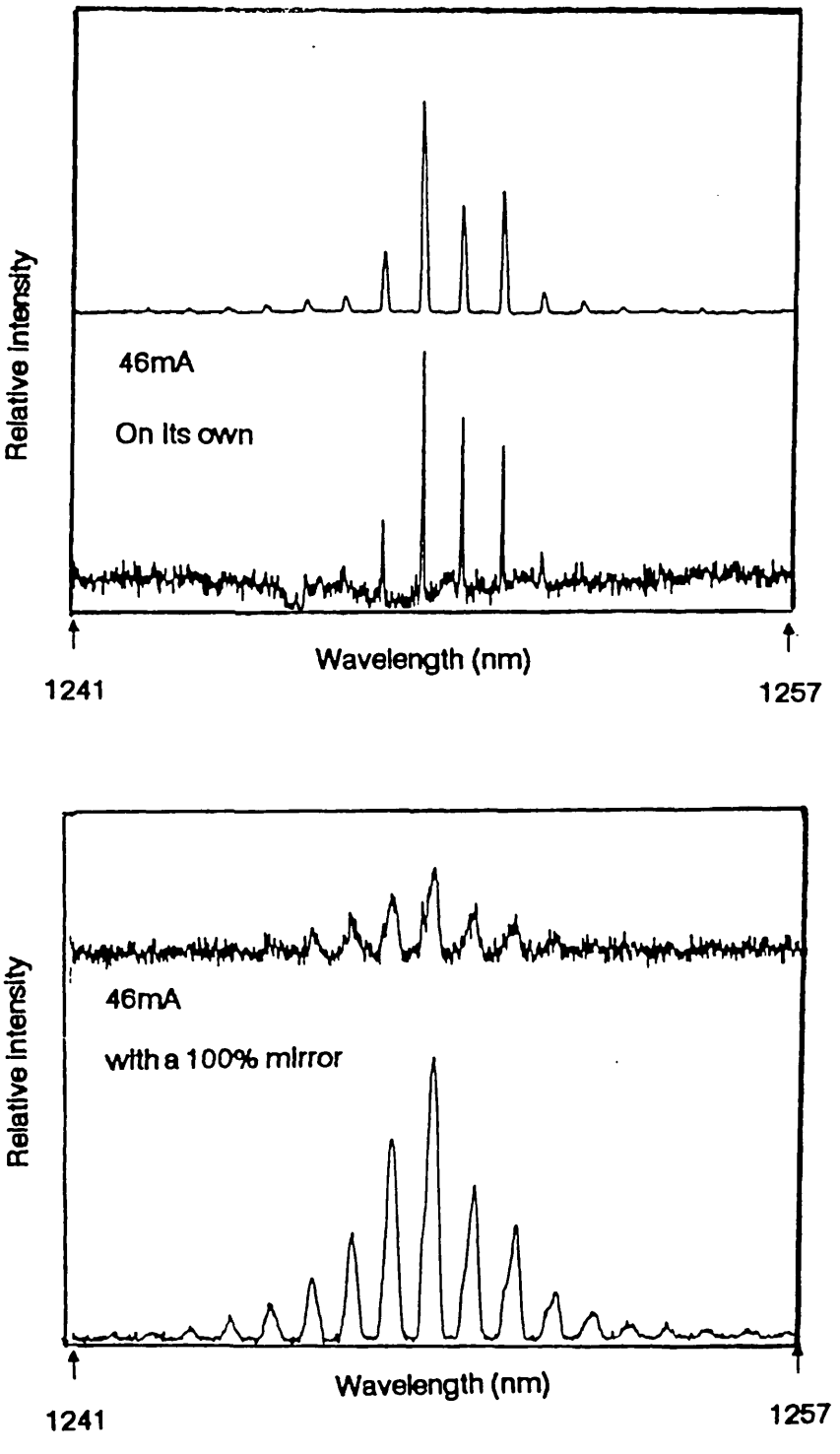

Figure (4.15b) : Spectra of external cavity zero-degree laser for different couplings with the external mirror.

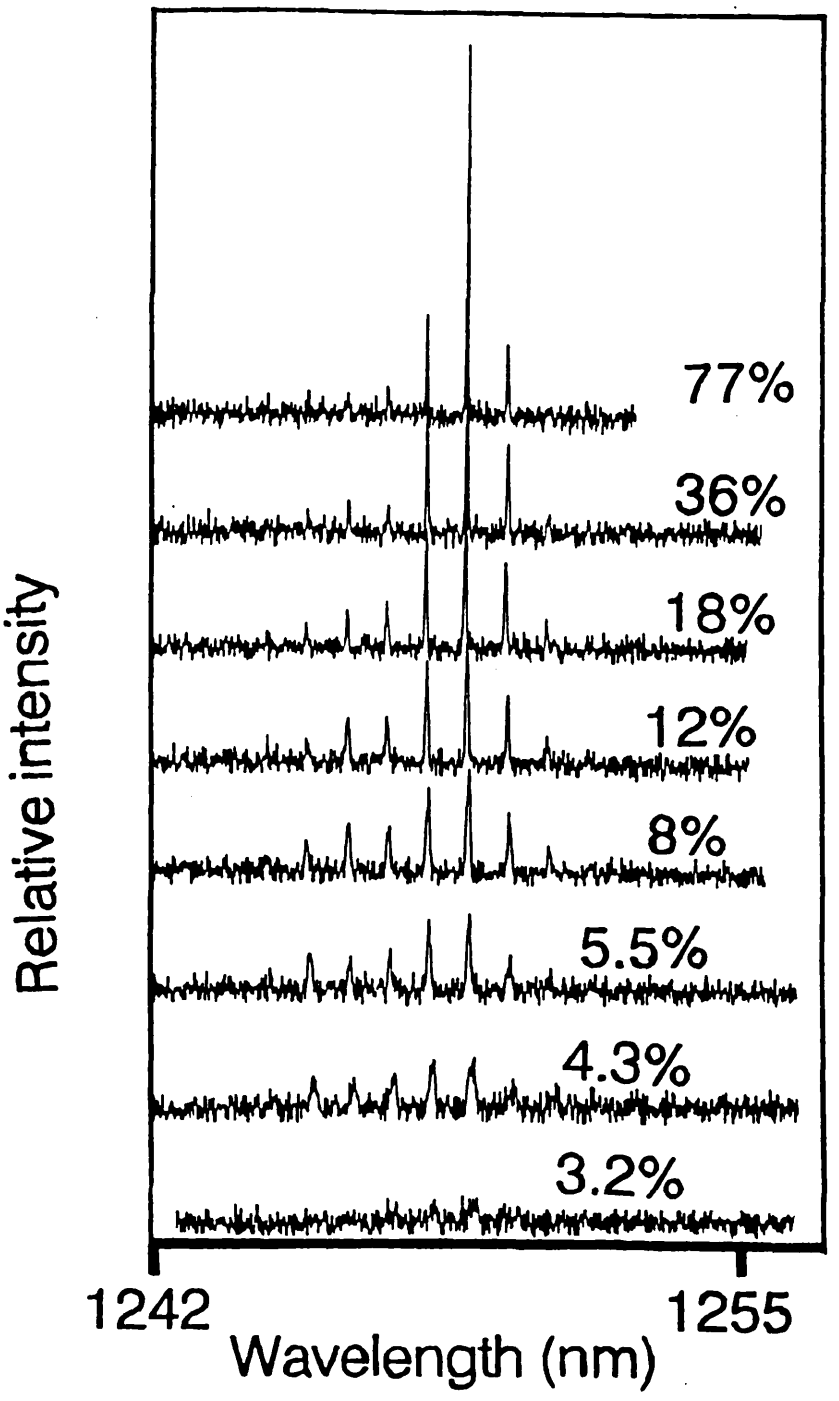

external reflectors which increases the quantum efficiency of the carrier recombinations. As expected, higher reflectivities would further reduce the threshold currents. In some cases, it was also noted that the "new" stimulated emission slope was less steep than that of the laser on its own.

The second interesting feature of an external cavity zero degree laser was the behaviour of the axial modes upon either varying the bias current or reducing the reflectivity of the external reflector. Figure (4.14) shows the spectra of two different external cavity zero degree lasers. When the bias current was just above the "new" lasing threshold, the lasers emitted at longer wavelengths than when they were on their own. As the currents were increased, two significant changes were observed. These were:

(1) the whole envelope which enclosed the mode-clusters shifted towards the shorter wavelengths,

(2) the envelope width as well as the individual clusters were broadened.

The broadening of each cluster was because the higher gain allows more "external cavity" modes to be excited within the cluster. The increase in gain also explains the broadening of the lasing envelope. These broadened mode-clusters were re-scanned at a much higher resolution (fig. (4.15)) and the noisy structures in each cluster can be clearly seen. Since the "external cavity" modes were so close to each other, strong mode competitions are bound to occur.

The dependence of the broadening on external feedback was investigated by placing an attenuator within the external cavity. At the lowest attenuation setting ($T \approx 10\%$), a large broadening was observed along with a wide lasing envelope (fig. (4.15)). When the isolation between the laser and the external cavity was increased, both the lasing envelope and individual mode-clusters seemed to become narrower.

4.6b A.R. coated lasers

Silicon monoxide of refractive index 1.9 was used as the coating material. The

Figure (4.16) and (4.17) : L/I curve of an one-side coated external cavity laser and the lasing spectrum of a two-side-coated external cavity laser.

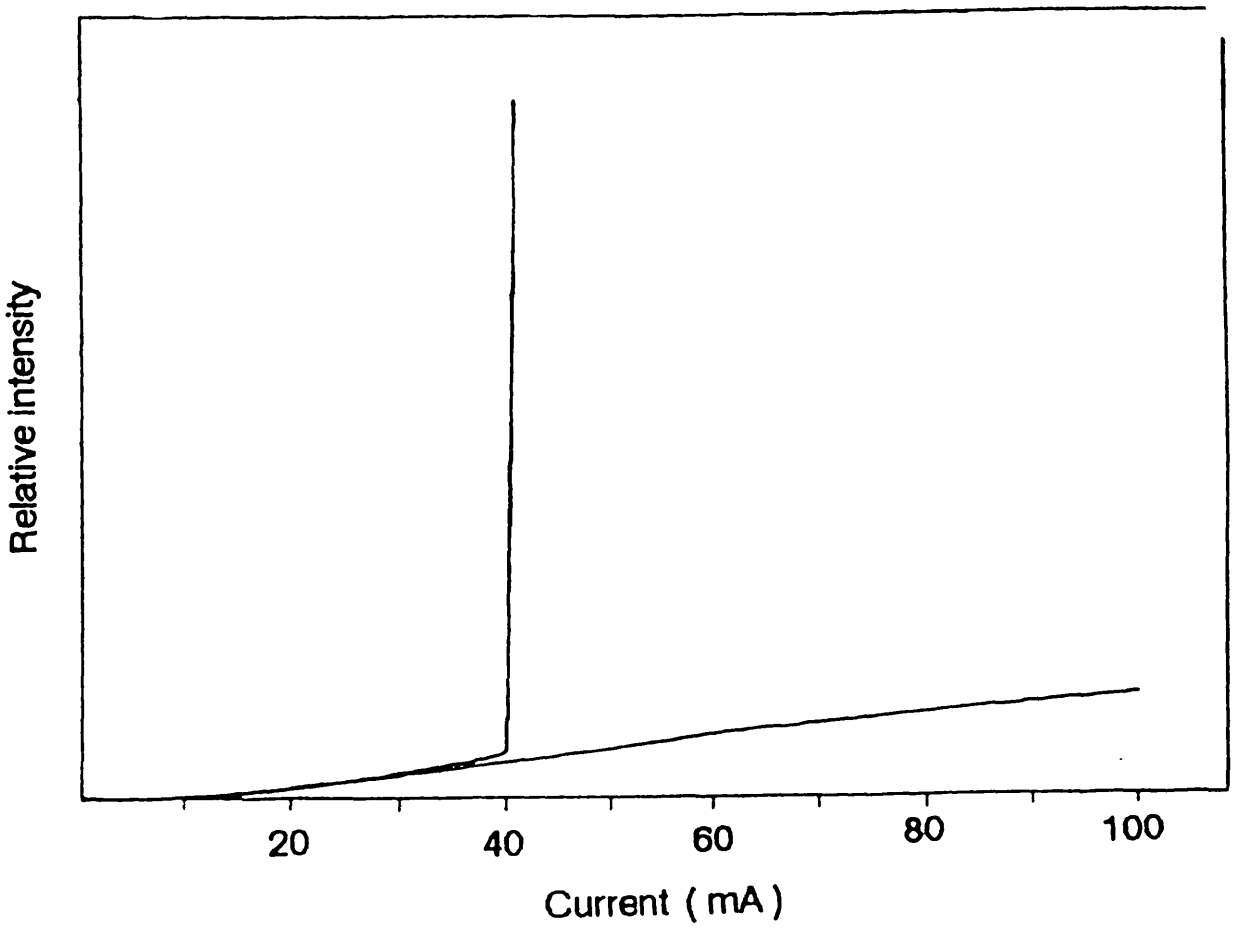

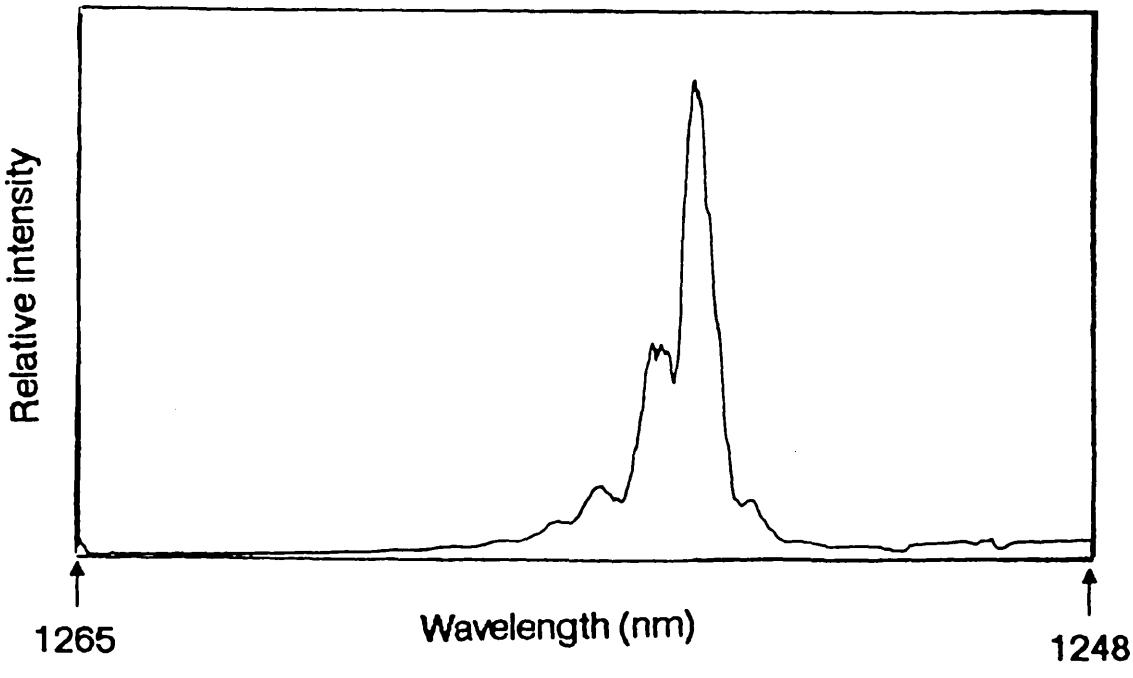

residual reflectivity of the coated facet was estimated to be around 5%. Prior to coating, lasers usually lased at around 40mA. When one facet was coated, self-lasing did not occur within the applied currents upto 100mA (fig. (4.16)). With an external reflector (100%), most of the A.R. coated lasers lased at 60mA and with an additional reflector (50%), the threshold current dropped by another 30%.

Despite the "good" light output characteristics, multiple mode-clusters were observed corresponding to the diodes' length. Thus, the residual reflectivities were still strong. The current dependence was the same as those of the uncoated lasers. In some cases, the clusters were so unstable that they kept changing from one scan to the next, despite all efforts to stabilise the system. A possible reason may be that these lasers are sensitive to the reflective phase changes induced by the A.R. layer.

Another interesting feature was the low spontaneous emission from the A.R. coated facets compared with the Brewster angled facets which will be described in the next subsection. Ideally, there should be more fluorescence emissions from a facet of zero reflectivity than the natural cleaved (R=30%) facet. However, it was noted that for these A.R. coated lasers, the ratio between the fluorescence from the coated and uncoated facets was only about 1:2 respectively. This is probably caused by absorptions within the coating layer. This absorption may also account for the significant increase of the threshold currents of lasers coated on both sides which could not lase with D.C. pumping alone. For these lasers, lasing was only possible if a strong R.F. current was also added. Because of this, It was not possible to measure the light output characteristics. However, scanning the lasing spectrum was still feasible, the results of which are shown in figure (4.17). From the spectrum, it is apparent that multiple mode-clusters still existed even though they have merged together due to the strong R.F. modulation.

4.6c One-side-Brewster-angled (OSBA) lasers

In principle, when the facet of a zero degree laser is polished (or cleaved) at

Figure (4.18a) and (4.18b) : L/I curve of the "good" and "bad" O.S.B.A. laser diodes.

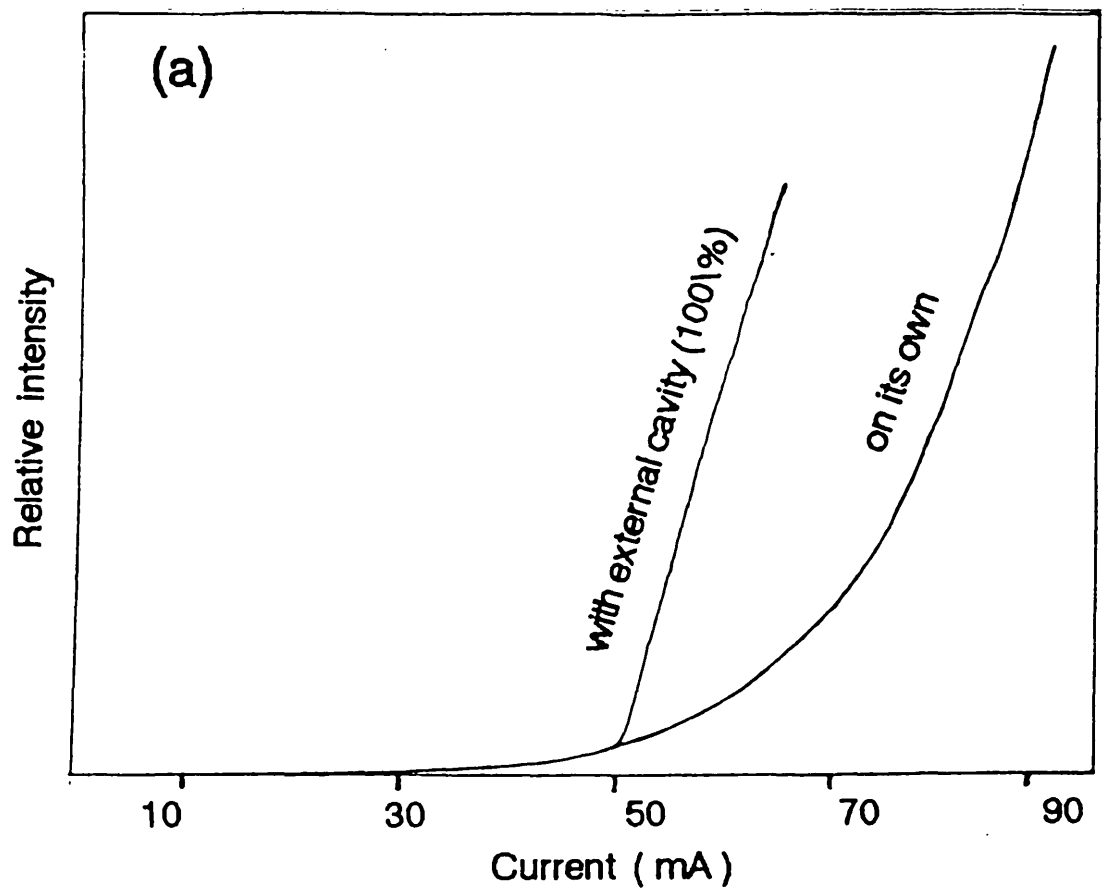

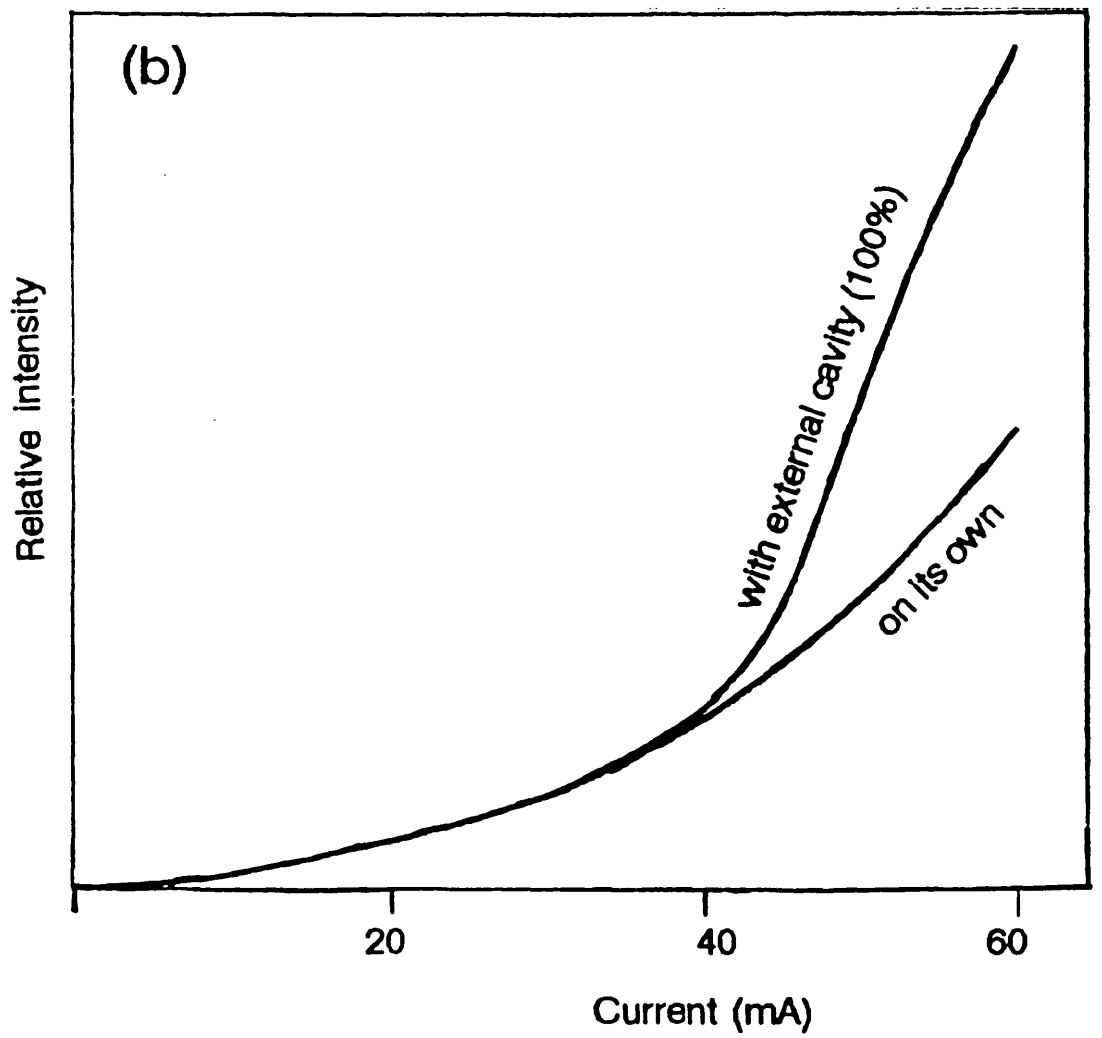

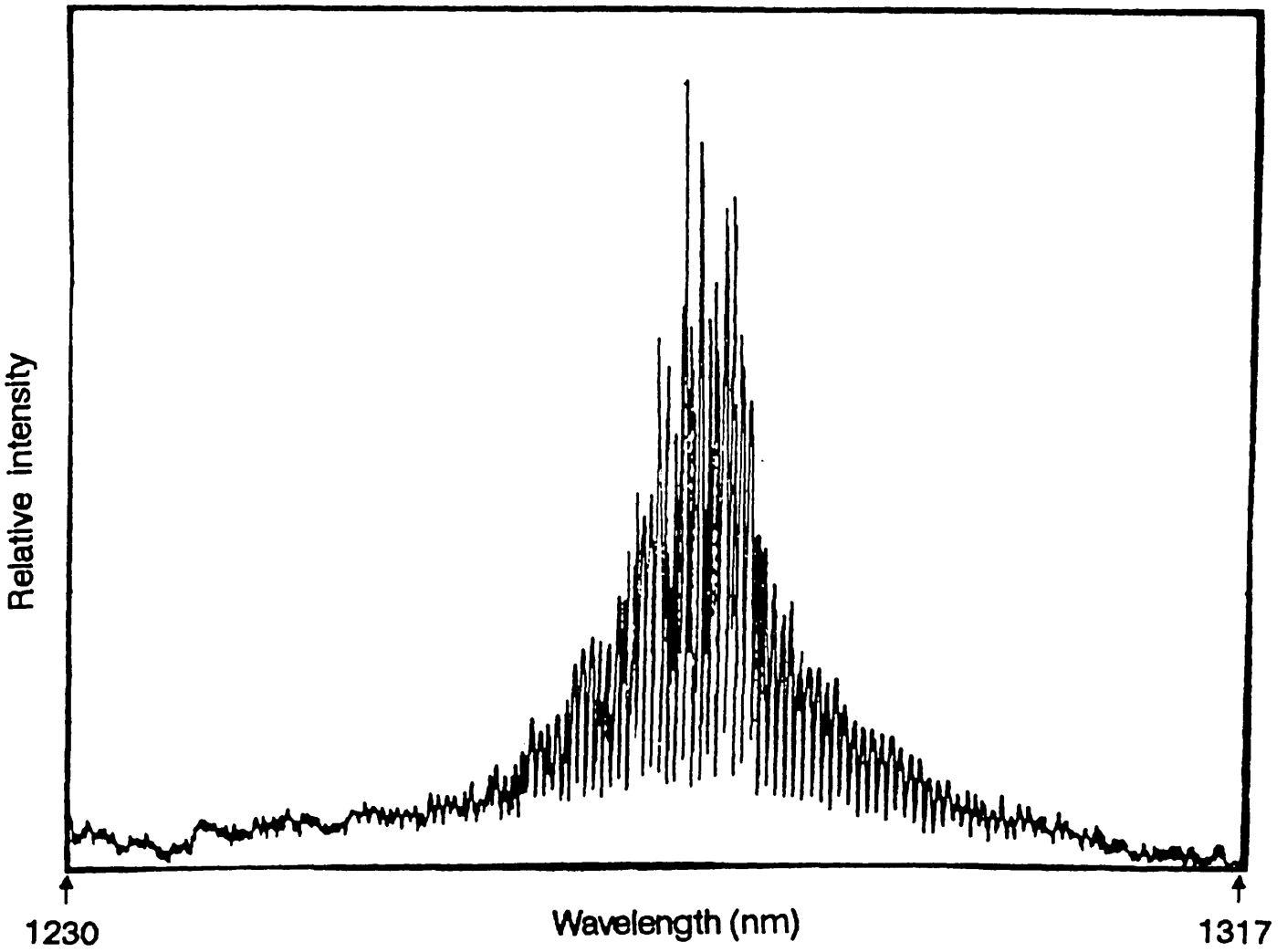

Figure (4.19) : Lasing spectrum of an O.S.B.A. laser.

the Brewster angle, the Fabry-Perot effect will be destroyed, making lasing on its own impossible unless optical feedback is provided by an external reflector. However, in practice, this has not been observed. The main reason could be due to the inherent high optical gain that allows resonance to occur even from the weak back-scattering at the polished facet. Nevertheless, the operational characteristics of the OSBA lasers were different from the zero degree lasers in terms of:

(1) higher self-lasing threshold currents,

(2) lack of a distinguishable "threshold knee" in the light output characteristic,

(3) sharper mode-clusters in the lasing spectra when coupled to external cavities.

The increase of the threshold current is obvious because of the high transmission losses at the angled facets. A few of the polished lasers could not lase even under c.w. pumping conditions. This was probably due to additional losses caused either by damages in the active region near the polished facet, or by damages incurred during the mounting process. The overall losses for these lasers were so high that even with external feedback, they still could not lase. A typical light output characteristic of such a "bad" OSBA laser is illustrated in fig. (4.18), which clearly shows the extra feedback from the external reflectors did not have much effect on the light output curve. For a "good" OSBA lasers coupled to an external cavity, the light outputs behaved like a zero degree laser; i.e. it consisted of a well defined "threshold knee" and a linear "stimulated emission" slope.

For OSBA lasers, a broadening of the "threshold knee" can be explained by the large differences between the facet reflectivities. For a zero degree laser, both cleaved facets have the same reflectivities, i.e. a "symmetrical" cavity; the transition from spontaneous emission to stimulated emission takes place at the point where the gain is greater than the losses within the laser resonator. Whereas for an OSBA laser, the transition is poorly defined due to the large imbalance between the cleaved facet and polished facet reflectivities. At low currents, the OSBA laser just fluoresces like a zero degree laser biased below threshold. As the current is increased, the gain

becomes positive so that the spontaneous emissions reflected from both facets are amplified, i.e. the so called "Amplified Spontaneous Emission (ASE)". However, lasing is still not possible until the gain is high enough to sustain the oscillations of any stimulated emissions (i.e. standing waves) within the cleaved and polished facets. Therefore, unlike a zero-degree laser, the light output curve of an OSBA laser consists of three parts: spontaneous emission, amplified spontaneous emission, and stimulated emission.

Figure (4.19) shows the lasing spectrum of an OSBA laser operating on its own. Here a large number of axial modes were excited probably due to a mixture of A.S.E. and stimulated emissions. The modes were very unstable which may be due to a gain competition between the two recombination processes. When it was coupled to an external reflector, the lasing peak shifted towards the longer wavelengths as compared with before. Also, the overall lasing bandwidth became much narrower and the modes were more stable than before, i.e. the recombination of the injected carriers was dominated by the stimulated emission process.

For external cavity OSBA lasers, the feedback was provided by the cleaved facet and external reflector. Multiple mode-clusters which corresponded to the diode length (i.e. between the cleaved and polished facets) were seen in the lasing spectra. These clusters were in fact the modulated "external cavity" modes. This spectral modulation was due to the interferometric effect of multiple reflections between the cleaved facet ($\approx$30%) and the polished facet where the reflections are caused by dust particles and by the surface roughness.

Using an external grating with the "collimated" alignment, one of the mode clusters could be selected (fig. (4.20)). The tuning range was typically 32nm which increased with the biased currents. Due to the existence of the mode clusters, the wavelength tunability could only be carried out by discretely selecting one cluster to another, instead of a more desirable continuously tunable selection.

4.6c Both-side-Brewster-angled (BSBA) lasers

Figure (4.20a) and (4.20b) : Lasing spectra of an O.S.B.A. laser coupled to a mirror and grating respectively.

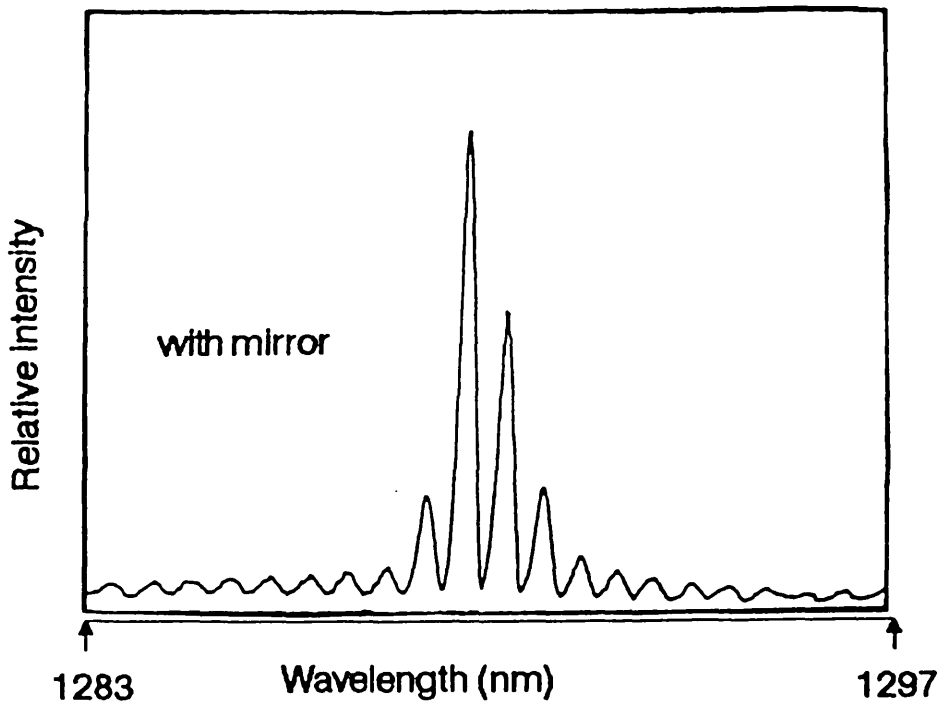

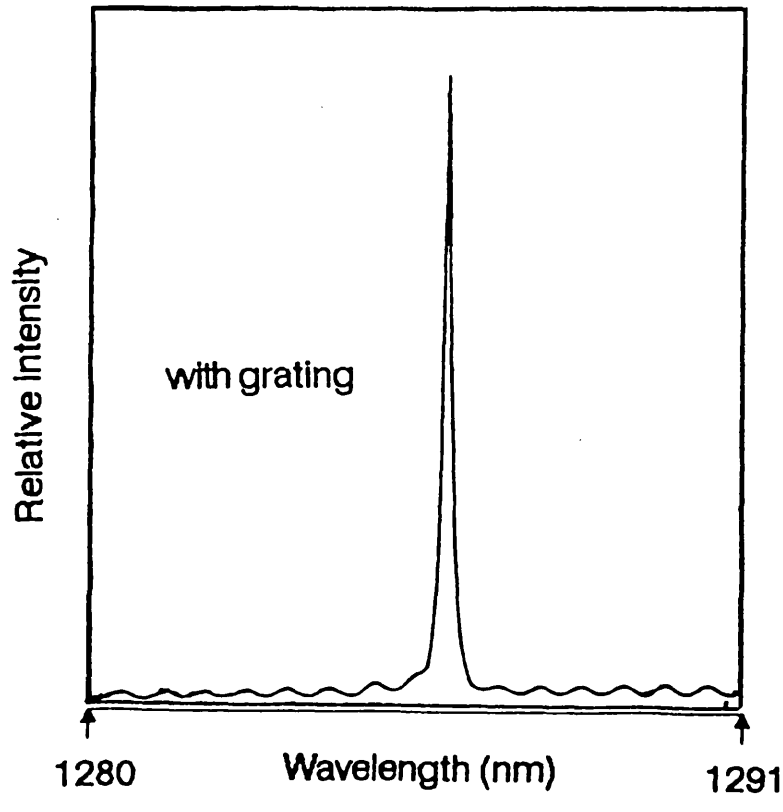

Figure (4.21) and (4.22) : L/I curve and flourescence spectra of a B.S.B.A. laser diode respectively.

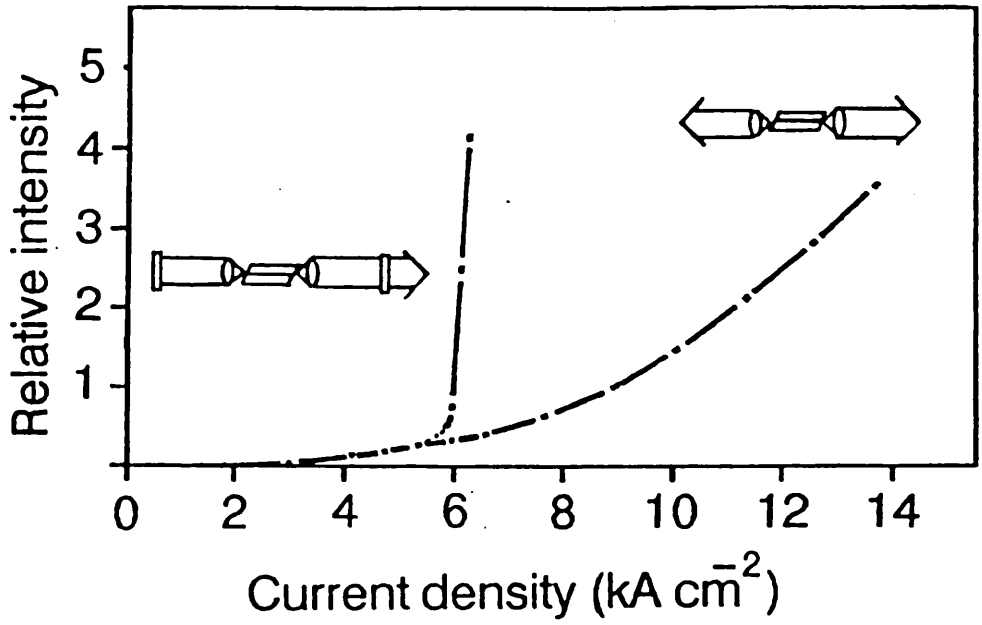

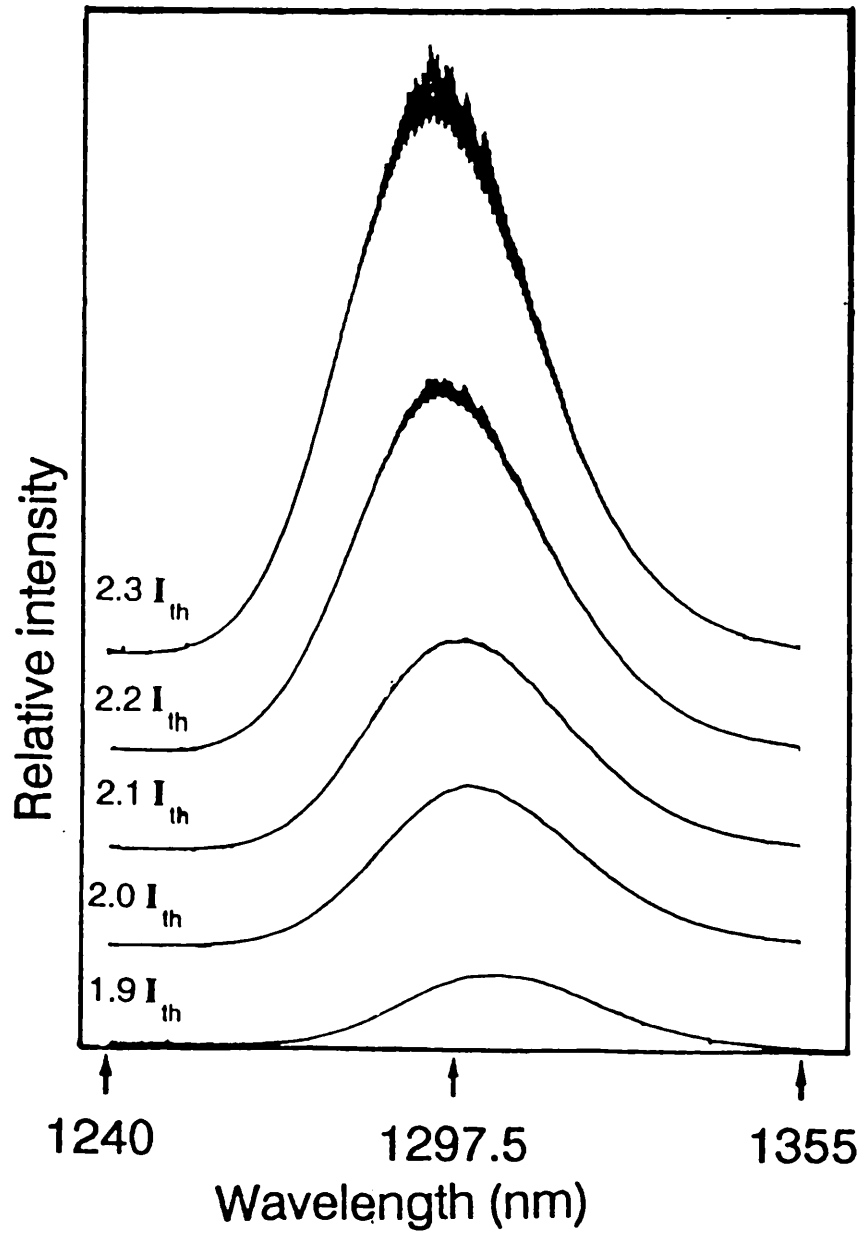

Figure (4.23) : Lasing spectra of an external cavity B.S.B.A laser near the threshold currents.

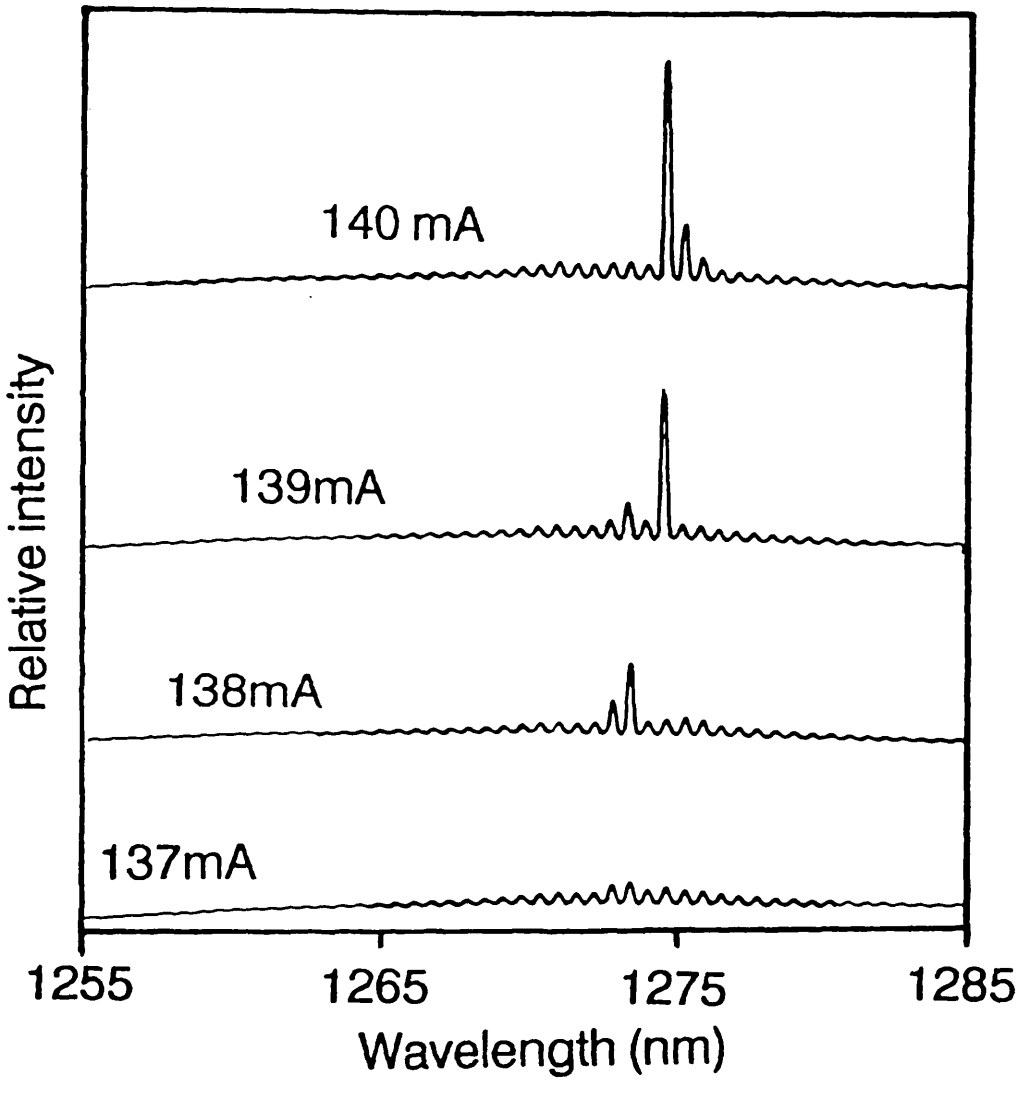

Figure (4.24) : Lasing spectra of an external optical fibre grating B.S.B.A. laser.

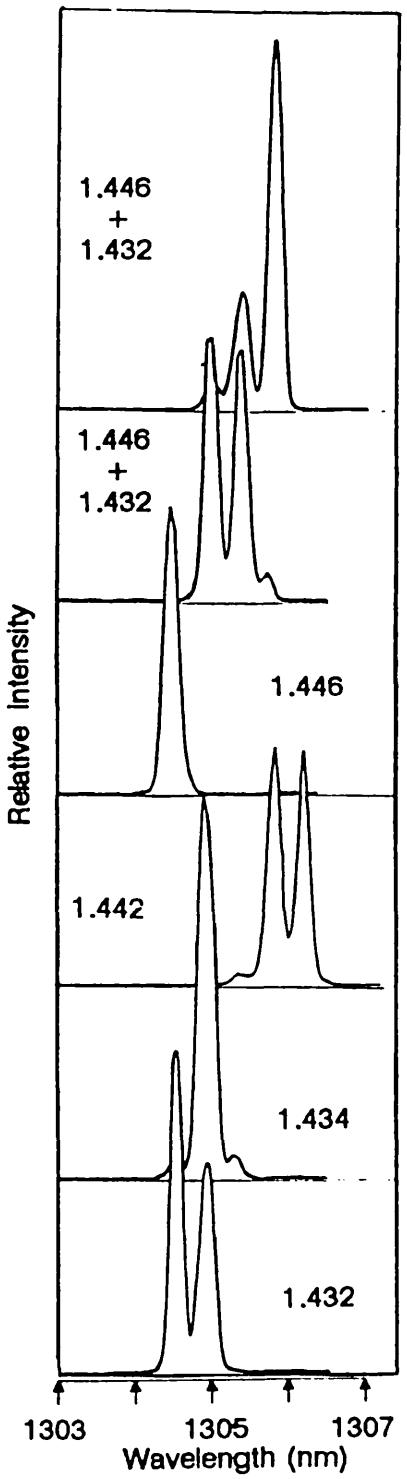

Figure (4.25) and (4.26) : Lasing spectra of an external optical fibre grating B.S.B.A. laser using other types of index-matching fluids and for various currents respectively.

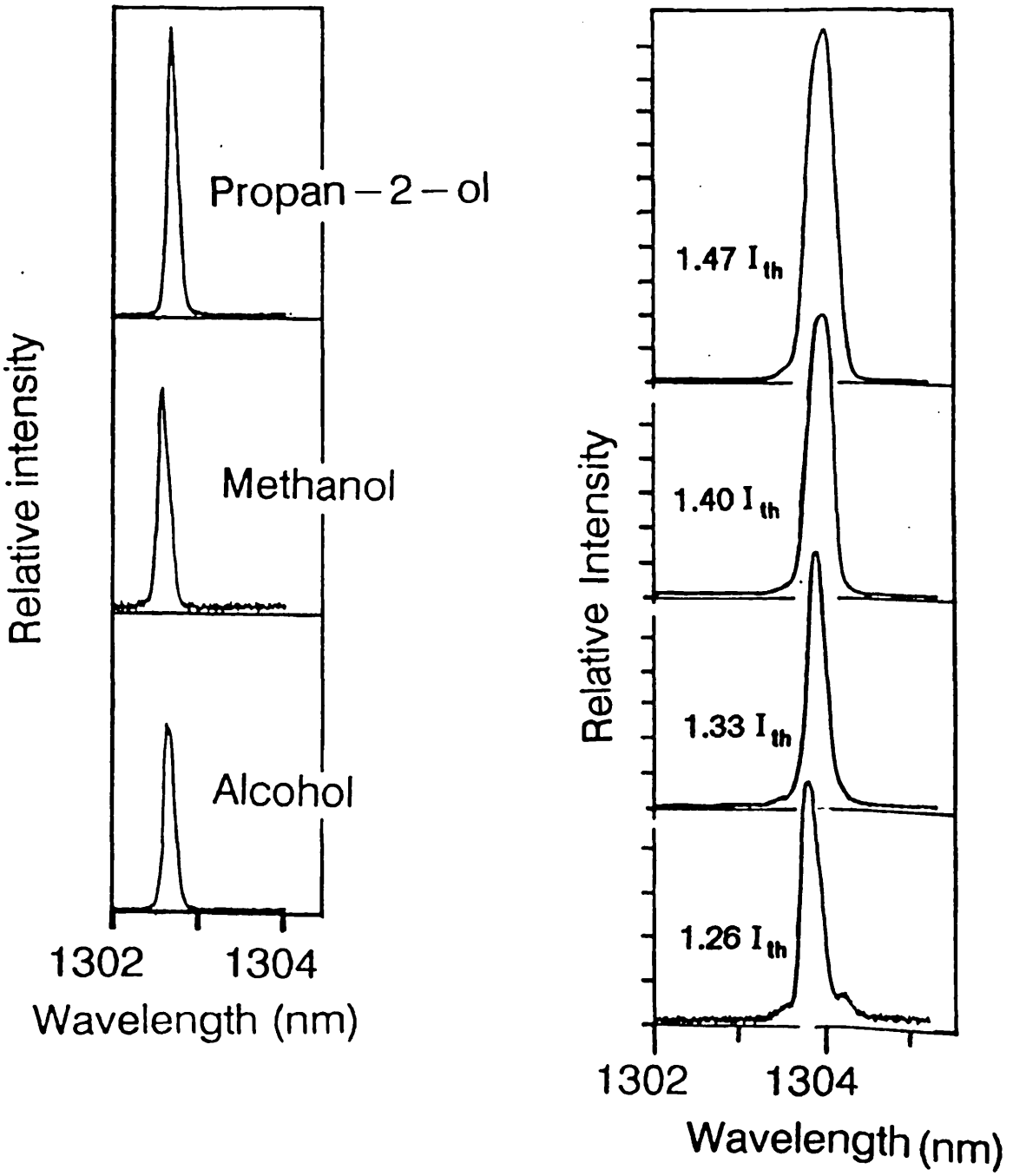

While characterising OSBA lasers, it was found that even though the self-lasing threshold has been significantly suppressed, the "diode cavity" effect still persisted producing mode-clusters in the lasing spectra. Initially, it was thought that the net transmission losses due to the Brewster angled facet was not strong enough to suppress the resonance effect; and that if both facets were to be Brewster angled then the cavity effect would be severely reduced or completely eliminated. At least, in principle, this should be the case. However, investigations have shown that the BSBA lasers still possessed the internal resonance which eventually led to lasing in multiple mode-clusters when coupled to an external cavity.

On its own, a BSBA laser diode could not lase even when biased at twice the threshold current of a zero degree laser of equivalent length. This was verified by both the light output characteristics (fig. (4.21)) and the fluorescence spectra at various biased currents (fig. (4.22)). Note that the light output curve resembled that of the light emitting diodes (LED) and the widths of the fluorescence spectra remained the same for various currents. If the BSBA lasers were able to lase on their own, the fluorescence spectra would have sharpened with increasing currents. Also sharp axial modes would have been observed above the threshold. It was noted that, similar to OSBA lasers, the fluorescence peaks from the BSBA lasers were also shifted toward shorter wavelengths with increasing currents.

Despite a good suppression of the self-lasing induced by the two Brewster angled facets, these BSBA lasers still showed some weak resonance effects corresponding to reflections at both polished facets. As mentioned before, these residual reflections may be caused by optical scattering. From the facets, the weak resonance effect clearly manifested itself in the fluorescence spectra, in which small intensity modulations appeared around the fluorescence peak especially at high biased currents (fig. (4.22)). By providing external optical feedback, the weak resonant modulations evolved into multiple mode-clusters.

A single mode-cluster was sometimes observed at bias currents just above the

threshold current. Figure (4.23) shows the evolution of the lasing spectrum from a two-mirror cavity (100% and 50%) BSBA laser in which a single dominant cluster was formed just above the threshold. The single cluster also shifted slightly towards longer wavelengths with increasing currents.

Using a wavelength selective element such as an optical fibre grating allows the selection of a single cluster. Figure (4.24) shows the spectra of both the single and multiple clusters from such an external cavity BSBA laser. The average bandwidth (or spectral window) of the grating was about 12Å compared to the diode's F.S.R. of 5Å for a 500μm diode. This is why the multiple clusters (three clusters at the most) were excited whenever the spectral window was not centred on a mode-cluster. Wavelength tunability was controlled by using different index-matching oils (fig. (4.25)) though chemical solvents such as alcohol, and acetone (fig. (4.26)) were also used as index-matching liquids.

For the emission of a single mode-cluster, an increase in currents increases the cluster intensity (fig. (4.26)) and broadens the cluster linewidth. This is simply due to the increase of available optical gain allowing more "external cavity" modes to be excited in each cluster.

4.8 Conclusion

Lasing characteristics of zero-degree, A.R. coated, and Brewster angled laser diodes have been discussed. The main emphasis were on both the spectral and intensity outputs. Multiple mode-clusters have been observed for all the tested lasers. Although Brewster angled lasers cannot lase on their own, but when coupled to an external cavity, emissions in multiple clusters were seen. The clusters separation corresponds to the length of the laser, i.e. they are caused by reflections at the facets. These reflections are possibly the back-scattering due to dust particles and surface roughness. Nevertheless, single clusters can be obtained either by biasing the lasers just above the threshold currents, or by using a wavelength selective element (e.g. grating). But

due to the diode's resonant effect, wavelength tunability can only be carried out by discretely selecting one cluster to another. Ideally, if the facets' reflectivities were zero, then the lasing wavelengths can be selected continuously across the whole gain bandwidth. At present, continuous wavelengths tunability in semiconductor lasers still has not been achieved, not even those workers [13,15,36] who have claimed to have completely eliminated the facets' reflectivities.

It seems that the intrinsic problem of getting zero reflectivities is the high optical gain of semiconductor lasers. Since high optical gain can cause a large build-up of the residual reflections they propagate through the gain medium. Thus, the obvious approach would be to minimise such a continuous amplifications. One solution is to use a long ($\approx$1mm or longer) Brewster angled laser diode, which has three split metallic contacts. The centre contact is used for injecting electrons into the active layer and gives rise to the gain region. This gain region is the only part of the laser which is responsible for lasing. The applied currents through the two outer contacts are adjusted such that the active layer below them acts as absorber (just below the threshold of transparency of semiconductor materials). Therefore these absorbing regions act as "buffer" zones to shield off any unwanted residual reflections (occurred at the facet) back into the gain region.

CHAPTER FIVE

Principles of mode locking of semiconductor lasers

5.1 Introduction

Intensive theoretical work on dye and solid state lasers had already been conducted before the first successful mode locking experiment of a semiconductor laser. Since the nature governing the lasing action for semiconductor lasers is different from other laser systems, the search for new theoretical models was needed. At the time of writing, there were no fewer than ten theoretical papers on this subject. These investigations can be grouped into three types. These are:

(1) the time analysis: in which the effects of pulse shaping are studied in the time domain and the spectral mode distribution is ignored. A steady state temporal equation is formulated so that the effects due to all cavity elements balance out with each other, and its solutions define the peak pulse power, the phase of the pulse relative to the pumping modulation, and the pulse width.

(2) the spectral analysis: which starts with the generation and coupling of an axial mode to its neighbouring modes caused by gain or loss modulation. Effects on the spectral distribution of a pulse due to elements of the cavity are formulated in terms of spectral dependence. Once again, a steady state equation is deduced for a zero net pulse shaping effect and the pulse parameters are calculated by solving the equation.

(3) the rate equations analysis: in which the mode locking mechanism due to the interaction between the photon and injected carrier densities within the active

region is considered. This interaction of photons and electrons is described by two simultaneous, first order time derivative, nonlinear differential equations which can only be solved numerically. The numerical iteration stops whenever the change in pulse shape after each transit through the cavity is smaller than an initially imposed tolerance.

In this chapter, the formation of cavity modes and general concept of mode locking will be discussed. This is followed by the above three analyses and an examination of the various boundary conditions as well as their validity.

5.2 Cavity modes

Cavity modes are defined as the quantised states of a cavity in which resonance can occur. There are two types of cavity modes. One is called axial or longitudinal modes which basically result from the standing wave criteria and thus, strongly depend on the optical length of the cavity. The other type of modes are called transverse modes. These depend strongly on the spatial geometry of each reflector in the cavity, since a transverse mode can only be formed if the reflected wave front matches its incident counterpart along every point of the cavity. An ideal fundamental transverse mode has a gaussian distribution and higher order modes always have at least one intensity minimum. The presence of these higher order modes is due to the large cavity volume in comparison to the wavelength. First generation laser diodes usually emit in higher transverse mode, especially under strong pumping, which is mainly due to the wide active stripe. Nowadays, stripe widths down to 3μm can be readily achieved with high resolution lithography which restricts the transverse mode to the fundamental gaussian distribution.

For a zero order transverse mode, the wavelength of the axial mode can be written as:

$$\frac{m\lambda}{2} = nL \qquad (5-1)$$

where nL is the optical length of the cavity. This equation basically implies that at

resonance, the optical length of the cavity must be able to fit an integral number of half wavelengths and the mode separation is expressed as:

$$\Delta\nu = \frac{c}{2nL} \qquad (5-2a)$$

or

$$\Delta\lambda = \frac{\lambda^2}{2nL} \qquad (5-2b)$$

In practice, not all the modes can be excited simultaneously when a laser gain medium is inserted into the cavity and only those modes which are encompassed within the gain bandwidth can be excited. There is also a dependence on the nature of the gain medium. For an inhomogeneously broadened gain medium, in which every atom emits radiation independently, no correlation exists between the gain in each mode so multi-mode emission is possible, and an increase in pumping above threshold will cause the spectral hole-burning. In a homogeneously broadened gain medium, the indistinguishable nature of the atoms leads to the formation of strong mutual interactions between the individual modal gain, so if lasing occurs at one particular wavelength, the gain in other wavelengths will be automatically drained in order to maintain lasing action and therefore, in principle, there should only be one axial mode excited. Semiconductor lasers are known to have quasi-homongeneously broadening characteristics, i.e. a combination of the two broadening effects. It was found that only a single mode can be excited just above the lasing threshold because of the homogeneously broadening effect. But at large injection levels, the gain becomes a partial inhomogeneously broadened medium so that multi-mode emission is possible. In the case of an external cavity semiconductor laser, these multiple axial modes become the multiple mode-clusters.

5.3 General concepts of mode locking

Mode locking, as explained by its name, is to force the laser's axial modes to oscillate simultaneously, i.e. to lock together the relative phases of every mode. The two most common ways of forcing the modes to oscillate in phase are the passive and

active mode locking. The former technique requires an intracavity saturable absorber such that its absorption bleaches at high intensity, i.e. only the intense intracavity flux can circulate with the cavity, while the weak flux will get absorbed by the absorber. Thus, due to this pulse shaping effect, a short and intense pulse will form itself after many transits through the cavity. The corresponding axial modes are then said to be passively locked without any external intervention. Active mode locking on the other hand, requires an active modulation of either the cavity gain or cavity loss in order to force each mode to interfere with its neighbouring modes and hence, the mode locking mechanism is introduced externally.

5.4 Review of various mathematical models

5.4a The time analysis

In the time analysis, the derivation of a mode locked pulse is always expressed in the time domain. The pulse shaping effect on the pulse profile due to each intracavity element (fig. (5.1)) such as the gain medium, saturable absorber etc, are also formulated in the time domain. At the steady state condition, the overall effects due to all the intracavity elements must balance out with each other such that the pulse shape remains unchanged after each transit through the cavity.

A well known time analysis for the actively mode locked semiconductor laser has been developed by Van der Ziel [88] based on these principles. The corresponding steady state equation which describes the net effects due to the pulse shaping elements is given by:

$$\left(G(t) - L(t) + \delta T \frac{d}{dt} + \frac{1}{\omega_c^2}\frac{d^2}{dt^2}\right)v(t) = 0 \qquad (5-3)$$

There are four terms in the equation which correspond to the gain medium, the saturable absorber, the disperse element and the effect of the frequency mismatch, $G(t)$ is the time dependent round trip gain, $L(t)$ is the time dependent loss, and δT is a normalised parameter of the detuning effect. ω_c^2 is the transmission bandwidth

Figure (5.1): Schematic diagram of an mode-locked system in the time analysis.

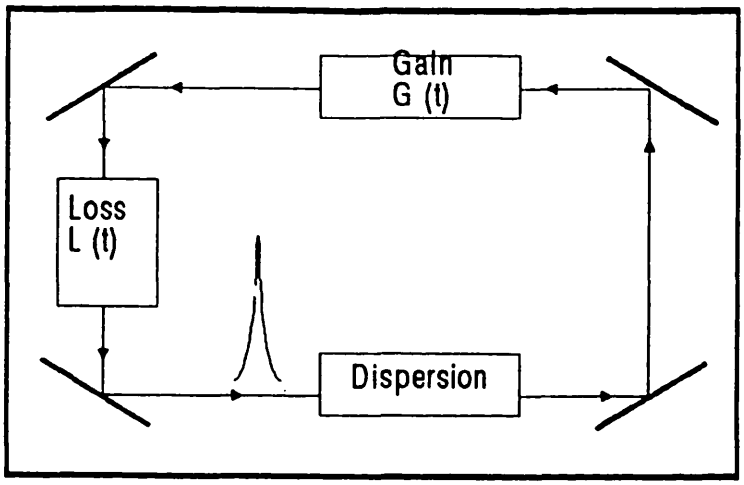

Figure (5.2): The derivatives of the gain function.

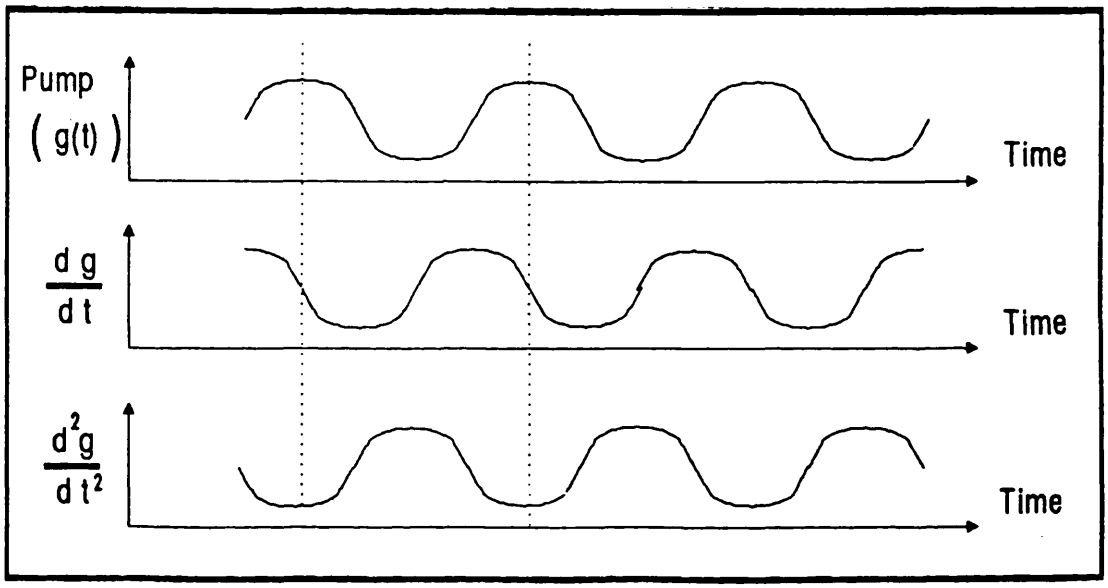

of a disperse tuning element such as a Fabry-Perot etalon or grating, and $v(t)$ is the pulse profile.

In order to simplify the above equation to the one which can be solved analytically, various important assumptions have been imposed. In the following, explanations for each of these boundary conditions, and their validity are given.

a1. The time dependent gain is calculated from the single mode rate equations in which, both the carrier density equation dn/dt and the net photon density $P(t)$ is represented by $|v(t)|^2/Ac$ where A is the cross section of the laser beam. However, since any mode-locking technique would involve more than one axial mode, thus in principle, the use of a multimodes rate equation would be more appropriate, i.e. the net photon density should be represented as the sum of all the photon densities in every excited axial mode. Therefore, this assumption has neglected the spectral distribution of a mode locked pulse. Perhaps this is the main weakness of this method because it ignores the existence of a spectral distribution and therefore completely neglects the correlation between the axial modes.

a2. In order to solve the carrier density rate equation near $t = 0$, the stimulated emission term is assumed to be zero between $-T_{R.F.} < t < 0$. This is quite acceptable since in an active mode locking experiment, the diode is normally biased just below the threshold. The stimulated emission can only occur during the passage of a pulse through the active medium and after which, there is very little or zero amount of stimulated emission generated by the D.C. pumping.

a3. For simplicity, the time dependent gain, $G(t)$, is also expanded in series as function of time, t, and only coefficients up to the second order are taken. Higher terms are neglected because of their small magnitudes. The truncated series is written as:

$$G(t) = k_1 G_{io} + T_{R.F.} G_i + \left(G'_{io} - G_{io} k_2 P_o\right) t + \frac{1}{2}\left[G''_{io} - \left[G'(io) - G_{io} K_2 P_o\right] k_2 P_o\right] T^2 \qquad (5-4)$$

where the apostrophe denotes the differentiation with respect to time, the subscript o denotes an evaluation of a parameter at $t = 0$, the constant (k_2) is a measure of the coupling strength between the gain and photon density. k_1 is a zero order coefficient which is a function of k_2 and the width of mode locked pulse [88]. Higher terms can be neglected if the rate of change of the gain is small. The use of such a truncated series can only be justified if the carrier depletion due to an optical pulse is small. But in the case of an intense optical pulse and if it is strong enough to cause an abrupt change in the carrier density, then more higher terms must be taken into account.

a4. The saturable absorption is written as:

$$\frac{dL}{dt} = \frac{1}{\tau_b}(L_s - L) - c\sigma_b LP \qquad (5-5)$$

where L_s is the loss, σ_b is the absorption cross section. L is the saturable loss. τ_b is the absorber relaxation time which is assumed to be much shorter than both the spontaneous decay time and the pulse separation. This implies that the absorber recovers to its fully populated state before the next arrival of an optical pulse. Once again, the loss is expanded in a series of t which is taken up to the second order term. The truncated series is given as:

$$L(t) = L_{so}A_1 - L_{so}c\sigma_b P_o t + \frac{1}{2}L_{so}(c\sigma_b P_o)^2 t^2 \qquad (5-6)$$

In the case of an intense optical pulse, the absorption (depletion of absorbing centres) may occur very abruptly so that extra higher order terms are needed in order to give a better description of the rate of change in losses.

With these assumptions, three simultaneous equations [88] can be derived. These equations connect together the pulse width $(t_{\frac{1}{2}})$, the peak pulse power (P_o), and the phase of the pulse relative to the R.F. current. In general, their corresponding solutions can only be obtained numerically. However, a qualitative understanding of the pulse width behaviour can be obtained from one of these equation. This equation is written as :

$$-G''_{io} + (\frac{\delta T}{t^2_{1/2}})(\frac{ac}{n})P_o + \sigma_b P_o^2 L_{so}c^2(\sigma_b - \frac{a}{n_a}) = \frac{2}{\omega_c^2 t^4_{1/2}} \qquad (5-7)$$

In the absence of detuning and saturable loss, the second and third terms would vanish and the equation becomes:

$$-G''_{io} = \frac{2}{\omega_c^2 t_{1/2}^4} \qquad (5-8)$$

The pulse width is thus determined solely by the curvature of the gain function $-G''_{io}$. To achieve the shortest pulse, G''_{io} must be as large as possible and of negative value in order to cancel the negative sign. According to figure (5.2), this point occurs at the peak of the pump modulation. When detuning is introduced, two cases can occur for positive and negative frequency mismatch. With positive detuning, i.e. the periodic time of R.F. modulation, $t_{R.F.}$, is greater than the cavity transition time, t_{cavity}; the detuning factor δT becomes greater than zero. This also means that the pulse will arrive earlier than the gain peak. According to equation 5-7, the L.H.S. will increase and the corresponding pulse width would become narrower. On the other hand, if δT is negative for negative detuning, a broader pulse width will be formed instead. This implies that the optimum mode-locked frequency may not be the same as the cavity frequency (i.e. the inverse of the cavity round-trip time).

If the saturable absorption is presented in the cavity, pulse narrowing will also occur. But this will only happen when the absorption coefficient (σ_b) is larger than the effective optical section (a/n_a), where a is the cavity loss parameter which is typically 200cm^{-1} for a stripe geometry laser diode. n_a is the nominal carrier density needed to overcome the cavity losses. Therefore, the presence of a large amount of saturable absorbers will reduce the mode locked pulses. In fact, the pulse shaping effect in passive mode-locking is attributed to this phenomena.

The pulse shaping effect due to a disperse element can also be understood from equation 5-7. Assuming the net contributions of the L.H.S. is constant, the pulse width is then inversely proportional to the square root of transmission bandwidth (ω_c) of the disperse element. Therefore, in order to generate shorter pulses, the use of a disperse element inside the cavity should be avoided, in which case, the bandwidth (ω_c) will become infinitely wide and accordingly, the pulse width will be infinitesimal small.

5.4b The spectral analysis

Consider figure (5.3), when the gain of an axial mode (V_n) is modulated externally at frequency ω. It generates two side-modes each on either side of the main axial mode and the mode separation is determined by ω. These side-modes oscillate in phase with respect to the "parent" mode. If the gain in these side-modes is also modulated, then more side-modes will be generated. In certain respect, all the possible side-modes can be regarded as originating from a single mode and have the same phases; these modes are therefore "locked" to each other. This is why it is named as "mode-locking".

At resonances, i.e. the frequency of the applied modulation matches the cavity mode spacing ($\omega_{R.F.}=\omega_{mode}$), the rate of change in the mode amplitude is then written as[31]:

$$0 = -M\left[\frac{\omega_{n+1}}{2Q_{n+1}}g(n+1)V_{n+1} - 2\frac{\omega_n}{2Q_n}g(n)V_n + \frac{\omega_{n-1}}{2Q_n - 1}g(n-1)V_{n-1}\right] + \frac{\omega_n}{2Q_n}g(n)V_n \qquad (5-9)$$

where $\frac{\omega}{2Q}$ is the rate of decay of the mode amplitude and $g(n)$ is the gain of the n^{th} mode. The derivation of a steady state equation in this analysis is much simpler than in the previous analysis. The necessary assumptions are:

b1. The factor $\frac{\omega_n}{2Q_n}$ is neglected and replaced by a constant $\frac{\omega_o}{2Q}$. Since the gain bandwidth is usually much larger than the pulse bandwidth, thus the term, $\frac{\omega_n}{2Q_n}$, has a weaker dependence on axial modes.

b2. The rate of decay (or loss) in amplitude of an axial mode is defined as $\frac{\omega_o}{2Q_n}V_n$ which at equilibrium is equal to the rate of growth (or gain) in equation 5.9. This is true if the noise is not present. Otherwise, a noise source has to be included.

b3. The origin of any noise is from spontaneous emission which is negligible compared to the stimulated emission when lasing. Thus, the noise can be neglected.

b4. Since the analysis is based on the interaction between discrete axial modes, the

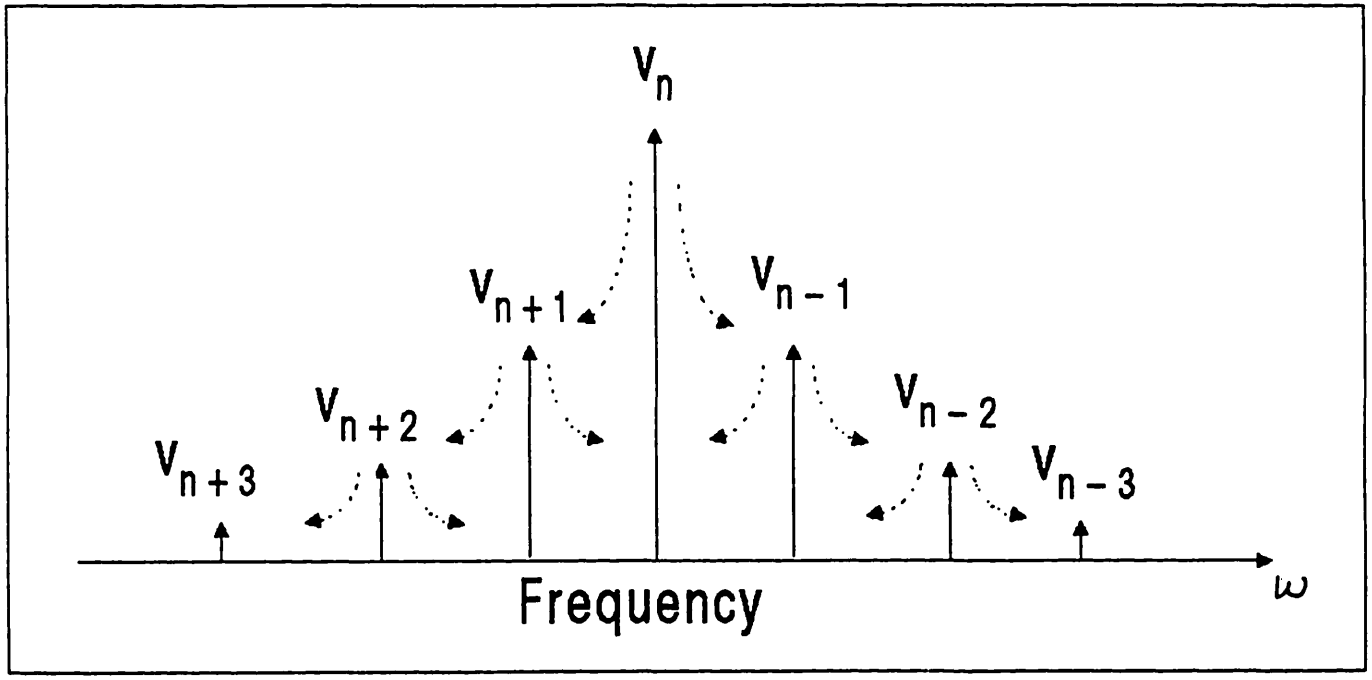

Figure (5.3): The locking between different axial modes.

equation will also have a nature of discreteness. Consequently, a difference equation will be formed. However, in order to obtain analytic solutions for mode locked pulses, a continuum approximation is needed. This is to transform the discrete mode spectrum, V_n, to a continuous spectrum, $V(\omega)$. As a result, the difference equation is transformed into a differential equation. This supersession is legitimate if the mode separation is smaller than the central mode frequency ω_o. i.e.:

$$V_{\omega_o+n\delta\omega} = \lim_{\frac{\delta\omega}{\omega_o}\to 0} V(\omega) \qquad (5-10)$$

Under this boundary condition, the discrete gain factor $g(n)$ will also become a continuous function, $g(\omega)$. These transformations are allowable because for external cavity 1.3μm InGaAsP semiconductor lasers of ,say, 50cm long; the mode spacing is 1.69x10^{-12}m (or 30MHz) which is much smaller than the emission wavelength.

With these assumptions, the equilibrium condition (as defined in **b2**) can be written as:

$$[1-g(\omega)]V(\omega) - M\omega_M^2 \frac{d^2}{d\omega^2}[g(\omega)V(\omega)] = 0 \qquad (5-11)$$

The above equation can be further simplified by substituting $U(\omega)$ for $g(\omega)V(\omega)$. The recast equation is expressed as:

$$[1-\frac{1}{g(\omega)}]U(\omega) + M\omega_M^2 \frac{d^2U(\omega)}{d\omega^2} = 0 \qquad (5-12)$$

Assuming the semiconductor laser is an ideal homogeneously broadened medium, the function $g(\omega)$ can be represented as:

$$g(\omega) = \frac{g_o}{1+(\frac{\omega-\omega_g}{\Delta\omega_d/2})^2} \qquad (5-13)$$

where g_o is the gain peak, ω_g is the gain peak frequency, $\Delta\omega_d$ is the gain bandwidth.

When a disperse element is inserted inside the cavity, additional losses are introduced. An extra loss term must then be added to the R.H.S. of equation 5.13. With a Fabry-Perot etalon and with the assumption that the lasing wavelength is near the transmission peak, i.e. $\omega \to \omega_{F.P.}$, the net gain is given as:

$$g(\omega) = \frac{g_o}{1+(\frac{\omega-\omega_g}{\Delta\omega_d/2})^2} - \frac{\omega-\omega_{F.P.}^2}{(\Delta\omega_{F.P.}/2)^2} \qquad (5-14)$$

where $\omega_{F.P.}$ is the transmission peak. With this gain function, the steady state equation can be reduced to a linear harmonic oscillator equation as in quantum mechanics and the solutions constitute a set of Hermitian-Gaussian polynomials, namely the "supermodes". Haus[31] has pointed out that under a steady state condition, only the fundamental supermode can be formed while the higher order supermodes cannot exist due to instabilities. Through the Fourier transformation, the pulse width, τ_{pulse}, can be derived for a cavity with and without the insertion of disperse element. These solutions are written as[108]:

$$\tau_{pulse} = \frac{\sqrt{2Ln2}}{\pi\sqrt{\nu_M \Delta\nu_d}\ \sqrt[4]{Mg_o}} \qquad (5-15a)$$

$$\tau_{pulse} = \frac{\sqrt{2Ln2}}{\pi\sqrt{\nu_M}\ \sqrt[4]{Mg_o}} \sqrt[4]{\frac{g_o}{(\Delta\nu_d^2)} + \frac{1}{(\Delta\nu_F^2)}} \qquad (5-15b)$$

Equation 5-15b shows that the insertion of a tuning element will broaden pulse width. The broadening factor is partly inversely proportional to the square root of free spectral range of the frequency selective element. It follows that if a short pulse width is of the main concern, frequency selective element should not be used. If it is to be used in the cavity, a broader pulse will form, but single-mode emission can be selected.

According to equations 5-15a and 5-15b, the mode-locked pulse width is inversely proportional to the square root of the modulation frequency, ν_M. It also depends on the lasing bandwidth, $\Delta\nu_d^2$. The dependence of τ_{pulse} on the modulation depth M is very weak. In fact, it is inversely proportional to the forth root of M.

5.4c The rate equations analysis

The study of mode-locked semiconductor laser was first reported by Aspin and Carroll [10]. Later on, AuYeung [6], Figueroa [26] , Chen et al [14] and Demokan [77] have also applied rate equations to investigate active mode-locking.

Chen et al used a simplified set of single-mode rate equations to obtain analytical solutions. From these solutions, important parameters such as the time evolution of the injection carrier density, secondary pulses, and the optimum arrival time of the main pulse in an actively mode-locked diode laser can be determined. They have

shown that the gain usually recovers very quickly and can sustain the generation of a secondary pulse. But the intensity is weaker because of the smaller recovered gain compared to the undepleted gain before the arrival of the main pulse. However, their analysis cannot be used to calculate the evolution of a mode-locked pulse.

Figueroa also used the single-mode rate equations which were modified to take into account the extra feedback from an external reflector, and the saturable absorption due to the presence of electron traps. This modification required another rate equation which described the change of electron-trap density. His numerical solutions showed that in the case of passive mode locking, both the pulse amplitude and pulse duration depend strongly on the amount of electron traps. This explains why mode-locking an aged diode laser can generate much shorter pulses[34].

Demokan's analysis is probably the most complete rate equation study reported on active mode-locking of a laser diode. This analysis considered the effects of sinusoidal and pulse injection current, spatial and temporal gain saturation, frequency mismatch as well as the material parameters. The rest of this section will concentrate on this analysis and its numerical solutions. The rate equations that Demokan used are:

$$\frac{\partial S(x,t)}{\partial x} = [\frac{\Gamma g \eta}{c}[n(x,t) - n_o] - \alpha_t] + \frac{M\Gamma k \eta B}{c} n^2(x,t) \qquad (5-16a)$$

$$\frac{\partial n(x,t)}{\partial t} = \frac{J(t)}{ed} - Bn^2(x,t) - g[n(x,t) - n_o]S(x,t) \qquad (5-16b)$$

where B is the radiative band to band recombination coefficient, Γ is the confinement factor, n_o is the nominal electron density, g is the optical gain coefficient, $S(x,t)$ and $n(x,t)$ are the photon and electron carrier densities respectively.

The novelty about this set of rate equations is that it deals simultaneously with both the time and space dependence; whereas the usual rate equations which all other workers used have only the time dependence. It has become well known that the time derivative rate equations are only valid for a laser diode which has a facet reflectivity greater than 10%[110]. It is also assumed that the laser diode is biased at or above

Figure (5.4): Numerial results computed by Demokan [77].

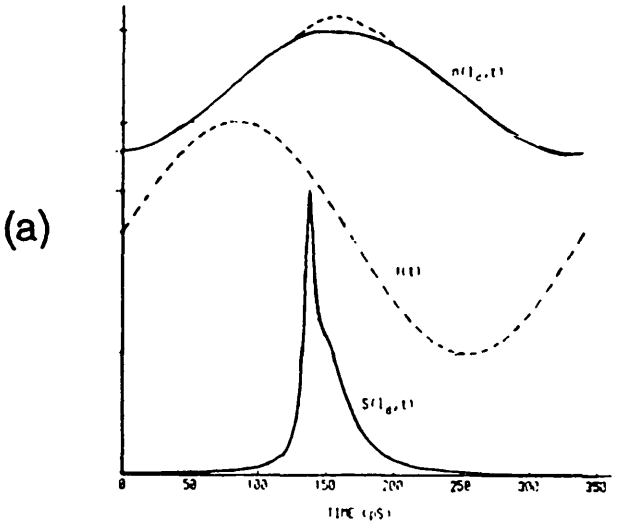

The injection current density $J(t)$, the electron density $n(l_d, t)$ and the photon density $S(l_d, t)$ for $0 < t < T$ after 600 round-trips of gain modulation. $J_{dc} = 1{\cdot}02\ J_{th}$, $J_{ac} = 0{\cdot}5\ J_{th}$.

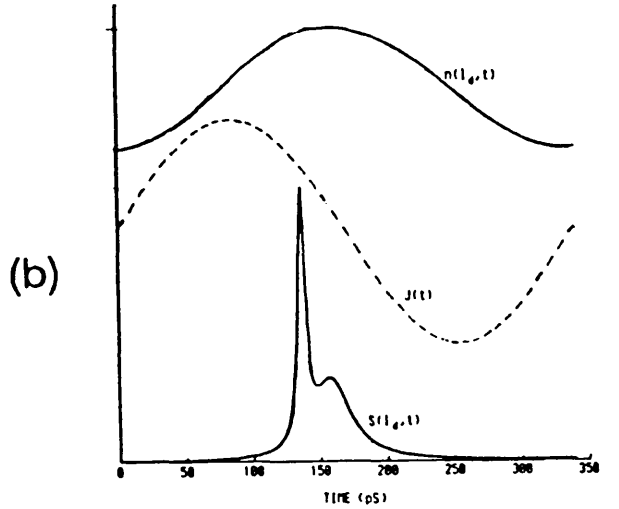

Double-pulse generation when k is changed to 1×10^{-3} while the rest of the parameters retain the values in Table 1.

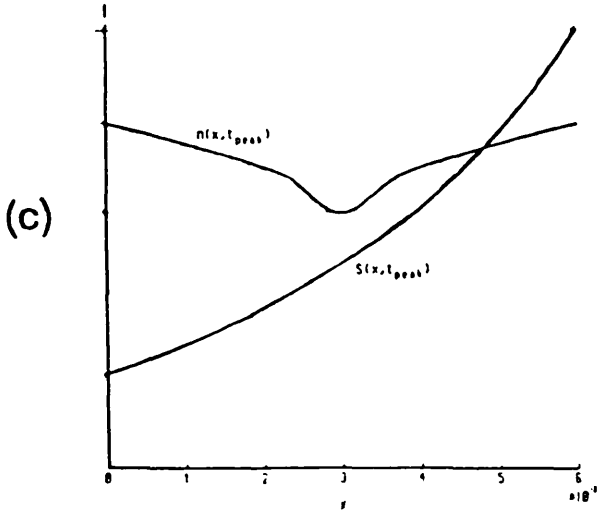

Electron density and photon density as functions of position along the diode axis at a time that corresponds to the peak of the photon density.

its lasing threshold. These assumptions lead to the approximation that photon and carrier densities are uniform over the whole length of the diode. In the case of laser amplifiers of reduced facet reflectivities, the time-only derivative equations therefore cannot be used. It has been shown[54] that photon and carrier densities are functions of the axial co-ordinates of a laser diode. It therefore seems that the rate equations should also take into account the space dependence as in equations 5-16a and 5-16b.

However, in these two rate equations, the space derivative only appears in the photon density equation while the carrier density equation has only the time derivative. This implies that only the carrier density changes primarily with time but does not vary primarily with space. The space dependence in the carrier density is only introduced by the photon density which is primarily space-dependent. Similarly, the photon density $S(x,t)$ has a "indirect" dependence on the time co-ordinates.

According to the travelling-wave rate equations[54], this would mean that the photon density $S(x,t)$ is "partially" independent of time and that the carrier density $n(x,t)$ is "partially" independent of space. Using these equations, he calculated various important parameters, in particular the pulse duration and pulse shape which agreed well with experimental results obtained by Chen [15,108]. Thus, it seems that the carrier density, $\frac{\partial n(x,t)}{\partial t}$, does indeed have a more stronger time-dependence such that its space derivative, $\frac{\partial}{\partial x}$, can be ignored and vice versa for the photon density.

In the following, various assumptions and definitions which were imposed in deriving these rate equations are given, and the numerical solutions relating to active mode-locking of laser diodes are discussed.

c1. The diode facet through which, the light is coupled to an external reflector is assumed to have an ideal zero reflectivity. In practice, this may be impossible to achieve because semiconductor lasers have very high internal gain (greater than 30dB) so that even the feedback due to optical scattering at the facets can be amplified significantly enough to give rise to a finite residual reflectivity.

c2. Only band to band radiative recombinations are taken into account. Other types of recombinations are neglected because they usually have negligible effect. But in the cases of long wavelength laser devices or laser diodes exhibiting self pulsation characteristics, other recombinations may be needed.

c3. Both the spontaneous emission and the gain factors of individual axial modes are assumed to be constant with wavelength. This is legitimate because the spectral bandwidth of a mode locked pulse is usually much smaller than the gain and fluorescence bandwidths. Also, with these assumptions, the discreteness of the rate equations are superseded by the continuum.

c4. Since only the zero-order transverse mode is assumed to be excited, this would imply that the stripe width is small (less than 5μm).

c5. Diffusion of injected carriers is ignored. This is acceptable in the case of index-guided lasers which usually have very small leakage currents. However, for some gain-guided lasers, carrier diffusion could be very large such that it cannot be neglected.

c6. The change in refractive index with electron density is neglected. In practice, this effect could become very strong in the case of a large current modulation. This effect also partly accounts for the frequency chirping within a pulse.

c7. Dispersions due to the laser medium or tuning element are ignored. Thus, the corresponding frequency chirping or pulse broadening due to bandwidth limitation cannot be determined.

c8. Phase spectrum is ignored. This is an inherent handicap of the rate equations study. In fact, this nature is similar to Van der Ziel's [88] time analysis in which the relative phases between axial modes were neglected. Demokan estimated the number of modes using the inverse time-bandwidth equation, which divides the cavity round tripe time by the pulse width calculated from the previous iteration. Thus, in every iteration, "all" the axial modes are assumed to be oscillating in phase, i.e. the system is always mode-locked.

Having outlined various assumptions and definitions, the discussion will now proceed to the numerical results computed by Demokan using the difference step numerical method. Figure 5.4a shows that under the optimum mode locking condition, a pulse must arrive in the gain medium before it reaches its unperturbed maximum gain. There is a time delay in the gain peak compared to the periodic pumping modulation peak. This is due to the presence of the cavity and material losses such that the gain needs some time to overcome these losses before it can build up to a significant value. The pulse consists of a spiky top part and a bottom part which is usually very wide. A waist in the trailing part is also apparent. For a smaller spontaneous emission factor, double-pulse generation was seen (fig. (5.4b)). This agrees well with the experimental results obtained by Chen et al[15] in which the mode locked pulses usually have broad bases and under certain operating conditions, secondary pulses will appear in the trailing part of the main pulse .

Perhaps, the most interesting feature of this numerical analysis is that it shows a strong space-dependence in photon and electron carrier densities (fig. (5.4c)). It follows that theoretical modelling on mode locking a semiconductor laser of zero facet reflectivity must also consider the nonuniform distributions of photon and carrier densities along the active stripe.

Conclusion

Basic concepts of cavity modes and mode-locking have been given. This was followed by a review of three different mathematical models, namely, the:

(1) Time analysis,

(2) Spectral analysis,

(3) Rate equations analysis.

In the spectral analysis, solutions for the mode-locked pulse-widths can be found analytically. A pulse-width is inversely proportional to the forth-root of the modulation currents, i.e. the current dependence is very weak. If a frequency selective element is placed within the cavity, the mode-locked pulse-width is broadened as

described by equation 5-15b. Similar conclusions can also be drawn from the time analysis, in which the pulse shaping effects are expressed in the time domain. In addition, from the time analysis, it is shown that the presence of saturable absorbers can also reduce the pulse-widths.

For the third analysis, the time and space dependent rate equations have been described. Due to the reduced facet reflectivity, both the photon and electron densities strongly depend on the axial position along an active stripe. The corresponding pulse profiles have broad bases and in some cases, double pulses can occur. This agrees well with experimental results [119]. In addition, at an optimum mode-locking condition, the pulses should arrive at the active medium slightly before the gain reaches its peak. Such an optimum condition can also be predicted using the time analysis.

Thus, in order to generate shorter pulses, the r.f. frequency should be smaller than the mode-locked frequency given by the external cavity length. The laser must also contain some saturable absorbers and the use of disperse (or wavelength selective) elements should be avoided.

CHAPTER SIX

Active mode locking of 1.3μm InGaAsP lasers

6.1 Introduction

In this chapter, a series of active mode-locking experiments on semiconductor lasers are compiled and for completeness, the work on passive mode-locking is also briefly outlined. Two different ways of directly measuring the pulse-widths are given. These are the photodiode/sampling oscilloscope pair and the synchronscan streak camera. The latter is the main diagnostic system used throughout this project. Active mode-locking of three different types of external cavity lasers are described with emphasis on the mode-locked spectra and the corresponding pulse-widths. Finally, these results are summarised in the conclusion.

6.2 Review on active mode-locking of laser diodes

The first active mode-locking of a c.w. semiconductor laser in an external cavity was reported in 1978 [34]. The external cavity was a silvered spherical mirror

with a 5cm radius. The laser was an AlGaAs double heterostructure laser emitting at around 850nm. No antireflection coating was deposited on the facets. The diode facet was placed at the centre of curvature of the spherical mirror so that light could be focused back into the diode. The threshold current decreased from 190 mA to 140 mA and current modulations at 3GHz were superimposed on the d.c. bias. The intensity autocorrelation was obtained from a second harmonic generating ($LiIO_3$) crystal. By assuming a gaussian pulse profile, pulse-width of 23 ps was calculated. The autocorrelation trace also contained a series of sharp peaks separated by 6.8 ps which corresponded to the round trip time within the diode. Since the facet reflectivity was not suppressed, part of the optical pulse was reflected back to the active region causing oscillations within the diode cavity. This is why most of the subsequent work has concentrated on suppressing the facet reflectivity.

To date, active or passive mode-locking still requires the semiconductor lasers to have external (or extended) cavities. Without the external cavities, "direct" mode-locking of semiconductor lasers requires modulation frequencies in the 100GHz region which are well beyond the reach of present day technologies. In addition, today's laser diodes cannot sustain such high modulation frequencies due to the parasitic elements.

In the following, the reviews on active mode-locking, experiments are divided into three groups in terms of different cavities. These are:

(1) the spherical-mirror and plane-mirror cavities,

(2) optical waveguide cavities such as the double channelled $LiIO_3$ waveguides or optical fibres,

(3) the grating cavities.

Lists containing most active and passive mode-locking experiments are compiled and outlined in figures 6.1 and 6.2 respectively.

6.2a Spherical and plane mirrors

Shortly after the announcement of actively mode-locking a semiconductor laser

by Ho et al[34], Glasser[27] reported similar results using an InGaAsP laser with emission wavelengths at around 1.2μm. A spherical mirror which had a radius of 3.88cm was used as an external reflector. An autocorrelator was used to measure the pulses and pulse-widths of 18ps were calculated assuming the pulses had gaussian profiles. The repetition rate was 2.1 GHz which corresponded to a cavity length of 7cm.

Holbrook et al[36] used both the spherical and plane mirrors to form an external cavity. The spherical mirror had a radius of 5cm. The diode was a 5^o angled stripe AlGaAs laser which was also A.R. coated to further suppress the internal cavity effect. A Fabry-Perot etalon was also used to limit the laser bandwidth and pulse width of 15ps was measured on a synchronscan streak camera.

A similar cavity configuration was used by Chen et al[15] to mode-lock a Brewster angled stripe semiconductor (AlGaAs) laser at 870nm. The Brewster angle was around 15^o between the facet and active stripe. The external cavity was a pair of plane and spherical mirrors. Such a cavity configuration will be referred to as a "two-mirror" cavity. A Fabry-Perot etalon was inserted into the cavity which limited the spectral width to 4.5Å. The cavity length was 90cm which corresponded to a modulation frequency of 333MHz. Pulse-widths of 13ps were obtained. After deconvolving with the system response of the streak camera, pulse-widths of 11ps were deduced.

Using plane mirrors as external reflectors instead of the spherical mirrors, required additional optics to couple the light out and back into the laser diode. Microscope objectives are commonly used for such purposes. One of the first mode-locking experiments using plane-mirror cavity was reported by Van der Ziel[88]. An AlGaAs laser with emission wavelengths around 870nm was coupled to a single external plane mirror using a 0.85N.A. lens. A mode-locking frequency of 1.9GHz was applied. Using the second harmonic method, pulse-widths of 35.7ps were observed assuming gaussian pulse profiles. Fine periodic structures separated by 1.6ps were also seen on the autocorrelation trace. These structures resulted from the reflective facets are sometimes

referred to as cluster mode-locking[30].

A similar experimental set-up was reported by Ho[34]. The external cavity was made of microscope objectives and plane mirrors. In addition, an intracavity tuning element (F.P. etalon) was inserted into the cavity and pulses of 60ps were generated at a repetition rate of 433MHz. The diode was an one-side A.R. coated GaAsAl laser.

Olssan and Tang[64] have also reported a mode-locked external cavity semiconductor laser using the two-mirror (plane mirrors) cavity. The lasing wavelength was 850nm and the cavity length was 1.2m which corresponded to a mode-locked frequency of 250MHz. An electro-optic tuner was used to restrict the oscillating bandwidth and to allow convenient tuning of laser wavelength. The shortest pulse-widths of the order of 6 to 8 ps were measured on an intensity autocorrelator assuming the pulses were of $sech^2$ profiles. They have also tried the ring cavity-configuration and obtained slightly longer pulses of 16ps. They reckoned that the difference in pulse-widths for the two cavity-configurations was not due to the cavity itself but because of the different internal parameters.

Mode-locking of a laser diode in a ring cavity has also been reported by Van der ziel[86]. He has produced the shortest pulses of 0.56ps measured on an autocorrelator. The generation of subpicosecond pulses was possible, largely due to the presence of saturable absorbers which were introduced by proton bombardments. Therefore, both active and passive mode-locking mechanisms were involved simultaneously. However, due to the crystal damages caused by proton bombardments, the diodes were usually short lived.

McInerney et al[55] also used this hybrid technique of combining both passive and active mode-locking, but instead of introducing the saturable absorption inside the active region by a destructive method such as proton bombardment, they used two diodes. One of which served as a linear gain device by biasing it near the threshold and subsequently, adding the R.F. currents. The other diode acted as a saturable absorbing device by biasing it below the threshold. Thus, the amount of gain and

absorption could be controlled electronically and independently. A Fabry-Perot etalon was used to limit the laser's spectral bandwidth. Pulse-widths of 25ps were measured on a streak camera and were calculated to be bandwidth limited.

Perhaps the disadvantages of a ring cavity are the difficulties in setting up the cavity, and in maintaining cavity stability. Cavity stability is more critical because more intracavity elements are involved. The alignment of a ring cavity is more difficult, and particularly in the case of using two diodes. This is because the diodes have to be positioned symmetrically to ensure a correct synchronisation between the two counter-propagating pulses in both diodes. Thus, practically speaking, the ring cavity may not be a convenient or good cavity configuration.

6.2b Optical waveguides

Mode locking experiments have also been carried out on external cavities in the form of optical fibres with high reflective ends, self focusing (GRIN) lenses, and double-channel waveguides which can be switched electrically at gigahertz frequencies. Alferness et al[3] have used a Ti:$LiNbO_3$ (Titanium diffused lithium niobate) waveguide as an external cavity. Light from an A.R. coated laser was coupled into the waveguide using a lensed fibre. Electrical sinusoidal-waves at a repetition rate of 7.2GHz were applied to the two coplanar travelling-wave electrodes and mode-locked pulses of 22ps were generated. The uniqueness of this experiment is that the diode was only pumped by a D.C. current, unlike all other mode-locking experiments in which the diodes were pumped by both D.C. and R.F. modulated currents.

Mode-locking an external cavity with an optical fibre was first demonstrated by Tucker et al[83] and later, by Lau et al[46]. The optical fibre could be a single mode or graded-index fibre. The fibre usually has one high-reflective end coated with metallic film, and the other end has a built-in microlens for coupling to the laser diode. Mode-locking frequency is determined by the total transit time within the fibre core and the laser. The first optical fibre external cavity laser generated mode-

Figure (6.1): List of active mode-locking experiments.

Active mode locking

Authors	τ_{width}	ν	Cavity type	λ	diode	Year
Ho	20ps	3.000GHz	Single mirror	850nm	Uncoated	1978
Glasser	18ps	2.100GHz	Single mirror	1.21μm	Uncoated	1978
Ho	60ps	0.433GHz	Single mirror	850nm	A.R.	1979
Ito	30ps	0.255GHz	Single mirror	850nm	Uncoated	1980
Olsson	7.0ps	0.250GHz	Twin mirror	850nm	A.R.	1981
Olsson	16ps	0.250GHz	Ring cavity	850nm	A.R.	1981
Van der Ziel	0.56ps	1.000GHz	Ring cavity	850nm	A.R.	1981
Bradley	16ps	0.380GHz	Twin mirror	850nm	5^o angle	1981
Akiba	30ps	5.300GHz	Selfoc lens	1.55μm	A.R.	1981
Chen	11ps	0.285GHz	Twin mirror	850nm	Brewster	1982
AuYeung	10ps	0.500GHz	Single mirror	820nm	A.R.	1982
Bessonov	15ps	0.250GHz	Single grat.	850nm	Uncoated	1982
Tucker	30ps	10.00GHz	Fibre cavity	1.3μm	A.R.	1983
Tada	37ps	3.600GHz	Selfoc lens	850nm	A.R.	1983
Lundquist	30ps	1.000GHz	Single grat.	850nm	Uncoated	1983
Dimmick	31ps	3.3GHz	Selfoc lens	850nm	A.R.	1984
Alferness	22ps	7.200GHz	Waveguide cav.	1.3μm	A.R.	1984
Lau	12ps	17.50GHz	Fibre cavity	850nm	A.R.	1985
McInerney	25ps	0.998GHz	Ring cavity	850nm	A.R.	1985
Tucker	5.0ps	20.00GHz	Fibre cavity	1.5μm	A.R.	1985
Vasil'ev	3.5ps	0.350GHz	Single grat.	850nm	A.R.	1985
Andrews	50ps	0.250GHz	Single mirror	850nm	A.R.	1986

Figure (6.2): List of passive mode-locking experiments.

Passive mode locking

Authors	τ_{width}	ν	Cavity type	λ	Absorber	Year
Ippen	5.00ps	0.85MHz	Single mirror	850nm	Aged	1980
Van der Ziel	35.7ps	1.90GHz	Single mirror	850nm	Aged	1980
Van der Ziel	0.65ps	1.00GHz	Single mirror	850nm	P-bombar.	1981
Yokoyama	0.58ps	5.00GHz	Single mirror	850nm	Aged	1982
Harder	35.0ps	1.50GHz	Single mirror	850nm	Split contact	1983
Tsang	200ps	0.20GHz	Single grating	850nm	C^3 laser	1983
Silberberg	1.60ps	1.00GHz	Single mirror	850nm	M.Q.W.absor.	1984
Vasil'ev	0.80ps	0.71GHz	Single mirror	850nm	Split contact	1986
Silberberg	0.83ps		Single mirror	850nm	M.Q.W.absor.	1986

locked pulses of 30ps at 10GHz. After which, Lau et al generated mode-locked pulses of 12ps at 17.5GHz. In the ultrahigh frequency experiments such as those mentioned, the laser chip is normally mounted in a broad-band 50Ω microwave test fixture. In addition, high-frequency cables are used in order to minimise the attenuation losses and the background interference.

6.2c Ruled gratings

For mirror cavities, the wavelength selectivity and tunability can only be controlled by using an intracavity Fabry-Perot etalon. Alternatively, this can be done by replacing one of the mirrors by a grating. The grating's wavelength selectivity depends on the number of lines per length and on the beam cross-section.

Lundquist[52] used a single grating coupled to an uncoated 850nm AlGaAs laser. The mode-locking frequency was 1GHz and pulse-widths of 30ps were measured. Later, Vasil'ev[90] also used an external grating cavity but the AlGaAs laser was A.R. coated. Mode-locked pulses of 3.5ps were generated at a repetition rate of 350MHz.

6.3 Review of passive mode locking experiments

Subpicosecond pulses from passively mode-locked semiconductor lasers were first observed by using a buried optical guided geometry laser[87]. Saturable absorption was introduced at the exit facet by photon bombardment with $3x10^{15}$ cm^{-2} at 600keV. The penetration depth into the active region was about 6μm. The laser facets were coated with SiO layers. The external reflector was a plane mirror. The coupling between the reflector and laser was via a microscope objective lens. Cavity length was 15cm corresponding to a round trip transit time of 1 ns. The intensity autocorrelation trace has a series of peaks of 1ps wide. Assuming a $sech^2$ pulse profile, pulse width of 0.65ps was calculated.

Passive mode locking was also achieved with an aged laser diode which has an increased threshold and exhibited self-pulsations. This effect is due to the presence of

a substantial amount of absorbing traps inside the active region. Using such a laser diode, pulse-widths of 0.78ps were generated by Yokoyama[96]. The cavity length was 23cm and the applied current was $1.5I_{th}$. The pulses envelope was 16ps and broadened with increasing cavity lengths. Passive mode locking could not be observed for external cavity greater than 6cm. This is because the self pulsation frequency limits the cavity length. Ippen et al[37] also used an aged laser diode for passive mode locking and obtained a burst of pulses of pulse-width 5ps. However, the introduction of saturable absorption by ageing process is less reliable and the life time of the passively mode locked laser is relatively short. Van der Ziel et al[86] have also reported the passive mode-locking of an aged laser diode and produced pulses of durations of 35.7ps.

Saturable absorbers can be introduced into diodes without causing any damage by either using two laser diodes as already mentioned, or using nonuniform current injection. The latter method can be achieved by splitting the metallic stripe into two and each section is pumped independently. Thus, the diode can have a section of linear gain and the other section of saturable absorption. Harder et al[29] used a buried heterostructure geometry laser with split contacts consisting of a long gain section and a short absorbing section. A SiO A.R. coating was also applied to the mirror facet of the gain section to increase the coupling to the external cavity. The cavity length was varied between 30 and 10cm corresponding to a frequency of 0.5 to 1.5GHz respectively. The shortest pulses of 37ps were observed for the gaussian shape approximation. Later, Vasil'ev et al[91] have also applied the same technique and obtained a burst of pulses, each of durations of 0.58ps. Tsang et al[81] extended the technique to form the cleaved-coupled-cavity lasers (C^3). In this geometry, the laser is cleaved into two sections with each section separated by an air gap of a few μm. The gain of the first section and the saturable absorption of the rear section can be controlled electronically. Light from the rear absorber facet was collimated by a lens and focused onto a grating. Detector-limited pulses of 200ps were obtained.

Saturable absorptions of the optical pulses need not to occur inside the laser

diodes. Passive mode-locking can also be achieved by placing absorbers in the external cavity. This was demonstrated by Silberberg et al[74] using GaAlAs multiple-quantum-well material deposited on a external 100% mirror. Pulse-widths of 1.6ps were generated for the gaussian pulse approximation.

6.4 Direct detection of optical pulses

Temporal profiles of the ultrashort optical pulses can be measured either directly or indirectly. The direct detection scheme measures directly the intensity profile of a pulse. Whereas the indirect method usually measures the intensity correlation of a pulse from which the pulse width can be estimated by assuming a certain pulse profile. In this project, only the direct detection methods, namely the photodiode/sampling oscilloscope and the synchronscan streak camera, were used.

6.4a Photodiode/sampling oscilloscope

Both the PIN and the fast Germanium diodes were employed to detect the mode-locked pulses which were subsequently viewed on a sampling oscilloscope with a S-4 sampling head.

The Germanium photodiode has an active area of 0.1mm in diameter but because the sensitivity was low, electrical amplifiers were used to amplify the signals. Because the amplifiers have built-in low pass band filters, the Germanium/amplifier detector cannot detect any d.c. signals. An overall risetime of 250ps was measured which included the effects due to the diode, amplifiers, cables, and the sampling oscilloscope. The minimum detectable optical power was about 300μWatts. A photograph of an oscilloscope trace is shown in figure (6.3). The power transfer characteristics (fig. (6.4)) are not linear and the sensitivity increases with lower input powers. However, this nonlinear response does not matter since the detector is merely used to monitor the outputs of a mode-locked laser. If the detector were to be used as the optical power measuring device as in the case of an optical amplification experiment, the

absolute powers can be calibrated using the power transfer characteristics.

6.4b Streak camera and image intensifier

A diagram of the streak camera-intensifier system is shown in figure (6.5). A light pulse incident on the photocathode will liberate a burst of photoelectrons which have a temporal distribution corresponding to the intensity profile of the light pulse. These are then accelerated down the tube by the mesh which is usually operated at 1KVolt. After which, the photoelectrons are then accelerated through the cone and anode electrodes. The net voltage difference between the cathode and the phosphor is 16.5KVolts. The cone and anode act as electron lenses to focus the electron beam onto the phosphor. Beyond the anode, the electrons pass through a pair of deflection plates. A sinusoidal voltage is applied to the plates to streak the burst of electrons across the phosphor screen. The frequency of the A.C. driving voltage is supplied from the synthesiser (fig. (6.6)) and amplified by the R.F. amplifiers before reaching an L-C resonant circuit. To achieve the best coupling, the inductance L of the coil is adjusted so that the LC circuit resonances at around the mode locking frequency. The synchronisation between the streak camera and mode-locked pulses is controlled via a variable delay line and by adjusting the capacitance of a variable air-gap capacitor.

The repetitive deflection-ramps enable each streaked line to overlay on top of each other and as a result, the overall sensitivity is increased. The spectral sensitivities of most streak tubes are very good for wavelengths which are within or just outside the visible spectrum and that the image intensifiers are not normally needed. However, if the wavelengths are well beyond the visible band but are still encompassed by the spectral response of the photocathodes such as for the wavelengths of 1.3 and 1.55μm, then the use of intensifier is necessary in order to boost up the streaked images. In this project, a channel plate intensifier of diameter 5cm was used which has a gain 10^5 and 1:1 magnification.

Calibration on the streak camera was carried out using a Michelson (two-arm)

Figures (6.3) and (6.4): A typical sampling oscilloscope trace using a PIN detector and the power transfer characteristics of the GM3/amplifier detector respectively.

(6.3)

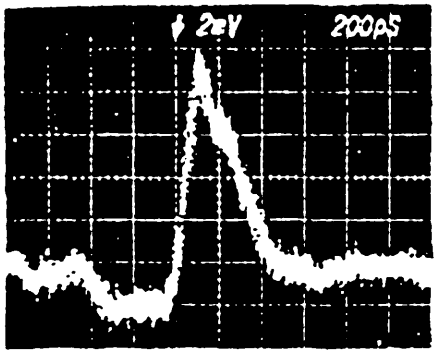

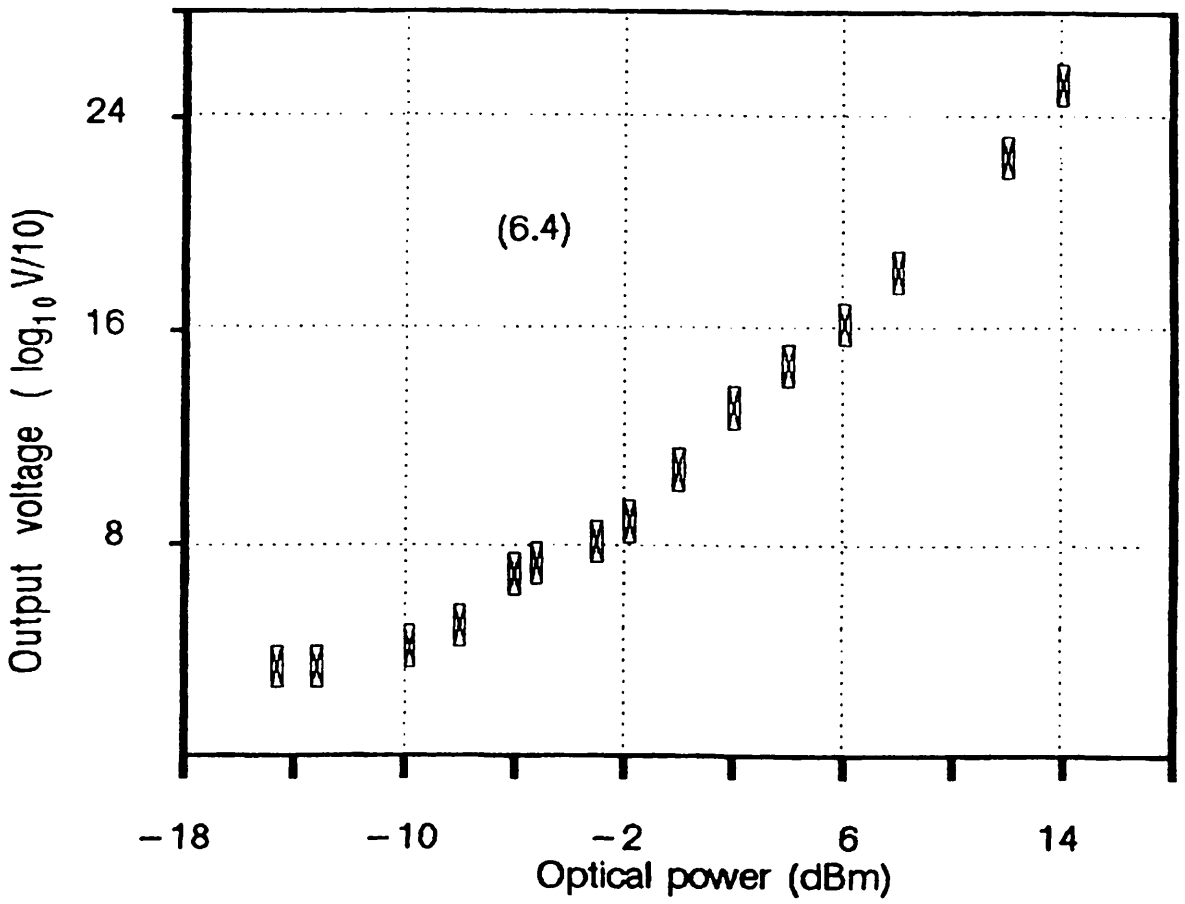

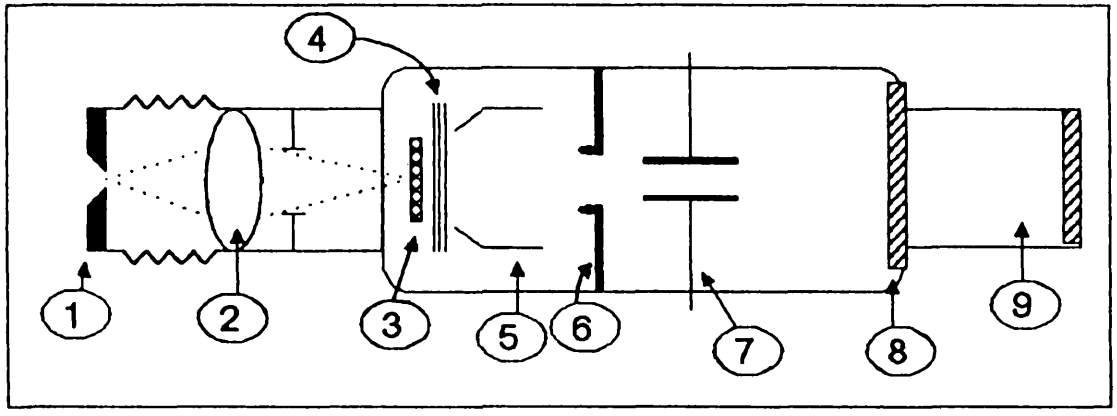

1. Slit
2. Focusing lens
3. Photocathode (– 16.5kV)
4. Mesh (– 15kV)
5. Cone
6. Anode (0 V)
7. R.F. deflection plates (10W R.F. power)
8. Phosphor
9. Image intensifier (7.5kV)

Figure (6.5): Schematic diagram of the streak camera and image intensifier.

Figure (6.6): The r.f. driving and deflection circuits for the synchroscan.

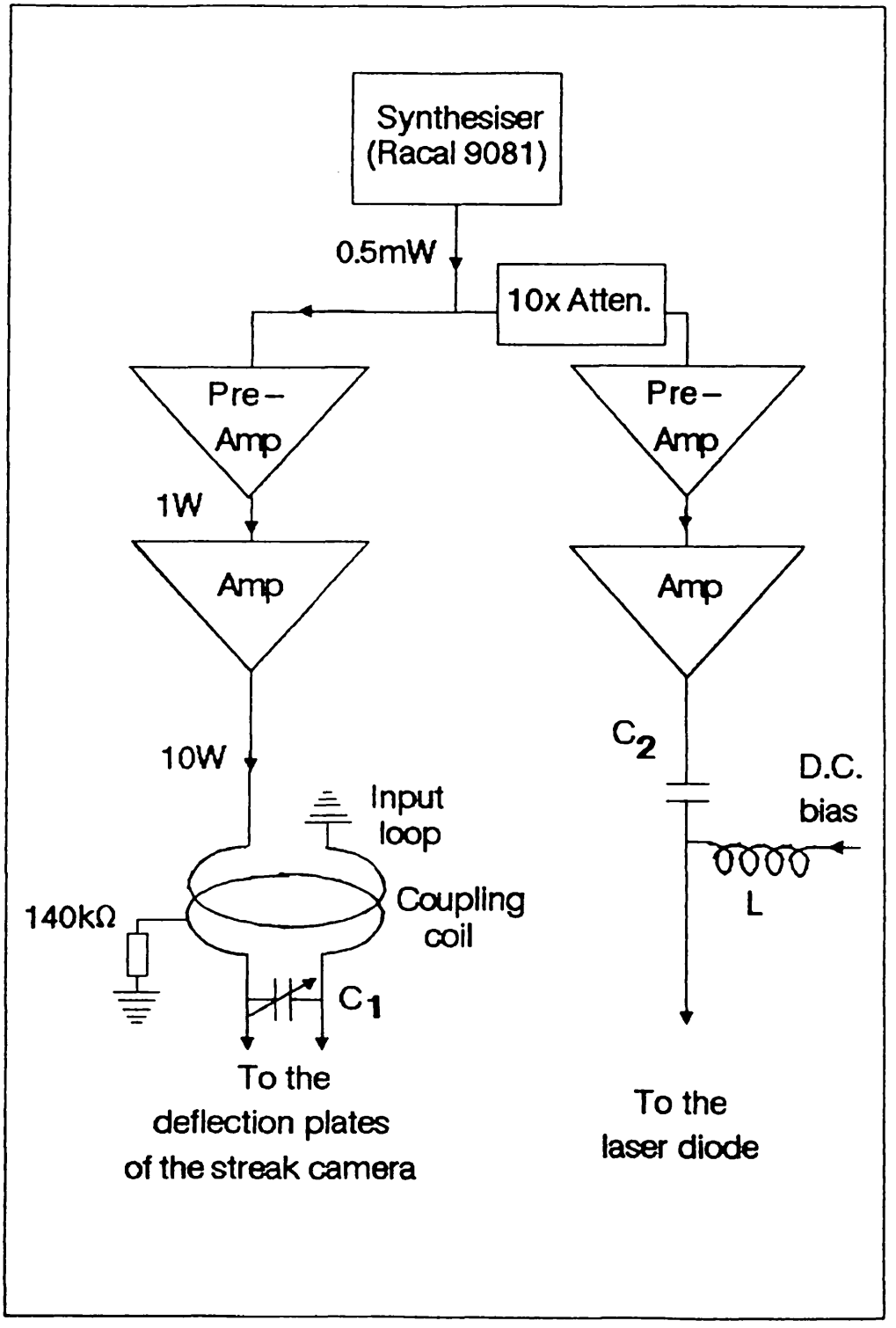

interferometer. When a pulse is incident onto the 50%/50% beam splitter of the interferometer, it is split into two smaller but identical pulses which travel further down each arm. Plane mirrors are normally placed at the end of each arm so that the replicas will be reflected back to the beam splitter. If both arms are of equal length, the replicas will arrive at the same time and recombine together. Suppose that the lengths are different by ΔL, then there will be a time difference of $2\Delta L/c$ between the replicas. As a result, the streaked lines will have a spatial separation which corresponds to this time difference.

The difference in optical paths, ΔL, was controlled by a micrometer which was mounted on a translational stage at one of the mirrors and ΔL was normally set at 1cm which corresponded to a time difference (or the streaked pulse separation) of 66ps.

6.5 Experimental alignments and results

The external cavities were initially set-up as mentioned in chapter four. After which, the bias currents were reduced below the lasing threshold. Usually, the lasers were biased near to the threshold-current. It was found that this can generate the shortest pulse-widths. To mode-lock an external cavity laser, the r.f. current corresponding to the cavity-transit-time was superimposed onto the d.c. bias current. For a 1 metre long cavity, the corresponding mode-locking frequency is about $\frac{1}{3}$GHz.

The frequency of the r.f. current was scanned around a pre-estimated mode-locking frequency until a maximum output was obtained. It was found that such a condition was always very close (less than 0.2MHz) to the optimum mode-locking frequency at which, the shortest pulses were produced. Sometimes, the search for a maximum output frequency may not be an accurate way of optimising the system. Especially, in the cases where the r.f. currents have transmission peaks near to the pre-estimated mode-locking frequency. Such peaks may be caused by mismatching between the impedance of the laser diode and the synthesiser. To double-check the

condition of a maximum output, the light output was compared to the light output when the external cavity was blocked out. For a "real" maximum output frequency, lasing action should be quenched very rapidly as the external cavity is blocked.

Having found the optimum output frequency, the detector/sampling oscilloscope was used to further optimise the pulse intensity. However, since this diagnostic system has a resolution of 250ps, quantitative studies of the mode-locked pulses could not be carried out. This is where the second diagnostic system, namely the synchron-scan streak camera, takes over because of its high resolution ($\approx$ a few picoseconds). In the following, various mode-locked pulse profiles and their corresponding time-averaged spectra are discussed.

6.5a Uncoated zero-degree lasers

It has been described in chapter four that when a zero-degree laser was placed inside an external cavity, its threshold current became smaller than when it was on its own. Although the stimulated recombinations occurring within the active region relied strongly on the feedback from the external reflector rather than on the feedback from the facets. However, the excitations of multiple mode-clusters could still be possible due to the additional feedback provided by the facets. Nevertheless, mode locking can still be carried out on such external cavity laser as long as the net R.F. and D.C. currents are below the laser's self-lasing threshold. This is sometimes referred to as "pseudo" mode locking in which all the "external cavity" modes within a cluster are locked together but the locking between clusters cannot be established. Due to this reason, "pseudo" mode-locked pulses are usually wider than pulses of "real" mode locking. In addition, a "pseudo" mode-locked pulse consists of many sharp spikes which are caused by multiple reflections between the facets. This is why many researchers have tried to reduce the facet reflectivity to eliminate the multiple mode-clusters and thus, suppress the fine structures within the pulses.

Figure (6.7) shows the mode-locked pulses from a zero degree laser which was

Figure (6.7): Mode-locked pulses of an uncoated zero-degree external cavity laser.

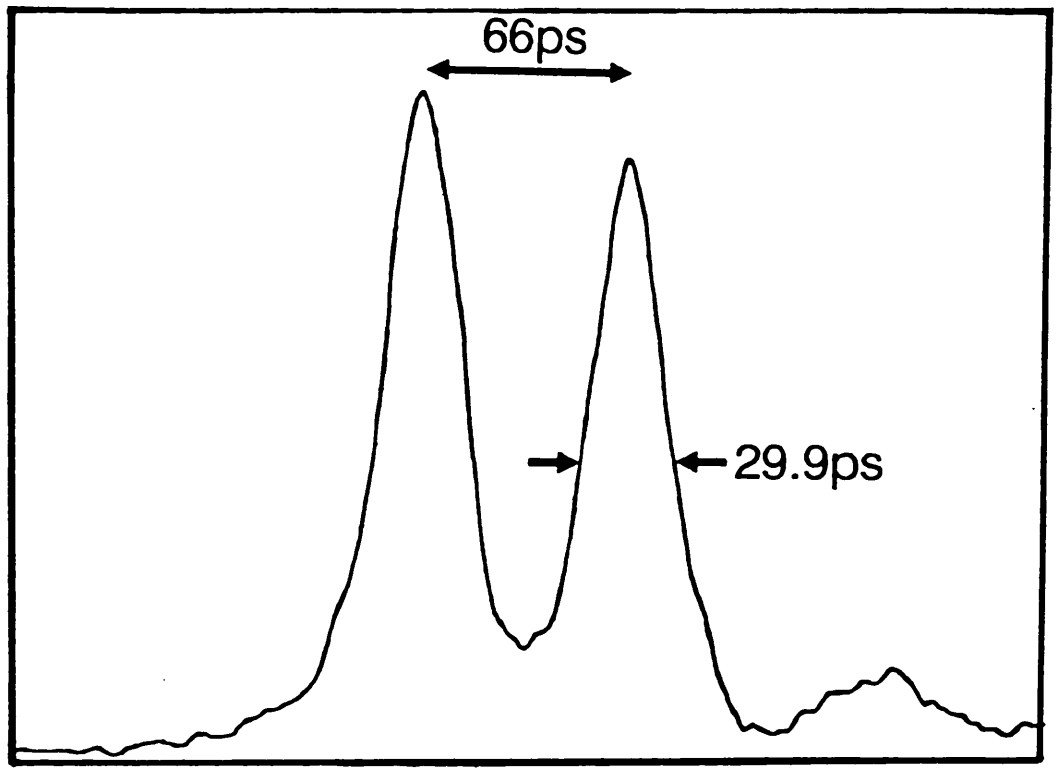

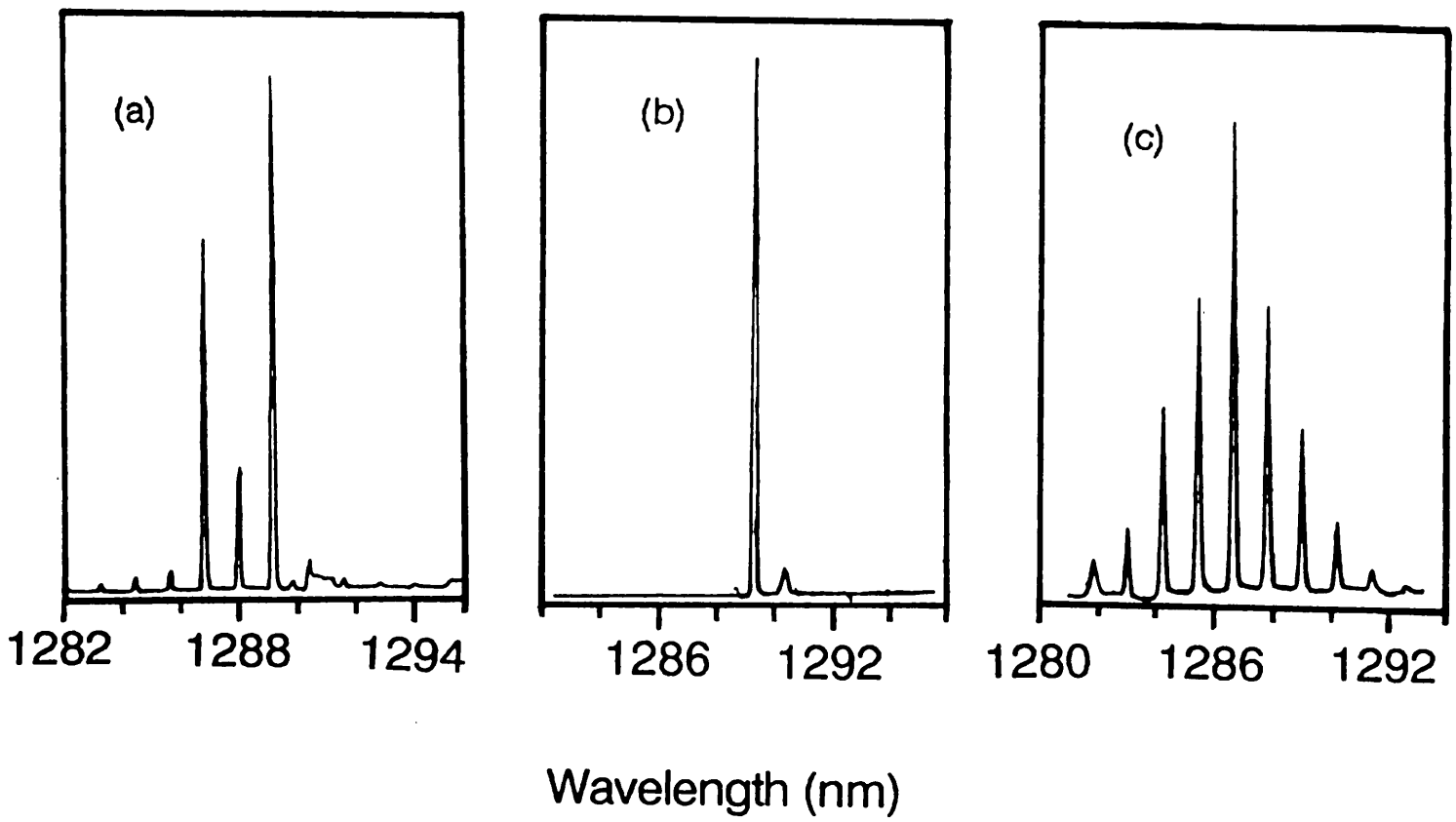

Figure (6.8): Emission spectra of an uncoated zero-degree laser, when (a) on its own, (b) collimated onto a ruled grating, and (c) focused onto the grating.

Figure (6.9): Mode-locked pulses from a uncoated zero-degree external (two-mirror) cavity laser.

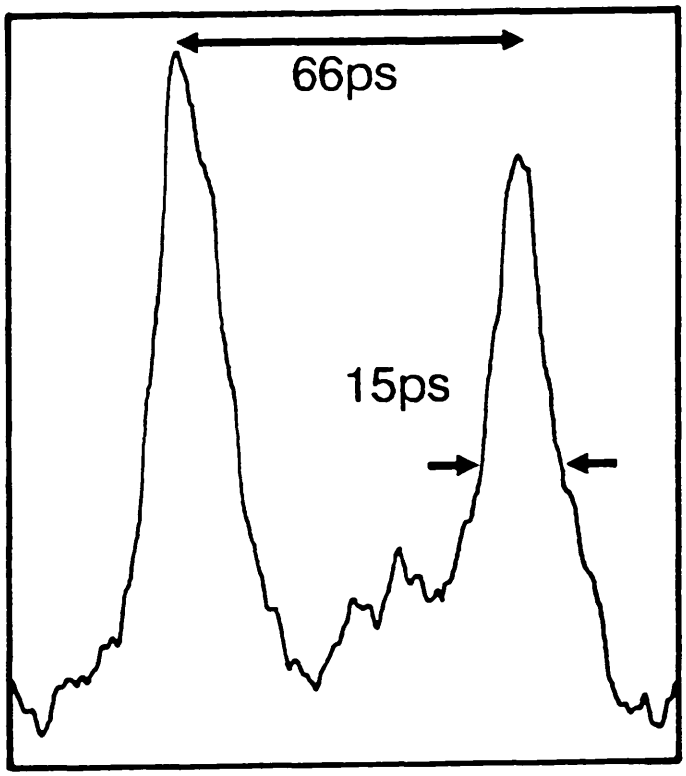

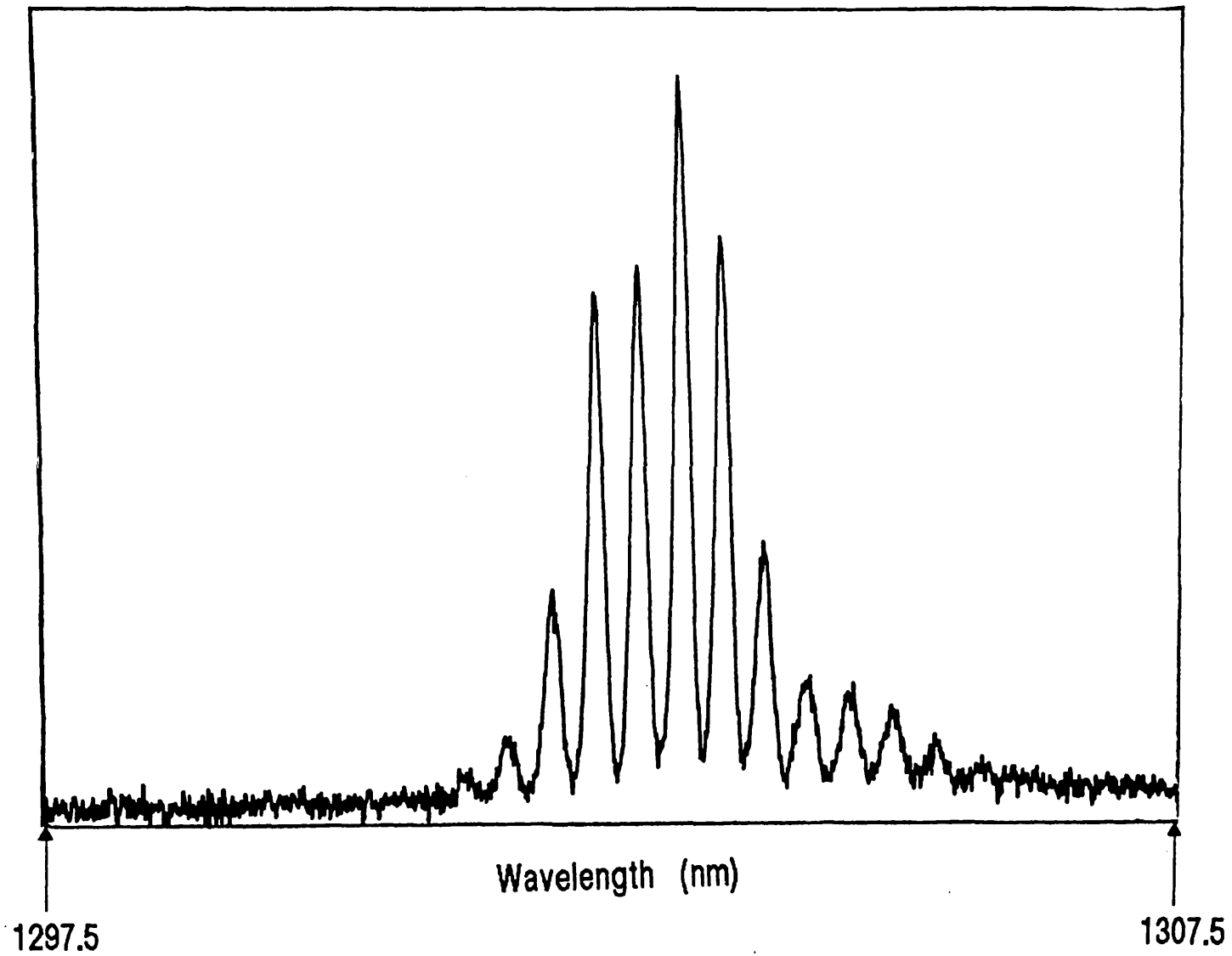

Figure (6.10): Emissio spectum corresponds to the mode-locked pulses in figure (6.9).

"focused" on to an external grating of 600 line pairs per mm. They were mode-locked because if the intracavity flux was blocked, the pulses would disappear. The peak to peak separation was set at 66ps and from which a pulse width of 29ps was calculated. The expected fine structures within the pulses were not observed. When on its own, the laser emitted multiple axial modes and each mode intensity varied randomly. But under the mode-locked condition, the intensities of the mode-clusters were bound by a smooth envelope (fig. (6.8)), also, the spectral envelope was wider than the d.c. pumping.

A single mode-cluster could be selected by collimating the beam onto the grating but this pushed up the threshold current near to the self-lasing threshold and "good" mode-locking could not be achieved. The pulses from a "collimated" external cavity laser were often very wide ($\approx$50ps) and of low peak-intensities. When increasing the R.F. or D.C. currents, the self-pulsation would occur and this is the so called "gain-switching". Unlike the mode-locked pulses, the gain-switched pulses were not affected by the presence of an external cavity. i.e. the pulses did not disappear when the coupling was blocked.

Mode-locked pulses from the uncoated zero-degree lasers were found to be improved by adding another external reflector. The extra optical feedback from the second reflector reduced the threshold current further from the self-lasing threshold. Thus, larger R.F. currents can be accommodated without overshooting the self-lasing threshold. Figure (6.9) shows the shortest pulses of 15ps obtained from such two-mirror cavities. The narrowing of pulses compared to before were probably due to the increase in broadening of each mode-cluster caused by the strong R.F. currents. Figure (6.10) shows the mode-locked spectrum in which the increase in both the cluster's broadening and the cluster-cluster overlapping can be clearly seen. Perhaps, it was due to this overlapping that a "weak" locking effect was established between neighbouring clusters which led to a significant improvement in the mode-locked pulses.

It is noted that according to the theoretical predictions described in the pre-

vious chapter, the pulse width reduces proportionally to the minus-forth-root of the R.F. modulation depth i.e. the dependence of pulse width on R.F. currents is very weak. Thus, the increase in R.F. current on its own cannot explain such large reduction in the pulse-widths implying that other effects must also be involved. One possible effect is the "weak" locking between mode-clusters as mentioned. The other could well be that in the case of a two-mirror cavity, the active medium is placed at the centre such that there are two counter-propagating pulses inside the cavity. These pulses interact with each other inside the active medium and perhaps it is this interaction which causes the pulse-narrowing.

6.5b A.R. coated lasers

In the study of external cavity A.R. coated lasers as described in chapter four, it was found that although the presence of SiO coatings made the self-lasing impossible, multiple mode-clusters still appeared in the emission spectra. This may be due to the absorption in the coating that fluorescence were much smaller than expected. Perhaps, it is due to the second reason that the mode-locked pulses were very weak. Figures (6.11) and (6.12) display a trace of the mode-locked pulses and its corresponding emission spectrum respectively from an one-side-coated laser which was placed within an (100%,40%) external cavity. The measured pulse-widths were 29ps but due to the weak pulse intensities, the signal to noise ratio was very poor even though the intensifier was operating at its most sensitive state. Probably, for the same reason that mode-locked pulses from a two-side-coated external cavity laser could not be detected on the streak camera/intensifier. Thus, in addition to the current characteristics, the intracavity losses also play an important role in the mode-locking.

6.5c One-side Brewster angled strip lasers

The mode-broadening in a r.f. modulated O.S.B. laser was the widest compared to the other two types of lasers. The increase in mode-width was typically

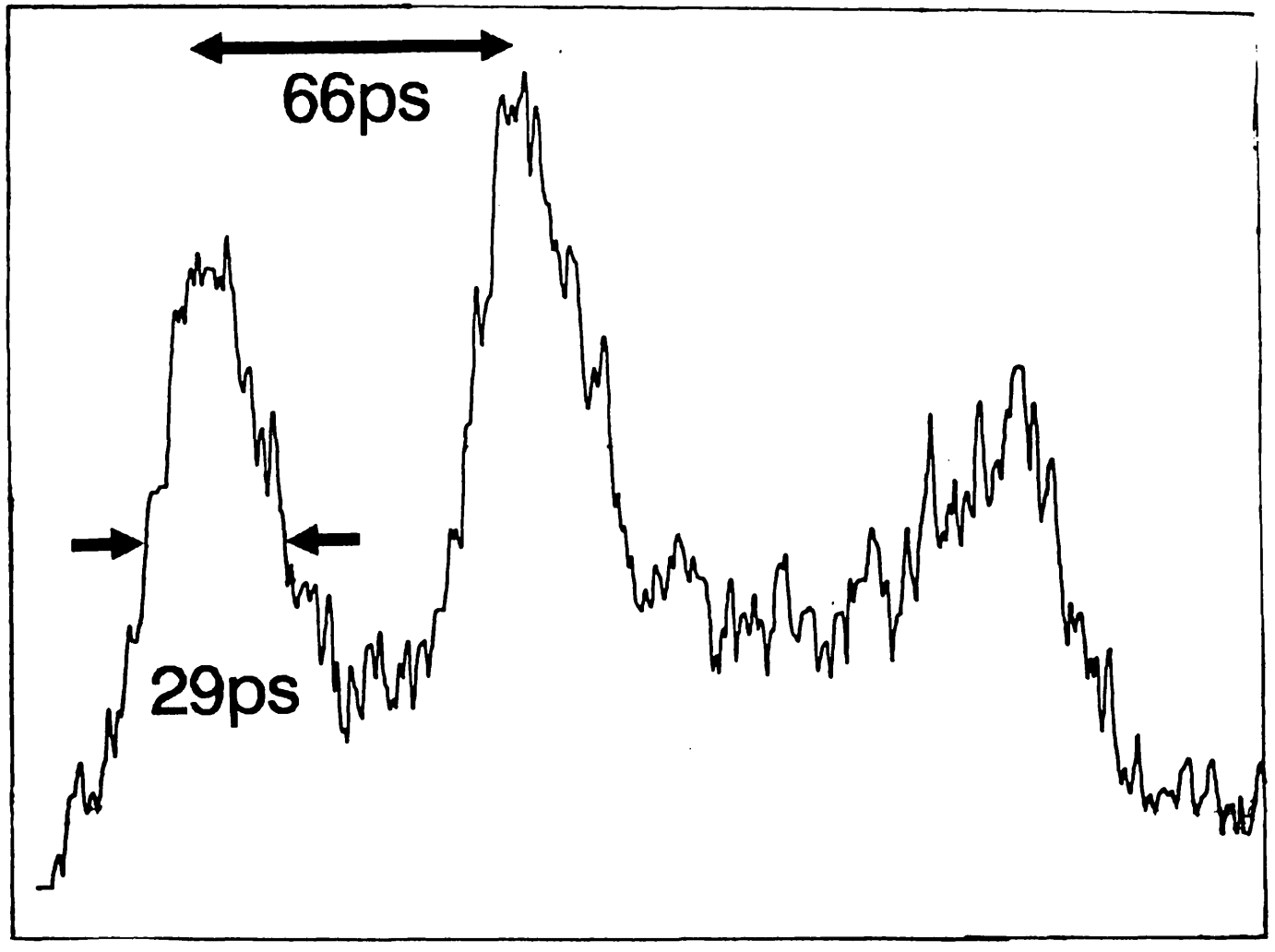

Figure (6.11): Mode-locked pulses of an one-side-coated external cavtiy (two-mirror) laser.

Figure (6.12): Emission spectrum corresponds to the mode-locked pulses in figure (6.11).

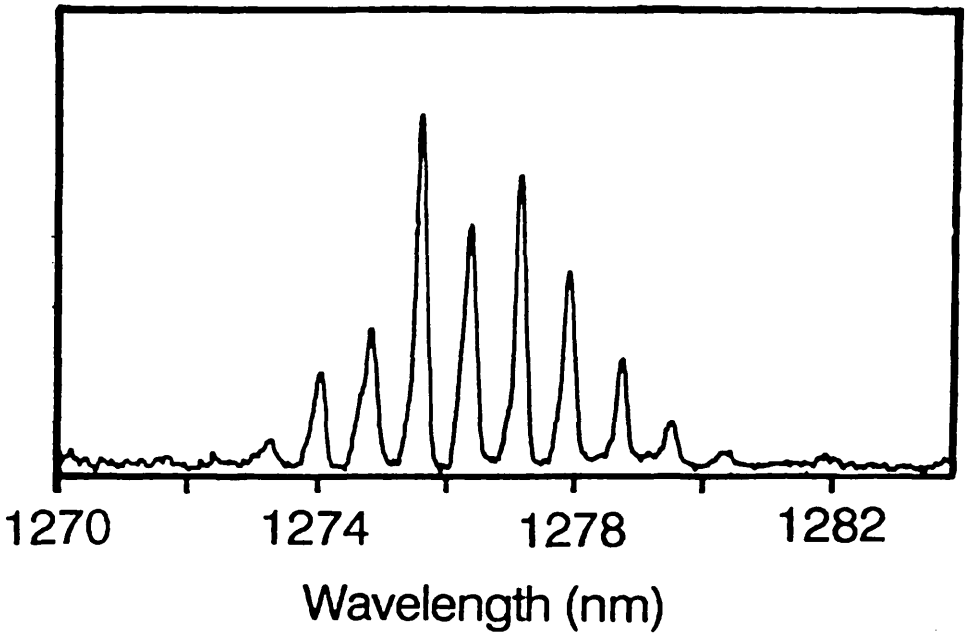

Figure (6.13): Broadening of a single mode due to r.f. modulation.

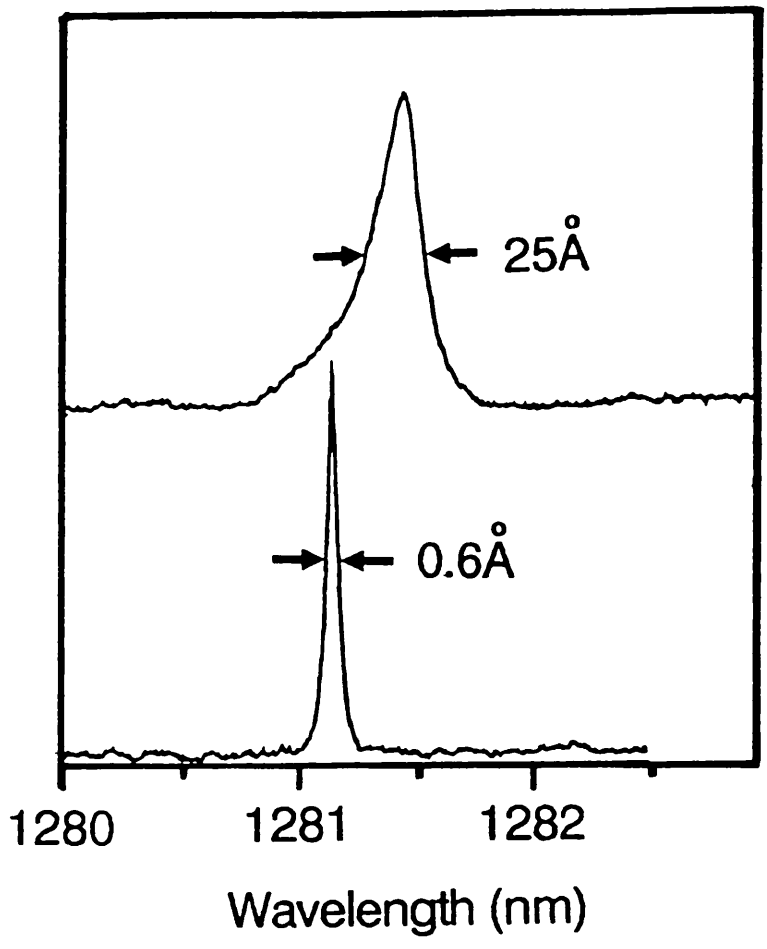

Figure (6.14): Emission specta of "collimated beam" and "focused beam" external grating lasers.

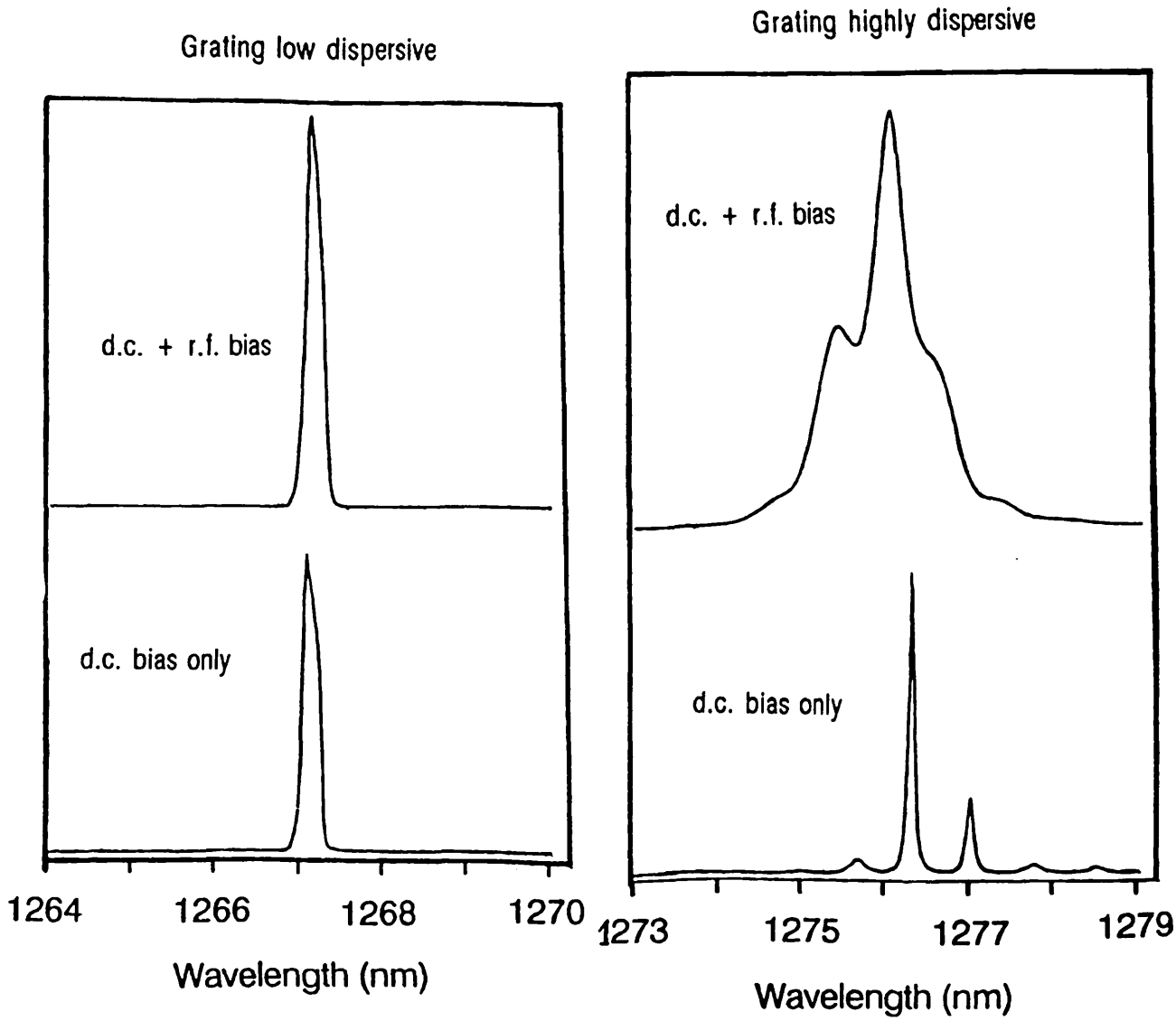

Figure (6.15): Mode-locked pulses of a "focused beam" external cavtiy O.S.B. laser.

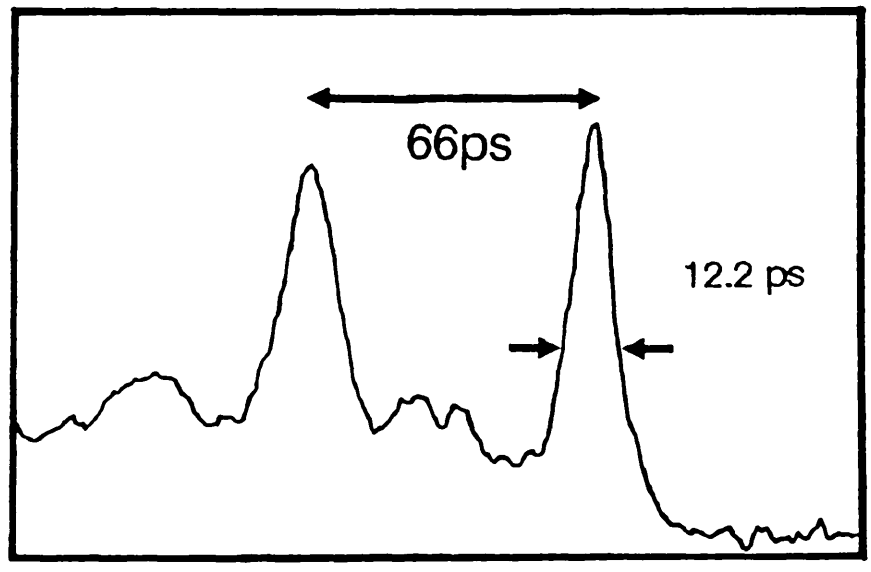

about four times that for the pulse-narrowing. of d.c. pumping. Figure (6.13) shows the emission spectra of a single-mode laser for d.c. and d.c.+r.f. pumping. In this pulse-narrowing., there is a shift of about 4Å towards longer wavelengths.

The shifting of the peak wavelength is due to the depletion effect. When the r.f. modulation is superimposed upon the d.c. bias, optical pulses are generated, and circulate inside the external cavity. Before a pulse arrives at the gain medium, a high carrier density has been established which causes a large separation between the two quasi-Fermi levels[110]. As the pulse is travelling through the gain medium, depletion occurs in the carrier density. Since the intraband relaxation time ($\approx$0.1ps) is much faster than the pulse transit time ($\approx$3.33ps for a 250μm long laser), the separation of the Fermi levels becomes closer as the pulse sweeps across the gain medium. Thus, the r.f. modulated lasing mode will sweep towards longer wavelengths. The amount of shifting is proportional to the change in carrier density. For more intense pulses, larger sweeps will occur.

Figure (6.14a) and (6.14b) show the mode-locked spectra of the "collimated" and "focused" external grating laser respectively. For the former pulse-narrowing., because of the tight spectral selectivity, there was no mode broadening. The corresponding pulse-widths were around 30ps. The shift was only about 1.8Å. Since the pulses were comparatively wide, the peak intensities were too small to cause a strong carrier depletion which led to a small shift.

For the "focused" alignment, the wide spectral window enabled the excitation of multiple mode-clusters. In fact, three clusters were observed but only one of which was strong. Upon applying the r.f. current, each cluster was broadened and started to overlap with its neighbouring clusters. Because of the strong overlapping, cluster to cluster locking was established, i.e. more "external cavity" modes were able to be locked with each other. This produced the shortest pulses of 12.2ps (fig. (6.15)). After deconvolution with the d.c. response of the streak camera ($\approx$7ps), pulse-widths of 10ps were calculated. From the emission spectra, the corresponding shifting was

about 4.5Å indicating that the strong carrier depletion due to the narrow mode-locked pulses.

At the optimum mode-locking conditions, small variations in either the d.c. bias or r.f. currents had little effect on the pulse-widths. This agrees with the theoretical predictions outlined in chapter five, in which the pulse-width is shown to be proportional to the minus-forth-root of the applied currents. However, at large currents, pulses became broader and in some cases, they disappeared completely. This is due to the disruptions caused by the increased fluorescence noise. At high currents, the laser diode itself will produce intense A.S.E. as mentioned in chapter four, causing these disruptions. If the intensity of generated A.S.E. is comparable to the pulse intensity, the mode-locking condition will be completely destroyed. This is why suggestions have been made on using lasers with low spontaneous emissions.

6.5d Frequency dependence of the pulse profiles

Even at the optimum mode-locking condition, a pulse profile always has the main and secondary pulses. As mentioned before, this is due to the fast recovery of the depleted gain after the formation of the main pulse. Both the main and secondary pulses were very sensitive to the detuning of r.f. modulations. It was found that at the optimum condition, the pulse profiles were typically sensitive to a 0.002% frequency shift. This sensitivity is smaller than that of Argon ion lasers[111] (0.05%) and synchronously pumped dye lasers[112] (0.001%). Thus, the mode-locking condition of a semiconductor laser is as tight as the dye laser. Therefore, for practical applications, good stability of both the cavity and frequency are needed.

The observed detuning effect on the mode-locked pulses were similar to those observed by Chen[113] and Holbrook[114]. The detuning frequency is defined as:

$$\Delta f = f_{applied} - f_{optimum} \qquad (6-1)$$

It was found that the detuning effect on the pulse-widths were asymmetrical with the frequencies. For small positive detuning (i.e. positive Δf), the secondary pulses

Figure (6.16): Frequency dependence of the pulse profile.

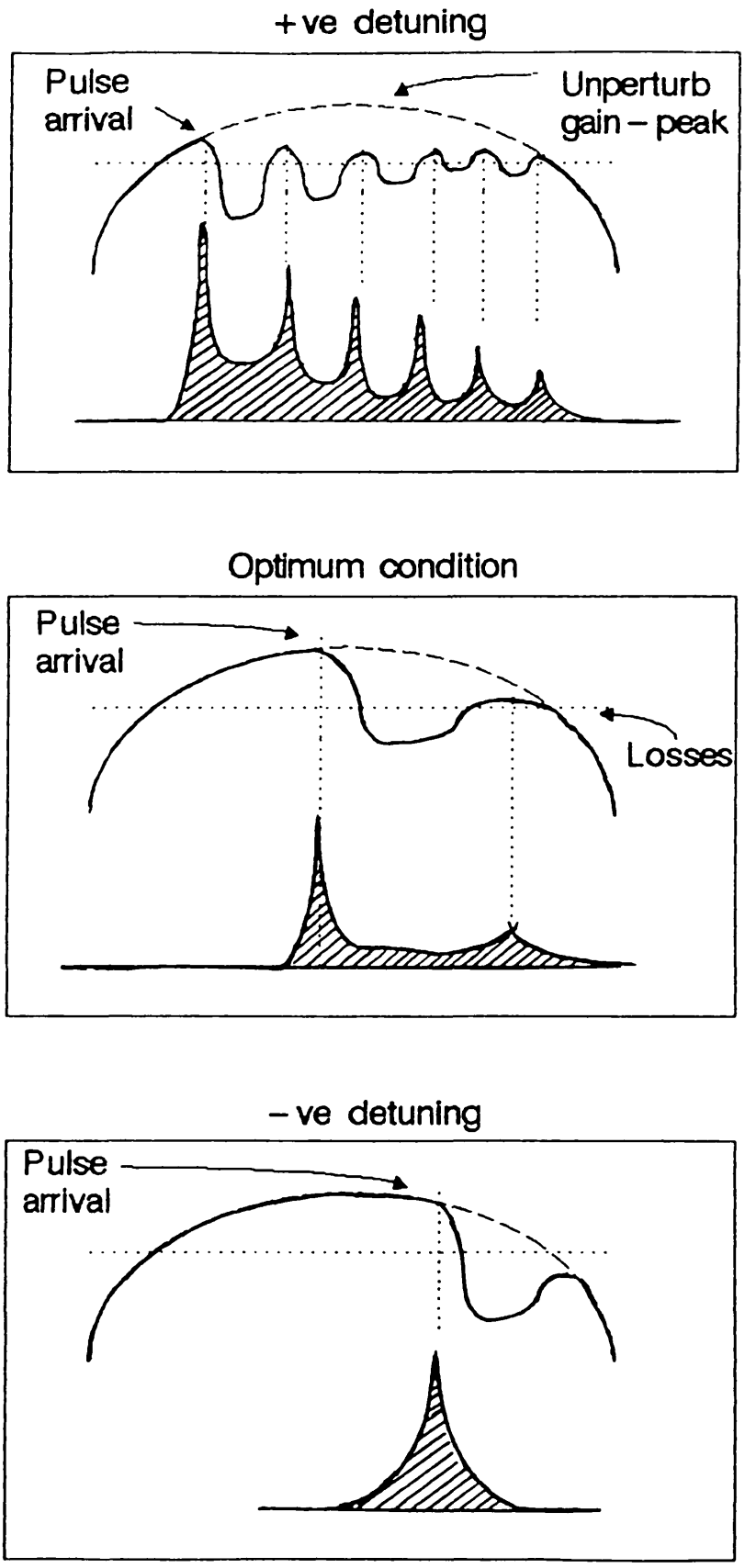

move closer to the main pulses to cause broadening. For detuning greater than 8KHz, both the main and secondary pulses merged together forming a single broad pulse. The broadening of this pulse continued with increasing detuning upto a few hundred KHz. Negative detuning on the other hand, was very sensitive to the frequencies. For a small amount of negative detuning (a few KHz), the pulses broadened substantially. A further increase in negative Δf causes the pulses to disappear completely. The observed asymmetry in detuning agrees with the theoretical predictions. [77,89]

As mentioned in chapter five, gain saturation by a pulse is an essential element of mode-locking. This enables the rear part of the pulse to experience a shortening effect. Thus, good mode-locking would demand the pulse to arrive slightly later in time than the peak of the gain (fig. (6.16)). This way, the pulse will saturate the gain and cause the sharpening of the rear part of the pulse. For a small positive detuning, an optical pulse arrives at the active medium slightly quicker than in the optimum condition. Because the pulse is now near to the gain peak, the depletion will be less severe and thus the depleted gain recovers more quickly. This leads to the formation of a secondary pulse which is closer to the main pulse. For a large positive detuning (i.e. beyond the gain peak), the arrival time of the pulse falls within the decaying period of the gain. Hence, there is not enough time for the depleted gain to recover and thus, the secondary pulse will disappear.

In the pulse-narrowing. of negative detuning, the pulse profile changes more rapidly. From figure (6.16), it can be seen that if a pulse arrives much sooner than the gain, both the front and main parts of the pulse will only see a small gain, i.e. the amplification will be small. As the rear part enters into the active medium, the gain has built up so the rear part will get amplified significantly. Thus, the overall pulse-width increases drastically. For a large negative detuning, the pulse will be completely washed out by the amplified rear part and the amplified spontaneous noise. Another crude explanation is that the r.f. modulated gain can be viewed as a r.f. chopper modulating the intracavity flux.

6.6 Conclusion

In this chapter, active and passive mode-locking experiments have been reviewed. To date, both kinds of these experiments require the semiconductor laser to be coupled to an external (or extended) cavities. Mode-locking results from a variety of external cavities have been outlined. These were the:

(1) Spherical and plane mirrors cavities,

(2) Optical waveguide and fibre cavities,

(3) Ruled grating cavities.

The early mode-locking experiments were usually carried out on zero-degree lasers. Later, in order to eliminate the fine structures observed in the mode-locked pulses, either the A.R. coated or the angled stripe lasers were used. However, the shortest pulses could only be generated from passively mode-locked lasers.

The pulse profile dependence of the r.f. modulation was discussed. Strong asymmetry was observed in detuning the mode-locked frequency from its optimum position. This agrees with work observed by other workers [113,114]. A simple diagrammatic explanation was given for such asymmetrical behaviour.

The diagnostic systems used in this experiment for aligning the lasers and recording the picoseconds mode-locked pulses were described. The pulse-widths, pulse-profiles, and their corresponding emission spectra were discussed. The main emphasis was on the broadening of cluster-modes due to the r.f. modulated currents. In the cases of multiple cluster emissions, the mode-locked pulse-widths were found to be dependent on the degree of the overlapping between adjacent clusters. It seems that a good overlapping can cause the clusters to weakly lock with each other, which otherwise, have on correlations between them. The shortest pulse-widths were about 12ps and after deconvolving with the system response of the streak camera, pulse-widths of 10ps were calculated. Also, the corresponding emission spectra had multiple clusters which overlapped strongly with each other.

CHAPTER SEVEN

Semiconductor laser amplifiers

7.1 Introduction

An optical amplifier is defined as a device which directly reproduces optical signals at a greater intensity without converting them into electrical signals. In many respects, its applications are fundamentally equivalent to that of its electrical counterpart. The main uses of optical amplifiers are:

(1) as preamplifiers to improve the detector sensitivity of photodetectors such as avalanche photodiodes.

(2) as power boosters to compensate the insertion losses incurred in coupling light into and out of passive elements.

(3) but the most important of all are as linear repeaters to expand the regenerative repeater spacing in the lightwave communication systems.

Recently, there has been a strong interest in semiconductor laser amplifiers because of their inherently high optical amplification by stimulated emissions and their compatibilities to passive elements such as optical fibres, and waveguides.

Semiconductor laser amplifiers can be grouped into two types. These are:

(1) the Fabry-Perot laser amplifier (F.P.L.A.) which is a conventional laser

diode operating just below its threshold. The amplification takes place as the incident light undergoes multiple reflections between the facets.

(2) the travelling-wave laser amplifier (T.W.L.A.) which has an ideal zero reflectivity at each end. The incident signal is amplified during a single passage and completely coupled out without reflecting any light back into the active region.

Studies on semiconductor laser amplifiers can be dated back to the early development of laser diodes. After its invention in 1963, amplification experiments were conducted on GaAs homojunction lasers at 77°K and despite the immature laser diode capability at the time, the principle and feasibility of optical amplification in semiconductor lasers was demonstrated.

The advent of heterostructure lasers which give continuous-wave emission at room temperature, has further stimulated work in this area. Both experimental [4,7,13,23,43,44,65,66,69,92,95,110] and theoretical [11,54,57,59,60] investigations have been intensively carried out on GaAs (1973 to 75), GaAlAs (1977 to 83), and InGaAsP (1980 to the present) devices. The main attraction of the quarternary laser amplifiers are that their emission bandwidths fall within the spectral windows (zero loss at 1.3μm and zero dispersion at 1.55μm) of the silica optical fibres which are widely used in optical communication systems.

The feasibility of inserting the laser amplifier into optical fibres has already been demonstrated on early GaAs devices by Schicketanz et al[73] and in their experiment, the amplifier was coupled to optical fibres which have rectangular cores, through which the incident light and the amplified signals were channelled.

Later, in the early 1980s, Mukai et al[59] have successfully demonstrated the applications of laser amplifiers and linear repeaters in single mode fibres. They found that the preamplifiers improve the minimum detectable power by 7.4dB over the silicon avalanche photodiode's direct-detection level; and the use of two linear repeaters have increased the regenerative gain by 37dB. During that period, important material and structural parameters of laser amplifiers have been established on GaAlAs

Figure (7.1): Travelling-wave and Fabry-Perot laser amplifiers.

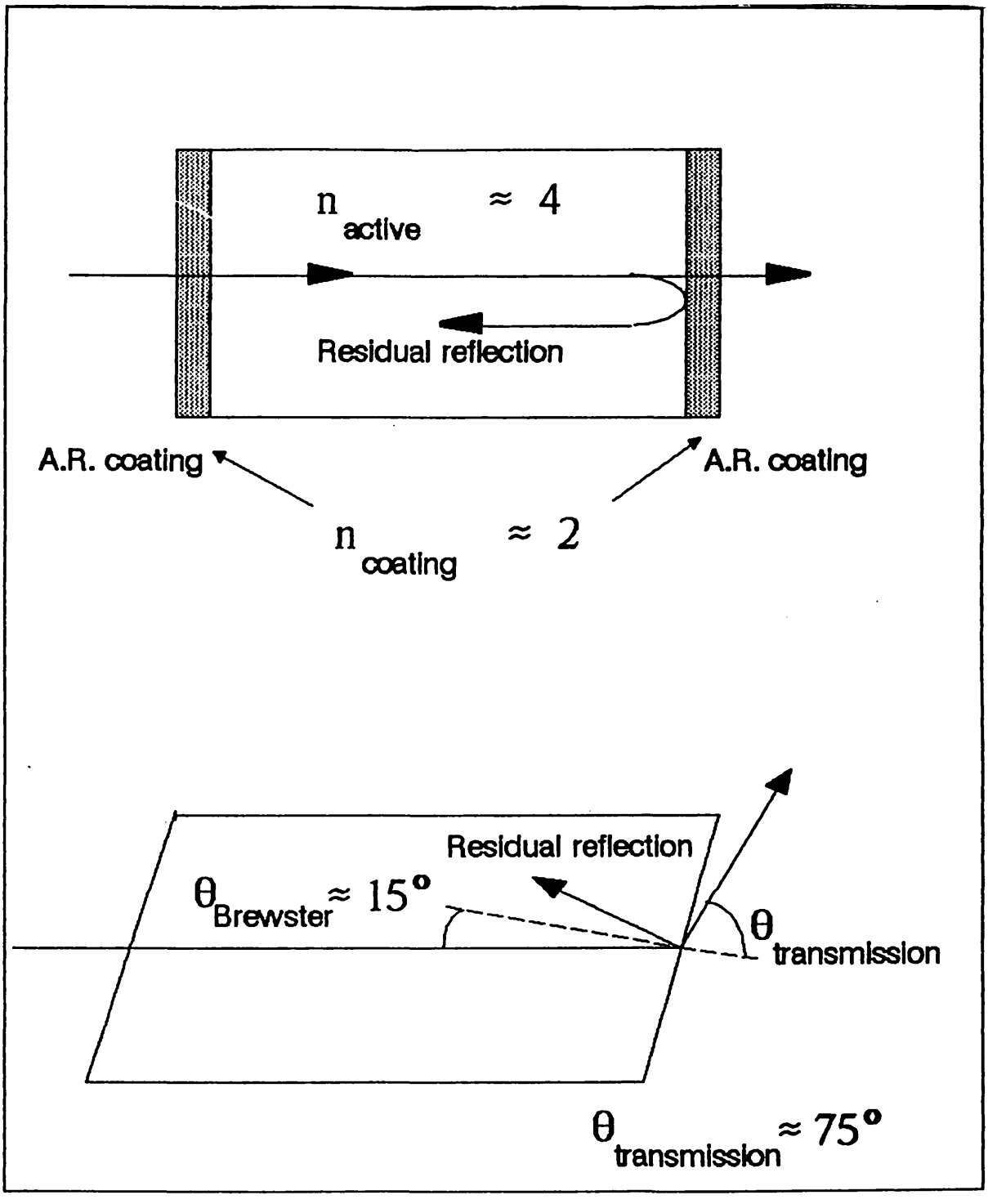

devices. These characterisation schemes can also be applied to the longer wavelengths of InGaAsP laser diodes.

Recently, most studies on InGaAsP amplifiers have been centred around the travelling-wave structure. This is because the T.W.L.A. has a broader amplification bandwidth, a high signal gain, and a high saturation power level, whereas, the Fabry-Perot laser amplifiers have narrow bandwidths and lower gain which is limited by the lasing threshold currents. A further constraint is necessity for maintaining good stability control in matching the gain peak to the wavelength of the incident signals.

At present, the transformation of a laser diode into a T.W.L.A. is normally carried out by depositing a single antireflection thin-film (fig. 7.1a) onto the facets. To achieve the ideal zero reflectivity, the film index has to be matched to the square root of the active region index. But in practice, perfect index matching is extremely difficult to achieved due to:

(1) the variation of index with injected carrier density,

(2) the fabrication of coating material of the desired index.

With a silicon monoxide (SiO) thin-film, the facet reflectivity can be readily reduced down to 0.1% but recently, Mukai et al[61] have achieved reflectivities as low as $13x10^{-6}$. Other workers [22,23] have used sputtered silicon nitride (Si_3N_2) on InGaAsP devices and obtained facet reflectivities of the order of 10^{-4} to 10^{-3}. Although high quality A.R. coating is possible, successful yields may not be good due to the high sensitivity of tailoring the film index to the processing parameters. In addition, it is difficult to achieve a perfect index matching because of the index variation with current densities.

Another way (fig. (7.1b)) of suppressing the facet reflectivity is to obtain a Brewster angled facet (with respect to the active stripe). The work on this type of laser diodes have already been mentioned in chapter two and thus will not be repeated here.

In this chapter, the basic principles of semiconductor laser amplifiers is presented, and experimental investigations on the performance and characteristics of Brewster angled stripe laser amplifiers is described. The gain measurements were carried out by probing the amplifiers with picoseconds pulses from a mode-locked external cavity laser. Finally, the results are summarised in the conclusion.

7.2 System gain

The signal gain G of an amplifier device is defined as the ratio of the increase in output signal over the input signal and it is given as:

$$G_{signal} = \frac{P_{output} - P_{spont.emission}}{P_{input}} \qquad (7-1)$$

where P_{input}, P_{output}, and $P_{spont.emission}$ are the powers of the input, output, and spontaneous emissions respectively. The signal gain, G_{signal}, is a measure of the net gain through the whole amplification device and is thus a dimensionless quantity. The signal gain is different from the gain coefficient, g, which was mentioned in chapter II. The g is a measure of the increase in photon numbers as they propagate through the active medium and its S.I. unit is normally expressed as cm^{-1}. In the case of an ideal T.W. laser amplifier, these two coefficients are connected by:

$$G_{signal} = e^{(\Gamma g - \alpha)L} \qquad (7-2)$$

where Γ is the light confinement factor, α is the total internal loss, and L is the length of the active stripe. In most optical amplification experiments, the performance of the amplifiers is often expressed in terms of the signal gain. This is because the main issue of these investigations is on the device performance rather than on the actual material characteristics.

In practice, the net coupling efficiency of the optical couplers which are used to feed the input into and to collect the output from the amplifiers, must also be taken into account. The modified G_{signal} is given as:

$$G_{signal} = \frac{P'_{output} - P'_{spont.emission}}{\xi_{in}\xi_{out}P'_{input}} \qquad (7-3)$$

where the apostrophe denotes a measurable quantity.

The coupling coefficients ξ_{in} and ξ_{out} can be determined experimentally by using the equilibrium equation which relates the internal gain and the losses at the lasing threshold. The equilibrium equation is given as:

$$gain = \frac{\Gamma n_g A}{c}(D_o n - n_o) \qquad (7-4a)$$

$$loss = \alpha_{cavity} + \alpha_{internal} \qquad (7-4b)$$

where A is the emission factor, $\alpha_{internal}$ is the material loss due to optical scattering and carrier absorption, α_{cavity} is the transmission loss due to the facets or external reflectors and is given as $\frac{1}{L}ln\frac{1}{r_1 r_2}$, D_o is the linewidth function at the gain peak and n_o is the nominal carrier density. When lasing, the losses and gain cancel out with each other.

Suppose that a Brewster angled stripe laser is coupled to a two-mirror external cavity of reflectivities R_{B1} and R_{B2} and also to a Fabry-Perot laser of the same length as the amplifier which can lase on its own (i.e. with facet reflectivities of $R_{F.P.1}$ and $R_{F.P.2}$) without the use of an external cavity. The threshold currents are ${}_{Brewster}I_{th}$ and ${}_{F.P.}I_{th}$ respectively. By substituting these parameters into the above gain and losses equations the difference in the lasing threshold gain and losses can be written as:

$$Change\ in\ gain = (\frac{\Gamma n_g A D_o \tau_{sp}}{cedL\omega})({}_{Brewster}I_{th} - {}_{F.P.}I_{th}) \qquad (7-5a)$$

$$Change\ in\ loss = \frac{1}{L}ln(\frac{r_{F.P.1}r_{F.P.2}}{r'_{B1}r'_{B2}}) \qquad (7-5b)$$

Equating and solving these equations for $r'_{B1}r'_{B2}$ and the net coupling efficiency can then be calculated using the following equation:

$$r'_{B1}r'_{B2} = \xi_{in}\xi_{out}\sqrt{r_{B1}r_{B2}} \qquad (7-6)$$

Using this estimation, a coupling efficiency of about 10% to 15% was calculated for the x20 microscope objectives. These values are similar to those obtained by Chen[13] who used the same procedure. There may be a small error in this estimation due to

the stray light that transmits through the cladding which has not been taken into account. However, because of the high signal gain the amplified signal will normally be much larger than the stray light intensity and so the error has a negligible effect on the experimental results.

7.3 Principles of semiconductor laser amplifiers

In the previous section, the measurable parameters were defined for characterising the performance of laser amplifiers. In this section, basic principles of optical amplification in semiconductor lasers is presented. i.e. how the operational parameters such as the gain saturation and the highest attainable gain vary with the material and cavity characteristics.

7.3a Spectral gain bandwidth

The variation of optical gain with wavelengths is dependent on two factors:

(1) the material (intrinsic) gain bandwidth,

(2) the cavity gain bandwidth.

The first factor is determined by the material parameters such as the injection carrier densities, material compositions and the bandgaps. The cavity gain bandwidth can be viewed as the spectral window (i.e. transmission) of the laser amplifier which can be calculated from the multiple beam interference equation.

Referring to figure (7.2) the Fabry-Perot laser cavity is filled with a gain medium which has a single-pass-gain of g_s and the incident light intensity is unity. Due to multiple reflections within the mirrors of power reflectivities R_1 and R_2, the net transmission is given by:

$$t_{net} = \frac{E_t}{E_i} = t_1 t_2 \sqrt{g_s} e^{\frac{-2\pi i n L}{\lambda}} (1 + g_s r_1 r_2 e^{\frac{-2\pi i n L}{\lambda}} + \cdots)$$
$$= \frac{t_1 t_2 \sqrt{g_s} e^{\frac{-2\pi i n L}{\lambda}}}{(1 + r_1 r_2 g_s e^{\frac{-4\pi i n L}{\lambda}})} \qquad (7-7)$$

Figure (7.2): The signal gain of a Fabry-Perot laser amplifier.

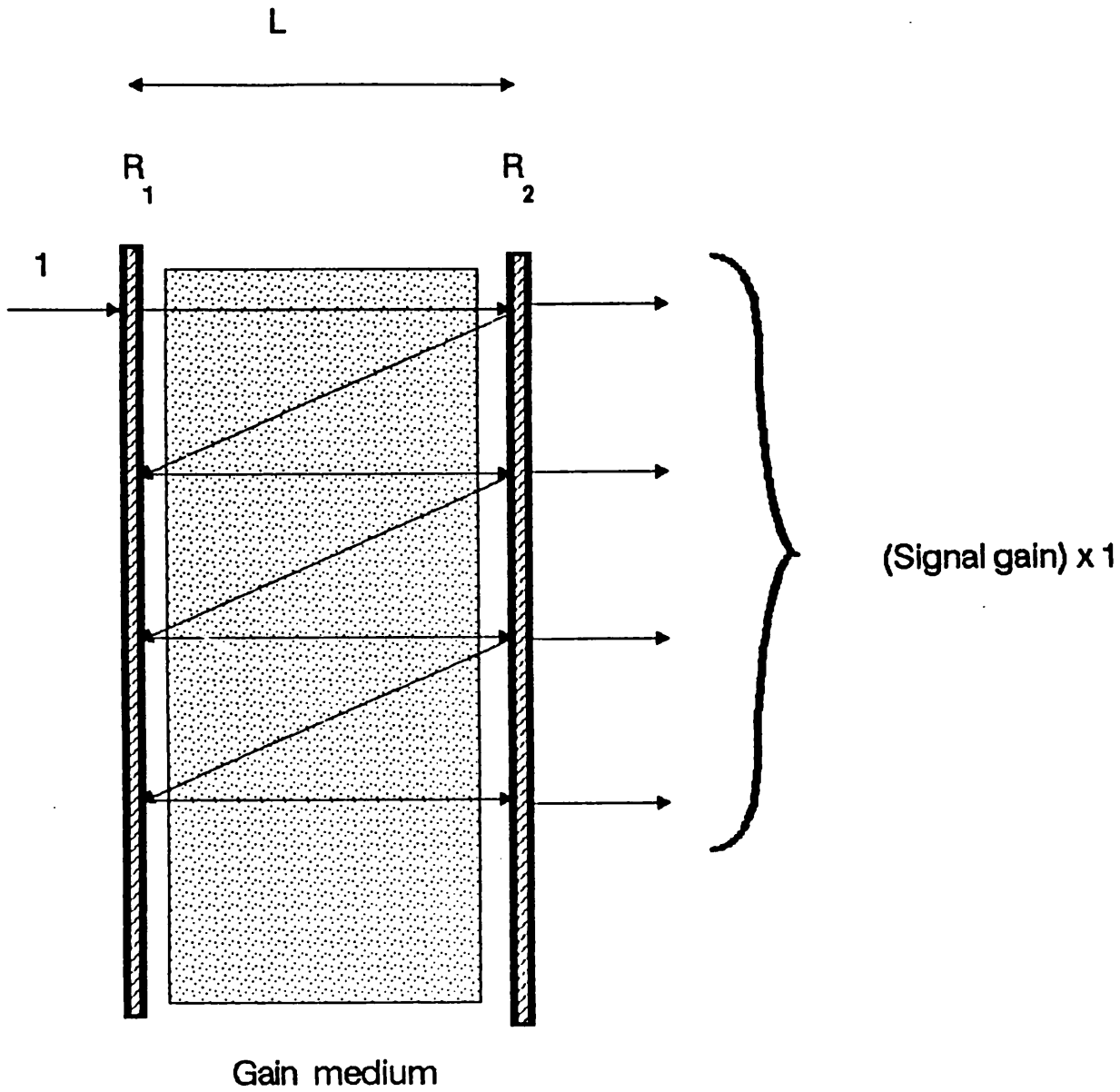

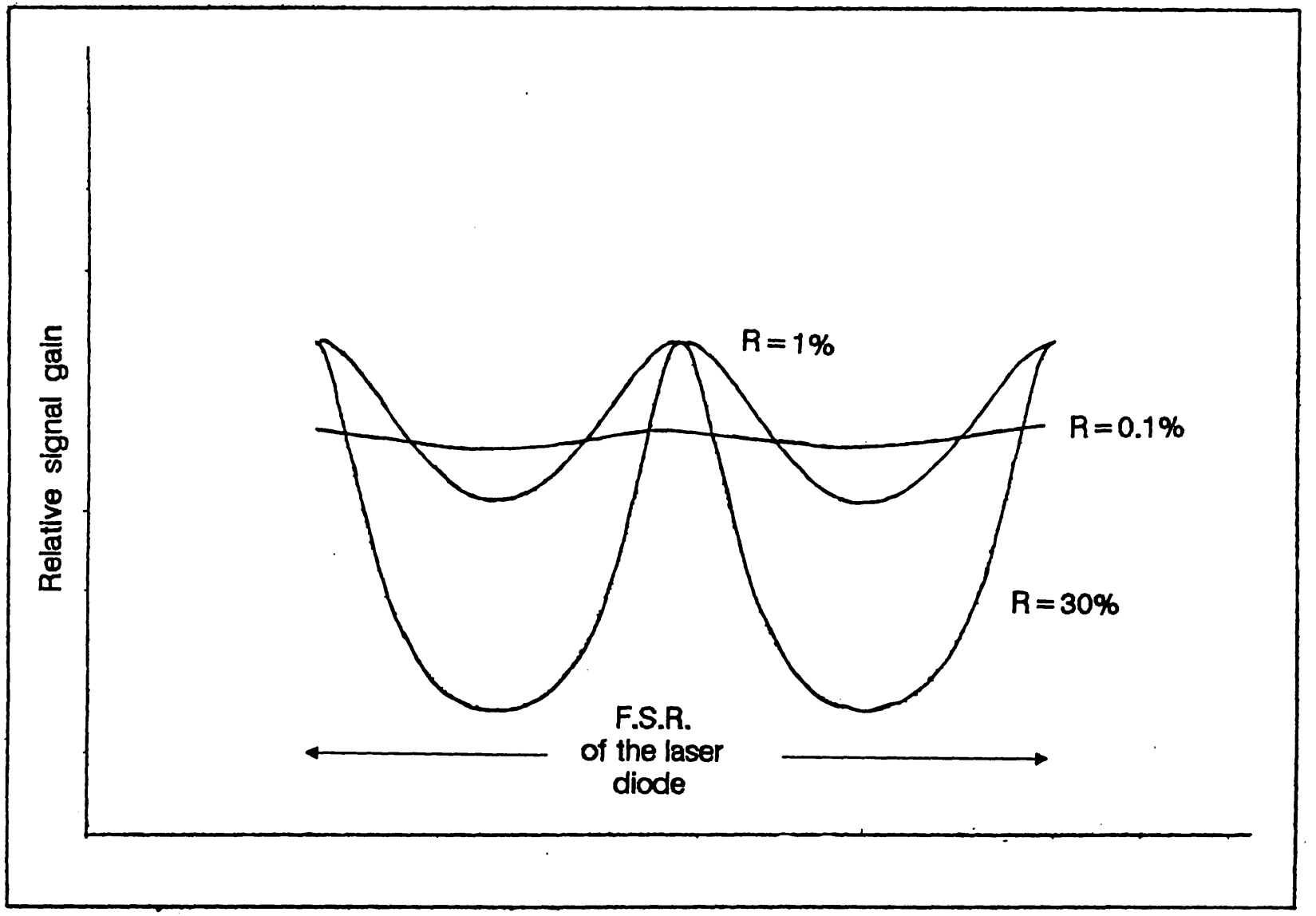

Figure (7.3): The gain bandwidths of Fabry-Perot and near T.W. laser amplifiers.

and the net intensity transmission is

$$T_{net} = |t_{net}|^2 = \frac{T_1 T_2 g_s}{(1 + R_1 R_2 g_s^2 - 2\sqrt{R_1 R_2} g_s \cos 4\pi n L/\lambda)} \qquad (7-8)$$

Equation 7-8 is essentially the signal gain, G_{signal}, and it is a periodic function which means that the signal gain varies periodically with wavelength. It was found that the FWHM of each cycle narrows with increasing mirror reflectivities.

For an ideal T.W. amplifier which has zero reflectivities, i.e. the R's are zero and the T's are 1, the above equation will be reduced to a single-pass-gain of g_s, i.e. the amplification is independent of the input wavelength provided that it is within the material gain bandwidth. Hence, an ideal T.W. laser amplifier should have a "white-light" response. Figure 7.3 shows how the signal gain G_{signal} varies with different combinations of mirror reflectivities.

7.3b Gain vs currents

The single-pass-gain (equation 7-2) depends exponentially on the material gain, $g(n)$. In most cases[53], the material gain can be approximated by a linear function with the carrier densities, n, i.e.:

$$g(n) = \frac{\Gamma A n_g}{c}(n - n_o) \qquad (7-9)$$

where Γ is the confinement factor, n_g is the group index, A is the stimulated emission factor, and n_o is the nominal carrier density at which, the active medium becomes transparent. Thus, according to this definition, the natural logarithm of the single-pass-gain should also be a linear function of the pumping current.

As mentioned before the usual rate equations are not appropriate for describing T.W. laser amplifiers because of the spatial variations in both photon and electron densities. Thus, the current dependence of the gain is not as straight forward as described by the above equation. Marcuse[54] used a set of travelling-wave rate equations to model the performance of a T.W. amplifier in which the spatial variations were taken into account. His numerical solutions showed that the single-pass-gain

was not linearly dependent on the current. It was also found that at large currents, the increase in gain occurs less drastically than at low currents, i.e. there is some sort of saturation at high pumping levels. Even in the absence of any input signals, the amplifier's gain becomes partially saturated at very high currents. It was suggested that this is due to the fluorescence generated by the amplifier which takes up some of the available gain, especially in the high gain regime.

In the case of a F.P. laser amplifier [73,95], the gain increases with increasing currents. But due to the Fabry-Perot effect, the spontaneous emissions are partially confined within the laser amplifier and subjected to stronger amplification than inside a T.W. amplifier. As a result, less gain is available for any input signals. Since the amount of fluorescence emissions increases with currents, the available gain will therefore become smaller at very high currents. Such an effect is similar to clamping of the lasing-gain of any laser despite further increase in the pumping levels beyond the lasing threshold.

7.4 Experimental arrangement and alignments

(i) The apparatus

The experimental set-up which was used, is depicted schematically in figure 7.4. The signal source was an external cavity Brewster angled stripe semiconductor laser which has been described previously in chapters IV and VI. When it was mode-locked, it generated optical pulses of around 10 to 30 picoseconds. A variable attenuator (transmission can be adjusted from 85% to 0.1%) was used and placed at the output mirror of the signal source, so that the input light level onto the amplifier could be adjusted. The absolute transmissions at various settings of the attenuator were calibrated by a photospectrometer and the output power from the laser source was measured by an optical power meter (photodyne).

Beyond the variable attenuator, light was then divided by a 50%/50% beam splitter ($B.S._1$) into two equal replicas. One was coupled into the laser amplifier by

Figure (7.4): Experimental set-up.

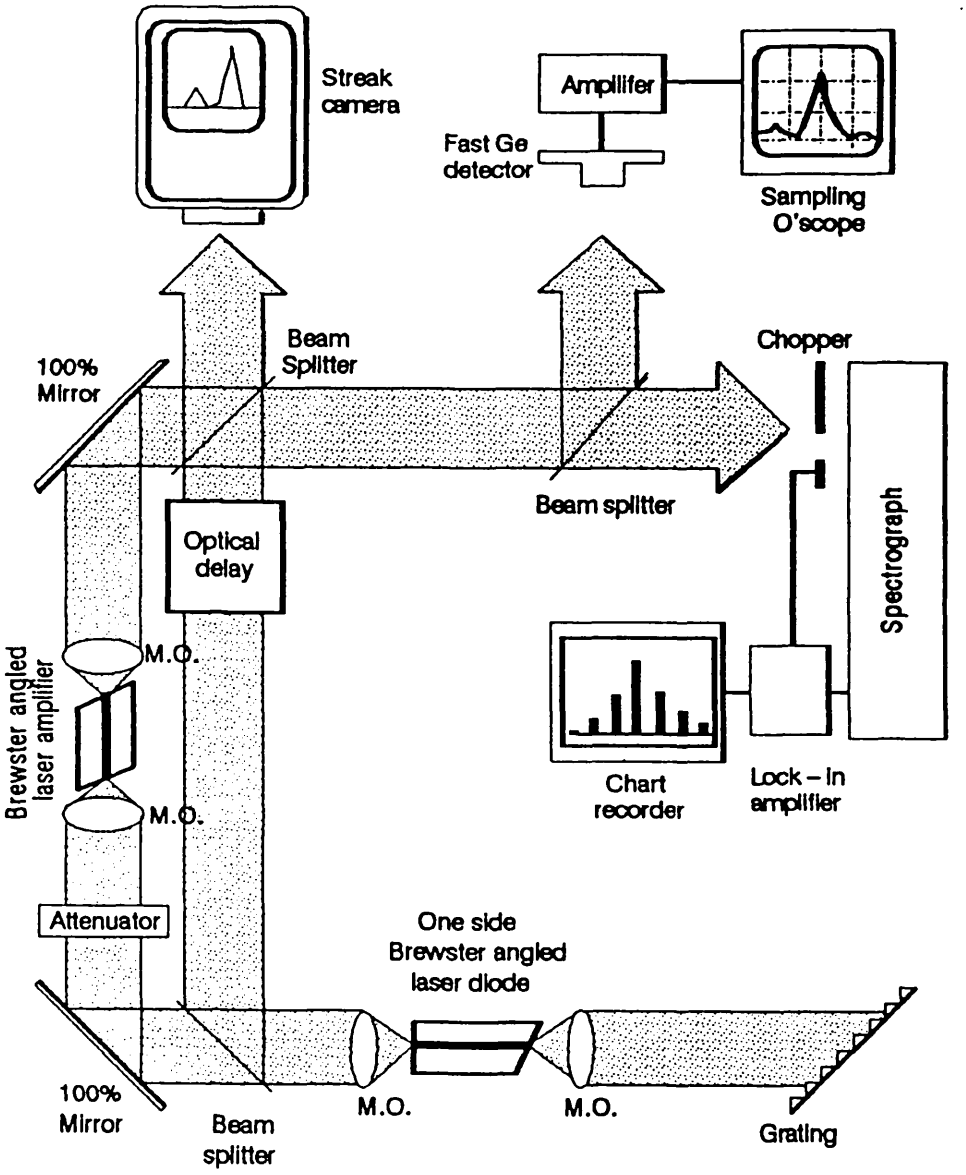

a x20 microscope objective and the amplified signal was then collected by another x20 objective. The other replica was partially reflected at 90° and recombined with the amplified beam at the second beam splitter ($B.S._2$) after which, the recombined beams were further divided into two parts. One part was chopped by a rotary chopper revolving at 1KHz before entering the spectrograph. The detected electrical signal from a large area germanium detector (GA-5) was amplified through a lock-in amplifier which was in-phase with the chopping frequency and the spectrum was then plotted on a chart recorder. The other part was either focused onto a fast germanium/amplifier detector (GM-3) and monitored on a sampling oscilloscope ; or focused onto a synchronscan streak camera/intensifier and the streak images were read out on an optical spectrum analyser (O.S.A.)

Initially, the pulse was viewed on the sampling oscilloscope and calibrated with the measured average power of the input beam using the photodyne power meter. Once, it had been calibrated, the applied voltage on the germanium/amplifier detector was fixed, otherwise any changes in the applied voltage would alter the gain and thus require a new calibration. The pulse-amplitudes of the amplified signals were measured for various input powers and for currents applied on the laser amplifier. The measured data was then converted into milli-Watts and were presented graphically using the equation 7.3.

(ii) The alignments

The copper stud which hosted the laser amplifier was mounted onto an piezo-electric x-y-z translational stage and the "source" laser stud was fixed inside a rotational base mount. The signal beam from the source was controlled by a x20 microscope objective ($M.O._2$) which was also mounted on a piezo-electric x-y-z translation stage. The other two x20 microscope objectives, $M.O._3$ and $M.O._4$, were mounted onto micrometer-controlled x-y-z translation stages.

Initially, the "amplifier" stud was removed from the stage, i.e. from between

Figure (7.5a): Emission spectra of the "source" laser, when the Brewster angled laser amplifier was switched on and off.

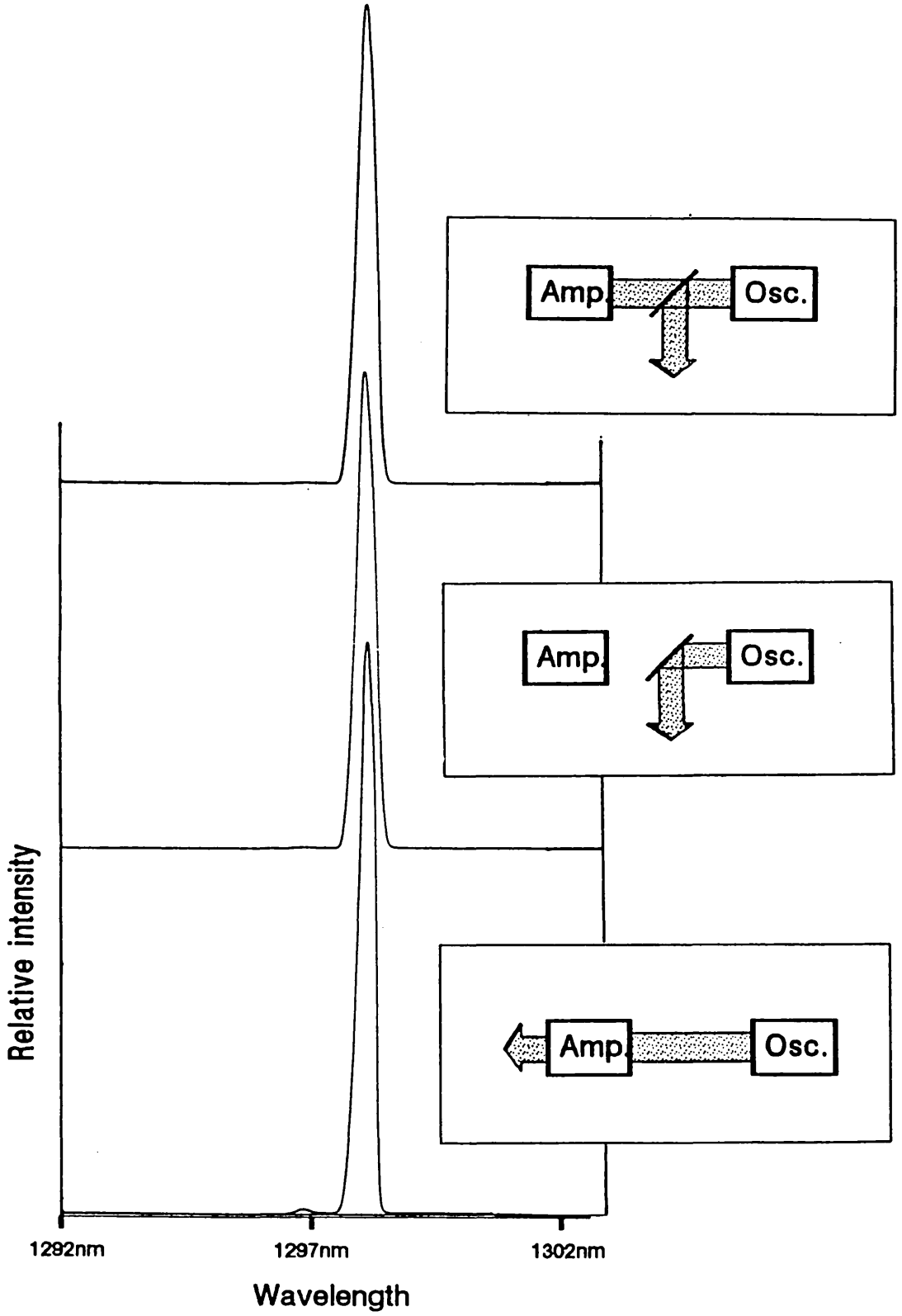

Figure (7.5b): Emission spectra of the "source" laser, when the Fabry-Perot laser amplifier was switched on and off.

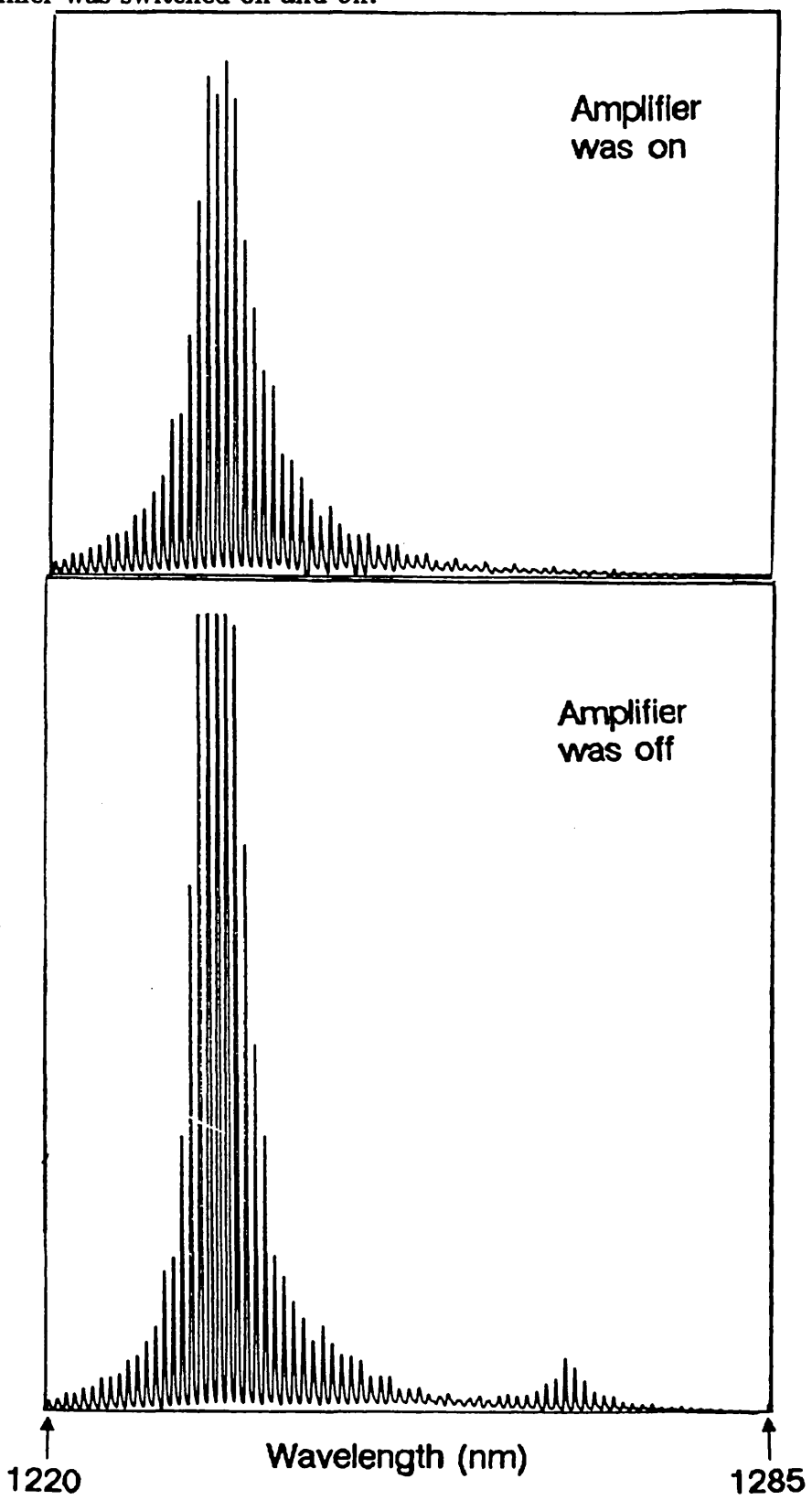

M.O.$_3$ and M.O.$_4$, and the "source" stud was placed in the mount. Light from the "source" laser was focused and steered onto M.O.$_3$ and the light emerging from M.O.$_4$ was adjusted so that its height remained the same as before. In this way, a position for the "amplifier" stud inside M.O.$_3$ and M.O.$_4$. was defined. The reason for maintaining a constant height from the optical table is because the thickness of the active region is about 0.2μm and so the matching in vertical position is quite critical.

The "amplifier" stud was then placed in the defined position and adjusted until the "amplifier" beam was focused, and coincided with the "source" beam spot on M_{steer}. In order to monitor the alignment, part of the "amplifier" beam was either focused onto a GA-5 detector (viewed on the chart recorder), or onto GM-3/amplifier detector (viewed on the sampling oscilloscope). The detected signal was then optimised by finely adjusting M.O.$_3$, M.O.$_4$, and M_{steer}. When the "source" beam was coupled into the "amplifier", a large increase in detected signal would be observed. It has been noted that even with an optimum alignment, small stray light through the cladding layers was detected at large input intensities. This is because the focused spot size of a "source" beam is always larger than the cross section of an active region. But this stray light can be neglected because:

(1) it decreases more rapidly than the attentuated "source" beam,

(2) its intensity is much weaker than the amplified signal.

(iii) Optical isolation

Since an optical isolator has not been used, it was therefore essential to check what effect the laser amplifier had on the "source" performance. This is because if strong coupling occurs between the two devices then the system will behave as a coupled-cavity-laser. To investigate the optical isolation, the "source" output was scanned using a spectrograph when the "amplifier" was switched on and off. It was found that for the case of a Brewster angled amplifier, the "source" spectrum remained unchanged but for F.P. laser amplifiers, strong coupling was observed especially at low attenuations. This is because F.P.laser amplifiers have 30% facet reflectivities

that allow some amplified light to be reflected back into the "source" laser and affect their performance. The "source" spectra of both F.P. and Brewster angled stripe laser amplifiers are shown in figure (7.5).

(iv) Streak camera

In order to simultaneously measure both the "amplified" and "source" pulses on a streak camera, the optical paths of both beams must be of equal length before entering the entrance slit of the streak camera i.e. the path of B.S.$_1$ to B.S.$_2$ must be the same as that from B.S.$_1$, to M_{steer}, to Amplifier, and to B.S.$_2$. The reason for this is that the calibration of spatial displacement to temporal separation requires the pulses of the two beams to coincide in time initially. This is why an optical delay device was placed in the path of the "source" beam because it acts as a compensator which equalises the paths of both the "source" and "amplifier" beams, as well as providing a facility for delaying one pulse by a known value.

7.5 Brewster angled stripe laser amplifiers

7.5a Spectra of amplified signals

The gain bandwidth of a laser amplifier is known to be dependent on the applied currents and on the types of materials, i.e. different bandgaps. For the 1.3μm InGaAsP lasers, the nominal gain bandwidth is about 40nm which increases with longer wavelengths. For instance, 1.55 μm InGaAsP lasers lase across a spectral range of 55nm[94] as compared with a tunable range of about 20nm[15] for the 850nm devices.

The spectra of amplified signals for different wavelengths are shown in figure (7.6). Since the tunable range of the "source" laser did not exactly match to the amplifier's gain bandwidth, the observed tunable range was smaller than expected. In fact, signal amplification was observed within a bandwidth of 25nm. It is believed

Figure (7.6): Emission spectra of the amplified signals for various input wavelengths.

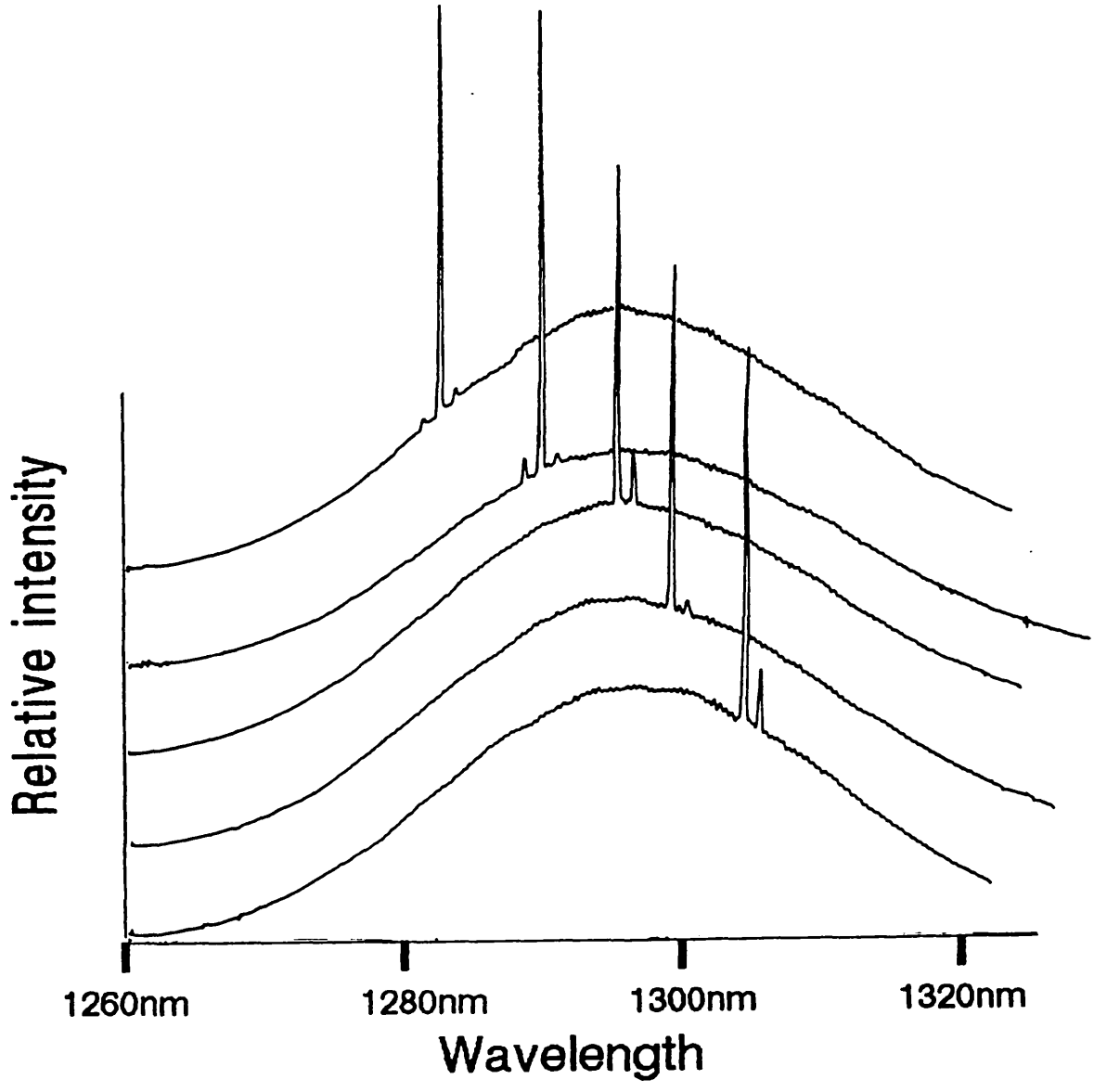

Figure (7.7): Emission spectra of the amplified signals for different input intensities.

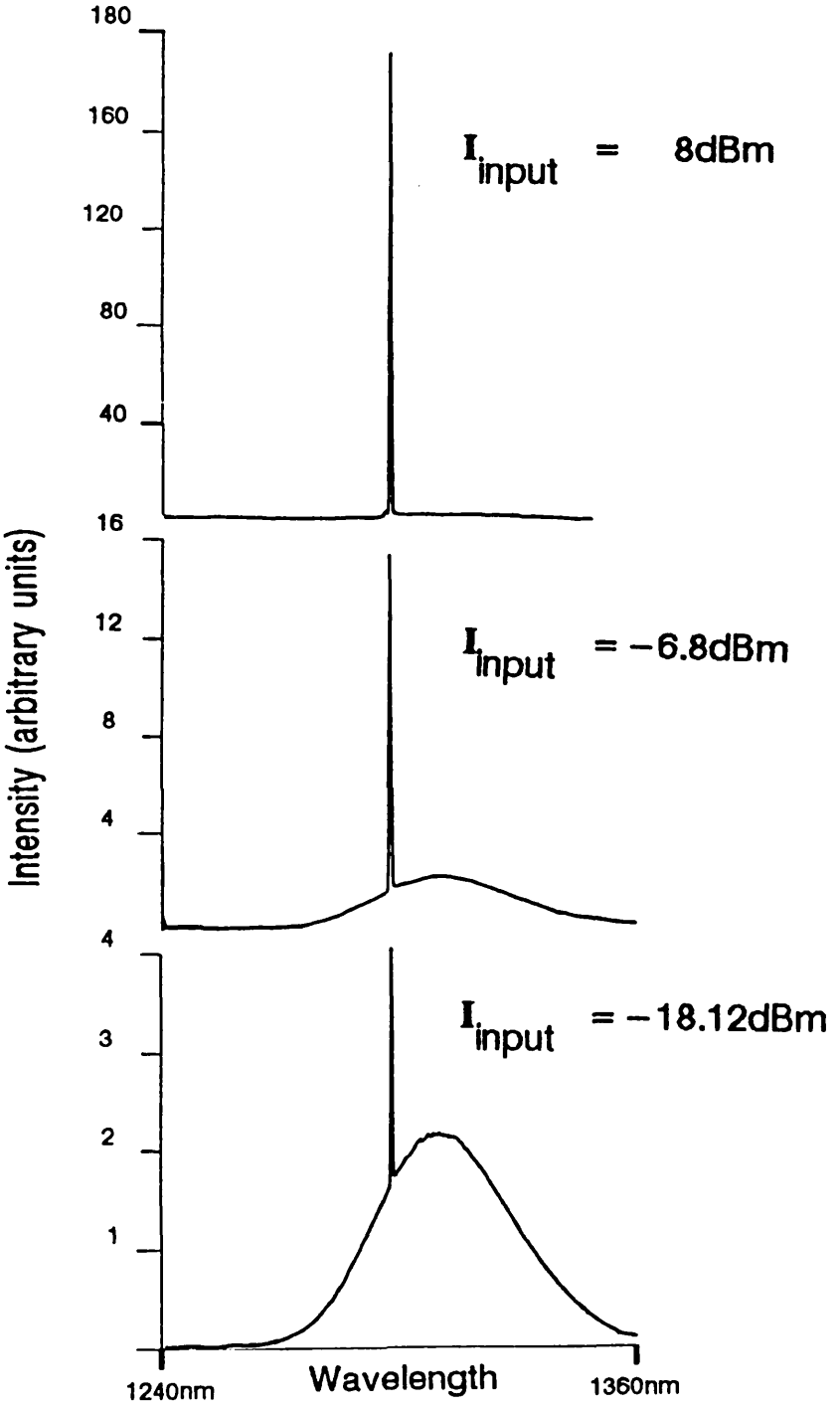

Figure (7.8): The output pulse-profiles for diferent input intensities.

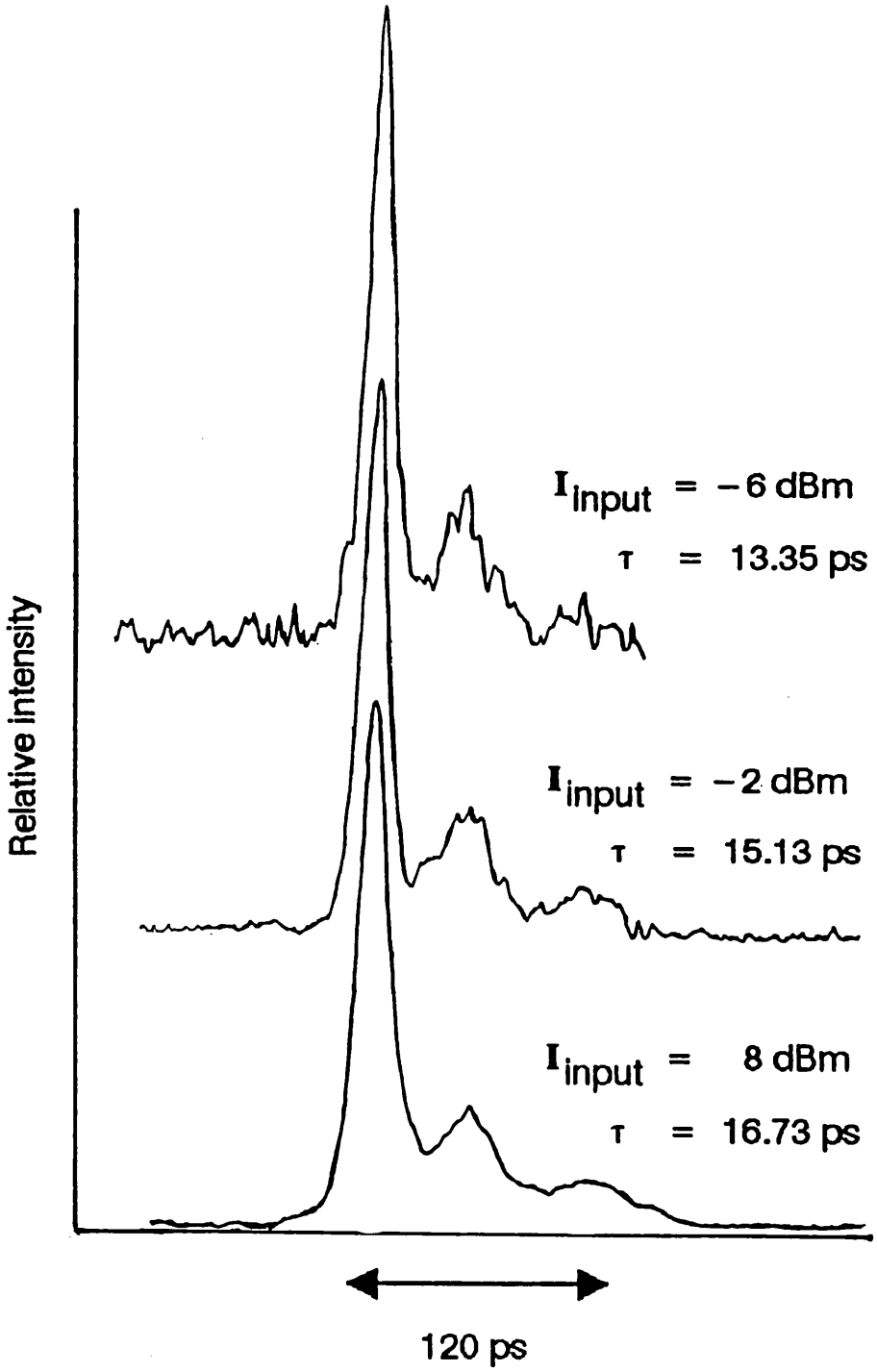

Figure (7.9): The output pulse-profiles for different pumping levels of the laser amplifier.

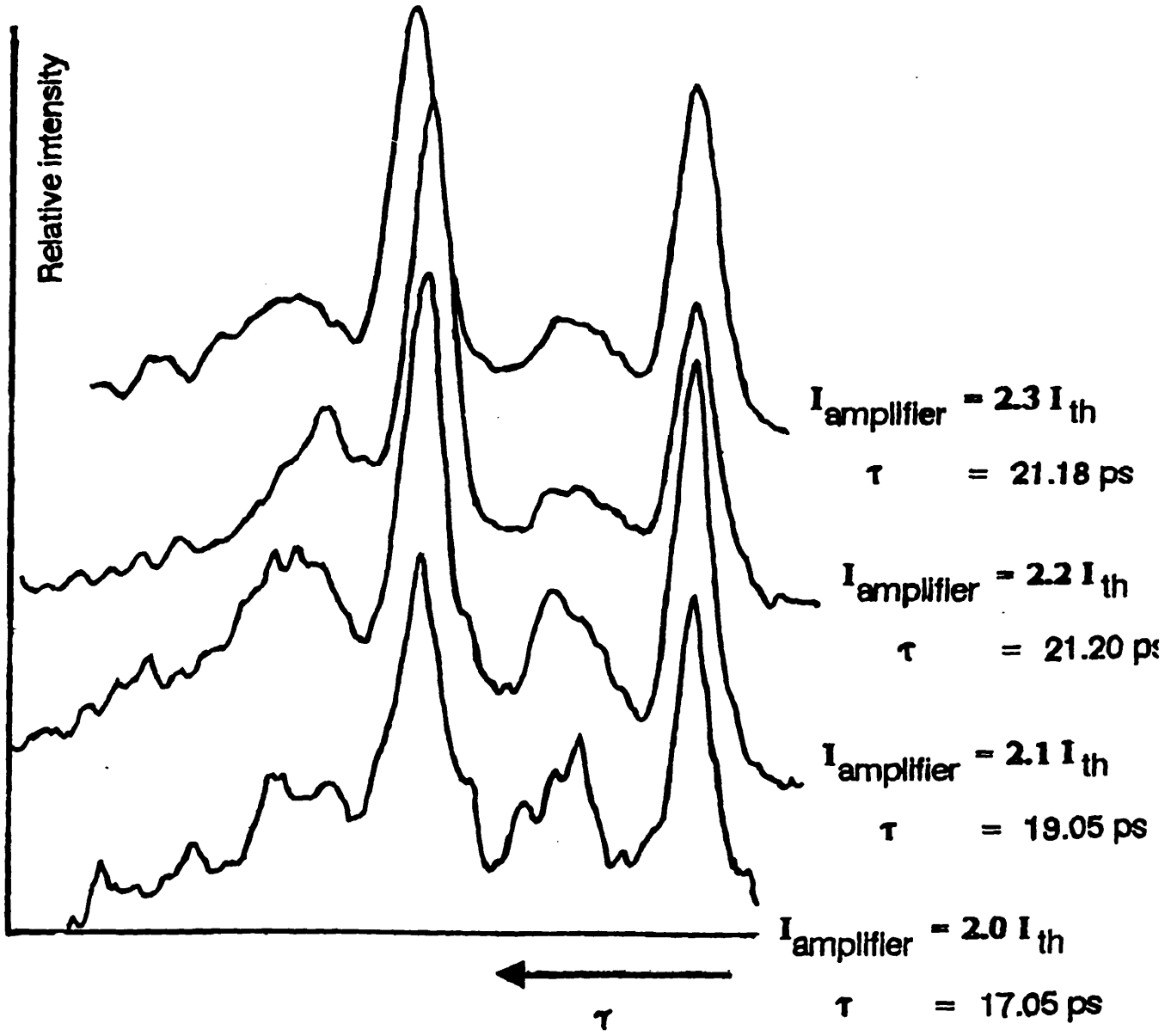

Figure (7.10): Power transfer and gain characteristics of the Brewster angled laser amplifier.

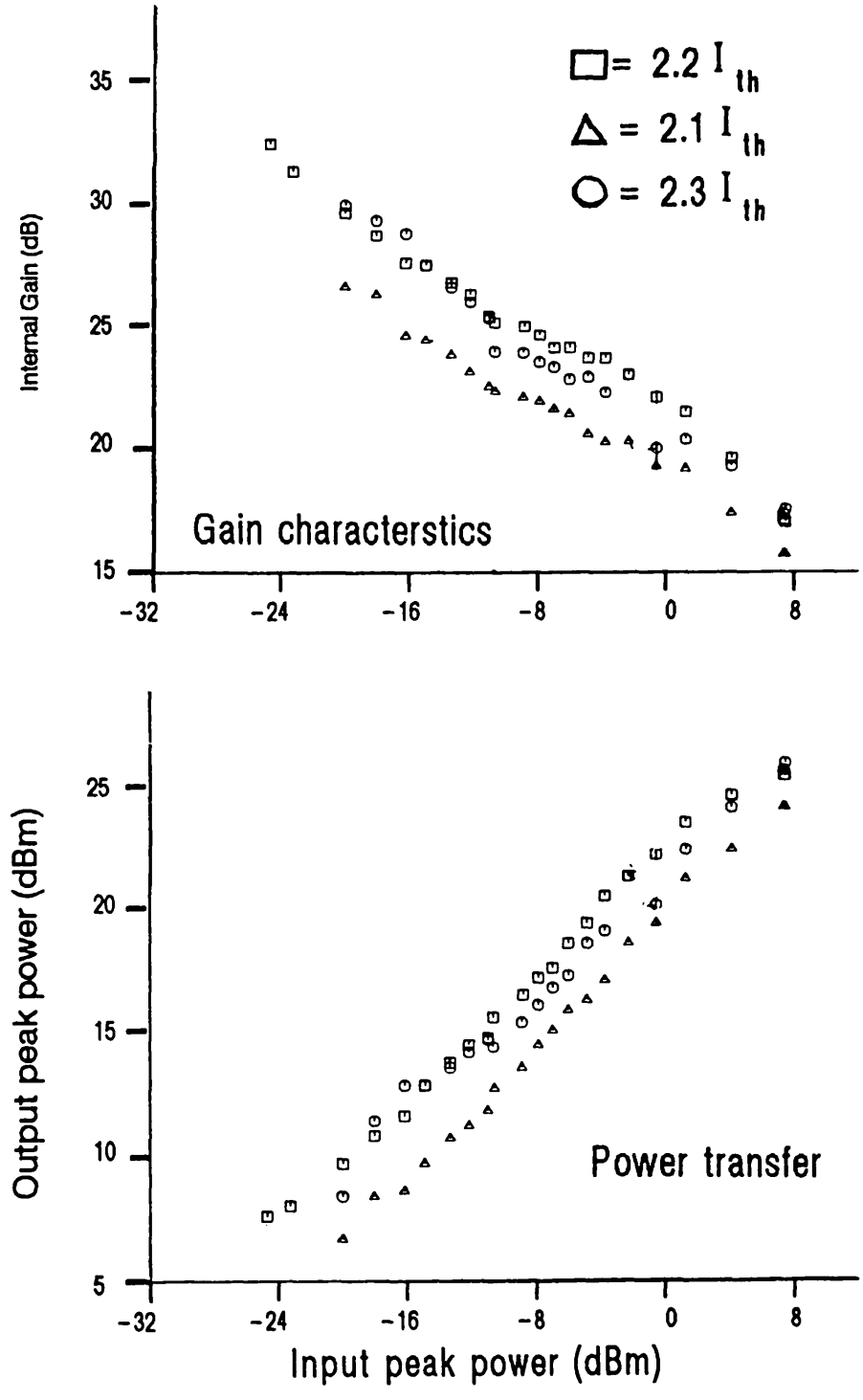

that if a good matching between the "source" and the "amplifier" is achieved, a wider tunable range will be seen. However, the operational bandwidth which is useful for amplification is normally smaller than the natural gain bandwidth.

The spectra of amplified signals at various input intensities are shown in figure (7.7). It is apparent that fluorescent noise plays an important role in the regime where small input signals are comparable to the noise level. In this case, the use of optical filters or electronic frequency filters are necessary in order to improve the signal to noise ratio. In this experiment, the latter method was used in which the detector can only measure the pulsed signals.

The wavelengths of the amplified signal did not shift with respect to the input wavelengths. However, it is believed that wavelength shifting did occur but it was too small to be resolved by the spectrograph. Because a laser amplifier possesses a modulated gain, if the input wavelengths are not matched exactly to the gain peak, the input wavelengths will experience a nonlinear gain and the amplification will be larger near the gain peak. As a result, the amplified signal will seem to be shifted from the input signal. But since the gain of a T.W. laser amplifier is only weakly modulated, this shifting will be extremely small.

7.5b Pulse distortion

Initially, both the amplified and oscillator pulses were simultaneously launched into the streak camera to observe whether there is any relative change. However, the amplified pulses were found to exactly follow the oscillator pulse at any input level and for different applied currents. The measured pulse widths were unchanged even when the mode-locked laser was deliberately detuned, in which case, the amplified pulses just followed the broadening of the "source" pulse widths. This is because the input intensity was below the required intensity level at which the gain saturates.

With increased intensity, a broadening of the amplified pulse was observed at large input intensities. Conversely, narrowing was seen at smaller inputs. This is

shown in figure (7.8). Although it is generally thought that for a large input intensity the carrier density will be heavily depleted during the arrival of leading part of the pulse such that there is very little gain left available for the trailing part. This will result in a sharp cut-off, i.e. the pulse will narrow. However, there is another factor which may also affect the amplified pulse-widths. This is the internal gain characteristic (gain vs intensity) of semiconductor laser amplifiers. It is well known [54] that at a high input intensity beyond the unsaturated gain region, a lower gain will be experienced by the larger intensity. Thus, the front and back of a pulse will experience larger amplifications than the centre part of the pulse. It may be due to this nonlinear temporal amplification that the pulses were seem to broaden at large input intensities. From figure (7.80, one can clearly see that for large inputs, the front and back of the amplified pulses were less sharp than at large inputs.

Another interesting feature was the distortion of amplified pulses for different gains. It was found that at large input intensities, the pulse narrowed with smaller gains. The nonlinear temporal amplification in this case may be caused by insufficient optical gain so the gain depletion by the leading part of the pulse becomes more severe. From figure (7.9), the pulses for the lower amplifier's gain have steep cut-off in the trailing part due to such gain depletion, whereas, the front ends have more or less the same curvatures. The sharpening of the trailing parts also resulted in an increase of the time-separations between the main pulse and the secondary pulse. Since the trailing part fall off sooner and they create a wider separation between the main and secondary pulses.

As explained before, the narrowing which can only be seen under low gain conditions is due to the severe gain depletion leaving little gain available for the trailing parts. One may argue that if the gain was depleted after the peak intensity, and subsequently caused the narrowing, then why there is still enough gain for exciting the secondary pulse. The reason is simply because of the fast gain recovery[14]. This also explains the generation of the secondary pulse from an actively mode-locked semiconductor laser. In which case, after the interaction between an optical pulse

and the carrier density, the normalised density will be reduced drastically. But there still exists a short period during which this density remains above one and thus, the system can sustain another pulse but of much weaker intensity. Therefore, it is not surprising to see that the amplifier's gain can recover quickly enough to amplify the secondary pulse.

7.5c Pulse-gain characteristics

Large amplifications for the signal gain were observed over a range of applied currents from 2.0 to $2.3I_{th}$ (fig. (7.10)). As expected, the signal gain increases with higher currents but there exists an optimum pumping current at which the internal gain reaches a maximum, beyond that the gain is reduced drastically. This has been explained before in section 7.3b that for a laser amplifier which possesses gain-ripples, the gain will reach a maximum with higher currents. Beyond this maximum, the gain will start to fall. The presence of gain-ripples in the Brewster angled stripe laser amplifier is probably a result of the feedback caused by optical scattering. The highest single-pass-gain was 32dB for an input power of -26dBm. Even at large input levels of 8dBm, an internal gain of 17dB was achieved.

Another interesting feature is the high amplified power. The largest output power was 25dBm for an input of 8dBm. Even at a minimum input power of -24dBm, the measured output power was 7.5dBm. The large output power is possible because of the large active area and weak guiding structure[11]. This may also explain why the power started to saturate at a relatively low value (below 24dBm). Perhaps, either with a smaller stripe width (a few μm) or by changing the length of laser amplifiers, the saturation input power (at which the gain starts to saturate) can be increased.

7.6 Conclusion

A high gain and large output power 1.3μm InGaAsP travelling-wave laser amplifier with Brewster angled facets has been described.. Together with a description

of the experimental set-up and alignments. Reflections from the angled facets are lost into the cladding regions which surrounded the active stripe. Thus, the nominal feedback mechanism is destroyed. Lasing was not possible without an external cavity. This was confirmed by both the light output characteristics and the measured spectra (both of these are illustrated in chapter four). However, as mentioned in chapter IV at high pumping levels, a weak intensity modulation was observed around the fluorescence peak. The corresponding feedback mechanism is possibly due to optical scattering at the facets.

Amplification was observed across a bandwidth of 25nm compared to the fluorescence bandwidth of 40nm. The optimum input wavelength was found to be 1.29μm which is near the fluorescence peak. Also, the wavelength of the amplified signal did not change with respect to the input wavelength. Besides the input mode, no other modes were excited by the laser amplifier. Thus, spectrally there was no observable change.

A maximum small-signal-gain of 32dB was attained for an input of -24dBm and the largest output power of 25dBm was measured for an input of 8dBm. Pulse narrowing in the amplified signals was observed on a synchronscan streak camera. A 4 ps pulse-width reduction was measured when the amplifier current was reduced from 2.3 to 2.0I_{th}. Pulse narrowing may be due to insufficient gain (or gain depletion) unable to sustain a constant temporal amplification across the whole pulse.

CHAPTER EIGHT

General Conclusions and prospects

8.1 Active mode-locking

Active mode-locking of InGaAsP semiconductor lasers has been demonstrated. Mode-locked pulses from various external cavity lasers were investigated with the aid of a repetitively-operating (Synchronscan) streak camera. The shortest pulse-widths obtained were about 10ps from a Brewster angled stripe laser coupled to an external grating. The repetitive rate was around 0.3GHz. Wavelength-tunability of about 30nm was measured. Most of the reported experiments (active mode-locking) on this type of III-V lasers generated pulses of durations around 20ps. This is induced by the sub-cavity effect due to the facet reflectivity, which has been alleviated by incorporating the Brewster angled geometry. Unlike A.R. coated facets, the direction of any reflected light from an angled facet is into the cladding instead of into the active medium. However, there could be some optical feedback due to the scattering at the facets. Lasers with two Brewster angled facets would not lase unless they were coupled to external cavities. Pulse formation was found to depend on both the d.c. bias and the r.f. currents. But these dependences were less critical than those of frequency detuning. Asymmetric broadening of pulse-widths were also observed on either side of the optimum mode-locked frequency. Such strong asymmetric behaviour can easily be explained in terms of the arrival of the pulse at the gain medium relative to the time at which the unperturbed gain reaches its peak.

Future work on generation of short pulses from laser diodes is likely to be continued in three different areas. These are:

(1) hybrid active-passive mode-locking,

(2) integrated or compact pulse generators,

(3) compression of the chirped pulses.

(1) Hybrid active/passive mode-locking:

Passive mode-locking is known to be a better way of generating pulses shorter than those due to active mode-locking. This is because in a passively mode-locked system, the pulses are generated by themselves within the cavity. Pulses are therefore continuously modulated by themselves (i.e. self-modulations) until an equilibrium condition has been reached such that the net pulse-shaping effect becomes zero. In other words, the pulse-width of a passively mode-locked system will always be at a "global" minimum which is characterised by the intracavity pulse-shaping elements. In the case of active mode-locking, the gain (or loss) of the system is externally driven, i.e. an external optical modulation. Thus, the pulses are forced to form for the benefit of the external parameters instead of for theirs. Even though an equilibrium condition can be reached, it only corresponds to a "local" minimum. As a result, the pulses are wider. However, passive mode-locking is less controllable and produces weaker intensities than active mode-locking. A compromise would be to combine the two techniques together.

A possible hybrid mode-locking experiment is shown in figure 8.1. The laser diode has two Brewster angled facets which anti-parallel to each other in contrast to that have been described in this thesis. The advantage of this is that sub-cavity resonance now becomes more difficult to form [115] and thus, the maximum r.f. currents can be increased without causing a strong amplified spontaneous fluorescence (i.e. A.S.E.). The top metallisation-contact can be split into two, three, or more sections for independent pumping. The gain or absorbing region would be formed in the active layer below one of these sections with the pumping set above or below a certain threshold value. The laser diode would therefore have sections of gain and absorbing regions dependent upon the injected carrier densities through the split contacts. In the case of a three split contacts diode, it is not certain whether there would be any difference between the configurations : gain/absorber/gain and vice versa.

Another way of improving the pulse-widths is to use two diodes forming a single cavity or double cavity as illustrated in figure 8.2. The r.f. current is applied onto one diode in such a way that the pulse arrival time (as determined by the cavity

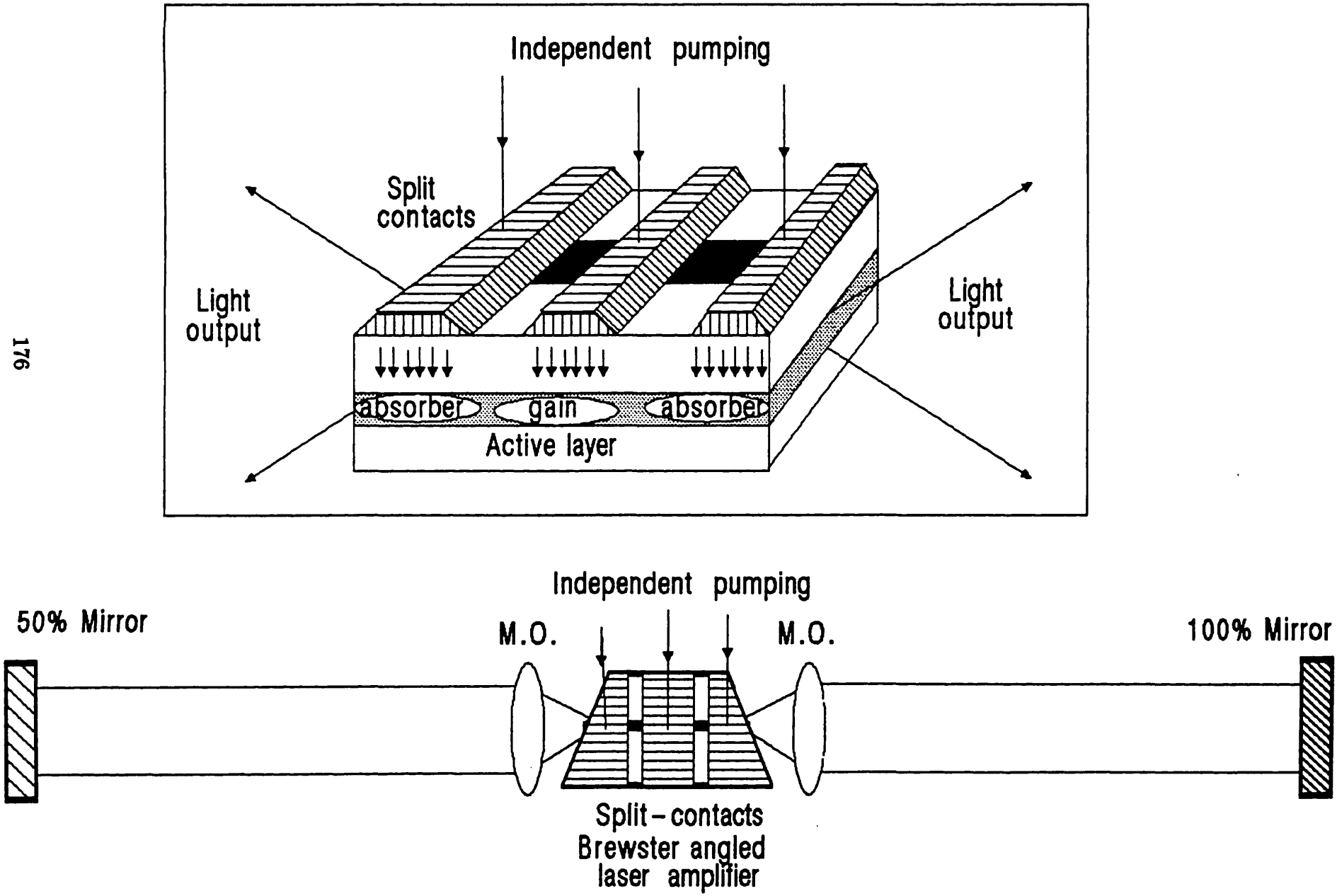

Figure (8.1): Hybrid mode-locking a multi-contact laser diode.

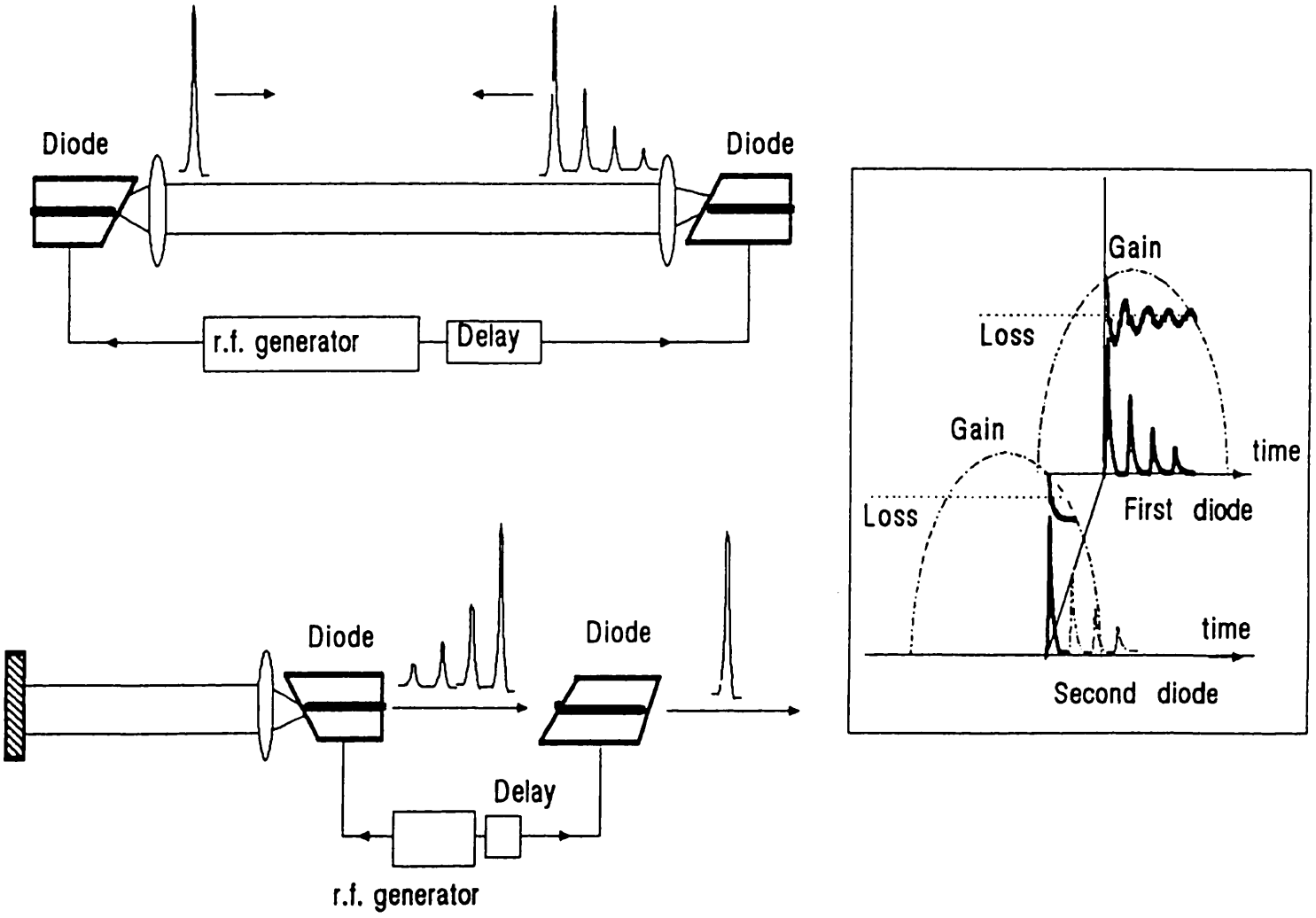

Figure (8.2): Generating pulses from two laser diodes, where one of the applied r.f. modulations is temporaly delayed with the other.

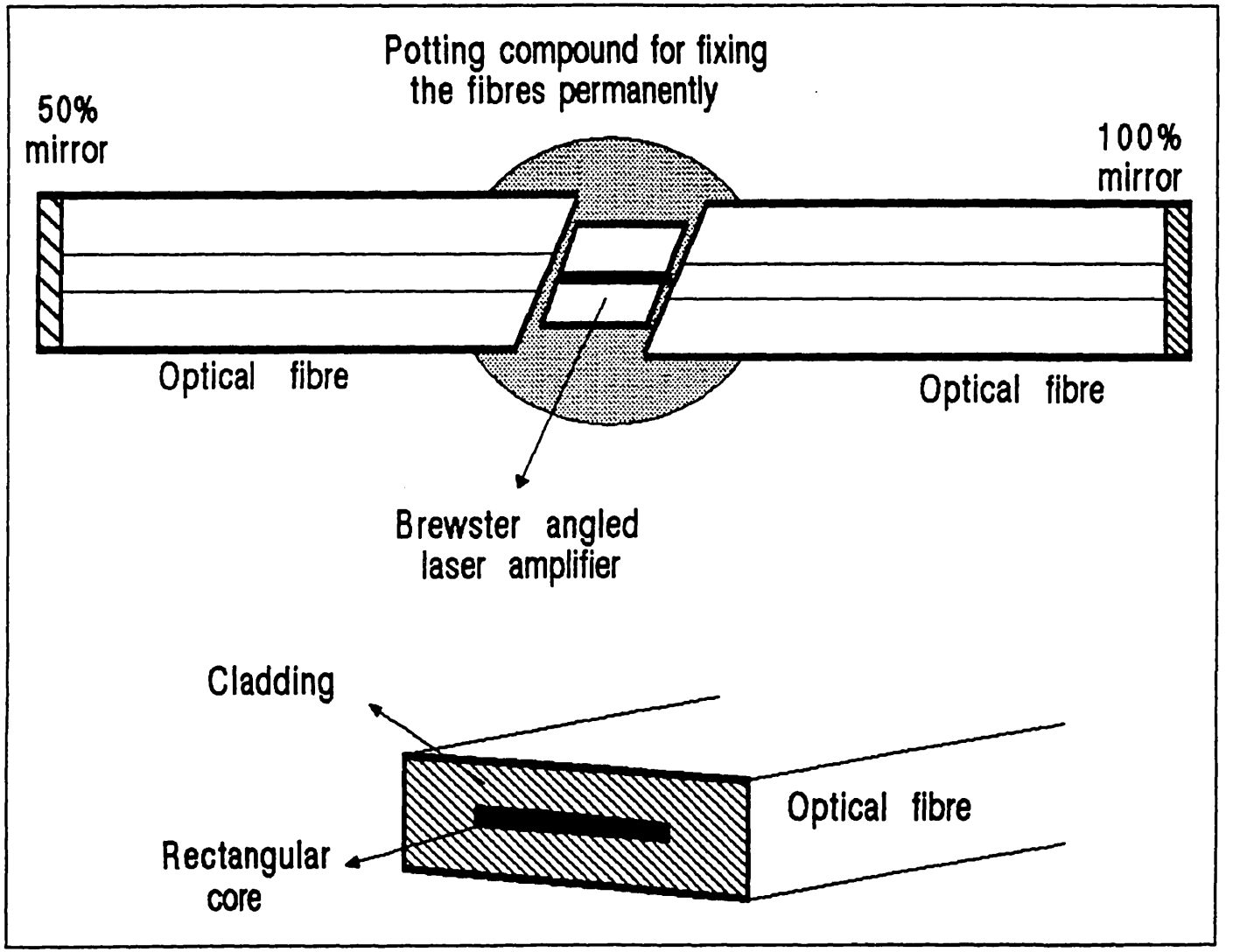

Figure (8.3):A permanently aligned external cavity laser using optical fibres.

length) is earlier than the unperturb gain peak. This will generate multiple pulses with very narrow pulse widths [116]. Conversely, the r.f. modulation on the second diode is arranged so that the pulse-packet will arrive at the gain medium later than the unperturb gain peak. As a result, only the first satellite-pulse will get amplified causing the gain to be reduced below the loss line as depicted in figure 8.2. Since the driving current is in the decaying cycle, the gain will find it very difficult to recover quickly enough to amplify the proceeding satellite-pulses. Therefore, the rear part of the pulse-packet will be cut off allowing only one pulse through. Even though, the gain in both diodes would be driven externally, the "self-modulation" of the pulses should now become much stronger. It is thought that future experiments for generating even shorter pulses from laser diodes could be based on self-modulation.

(2) Integrated or compact pulse generator:

Unless electronic technology reaches the THz regime, mode-locking of laser diodes will still require external (or extended) cavities. A permanently aligned external cavity would be the next step in the development of a compact ultrashort pulse generator, which would have applications in a wide spectrum of technologies. Recently, a strong interest has developed in incorporating such a device into an "optical sampling head" of the sampling oscilloscope.

The external cavity could be based upon an optical fibre or waveguide. In order to make them compatible to Brewster angled strip lasers, the coupling ends must be angle-polished. The cavity would be butt-jointed (fig. (8.3)) and then potted into position with the lasers to form a permanent structure. To achieve a good butt-coupling, the waveguiding properties of the cavities should be matched to the confinement of light within the lasers' active layers. In the case of an optical fibre cavity, a rectangular guiding-core would be more preferable than the conventional spherical core. Work has now started on this type of fibre cavity at Imperial college, U.K. [117].

(3) Compression of chirped pulses:

It is a well known fact that the refractive index of the active layer strongly depends on the injected carrier density. In addition, the dispersion of light within a semiconductor material may also be strong. Due to these two factors, it is very likely that the actively mode-locked pulses are chirped. This may be a possible reason why transform-limited pulses cannot always be achieved. At present, there is not much knowledge about the degree of chirping contained inside an actively mode-locked pulse and its dependence on the r.f. modulation (i.e. with detuning and current amplitudes). But if the chirping is large, a shorter pulse-width can be achieved by optical dispersion. As demonstrated in other laser systems, such a pulse-compression can be achieved by inserting an appropriate disperse element within the external cavities.

8.2 Theoretical studies

In chapter III, it was shown that the lasing bandwidth of an external cavity laser is not always a continuum. A continuous lasing bandwidth exists only for a "stable" laser resonator, where just the pure resonant modes can be excited. For the composite cavity laser, the required lasing gain (needed to overcome the cavity losses) is not constant over all the wavelengths. In some cases, even when the innermost mirrors' reflectivities have been reduced down to 0.001% (10^{-5}), the gain modulation still persisted. At present, most theoretical analyses of actively mode-locked external cavity semiconductor lasers do not take into account such an effect. They have all assumed that the cavity losses are constant for all wavelengths. Thus, practically speaking, it would be more appropriate for any future analysis to consider this spectral gain modulation.

Another important aspect in modelling the active mode-locking of semiconductor lasers is the axial variation of gain within the active medium. Such a variation becomes very strong in laser diodes, which have reduced facet reflectivities. In the case of a wide pulse (i.e. its corresponding optical path is longer than the gain medium), this axial variation can be ignored because as far as the pulse is concerned, the gain

appears to be constant (fig. (8.4)). But for a shorter pulse-width with a transit-distance comparable or shorter than the diode's length, then the axial variation must also be taken into account. This axial dependence of the gain may play an important role in shaping an input pulse in laser amplifiers.

8.3 Laser amplifiers

Preliminary studies of the Brewster angled stripe travelling-wave laser amplifiers operating at 1.3μm have been described. An actively mode-locked external cavity semiconductor laser was used as a signal source. For the picoseconds input pulses, maximum single-pass-gain of 32dB was attained for an input of -24dBm. A maximum output peak power of 25dBm was measured for an input power of 8dBm. Narrowing in the amplified pulse was observed whenever the amplifier gain was too weak to sustain constant temporal amplification across the whole pulse. The amplification bandwidth was about 25nm wide compared to the fluorescence bandwidth of 40nm. This broad operational bandwidth may possibly accommodate simultaneous-amplification of multiple wavelengths. If so, it can then be used in wavelength-multiplexing systems. Thus, the next step in the investigation of laser amplifiers would be on the gain broadening mechanism.

A possible experimental set-up for measuring such a spectral gain broadening is shown in figure (8.5). Two external grating lasers are used allowing the lasing wavelengths to be tuned separately. Both signals are coupled simultaneously into the laser amplifier. The single-pass-gain of one of the signals is measured as the other signal is tuned continuously across the gain bandwidth. A similar set-up could also be used to study the temporal gain recovery of a laser amplifier under different pumping conditions. Since it is this recovery time that determines the smallest temporal separation between two adjacent pulses so that a consistent amplification can be maintained.

Figure (8.4): The axial dependence of gain within the active medium becomes important for pulse-widths shorter than the diode length.

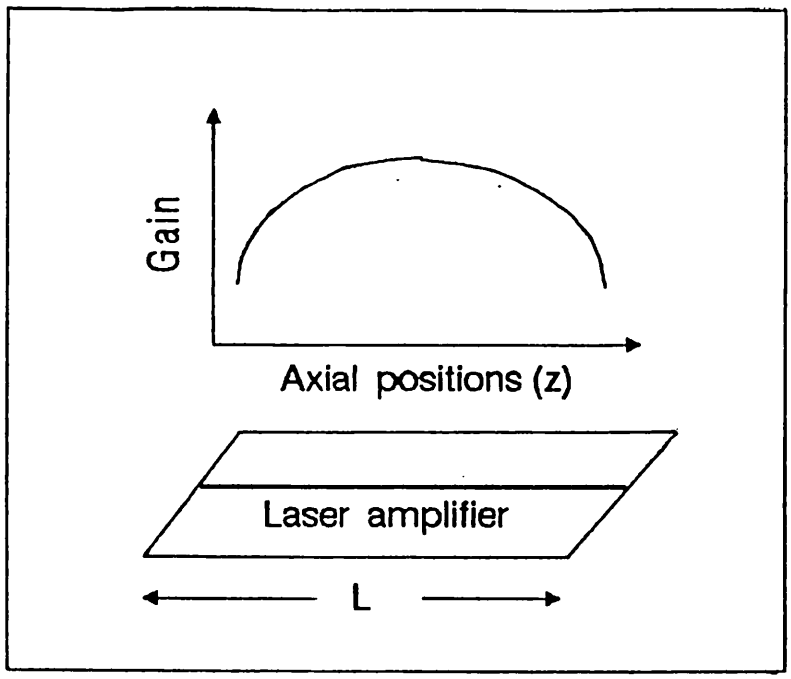

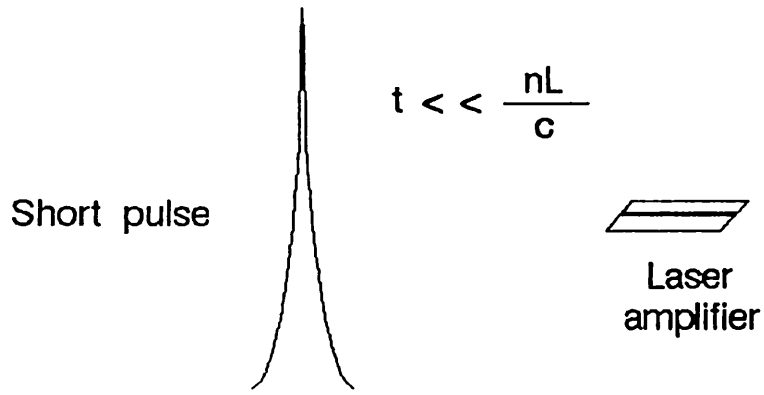

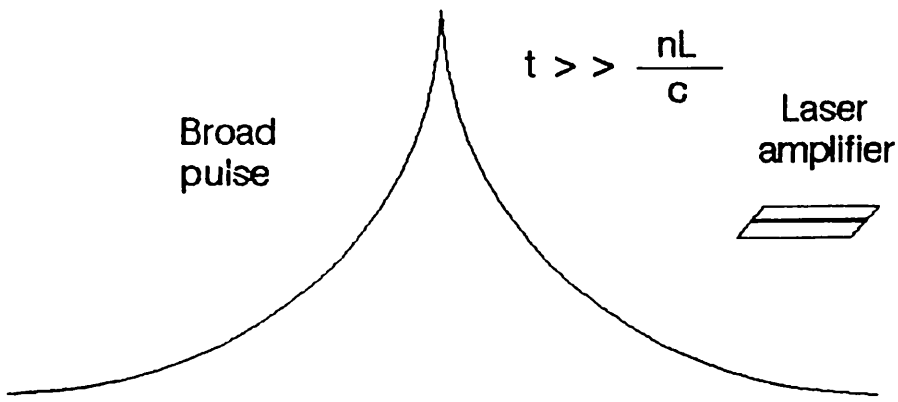

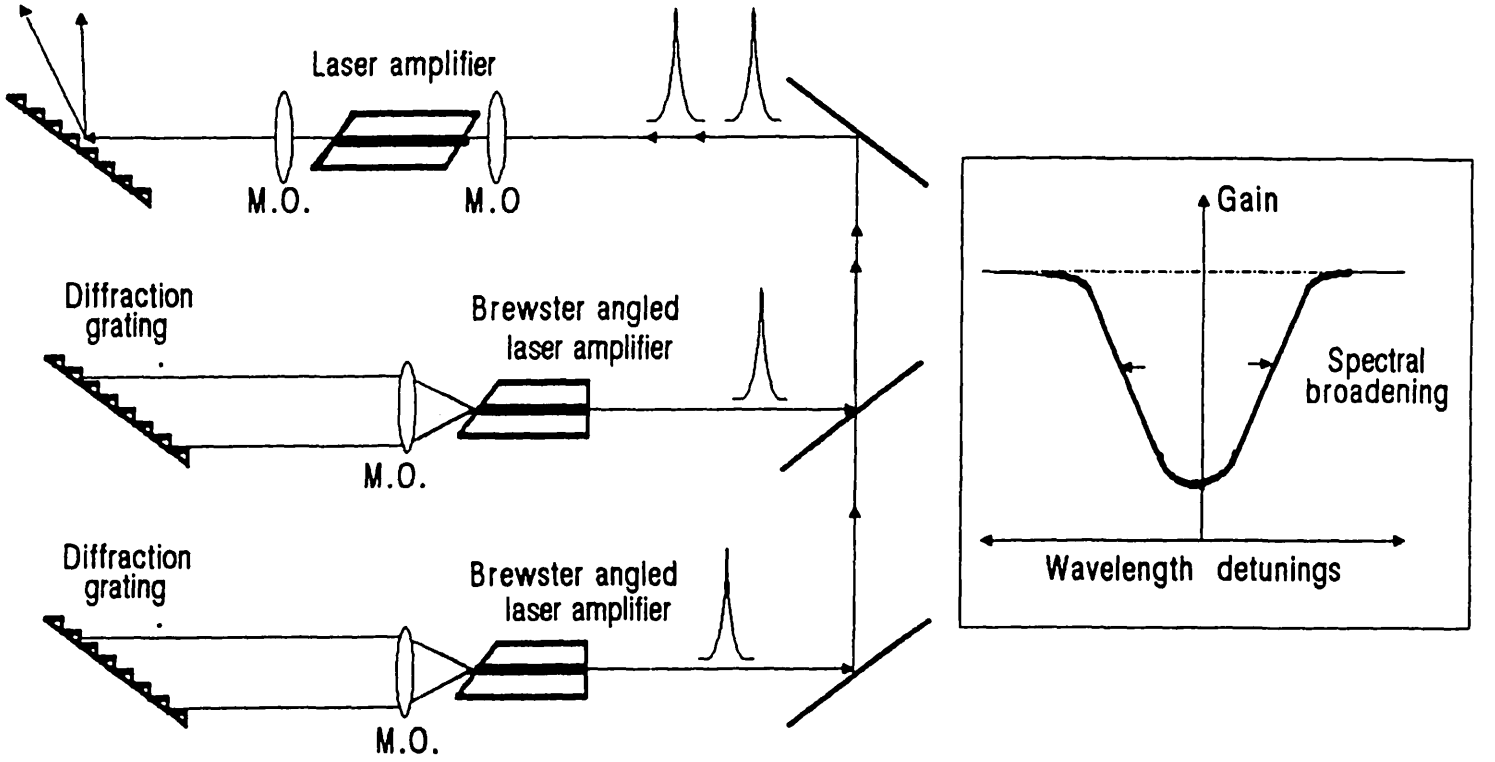

Figure (8.5): Expermiental set-up for measuring the spectral broadening, and temporal gain recovery of a laser amplifier.

Publications

[1] "**Active mode locking of InGaAsP Brewster angled semiconductor lasers**" by J.T.K. Chang and J.I.Vukusic, IEEE, J.Quantum Electron., QE-23, pp 1329-1331, 1987.

[2] "**Study of mode-locked InGaAs/InP lasers using synchroscan streak camera**" by J.T.K.Chang, S.Majumdar, and J.I.Vukusic. 5^{th} International Symposium on Ultrafast Phenomena in Spectroscopy, Vilna, USSR, August, 1987.

[3] "**Travelling-wave Brewster angled stripe InGaAsP laser amplifiers**" by J.T.K.Chang and J.I.Vukusic, Technical Digest of the 8^{th} National Quantum Electron. Confer., (St. Andrews, U.K.) Sept, 1987.

[4] "**Travelling-wave Brewster angled stripe InGaAsP laser amplifier at 1.3μm**" by J.T.K.Chang and J.I.Vukusic, to be published (has been accepted) in a special issue of Modern Optics, 1988.

References

[1] Akiba S.; *"Band to band Auger Recombination effect on InGaAsP laser threshold"* IEEE J.Quantum Electron. QE.17, pp627-635, 1981.

[2] Akiba S. et al; *"High rate pulse generation from InGaAsP laser in selfoc lens external resonator"* Electron. Lett. Vol.17, pp527-529, 1981.

[3] Alferness R.C. et al; *"Modelocking a Ti:$LiNbO_3$-InGaAsP composite cavity laser with an integrated high-speed directional coupler switch"* Appl. Phys. Lett. Vol.45, pp944-946,1984.

[4] Andrews J.R. et al; *"High peak power and gateable picosecond optical pulses form a diode array travelling wave amplifier and a mode-locked diode laser"* Appl. Phys. Lett. Vol.49, pp1004-1006,1986.

[5] Asada M. et al; *"The temperature dependence of the threshold current of GaInAsP D.H. lasers"* IEEE J.Quantum Electron. QE.17, pp611-618, 1981.

[6] AuYeung J.C. et al; *"Picosecond pulse generation from a synchronously pumped mode-locked semiconductor laser diode"* Appl. Phys. Lett. Vol.40, pp112-114, 1982.

[7] Bakker J. et al; *"Single pass gain measurements on optical pumped AlGaAs DH laser structures at room temperature"* IEEE J.Quantum Electron. QE.13, pp567-573, 1977.

[8] Bessonov Y.L. et al; *"Generation of picosecond pulses in an injection laser with an external selective resonator"* Sov. J. Quantum Electron. Vol.12, pp1510-1512, 1982.

[9] Bradley D.J. et al; *"Bandwidth limited picosecond pulses from an actively mode-locked GaAlAs diode laser"* IEEE J. Quantum Electron. QE-17, pp658-662, 1981.

[10] Butler J.K. et al; *"Lateral mode discrimination and control in high-power sin-gle0mode diode lasers of the large-optical cavity (LOC) type"* IEEE J.Quantum Electron., QE-20, pp879-891, 1984.

[11] Buus J. and Plastow R.; *"A theoretical and experimental investigation of Fabry-Perot semiconductor laser amplifiers"* IEEE J.Quantum Electron. QE.21, pp614-618, 1985.

[12] Casey H.C.Jr.; *"Temperature dependence of the threshold current density in InP-GaInAsP (1.3μm) D.H. lasers"* J. Appl. Phys., Vol.56, pp1959-1964.

[13] Chen J.; *"Brewster angled diode amplifiers"* Ph.D. Thesis, London University, Chapter 7, pp202-236, 1983.

[14] Chen J. and Pan D.; *"A rate equation analysis of active mode-locked semiconductor lasers"* IEEE J.Quantum Electron., pp26-31, 1986.

[15] Chen J. et al; *"Modelocking of Brewster angled semiconductor lasers"* Electron. Lett. Vol-18, pp426-427, 1982.

[16] Chen K.L. et al; *"Effect of Mirror imperfections on phase-locked semiconductor laser arrays"* IEEE J.Quantum Electron. QE-21, pp264-270, 1985.

[17] *"Coherent optical transmission: A status report"* Lasers & Applications, pp36-37,

July 1986.
[18] Dimmick T.E. et al; *"Coherent pulse generation by active mode locking of a GaAlAs laser in a selfoc lens extended resonator"* Electron. Lett. Vol.20, pp831-833, 1984.
[19] Domura E. et al; *"InGaAsP/InP buried crescent laser diode emitting at 1.3μm wavelength"* IEEE J. Quantum Electron., QE.20, pp866-873, 1984.
[20] Dutta N.K.; J.Appl. Phys., Vol.51, pp6095, 1980.
[21] Dutta N.K. et al; *"Gain measurments in 1.3μm InGaAsP-InP DH lasers"* IEEE J.Quantum Electron., QE.18, pp44-49, 1982.
[22] Eisenstein G.; *"Theoretical design of single layer antireflection coating on laser facets"* AT& T Bell Lab. Tech. J. Vol.63, pp357-364, 1982.
[23] Eisenstein G. et al; *"Travelling wave optical amplifier at 1.3μm"* Electron. Lett. Vol.23, pp1020-1021, 1987.
[24] Eisenstein G. et al; *"Active modelocking characteristic of InGaAsP single mode fibre composite cavity lasers"* IEEE J.Quantum Electron. QE.22, pp142-148.
[25] Favre F. et al; *"Autostabilization technique for achieving highly stable resonant feedback in fibre resonantor loaded injection laser"* Electron. Lett., pp1046-1048, 1983.
[26] Figueroa L.; *"Study of modelocking in GaAlAs injection lasers"* IEEE J.Quantum Electron. QE.17, pp1074-1085, 1981.
[27] Glasser L.A.; *"C.W. mode locking of a GaInAsP diode laser"* Electron. Lett. Vol.14, pp725-726, 1978.
[28] Glasser L.A.; *"A linearized theory for the diode laser in an external cavity"* IEEE J. Quantum Electron., QE.16, pp525-531, 1980.
[29] Harder C. et al; *"Passive mode locking of buried heterostructure lasers with nonuniform current injection"* Appl. Phys. Lett. Vol.42, pp772-774, 1983.
[30] Haus H.A.; *"Modelocking of semiconductor laser diode"* Japan. J. Appl. Phys. Vol.20, pp1007-1020, 1981.
[31] Haus H.A.; *"Theory of modelocking of a laser diode in an external resonator"* J.Appl. Phys., pp4042-4049, 1980.
[32] Haus H.A.; *"Mode locked semiconductor diode lasers"* Phil. Trans. R. Soc. Lond. A298, pp257-266, 1980.
[33] Haus H.A.; *"Effect of noise on active mode locking of a diode laser"* IEEE J.Quantum Electron. QE.15, pp1258-1265, 1979.
[34] Ho P.T.; *"Coherent pulse generation with a GaAlAs laser by active modelocking"* Elec-tron. Lett. Vol-15., pp526-527, 1979.
[35] Ho P.T. et al; *"Picosecond pulse generation with a cw GaAlAs laser diode"* Appl. Phys. Lett. Vol.33, pp241-242, 1978.
[36] Holbrook M.B. et al; *"External cavity operated angled-stripe geometry DH lasers"* Ap-pl. Phys. Lett. Vol.36, pp349-350, 1980.
[37] Ippen E.P. et al; *"Picosecond pulses generation by passive mode locking of diode*

lasers" Appl. Phys. Lett., Vol.37, pp267-289, 1980.
[38] Ito H. et al; *"Bandwidth limited picosecond optical pulse generation from actively mode-locked AlGaAs diode laser"* Electron. Lett. Vol.16, pp620-621, 1980.
[39] Jain K. et al; *"Stabilisation of external optical feedback phase in a semiconductor laser"* Electron. Lett. Vol.21, pp957-956, 1985.
[40] Kam Y. et al; *"High frequency current modulation of semiconductor injection lasers"* Semiconductor & semimetals, Vol.22, part-B, pp69-148, 1985.
[41] Kapon E. et al; *"Controlled fundamental supermode operation of phase-loked arrays of gain-guided diode lasers"* Appl. Phys. Lett. Vol.45, pp600-602, 1984.
[42] Katz J. et al; *"Rate equations analysis of phase-losked semiconductor laser arrays under steady state conditions"* IEEE J.Quantum Electron. QE-20, pp875-878, 1984.
[43] Kawaguchi H. et al; *"Optical frequency selective amplification in a distributed feedback type semiconductor laser amplifier"* Appl.Phys. Lett. Vol.52, pp66-67, 1987.
[44] Kobayashi S. et al; *"Gain and saturation power of resonant AlGaAs laser amplifier"* Electron. Lett. Vol.16, pp230-231, 1980.
[45] Lau K.Y. et al; Appl. Phys. Lett., Vol.45, 316, 1984.
[46] Lau K.Y. and Yariv A.; *"Direct modulation and active modelocking of ultrahigh speed GaAlAs lasers st frequencies up to 18 GHz"* Appl. Phys. Lett. Vol46., pp326-328, 1985.
[47] Lee T.P. et al; *"Characteristics of linewidth narrowing of a 1.5μm DFB laser with a short GRIN-ROD external coupled cavity"* Electron. Lett. Vol.21, pp655-666, 1985.
[48] Lenth W.; *"Picosecond gain measurements in a GaAlAs diode laser"* Optics Lett. Vol.9, pp396-398, 1984.
[49] Lin C. et al; *"Measurement of 1.3 and 1.55μm gain switched semiconductor laser pulses with a picosecond IR streak camera and a high speed PIN photodiode"* Electron. Lett. Vol.21, pp1200-1202, 1985.
[50] Lin C. et al; *"11.2GHz picosecond optical pulse generation in gain-switched short-cavity InGaAsP injection lasers by high-frequency direct modulation"* Electron. Lett. Vol.20, pp238-239, 1984.
[51] Liou K.Y. et al; *"Narrow linewidth fibre-external-cavity injection lasers"* Electron. Lett. Vol.21, pp933-934, 1985.
[52] Lundquist S. et al; *"Generation of tunable single mode picosecond pulses from an AlGaAs semiconductor laser with grating feedback"* Appl. Phys. Lett. Vol.43, pp715-717, 1983.
[53] Marcuse D. & Lee T.P.; *"On approximate analytical solutions of rate equations for studying transient spectra of injection lasers"* IEEE J.Quantum Electron. QE-19, pp1398-1406, 1983.
[54] Marcuse D.; *"Computer model of an ijection laser amplifier"* IEEE J.Quantum Electron. QE-19, pp63-72, 1983.
[55] McInerney J. et al; *"Bandwidth limited picosecond pulse generation by hybrid*

modelocking in a ring cavity GaAlAs laser" Electron. Lett. Vol.21, pp117-118, 1985.
[56] Morishita M. et al; Solid-state Electron., Vol.22, pp951, 1979.
[57] Mukai T. et al; *"Gain, frequency bandwidth and saturation output power of AlGaAs DH laser amplifiers"* IEEE J.Quantum Electron. QE.17, pp1028-1034, 1981.
[58] Mukai T. et al; *"Optical amplification by semiconductor lasers"* Semiconductor and semimetal, Vol.22, part E, pp265-303, 1985.
[59] Mukai T. et al; *"Optical direct amplification for fibre transmission"* Review Electrical Comm. Lab. Vol.23 pp340-348, 1983.
[60] Mukai T. et al; *"S/N performance of an AlGaAs laser preamplifier and a linear repeater system"* Electron. Lett. Vol.18, pp382-384, 1982.
[61] Mukai T. et al; *"5.2dB noise figure in a 1.5μm InGaAsP travelling wave laser amplifier"* Electron. Lett. Vol.23, pp216-218, 1987.
[62] Nahory et al; Appl. Phys. Lett., Vol.33, pp659, 1980.
[63] Nielsen C.J. et al; *"Linewidth stabilization of semiconductor lasers in an external cavity"* J. Opt. Commun., Vol.41, 1984.
[64] Olsson A. and Tang C.L.; *"Active modelocking of linear and ring external cavity semiconductor lasers"* IEEE J.Quantum Electron. QE.17, pp1977-1978, 1981.
[65] O'Mahony et al; *"Low reflectivity semiconductor laser amplifier with 20 dB fibre to fibre gain at 1500nm"* Electron. Lett. Vol.21, pp501-502, 1985.
[66] O'Mahony et al; *"Semiconductor laser amplifiers for optical communication systems"* Br. Telecom. Technol. J. Vol.5, pp9-18, 1987.
[67] Oomura E. et al; *"Low threshold InGaAsP/InP buried crescent laser with double current confinement structure"* IEEE J.Quantum Electron., QE.17, pp646-650, 1981.
[68] Plastow R. et al; *"Low threshold current c.w. operation of multiple infill buried heterostructure 1.3μm InGaAsP laser"* Electron. Lett. Vol.186, pp262-263, 1982.
[69] Saitoh T. et al; *"Broadband 1.5μm GaInAsP travelling wave laser amplifier with high saturation output power"* Electron. Lett. Vol.23, pp218-219, 1987.
[70] Salathe R.P.; *"Diode lasers coupled to external resonators"* Appl. Phys. Vol.20, pp1-18, 1979.
[71] Sargent M. et al; *"Theory of a distributed feedback laser"* IEEE J.Quantum Electron., QE-16, pp465-472, 1980.
[72] Sato H. et al; *"Theory of spectral linewidth of external cavity semiconductor lasers"* IEEE J.Quantum Electrono., QE-22, pp1060-1063, 1986.
[73] Schicketanz et al; *"GaAs double heterostructure lasers as optical amplifiers"* IEEE J.Quantum Electron. QE.11, pp65-69, 1975.
[74] Silberberg Y. et al; *"Passive modelocking of a semicoductor diode laser"* Optics Lett., Vol.9, pp507-509, 1984.
[75] Silberberg Y. et al; *"Sub-picosecond pulses from a mode locked semi-conductor laser"* IEEE J. Quantum Electron. QE-22, pp759-761, 1986.
[76] Suematsu Y. et al; *"Dynamic single-mode semiconductor lasers with a distributed*

reflector" Semiconductor & semimetal, Vol.22, part-B, pp203-252, 1985.
[77] Suleyman Demokan M.; *"A model of a diode laser actively mode-locked by gain modulation"* Int. J.Electronics, Vol.60, pp67-85, 1985.
[78] Tada Y. et al; *"Ultrashort optical pulses generation from microwave modulated AlGaAs diode laser with selfoc rod resonator"* Optical Comm. Vol.47, pp183-189, 1983.
[79] Thomson G.H.B.; *"Physics of semiconductor laser devices"* John Wiley & sons Ltd, 1980.
[80] Tsang W.T. et al; *"Threshold-wavelength and threshold temperature dependences of GaInAsP/InP laseers with frequency selective feedback operating in the 1.3 and 1.5μm regions"* Appl. Phys. Lett., Vol.43, pp154-156, 1983.
[81] Tsang W.T. et al; *"Mode-locked semiconductor lasers with gateable output and electrically controllable optical absorber"* Appl. Phys. Lett. Vol.43, pp339-340, 1983.
[82] Tsang W.T.; *"C^3 lasers"* Semiconductors and semimetals, Vol.22, part-B, Chapter 5, pp257-373, 1986.
[83] Tucker R.S. et al; *"10GHz active modelocking of a 1.3μm ridge-waveguide laser in an optical-fibre cavity"* Electron. Lett. Vol.19, pp552-553, 1983.
[84] Tucker R.S. et al; *"20GHz active modelocking of a 1.55μm InGaAsP laser"* Electron. Lett. Vol.21, pp239-240, 1985.
[85] Utaka K. et al; *"Lasing characteristics of 1.5-1.6μm GaInAsP/InP integrated twin-guide lasers with first-order distributed Bragg reflectors"* IEEE J.Quantum Electron., QE-17, pp651-658, 1981.
[86] Van der Ziel J.P. et al; *"Generation of subpicosecond pulses from an actively mode locked GaAs laser in an external cavity"* Appl. Phys. Lett. Vol.39, pp867-869, 1981.
[87] Van der Ziel J.P. et al; *"Subpicosecond pulses from passively mode-locked GaAs buried optical guide semiconductor lasers"* Appl. Phys. Lett. Vol.39, pp525-527, 1981.
[88] Van der Ziel J.P. et al; *"Mode-locking of stripe buried heterostructure AlGaAs lasers using an external cavity"* J. Appl. Phys. Vol.51, pp3033-3037, 1980.
[89] Van der Ziel J.P.; *"Modelocking of semiconductor lasers"* Semi-conductor and semi-metal, Vol.22, part B, pp1-68, 1985.
[90] Vasil'ev P.P. et al; *"Bandwidth limited pico-second pulses from GaAlAs DH laser with an external dispersive cavity"* IEEE J.Quantum Electron. QE.21, pp576-581, 1985.
[91] Vasil'ev P.P. et al; *"Subpicosecond pulse generation by a tandem-type AlGaAs DH laser with colliding pulse mode locking"* IEEE J.Quantum Electron. QE.22, pp149-152, 1986.
[92] Westlake H.J. et al; *"Gain characteristics of a 1.5μm DCPBH InGaAsP resonant optical amplifier"* Electron. Lett. Vol.21, pp33-35, 1985.
[93] Wilcox J.Z.; *"Power characteristics of unstable resonator cavity semiconductor*

stripe lasers" Appl. Phy. Lett. Vol.47, pp1019-1021, 1985.
[94] Wyatt R. et al; *"10KHz linewidth 1.5μm InGaAsP external cavity laser with 55nm tuning range"* Electron. Lett. Vol.19, pp110-112, 1983.
[95] Yamamoto Y.; *"Characteristics of AlGaAs Fabry-Perot cavity type laser amplifiers"* I-EEE J.Quantum Electron. QE.16, pp1047-1052, 1980.
[96] Yokoyama H. et al; *"Generation of subpicosecond coherent optical puklses by passive mode locking of an AlGaAs diode laser"* Appl. Phys. Lett. Vol.40, pp105-107, 1982.
[97] Zah C.E. et al; *"Fabrication and performance of 1.5μm GaInAsP travelling wave laser amplifiers with angled facets"* Electron. Lett. Vol.23, pp990-992, 1987.
[98] Hijikata T.; *"Development and production of VSIS lasers"* Lasers & Applications, February, pp57-60, 1985.
[99] Razeghi M. et al; *"Very low threshold GaInAsP/InP double heterostructure lasers grown by LP-MOCVD"* Electron. Lett. Vol.19, pp336-337, 1983.
[100] Itaya Y. et al; *"1.6μm wavelength GaInAsP/InP lasers prepared by two-phase solution technique"* IEEE J.Quantum Electron., QE-17, pp635-639, 1981.
[101] Hirao M. et al; *"Fabrication and characterisation of narrow stripe InGaAsP buried gheterostructure lasers"* J.Appl. Phys. Vol.51, pp4539-4540, 1980.
[102] Ishikawa et al; *"V-grooved substrate buried heterostructure laser emitting at 1.3μm"* IEEE J.Quantum Electron., QE-18, pp1704-1711, 1982.
[103] Mito I. et al; *"InGaAsP planar buried heterostructure laser diode (PBH-LD) with very low threshold current"* Electrono. Lett. Vol.18, pp2-3, 1982.
[104] Mito I. et al; *"Double-channel planar buried heterostructure laser diode with effective current confinment"* Electron. Lett. Vol.18, pp953-954, 1982.
[105] Panish M.B. et al; IEEE J.Quantum Electron. Vol.QE5, pp211, 1969.
[106] Bennion I. et al; *"High reflectivity monomode-fibre grating filters"*, Electron. Lett., Vol.22, pp341, 1986.
[107] Mohn E. et al; Phys. Lett., Vol.2A, pp561-563, 1967.
[108] Lau K.Y. and Yariv A.; *"High-frequency current modulation of semiconductor injection lasers"* Semiconductors & Semimetals Vol.22, part B, pp70-148, 1985.
[109] Aspin G.J. and Carroll J.E.; *"Simplified theory for a mode-locking in injection lasers"* Proc. Instn elect. Engrs, Pt I, 3, pp220-223, 1979.
[110] Kressel H. and Butler, J.K.; *"Semiconductor lasers and heterojunction LED's"* Academic Press, 1977.
[111] Rayan, J.P.; Ph.D. Thesis, University of London, 1978.
[112] Korobkin V.V. et al; Sov. Phy., Tech. Phy., Vol.16, pp165, 1971.
[113] Chen J.; "Mode-locked frequency tunable Brewster angled diode laser" Ph.D. Thesis, University of London, Chapter 6, pp158-201, 1983.
[114] Holbrook M.B. Ph.D. Thesis, University of London, pp125-132, 1980.
[115] Zhou J.Y.; Private communication.

[116] Kelly S.; Private communication.

ERRATUM

Pg 14. Equation (2-3) is only valid for the case where the bandgap energy is independent of lattice matching parameter, namely, the x parameter.

Pg 26. Equation (3-11) and (3-12) are not the same. In fact, equation (3-11) is the modules of equation (3-12) and thus contains only the real parts.

Pg 28. The parameters "Γ" and "γ" in equation (3-15) are the propagation constants of the two subcavities, i.e. subcavities of the 3-mirror composite cavity.

Pg 30. The parameters "n_1" and "n_2" in equation (3-16) are the refractive indices within the subcavities. "L" and "l" are the lengths of these subcavities.

Pg 97. The last paragraph in the conclusion of Chapter Four, i.e. "*It seems that ..... into the gain region.*", should be withdrawn completely from the conclusion.

Pg 14. The lowest losses and dispersion of silica optical fibre should be at λ=1.55 and 1.3 μm.

Pg 83.

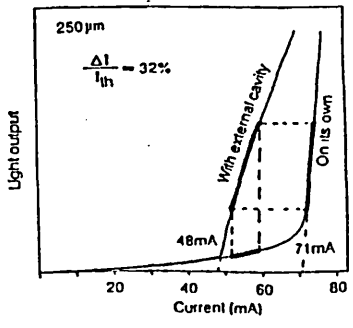

(a) Quantum efficiency has improved with the extra feedback.

(b) Quantum efficiency is less steep the the F..P. laser on its own. This is because the amount of optical feedback is smaller than 30%. (N.B. coupling loss via the lens is about 90%)

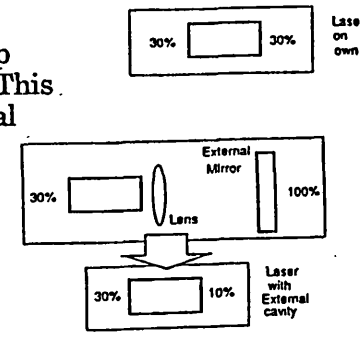

Pg 63.

The non-linearity of the temperature is mainly due to mounting process and the thermal resistance of the indium and copper stud.